**Illuminating the Regulation of the Dark Kinase PSKH1**

**McAloon, Luke**

Neurometabolism Group

Drug Discovery Biology

Monash Institute of Pharmaceutical Sciences

St Vincent's Institute for Medical Research

Australian Catholic University


**Thesis submitted for the degree of**

**Doctor of Philosophy**


**Illuminating the Regulation of the Dark Kinase PSKH1**


Mr. Luke McAloon

Student ID: S00287493

Bachelor of Science (Honours)


Principal supervisor: A/Prof. Jon Oakhill, Dr. John Scott

Co-supervisor: Prof. Bruce Kemp

日々旅にして、旅を栖とす


Every day is a journey, and the journey itself is home.


- Matsuo Bashō from Oku no Hosomichi, or The Narrow Road to the Deep North

**STATEMENT OF AUTHORSHIP**

This thesis contains no material that has been extracted in whole or in part from a thesis that I have submitted towards the award of any other degree or diploma in any other tertiary institution. No other person's work has been used without due acknowledgment in the main text of the thesis. All research procedures reported in the thesis received the approval of the relevant Ethics/Safety Committees (where required).

## ACKNOWLEDGEMENTS

**PUBLICATIONS**

Kaiser J, Nay K, Horne CR, **McAloon LM**, Fuller OK, Muller AB, Whyte, Means AR, Walder K, Berk M, Hannan AJ, Murphy JM, Febbraio MA, Gundlach AL, Scott JW (2023). CaMKK2 as an emerging treatment target for bipolar disorder. *Molecular Psychiatry* 28, 4500-4511.

Neopane K, Kozlov N, Negoita F, Murray-Segal L, Brink R, Hoque A, Ovens AJ, Tjin, G, **McAloon LM**, Yu D, Ling N, Sanders MJ, Oakhill JS, Scott JW, Steinberg GR, Loh K, Kemp BE, Sakamoto K, Galic S (2023). Blocking AMPK β1 myristoylation enhances AMPK activity and protects mice from high-fat diet induced obesity and hepatic steatosis. *Cell Reports* 41.12.

Nay K, Smiles WJ, Kaiser J, **McAloon LM**, Loh K, Galic S, Gundlach AL, Oakhill JS, Scott JW (2021). Molecular mechanisms underlying the beneficial effects of exercise on brain function. *International Journal of Molecular Sciences* 22, p4052.

Langendorf CG, O'Brien MT, Ngoei KRW, **McAloon LM**, Dhagat U, Hoque A, Ling NXY, Dite TA, Galic S, Loh K, Parker MW, Oakhill JS, Kemp BE, Scott JW (2020). CaMKK2 is inactivated by cAMP-PKA signaling and 14-3-3 adaptor proteins. *Journal of Biological Chemistry* 295(48), p16239-16250.

**PUBLICATIONS IN PREPARATION**

**McAloon LM**, Muller AG, Nay K, Lu E, Smeuninx B, Means AR, Febbraio MA, Scott JW (2024). CaMKK2 – Bridging the gap between $Ca^{2+}$-signalling and energy sensing. *Essays in Biochemistry*.

Smiles WJ, Ovens AJ, Yu D, Ling NXY, Morrison KR, Murphy E, **McAloon LM**, Scott JW, Langendorf CG, Kemp BE, Hoque A, Galic S, Petersen J and Oakhill JS. Torin1-sensitive phosphorylation sites on the metabolic regulator AMPK revealed by label-free mass spectrometry. Submission to *npj Metabolic Health and Disease*. Planned for July 2024.

**McAloon LM**, Horne CR, Ling N, Oakhill JS, Johnson JL, Murphy JM, Scott JW. The dark kinase PSKH1 is a metabolic sensor that promotes prostate cancer progression by regulating fuel switching to fatty acids. Planned for 2024.

## LIST OF ABBREVIATIONS

| | | |
|---|---|---|
| aa | – | amino acid |
| ADT | – | androgen deprivation therapy |
| AID | – | autoinhibitory domain |
| AKAP | – | A-kinase anchoring protein |
| ASD | – | autism spectrum disorder |
| ATP | – | adenosine triphosphate |
| CaM | – | calmodulin |
| CaMK | – | $Ca^{2+}$/calmodulin-dependent protein kinase |
| CaMK1 | – | $Ca^{2+}$/CaM-dependent protein kinase 1 |
| CaMK2 | – | $Ca^{2+}$/CaM-dependent protein kinase 2 |
| CaMK4 | – | $Ca^{2+}$/CaM-dependent protein kinase 4 |
| CaMKK | – | $Ca^{2+}$/CaM-dependent protein kinase kinase |
| cAMP | – | cyclic adenosine monophosphate |
| CARS | – | coherent anti-Stokes Raman scattering |
| CBD | – | calmodulin-binding domain |
| CHOL | – | cholangiocarcinoma |
| CMV | – | cytomegalovirus |
| CREC | | $Ca^{2+}$-binding protein of 45 kDa (Cab45), reticulocalbin, ER $Ca^{2+}$-binding protein of 55 kDa (ERC-55), and calumenin |
| CRPC | – | castration-resistant prostate cancer |
| CTKD | – | c-terminal kinase domain |
| DC | – | Doublecortin |
| DD/ID | – | developmental delay/intellectual disability |
| DKO | – | double knock-out |
| ECAR | – | extracellular acidification rate |
| ER | – | endoplasmic reticulum |
| ESCA | – | oesophageal cancer |
| ETC | – | electron transport chain |
| GA | – | Golgi apparatus |
| HDX | – | hydrogen deuterium exchange |
| eEF2K | – | eukaryotic elongation factor 2 kinase |
| HNSCC | – | head and neck squamous cell carcinoma |

| | | |
|---|---|---|
| KIRC | – | kidney renal clear cell carcinoma |
| ko | – | knock-out |
| LC-MS/MS | – | liquid chromatography mass spectrometry/mass spectrometry |
| LIHC | – | liver hepatocellular carcinoma |
| LKB1 | – | liver kinase B1 |
| MLCK | – | myosin light chain kinase |
| NF2 | – | Neurofibromatosis Type 2 |
| NLS | – | nuclear localisation signal |
| NTKD | – | n-terminal kinase domain |
| OCR | – | oxygen consumption rate |
| PCa | – | prostate cancer |
| PH | – | pleckstrin homology (domain) |
| PDAC | – | pancreatic ductual adenocarcinoma |
| PDE | – | phosphodiesterase |
| PhK | – | phosphorylase kinase |
| PKA | – | cAMP-dependent protein kinase |
| PSKH1 | – | serine/threonine-protein kinase H1 |
| RBD | – | Rho-binding domain |
| RCN | – | reticulocalbin |
| RSK1-4 | – | ribosomal S6 kinase 1-4 |
| TSSK | – | testis-specific serine/threonine-protein kinase |
| wt | – | wild-type |

# INDEX OF FIGURES

## INDEX OF TABLES

## TABLE OF CONTENTS

**ABSTRACT**

PSKH1 is a 48 kDa serine/threonine-protein kinase whose function, regulation and downstream effectors remain undefined. Discovered in the late 1980's, PSKH1 is increasingly implicated in an appreciating number of cellular processes, including vesicle trafficking, cell migration, and pre-mRNA splicing. More recently, PSKH1 was classified as a top-6 driver of prostate cancer progression. Precisely how PSKH1 mediates these effects is not currently understood. This thesis sought to resolve these questions using a combination of *in vitro* and *in vivo* experimental methodologies.

Chapter 3 details efforts to elucidate the mechanisms by which PSKH1 activity is regulated. It was revealed that PSKH1 autophosphorylates itself in a *cis*-apparent mechanism, a process that significantly enhances its catalytic activity *in vitro*. Further, as a *bona fide* CaM-kinase family members, PSKH1 is regulated by calmodulin, albeit via a distinct mechanism. Lastly, PSKH1 is negatively regulated by a novel family of low-affinity $Ca^{2+}$-binding proteins.

Chapter 4 established, for the first time, a function for PSKH1, providing a direct causative link between PSKH1 and prostate cancer progression. PSKH1 is a metabolic sensor kinase that is activated in response to glucose deprivation and drives prostate cancer cell growth by mediating fuel switching to alternative energy sources (fatty acids). Furthermore, PSKH1 may mediate these effects by modulating the action of RSK1/eEF2K, two proteins we recently identified as PSKH1 interacting. PSKH1 regulation of the RSK1/eEF2K signalling axis is currently preliminary but corroborates the growth-promotive phenotype of PSKH1 expression in prostate cancer. These data provide critical insights into PSKH1 regulation of prostate cancer progression.

# 1. INTRODUCTION

## 1.1. Illuminating the dark CaMK kinome

Reversible phosphorylation is an integral regulatory component of almost all facets of cellular biology, affecting key physiological programs such as transcription and translation, cell cycle and cytodifferentiation, metabolism and programmed cell death. Indeed, more than 500 kinases constituting ~2% of all encoded human genes have to date been described [1]. However, it was not until Edwin Krebs and Edmond Fischer's seminal papers in the mid-1950's that the importance of phosphoproteins and, by extension, their regulation by reversible phosphorylation was meaningfully appreciated. In their studies, which were initially focused on the regulation of glycogen phosphorylase by 5'-adenylic acid (henceforth, cyclic adenosine monophosphate; cAMP), it was revealed that paper filtration of crude muscle extracts converted glycogen phosphorylase from an inactive (phosphorylase b; PhB) to active (phosphorylase a; PhA) species [2]. These filter papers were later discovered to be contaminated by $Ca^{2+}$ cations. Given the prevalence of adenosine triphosphate (ATP) in crude skeletal muscle extracts, the authors reasoned that a kinase acting upstream and through calcium activated glycogen phosphorylase. The identity of this mysterious enzyme was revealed to be phosphorylase kinase (PhK) which, when stimulated by $Ca^{2+}$, catalyses the conversion of phosphorylase from the inactive to active species [3]. Importantly, subsequent work by Phil Cohen's lab demonstrated that PhK was itself under the direct regulation of phosphorylation by an additional, extrinsic protein kinase – the cAMP-dependent protein kinase, or PKA [4]. These studies collectively described, for the first time, the existence of a phosphoryl transfer cascade that, importantly, controlled the action of a crucial cellular process, such as carbohydrate metabolism.
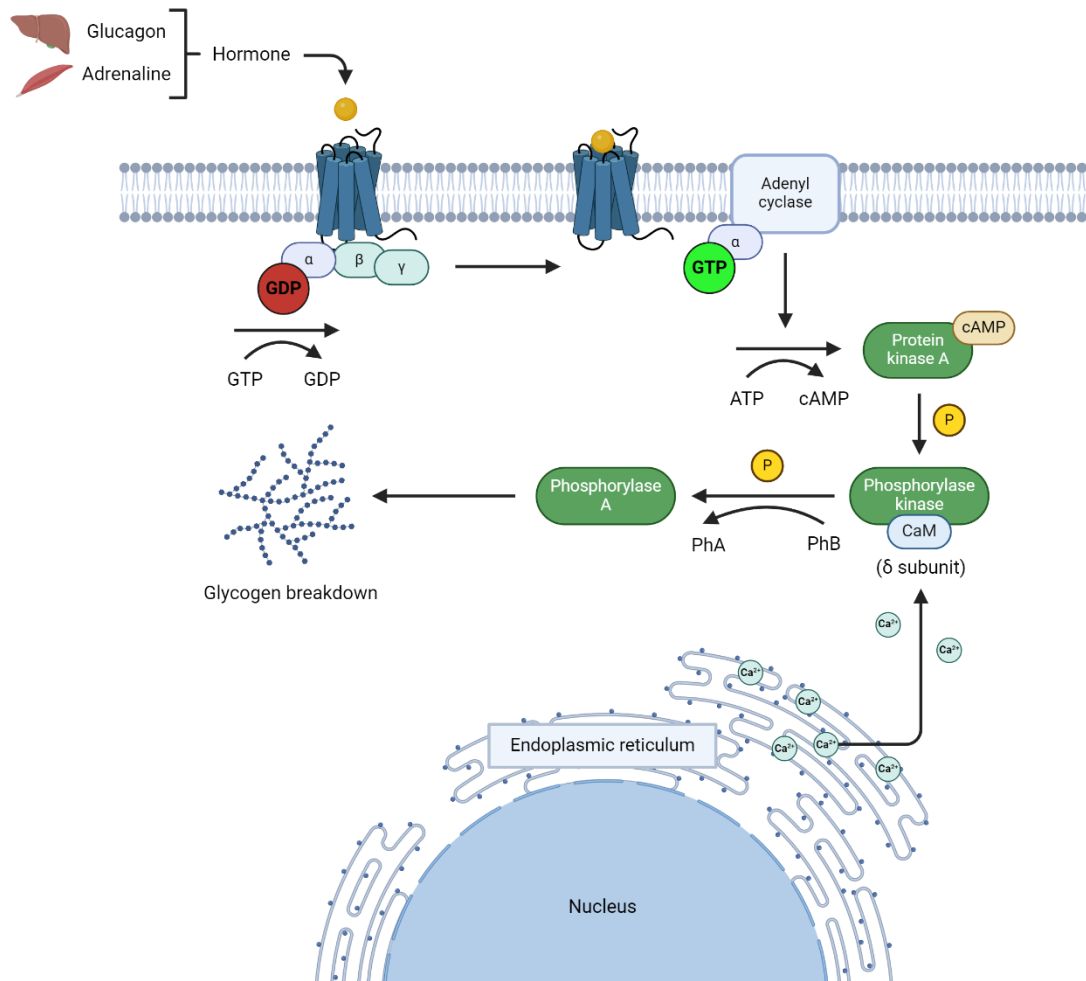
***Figure 1.1. Key biological processes, such as carbohydrate metabolism, are regulated by a protein phosphorylation cascade.*** In response to first messenger signalling at the plasma membrane, adenyl cyclase catalyses the conversion of ATP to cAMP, which liberates the regulatory subunits of protein kinase A (PKA) and stimulates catalytic activity. PKA phosphorylates the α and β subunits of phosphorylase kinase (PhK). Intracellular increases in [$Ca^{2+}$], either from internal stores (endoplasmic reticulum) or via ion channels at the plasma membrane, activate the integral σ subunit of PhK (calmodulin). Activated PhK catalyses the conversion of glycogen phosphorylase from the inactive (PhB) to active (PhA) species, promoting glycogen breakdown. Adapted from Han, Kang [5]. Created with BioRender.com.

Interestingly, since its discovery more than 70 years ago, many aspects of PhK biochemistry remain undefined. This is indeed the case for many members of the calmodulin-dependent protein kinase (CaMK) subfamily, more than two thirds of which remain poorly characterised (Figure 1.2). There is a pressing need to holistically evaluate the regulation and function of these enzymes, as members of the dark CaMK kinome are increasingly correlated with aggressive and often fatal disease phenotypes, such as metastatic prostate cancer and neurodegenerative diseases such as Huntington's disease [6, 7]. Further, according to a recent report by Essegian, Khurana [8], only 8% of the human kinase complement is currently targeted by FDA-approved small molecule anti-cancer drugs. Importantly, there are no FDA-approved small molecule compounds that specifically target the CaMK family [8]. Although details pertaining to the structure, function and effector substrates of many CaM-kinases currently remain undefined, this review will largely be restricted to CaM-kinases featured in the Dark Kinase Knowledgebase [9], including: Obscurin-MLCK, the testis-specific serine/threonine protein kinases, NIM1, BRSK1, BRSK2, NuaK2, MNK1, MNK2, DCAMKL3, CaMK1 and, notably, the serine/threonine protein kinase-H1 (PSKH1), of which this thesis is primarily concerned. The biochemical characterisation of these kinases, in addition to associated disease phenotypes, will be explored. This review will also be extended to the upstream effector of the CaM-kinase kinase (CaMKK) signalling cascade, CaMKK2, and will be discussed first. For simplicity, pseudokinases – catalytically deficient kinases – have been omitted.
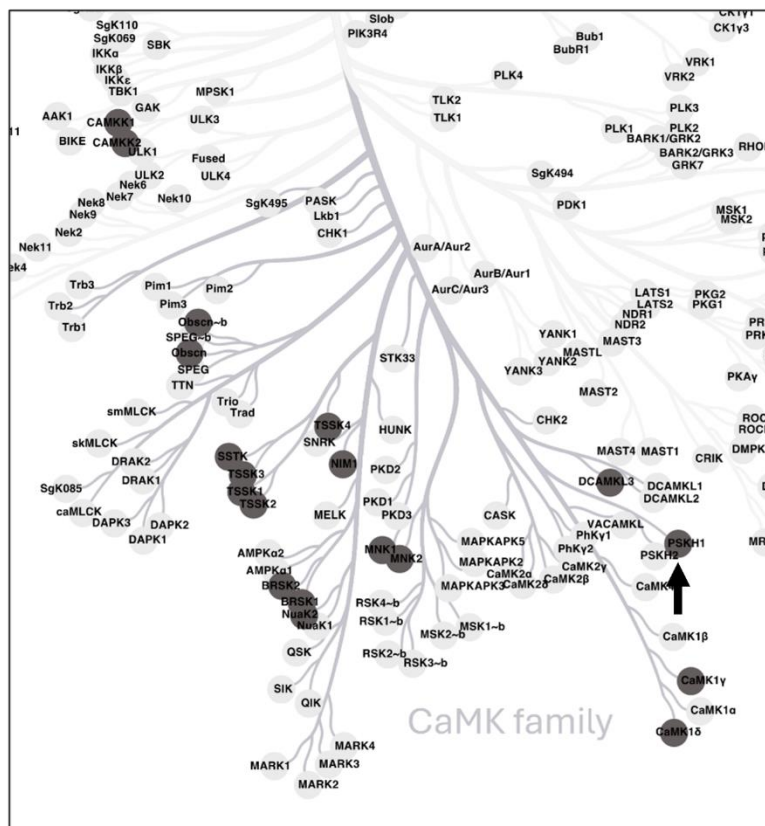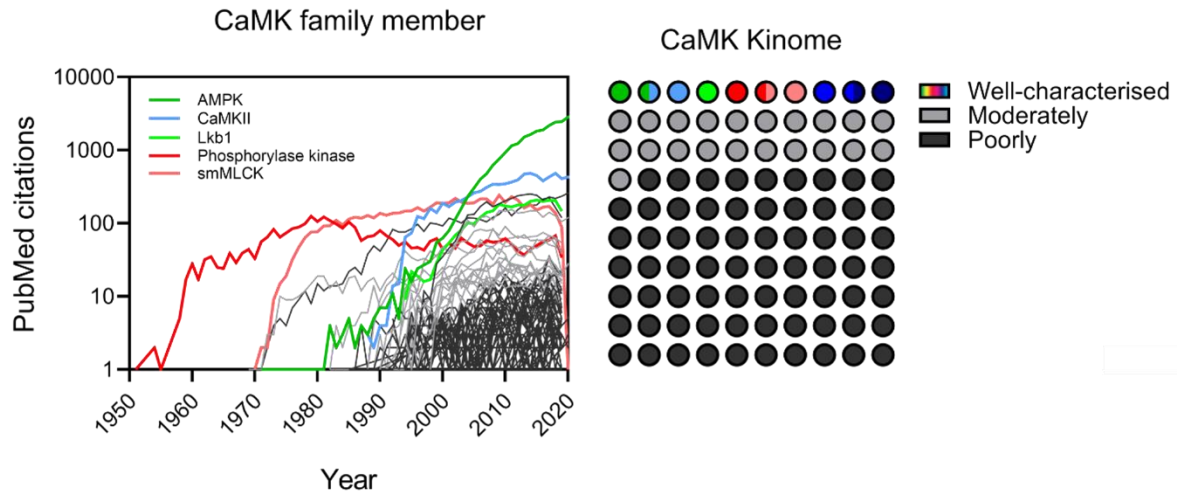
***Figure 1.2. The CaMK kinome remains largely uncharacterised.*** Annual citations (1950-2020) for each individual CaMK-family member were extracted from PubMed (for full list of search terms used, see Appendix) and plotted over time. The top five most highly cited CaM-kinases (AMPK, CaMKII, Lkb1, phosphorylase kinase and smMLCK) were used as a benchmark to categorise the kinome into: well-characterised (>3000 cumulative citations), moderately characterised (300-3000 cumulative citations) or poorly characterised (>300 cumulative citations). *Kinome tree*. Poorly characterised CaM-kinases also featured in the Dark Kinase Knowledgebase include: Obscurin-MLCK (Obscn-b), TSSK1, TSSK2, TSSK3, TSSK4, SSTK, NIM1, BRSK1, BRSK2, NuaK2, MNK1, MNK2, DCAMKL3, PSKH1 (indicated – black arrow), CaMK1γ and CaMK1σ [9]. Kinome tree prepared using Coral [10].

**Table 1.1. Current characterisation of the dark CaMK kinome**

| Dark Kinase | Tissue Expression | | Biochemical Characterisation | | | |
|---|---|---|---|---|---|---|
| | *Tissue* | *Cellular* | *CaM-binding domain* | *Autokinase activity* | *Extrinsic kinase/s* | *Substrates* |
| *Other* | | | | | | |
| **CaMKK1** CaMKKα CaM-kinase Ia kinase | Brain, thymus, spleen [11], retina [12] | | Yes: 438-463 [13, 14] | Yes: S24 [15] | **PKA**: S52/74/108/458/475 [15] | **CaMK1**: T177 [16, 17] **CaMK4**: T196 [18] |
| **CaMKK2** CaMKKβ CaM-kinase IV kinase | Brain, thymus, spleen, testis [19] | Granule cell layer [20] | Yes: 480-499 [19] | Yes: T85 [21] T482 | **CDK5**: S137 **GSK3**: S129/133 [22] **PKA**: S100/495/511 [23] **AMPK**: T145 | **CaMK1**: T177 [24] **CaMK4**: T196 [11, 25, 26] **AMPK**: T172 [27] **PKB**: T308 [28] **Syndapin I**: T355 [29] **SIRT1**: S27/47 [30] **GAPDH** [31] **Pex3** [31] |
| *CaMK1/4 branch* | | | | | | |
| **CaMK1γ** CLICK-III | Brain [32], amygdala, VMH [33] | Neurons, intracellular membranes [33] | Yes: | Undefined | **CaMKK**: T177 [17] | **CREB** [33] |
| **CaMK1σ** CKLiK | Ubiquitous [34] | Granulocytes [35] | Yes: 297-324 [34] | Undefined | **CaMKK1**: T180 [34] **CaMKK2.3**: T180 [34] | **CREB** [35] |
| **DCLK3** DCAMLK3 CLICK-I/II-related (CLr) | Adult brain (striatum), liver, kidney [36] | Diffuse (cytoplasmic, nuclear) [36] | No/undefined | Yes: [7] | CDK5? [37] | Undefined |
| **PSKH1** | Ubiquitous, testis [38] | Perinuclear/nuclear, Golgi, centrosome [38] | Undefined | Yes: S370 – C383 [38] | Undefined | Undefined |
| *AMPK branch* | | | | | | |
| **BRSK1** SAD-B | Brain [39] | Neurons [39], highly-membrane associated [40] | No | Yes: [39] | **LKB1**: T189 [41] **CaMKK1**: T189 [42] | **CAST**: S45 [43] **RIM1** [39] **Tau** [44] |
| **BRSK2** SAD-A | Brain, pancreas [39, 45] | Neurons, diffuse [40] | No | Undefined | **LKB1**: T174 [41] **PKA**: T260 [46] | **Cdc25C**: S216 [47] **PAK1**: [48] **Tau**: S262 [49] **TSC2**: S1387 [50] |

| | | | | | | |
|---|---|---|---|---|---|---|
| **NUAK2** Nuak2 SNARK | Ubiquitous, brain/adrenal (protein) [51, 52] | Nuclear [53] | | Yes: [51] | **LKB1**: T208 [41] | **LATS1**: T246, S613 [54] **MYPT1**: S445 [55] |
| **NIM1** | Ubiquitous [56] | Cilia [57] | No/ undefined | Yes: Putatively T229 [56] | Undefined | Undefined |
| **TSSK1** TSK-1 | Adult testis [58-61] | Post-meiotic spermatids, residual bodies [59, 61, 62] | No | Yes: [56] | Undefined | **TSKS**: S288 [59, 60] |
| **TSSK2** DGS-G | Adult testis [59-61] | Post-meiotic spermatids, residual bodies [59, 61, 62] | No | Yes: [60, 61] | Undefined | **TSKS**: S288 [59, 60] |
| **TSSK3** | Adult testis [61, 63] | Leydig cells [64] | No | Yes: S166 [65] | PDK1: T168 [65] | |
| **TSSK4** TSSK5 | Adult testis [61, 66] | Post-meiotic spermatids [61] | No | Yes: T197 [67] | Undefined | **CREB**: S133 [66] **ODF2**: S76 [68, 69] |
| **TSSK6** TSSK4 SSTK | Adult testis, ubiquitous [61, 70] | Post-meiotic spermatids [61, 70] | No | Yes: [70] | Undefined | **H1, H2A, H2AX, H3** [70] |
| *MAPK-regulated branch* | | | | | | |
| **MKNK1** MNK1 | Ubiquitious [71] | Cytoplasmic [72] | No | Undefined | **p38**: T250/255 [73, 74] | **eIF4E**: S209 [74] |
| **MKNK2** MNK2 MNK2a | Ubiquitious [71] | Cytoplasmic [75] | No | Undefined | **ERK/ p38MAPK α/β**: [74] | **eIF4E**: S209 [76] |
| *MLCK branch* | | | | | | |
| **Obscurin-MLCK** Obscurin-B | Striated skeletal muscle | | Yes (IQ) | Putatively | Undefined | Undefined |
| **Obscurin single-MLCK** Obscurin-associated kinase | Striated cardiac muscle [77] | Sarcolemma (extracellular) [77], myonuclei [78] | No | Yes [77] | Undefined | Undefined |
| **Obscurin tandem-MLCK** Obscurin-associated kinase | Striated cardiac muscle [77] | Sarcolemma (intracellular) [77], myonuclei [78] | Putatively [79] | Yes: S6789/ S6790 [77, 80] | Undefined | *N*-Cadherin: [77] |

## 1.2. The Ca2+/Calmodulin-dependent protein kinase kinase 2

Since its discovery in the mid 1990's, a growing body of literature has implicated the $Ca^{2+}$/Calmodulin-dependent protein kinase kinase 2 (CaMKK2) in a wide variety of biological processes, including whole-body energy homeostasis, memory formation and inflammation [20, 25]. These pleiotropic effects likely reflect CaMKK2's enduring phylogenetic history, being one of the most ancient kinases represented in the Manning kinome tree [1]. Unsurprisingly, dysregulation of CaMKK2 correlates with an appreciating number of disease phenotypes, including neuropsychiatric disorders, prostate and ovarian cancer, and non-NF2 meningioma [81]. However, many elements of CaMKK2's biochemistry remain incomplete and unresolved. The linearised domain structure of CaMKK2 consists of a central catalytic domain buttressed by variable N- and C-termini harbouring a regulatory phosphorylatable cluster and overlapping autoinhibitory and calmodulin-binding domain (AID/CBD), respectively [20, 82] (Figure 1.3). Alternative splicing yields 7 transcripts of variable function and domain organisation, including CaMKK2.7 which harbours a putative nuclear localisation sequence at its C-terminus [83].

Unlike the closely related CaM-kinase, CaMKK1, and its downstream effectors, CaMK1 and CaMK4, CaMKK2 exhibits $Ca^{2+}$/Calmodulin-independent activity [82]. CaMKK2 is regulated by several extrinsic kinases at its N- and C-termini. Sequential phosphorylation of the N-terminal regulatory region by CDK5 (Ser137) and GSK3 (Ser133, Ser129) impairs autonomous activity [22]. Additionally, cAMP-dependent protein kinase A (PKA)-mediated *trans*-phosphorylation of Ser100, Ser495 and Ser511 attenuates CaM binding and primes CaMKK2 for recruitment by 14-3-3 adaptor proteins [23, 84]. The transient CaMKK2:14-3-3 oligomer is stabilised primarily by kinase domain contacts and phosphopeptide interactions (p-Ser100, p-Ser511) which anchor the 14-3-3 dimer and sterically hinder Ser495 dephosphorylation [23, 85]. Following dissociation of the CaMKK2:14-3-3 complex, CaMKK2 is rapidly

dephosphorylated at Ser495, enabling recruitment of $Ca^{2+}$/Calmodulin to the C-terminal CBD. In most instances, calmodulin docks its cognate CBD through recognition of interspaced aliphatic side chains. These bulky, often aromatic residues serve to anchor the globular termini of calmodulin and sequester the CBD inside the $Ca^{2+}$/Calmodulin molecule. Several CaM:CaMK crystal structures have been solved using synthetic peptides derived from the respective CaMK-CBD, including rabbit skMLCK, chicken smMLCK, rat CaMK2α and rat CaMKK1 [14, 86-88]. In skMLCK, smMLCK and CaMK2α, the helical CBD adopts a distinct polarity, with the N- and C-termini associating with the C- and N-lobes of calmodulin, respectively. In CaMKK1, the electrostatic properties of the CBD result in a reversed binding orientation, whereby the highly basic C-terminus of the CBD peptide associates with the acidic channel outlet created by the C-lobe of calmodulin. This N-N/C-C orientation is unique to CaMKK1 and likely CaMKK2, albeit whose CBD structure remains unresolved [14]. How CaMKK2 remains autoinhibited in the absence of $Ca^{2+}$/Calmodulin is less clearly defined. In CaMK4, the overlapping AID/CBD sits across the face of the kinase domain, sterically occluding the substrate binding cleft and ATP binding pocket (Muniz et al. 2009). This traditional pseudosubstrate mechanism is less distinct in CaMK1, whose AID/CBD, in addition to forming electrostatic interactions at the αD-helix, folds back onto the N-lobe and distorts the catalytic architecture in the absence of $Ca^{2+}$/Calmodulin [89]. Recent efforts to illuminate the underlying mechanism of CaMKK2 autoinhibition have revealed new insights into CaMKK2's biochemistry. Hydrogen deuterium exchange (HDX) experiments involving kinase dead CaMKK2 demonstrate increased deprotection of the β4-β5 strands, αC-helix and Arg-Pro (RP)-rich insert upon $Ca^{2+}$/Calmodulin addition [90]. Kylarova et al. posit that this resultant increase is likely due to liberation of this region from the autoinhibitory domain. The RP insert (henceforth, RP loop) is critical for substrate recognition of the downstream CaMKK effectors, CaMK1 and CaMK4, which bind CaMKK2 in a $Ca^{2+}$/Calmodulin-dependent manner [91].

Indeed, the RP loop appears to be the primary mechanism by which CaMKK2 phosphorylates its downstream targets, as insertion of the RP loop between subdomains II and III of the AMPK activator liver kinase B1 (LKB1) imparts affinity for the CaMKK substrates, CaMK1 and CaMK4 [92]. Interestingly, in AlphaFold2 docking simulations between an RP-peptide (QAGFPRRPPPRGTRPAPGGCIQP) and the kinase domains of CaMK1 and CaMK4, the RP loop sits inside the substrate binding cleft, adjacent to the αD-helix (Figure 1.4). The αD-helix is important for substrate recognition of a multitude of kinases [93]. Strikingly, a conserved hydrophobic pocket formed by Phe104, Ile107, Val108, Tyr184 and Ile210 (CaMK1) anchors the RP loop aromatic Phe207 in both CaMK1 and CaMK4. Interestingly, this pocket is sterically obstructed in the autoinhibited CaMK1 crystal structure by Phe298 of the autoinhibitory/calmodulin-binding domain (Figure 1.4) [89]. Insertion of the CaMKK2 RP loop at the αD-helix/substrate cleft of CaMK would theoretically bring the CaMKK2 catalytic site and β4-αE loop near the activation loop residues of CaMK1 (T177) and CaMK4 (T200) (Figure 1.4), allowing phosphoryl transfer to occur. Future studies should interrogate the function of the RP loop-Phe207 residue by point mutation analysis end evaluate allosteric inhibition of the RP loop pocket by small molecules. Sterically occluding CaMKK2 from CaMK1 and CaMK4 may prove beneficial in disorders where CaMKK2 is overexpressed but where CaMK1/4 activity must remain low.
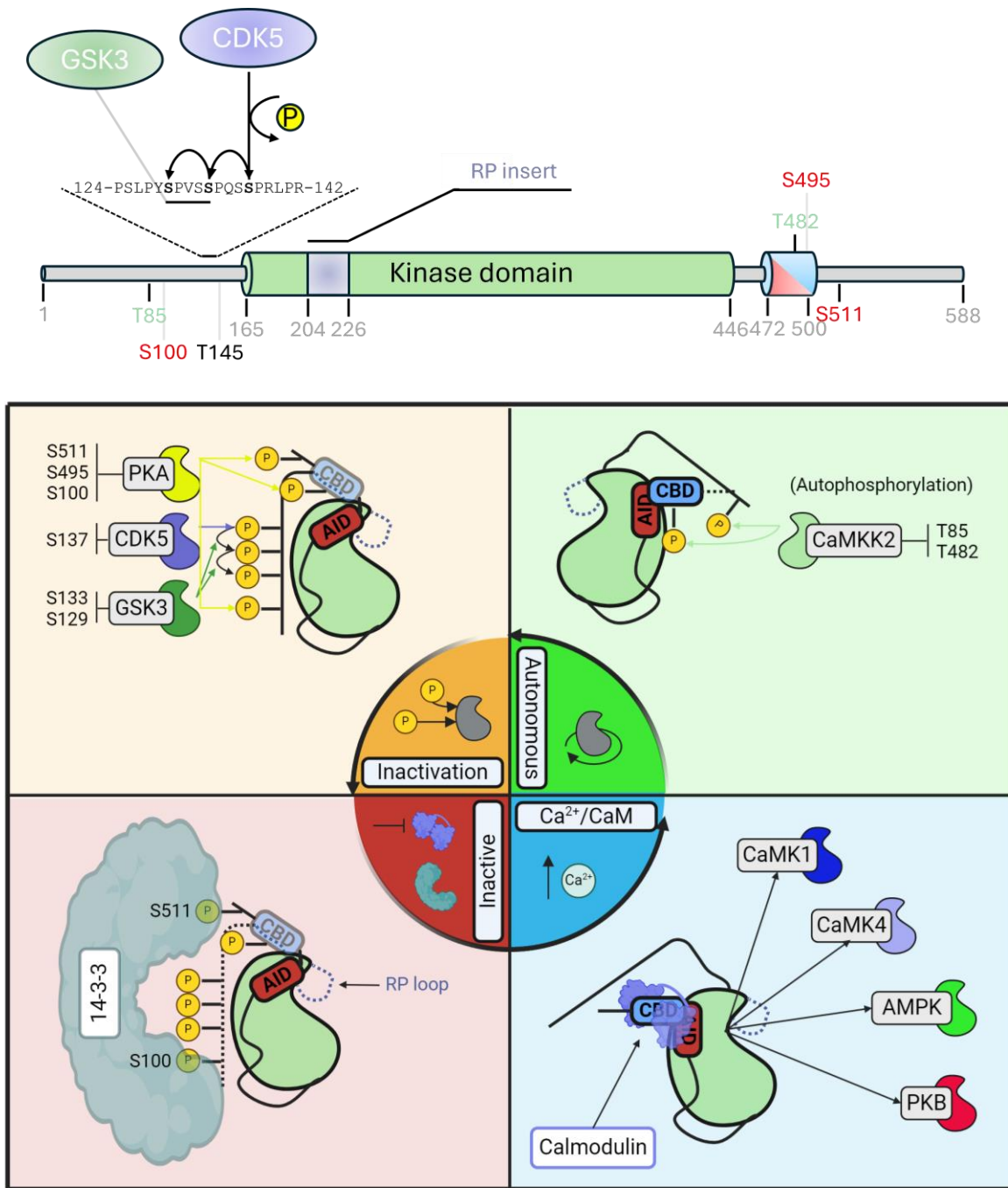
***Figure 1.3. Biochemical characterisation of CaMKK2.*** *Domain structure.* The linear domain structure of CaMKK2 consists of a central kinase domain flanked by variable N and C-termini harbouring an N-terminal regulatory region and C-terminal overlapping autoinhibitory and calmodulin-binding domain (AID/CBD), respectively [20, 82] Autophosphorylation sites are coloured green. PKA phosphorylation sites are coloured red Numbering is according to the human CaMKK2 UNIPROT designation (accession no. Q96RR4). *Regulation.* Unlike the closely related CaM-kinase CaMKK1, CaMKK2 exhibits significant $Ca^{2+}$/Calmodulin-independent activity [20]. Sequential phosphorylation of the N-terminal regulatory region by Pro-kinases and GSK3 suppresses autonomous activity [22]. Additionally, *trans*-phosphorylation of S100, S495 and S511 by PKA impairs $Ca^{2+}$/Calmodulin-activation (S495) and primes CaMKK2 for 14-3-3 recruitment (S100, S511) [23, 84]. The CaMKK2:14-3-3 transient oligomer is stabilised by kinase domain contacts and phosphopeptide interactions,

sterically hindering S495 dephosphorylation [23, 85]. Upon dissociation, CaMKK2 is dephosphorylated at S495, permitting $Ca^{2+}$/Calmodulin recruitment to the C-terminal CBD. Subsequent liberation of the RP loop by $Ca^{2+}$/Calmodulin enhances CaMKK2 affinity for its downstream effectors, CaMK1, CaMK4 and AMPKα [91, 92]. Autophosphorylation of T85 imparts autonomous activity via retention of the activating $Ca^{2+}$/Calmodulin signal [21]. Created with BioRender.com.
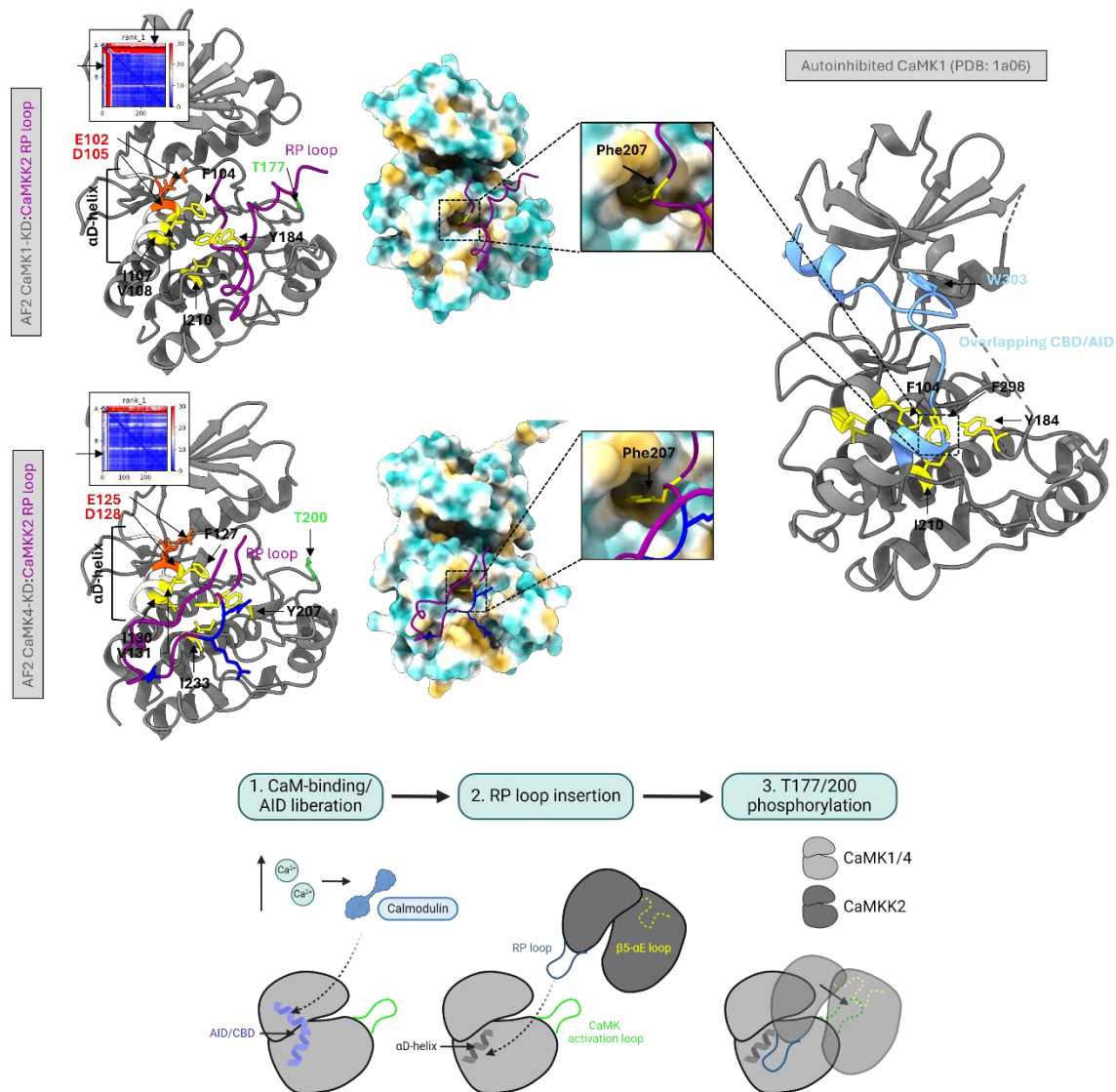


***Figure 1.4. CaMKK2 may mediate T-loop phosphorylation of CaMK1 and CaMK4 via insertion of the RP loop into a hydrophobic interface at the αD-helix.*** In all docking simulations (AlphaFold2) between an RP-peptide (QAGFPRRPPPRGTRPAPGGCIQP; purple) and the kinase domains of CaMK1 and CaMK4, the RP loop inserts into the substrate binding interface formed by the αD-helix (light grey) of the CaMK1 and CaMK4 kinase domains. Strikingly, a conserved hydrophobic pocket (yellow residues) anchors the RP loop Phe207. This pocket is sterically obstructed in the autoinhibited CaMK1 crystal structure (PDB ID: 1a06) by Phe298 of the autoinhibitory domain (cornflower blue) [89]. Insertion of the RP loop at the αD-helix would theoretically bring the catalytic site of CaMKK2 in close proximity

to the activation loop (green) residues of CaMK1 (T177) and CaMK4 (T200), allowing phosphoryl-transfer to occur. AlphaFold2 docking simulations were run via the ColabFold v1.5.5 Google notebook [94] using the MMseqs2 multiple sequence alignment protocol, with 6 recycles. Predicted aligned error (PAE) plots are shown as inserts overlaying the CaMK1/4 ribbon structures.

**Table 1.2. Associated disorders of the Dark CaMK kinome**

| Dark Kinase | Disorder | Expression | Phenotype | Mutation | Ref |
|---|---|---|---|---|---|
| CaMKK2 | Anxiety and bipolar | | ↓ activity | T85S | [21, 95] |
| | Bipolar | | ↓ activity ↓ T85 autophosphorylation | R311C | [96, 97] |
| | Colorectal adenocarcinoma | | | R91W | [98] |
| | Hepatocellular carcinoma | ↑ | | | [99] |
| | High-grade serous ovarian cancer | ↑ | Hyperactivation of PKB/Akt | | [28] |
| | Non-NF2 meningioma | | ↓ activity ↓ T85 autophosphorylation | G87R | [100, 101] |
| | Prostate cancer | ↑ | ↑ cell proliferation, migration | | [102-104] |
| CaMK1γ | Thyroid carcinoma, HNSCC, ESCA, LIHC and CHOL | | | | [8] |
| CaMK1σ | Acute myeloid leukaemia | ↑ | Poorer survival outcomes for AML patients | | [105] |
| | Breast cancer | ↑ | ↑ cell proliferation Epithelial-mesenchymal transition | | [106] |
| | Glioma | ↓ | ↑ cell growth, invasion ↑ PI3K/AKT/mTOR activity | | [107] |
| DCLK3 | Bipolar | | | | [108] |
| | Colorectal cancer | ↑ | | | [109] |
| | Huntington's disease | ↓ | | | [7, 110] |
| PSKH1 | Chron's Disease Ulcerative colitis | ↑ | | | [111] |
| | Colorectal cancer | ↑ | ↑ cell proliferation, metastasis | | [112] |
| | Osteosarcoma | | ↑ cell proliferation, metastasis | | [113] |

| | | | | | |
|---|---|---|---|---|---|
| | Prostate cancer | ↑ | ↑ cell proliferation, migration | | [6] |
| BRSK1 | Breast cancer | ↓ | ↑ cell proliferation (tumour suppressor) | | [114] |
| BRSK2 | ASD | | Speech delay, ADD/ADHD, auditory hallucinations, limb tremors | L148Cfs*39 G212E Q244* S466Qfs*83 E511Vfs*38 R612C | [115] [116] |
| | DD/ID | | Speech and motor delays | R65CQ | [116] |
| | Pancreatic ductual adenocarcinoma | ↑ | | | [50] |
| NuaK2 | Anencephaly | | Catastrophic brain deformities, foetal death | Y138_Q145delinsE | [117] |
| | Bladder cancer | ↑ | | | [54] |
| | Hepatocellular carcinoma | ↑ | | | [118] |
| | Melanoma | ↑ | | | [119, 120] |
| | Prostate cancer | ↑ | | | [121] |
| NIM1 | KIRC | | | | [8] |
| TSSK | Colorectal cancer (TSSK6) | ↑ | Reduced relapse-free survival | | [122] |
| MKNK1 | Melanoma | ↑ | | | [123] |
| MKNK2 | Breast cancer | | Increased MKNK2 activity correlates with HER2 overexpression | | [124] |
| Obscurin | Hypertrophic cardiomyopathy | | Impaired interaction of obscurin with titin at Z-disc of sarcomeres Ventricular cardiac arrythmia | Arg4344Gln | [125, 126] |

## 1.3. The Ca$^{2+}$/Calmodulin-dependent protein kinase 1

The Ca$^{2+}$/calmodulin-dependent protein kinase 1 (CaMK1) is highly implicated in neuronal processes, where it regulates synapse formation, axonal outgrowth and growth cone formation [127]. Importantly, it is a major effector of the CaM-kinase kinases CaMKK1 and CaMKK2, previously described. Upon binding Ca$^{2+}$/CaM, CaMKK phosphorylates Thr177 of the activation loop of CaMK1 [17, 128]. In the absence of CaM-binding, the C-terminal CBD sterically occludes the substrate binding cleft and distorts the small lobe of the kinase domain of CaMK1, preventing CaMKK-orchestrated activation [89]. Initially identified in rat brain homogenate, subsequent studies utilising synthetic peptides derived from its *in vitro* substrate synapsin 1 resulted in the purification of several species from murine and bovine brain extracts, representing the α and β isoforms [32, 129, 130]. An additional two isoforms, CaMK1γ and CaMK1σ, were later characterised by homology probing of embryonic rat brain and granulocyte cDNA [35, 131]. Like CaMK1α, the β, γ and σ isoforms harbour a central, catalytic core and C-terminal calmodulin-binding domain with variable C-termini (Figure 1.5) [132].
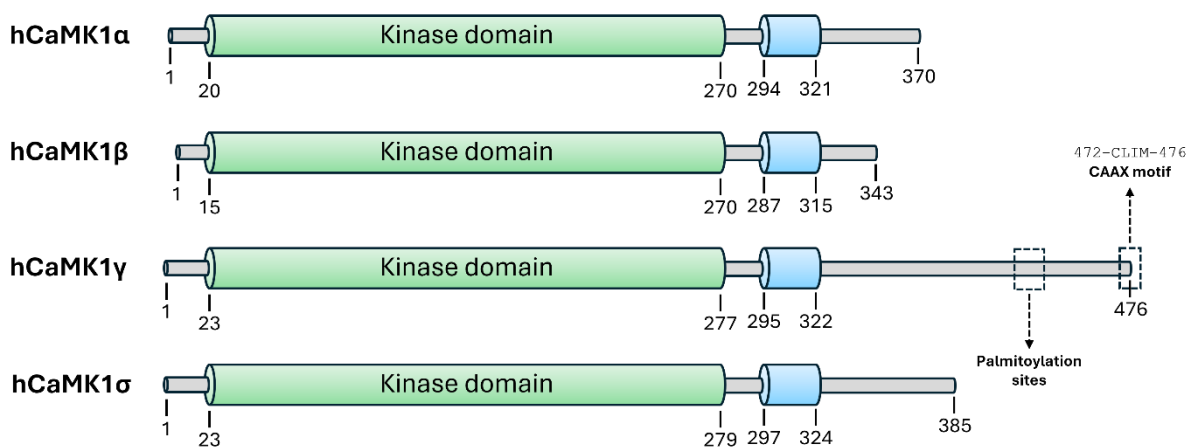


*Figure 1.5. Domain structure of the CaMK1 isoforms.* The CaMK1 isoforms are characterised by a central kinase domain and C-terminal CBD (blue) with variable C-termini [131, 132]. CaMK1γ is delineated by a C-terminal extension harbouring various palmitoylation and prenylation sites [33].

### 1.3.1. CaMK1γ

Little is currently understood of CaMK1γ due to the predominant and ubiquitous expression of the primary CaMK1 isoform, CaMK1α [131-133]. Unlike CaMK1α and CaMK1β, CaMK1γ expression is highly restricted to neural tissue of the amygdala and ventromedial hypothalamus [33]. CaMK1γ is uniquely characterised by an extended C-terminus capped by a CAAX motif (AA = aliphatic amino acid) that, when prenylated, promotes CaMK1γ's translocation to internal membranes (Figure 1.5) [33]. Following prenylation, CaMK1γ is palmitoylated at a C-terminal cysteine cluster which promotes CaMK1γ association with lipid microdomains of dendritic structures [134]. Interestingly, dual lipidation of CaMK1γ was demonstrated to promote its self-association in co-immunoprecipitation experiments [134]. These characteristics distinguish CaMK1γ from the α, β and σ CaMK1 isoforms.

### 1.3.2. CaMK1σ

CaMK1σ (CKLiK, henceforth CaMK1σ) exhibits strong similarity to the CaMK1α isoform in its primary structure, albeit with a marginal C-terminal extension (Figure 1.5). The function of these additional residues has not yet been characterised. Like CaMK1α, CaMK1σ is phosphorylated on its activation loop by CaMKK1 and CaMKK2 [34]. Interestingly, the CaMKK2.3 splice variant appears to be the primary kinase by which CaMK1σ T-loop phosphorylation is regulated and was concurrently discovered with CaMK1σ in a homology probe of a HeLa cDNA library [34]. Peculiarly, whilst CaMK1σ harbours an overlapping AID/CBD in its C-terminus, CaMK1σ exhibits substantial kinase activity even in resting cells [34]. The CaMK1σ isoform was also identified in granulocytes, namely eosinophils and neutrophils, where it regulates granulocyte function by mediating chemokine inputs [35].

*Therapeutic potential*

Corroborating CaMK1σ's expression in white blood cells, CaMK1σ was recently shown to provoke tumour immune resistance to cytotoxic T cell therapy (CTL) [135]. It was

hypothesised that increased CaMK1σ activity resulting from CTL-induced Fas-receptor signalling downregulated the action of effector caspases, inhibiting CTL-mediated apoptosis and tumour cell death [135]. CaMK1σ has also been recently implicated in aggressive malignancies of the brain (glioma) and breast [106, 107]. In breast cancer, CaMK1σ overexpression aggravates cell proliferation and promotes epithelial-mesenchymal transition [106]. Notably, in contrast, CaMK1σ downregulation enhances the proliferation and invasion of glioma *in vitro* and *in vivo* [107]. Analysis of differentially expressed genes in CaMK1σ-driven glioma cohorts revealed that CaMK1σ expression negatively correlates with PI3K/AKT/mTOR activity [107]. Rescue of CaMK1σ activity in U251 glioblastoma cells by transient transfection inhibited PI3K/AKT/mTOR activation and cell proliferation [107]. Thus, the mechanisms by which CaMK1σ is therapeutically targeted will invariably be highly context dependent and may prove challenging due to CaMK1σ's ubiquitous expression and diverse functions within the body.

## 1.4. Doublecortin-like kinase 3

Doublecortin-like kinase 3 (DCLK3) is closely related to CaMK1 and CaMK4, sharing <45% sequence identity within the kinase catalytic core [36]. Its' domain structure is characterised by a C-terminal catalytic domain buttressed by variable termini of unknown function. Further, DCLK3 lacks the tandem doublecortin domains (DC) present in DCLK1 and DCLK2 necessary for microtubule association [136]. Indeed, DCLK3's subcellular distribution is largely diffuse, with no apparent localisation to microtubule structures [36]. Unlike CaMK1 or CaMK4, DCLK3 has no discernible calmodulin-binding domain and is not regulated by calmodulin *in vitro*.

*Therapeutic potential*

DCLK3 is increasingly correlated with disorders of the brain, including bipolar (BD) and Huntington's disease [7, 108, 110]. Congruent with these observations, DCLK3 expression is largely restricted to adult brain, specifically neurons of striatal [7, 137] and hippocampal [36] origin. Further, recent findings by Liu, Ter Huurne [109] indicate DCLK3 may function to promote cell survival, as enhanced DCLK3 expression in colorectal cancer (CRC) positively correlates with disease progression. In contrast, DCLK3 is frequently downregulated in both murine and patient-derived brain samples presenting with Huntington's disease [110, 137], suggesting a neuroprotective function for DCLK3. Interestingly, active kinase domain of DCLK3, but not catalytically impaired mutants, protects wild-type mice from striatal lesions in mouse models co-transfected with mutant Huntington (mHtt) [7]. These data suggest that DCLK3's primary function is one of cell survival, protecting neurons and/or enhancing CRC progression. In a recent, genome-wide association study (GWAS) of more than 40,000 patients with bipolar disorder, DCLK3 expression robustly correlated with BD (top-15 candidate) and was noted for its inherent druggability [108].

Similarly, CaMKK2 has recently emerged as an attractive treatment target for bipolar disorder [138]. Interestingly, DCLK3 was initially discovered via homology probing using degenerate oligonucleotide primers targeting conserved catalytic motifs in the CaMKK2 effectors, CaMK1 and CaMK4 [36]. Further, proteomic analysis and network mapping of the CMGC kinase group indicate DCLK3 closely associates with CDK5 and GSK3, known regulators of CaMKK2 activity [22, 37]. DCLK3 also appears to be under activation loop regulation, as co-expression of an activation loop point mutant (murine T286A) with mHtt fails to ameliorate the Huntington phenotype in striatal neurons *in vitro* [7]. Collectively these data strongly implicate CaMKK2 as a potential, upstream activating kinase of DCLK3, of which no known regulators have to date been described. Analysis of DCLK3's primary structure reveals conservation of consensus residues surrounding the activation loop phosphorylation site and residues previously detailed to likely be important for RP-loop recognition (Figure). Importantly, activation of both CaMKK2 and DCLK3 ameliorates the effects of neurological disorders such as bipolar and Huntington's disease, respectively [7, 138]. Future research should interrogate the relationship, if any, between CaMKK2 and DCLK3.
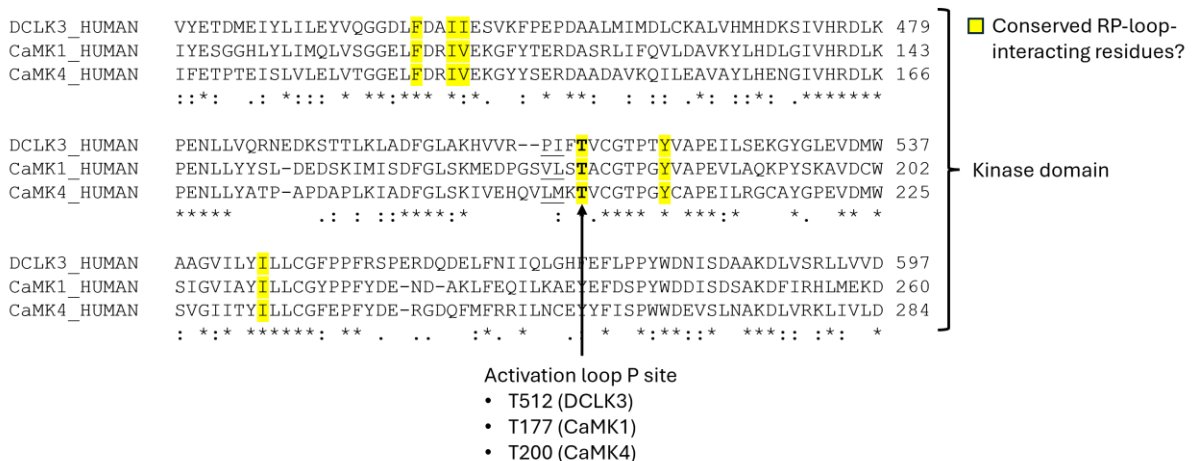


*Figure 1.6. Conservation of consensus residues in the kinase domains of CaMK1, CaMK4 and DCLK3 strongly implicate DCLK3 as a potential substrate of CaMKK2.* UNIPROT sequence alignment of the CaM-kinases CaMK1, CaMK4 and DCLK3 reveals conservation of

consensus residues that surround the activation loop phosphorylation site (underlined) and hydrophobic residues (yellow) that may participate in RP-loop recognition of CaMKK2.

## 1.5. Serine/threonine-protein kinase H1

Since its discovery by Hanks [139] in the late 1980's, a small but growing body of literature has implicated PSKH1 in a variety of cellular programs, including pre-mRNA splicing [140], anterograde vesicle trafficking [141] and cell migration [113]. However, a precise function for this elusive enzyme has to date not been defined. Furthermore, no substrates or upstream, extrinsic kinases of PSKH1 have been described. PSKH1 is the catalytically competent compliment to the pseudokinase, PSKH2. Both enzymes are believed to have arisen through a gene duplication event [142]. PSKH1 is ubiquitously expressed, although exhibits strongest expression in the testis [38]. The linearised domain structure of PSKH1, first characterised by Brede, Solheim [38], consists of a central catalytic domain flanked by highly basic N- and C-termini (Figure 1.7). Additional regulatory motifs identified include various membrane targeting motifs, including N-terminal acylation sites (N-myristoylated glycine 2, S-palmitoylated cysteine 3) and a putative post-Golgi membrane surface directing signal, an SH3-domain binding PxxP motif, a nuclear localisation signal, and a C-terminal calmodulin-binding domain (CBD), although the functional significance of these motifs has not been investigated. Unlike the closely related CaM-kinase, CaMK1, previously described, the putative C-terminal CBD of PSKH1 exhibits poor sequence conservation but is generally amphipathic. Overlapping with and extending from this region is a sequence empirically determined to exhibit intermolecular autophosphorylation of a serine cluster [38]. Although structural information on PSKH1 is severely lacking, yeast two-hybrid and gel filtration experiments have demonstrated that PSKH1 forms at minimum homodimers, with oligomerisation chiefly facilitated by kinase domain contacts [38].
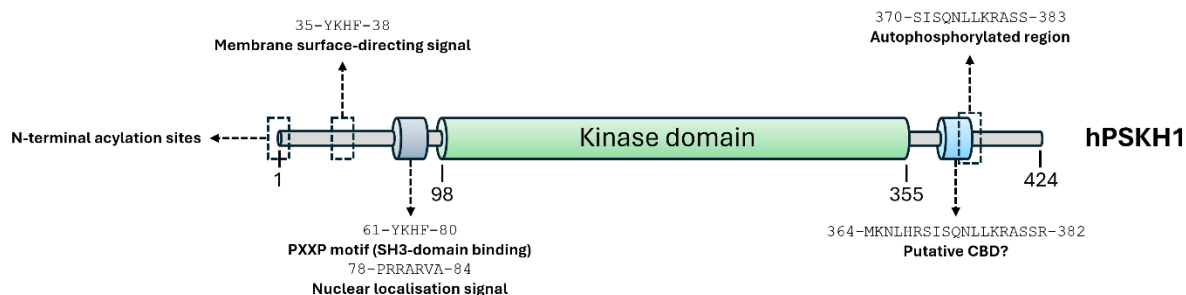
*Figure 1.7. Domain structure of PSKH1.* Linearised domain structure of the human PSKH1 polypeptide. The kinase is characterised by a central catalytic domain (98-355; UNIPROT accession #P11801) flanked by highly basic N- and C-termini. Putative motifs include N-terminal acylation sites, a post-Golgi membrane surface directing signal (35-38), an SH3-domain binding PXXP motif (61-80), a nuclear localisation signal (78-84) and a C-terminal calmodulin-binding domain (CBD), which shares poor sequence conservation with other kinases in the CaMK subfamily [38]. A region which overlaps with the C-terminal CBD (370-383) has been demonstrated to exhibit intermolecular autophosphorylation of serine residues [38].

*Therapeutic potential*

PSKH1 is a top 6 driver of prostate cancer progression [6]. Congruent with a role in neoplastic disease, PSKH1 was recently identified as a top-performing biomarker for cetuximab efficacy in metastatic colorectal cancer (mCRC) treatment regimens [143]. Further, PSKH1 has also been shown to promote the proliferation, migration and invasion of osteosarcoma cells *in vitro* and *in vivo* [113]. These studies strongly implicate a role for PSKH1 in cell proliferation and migration pathways. However, a precise function for this enzyme has, to date, not been assigned. PSKH1 ablation has proven efficacious in attenuating the growth of a battery of prostate cancer cell lines *in vitro*, including the androgen-sensitive and insensitive cell lines LNCaP and C4-2B, respectively [6]. Promisingly, these effects seem largely restricted to prostate cancer, as transient siRNA inhibition of PSKH1 in non-neoplastic cell lines has minimal effect on cell growth [6]. As no known function or downstream substrates for PSKH1 have to date been characterised, the potential pleiotropic effects of PSKH1 inhibition are not currently understood. These precise questions will remain the focus of this thesis and will be explored in later chapters.

## 1.6. Brain-specific serine/threonine-protein kinase 1/2

The brain-specific serine/threonine-protein kinases (BRSK) were first described in *C. elegans* in the early 2000's during genetic screening for novel regulators of presynaptic vesicle clustering in chemosensory neurons [144]. Human orthologues of *C. elegans* BRSK (SAD-1) were later characterised by Inoue, Mochida [39], revealing two kinases of 85- (SAD-B, henceforth BRSK1) and 82kDa (SAD-A, henceforth BRSK2), respectively. As their namesake suggests, BRSK1 and BRSK2 are almost exclusively expressed in the brain, particularly to the synaptic-rich and axonal regions of cortical neurons [39, 41, 49, 144]. BRSK is also present in the testis and pancreas [41, 145]. In both peripheral and neural tissues, BRSK coordinates the polarisation of acinar and neuronal cells. Polarisation, specifically of neuronal cells, is critical to directing the flow of electrical information from dendrites to the presynaptic terminal, where subsequent neurotransmitter release into the synaptic junction facilitates signal relay to adjacent cells. Reflecting this important function, BRSK1/2 double knock-out (DKO) mice present with debilitating neural phenotypes, die within two hours of birth, and exhibit defective polarisation of hippocampal neurons [49]. Further, inactivation of BRSK1/2 in murine pancreas results in polarity defects in pancreatic acinar cells [145]. Luminary work by Lizcano, Goransson [41] revealed that, like 11 closely-related kinases in the AMPK-related sub-branch, BRSK1/2 are under direct regulation by the tumour suppressor, liver kinase B1 (LKB1) [41]. LKB1 phosphorylates conserved threonine residues in the activation segment of BRSK1 and BRSK2 (Thr189 and Thr174, respectively), increasing the catalytic activity of these kinases by more than 50-fold [41]. Activation of BRSK1/2 by LKB1 is dependent on the concerted actions of two distinct, regulatory proteins: the pseudokinase STRAD and the scaffolding protein MO25, which allosterically activate LKB1 upon assembly of the LKB1:STRAD:MO25 heterotrimeric complex [146-148]. Further, whilst LKB1 has historically been viewed as a constitutively active enzyme *in vitro* and *in vivo*, various studies support the phosphorylation

of a C-terminal serine residue (Ser431) in regulating the action of LKB1 in cells. Ser431 is phosphorylated by the cAMP-dependent- and p90 ribosomal s6 kinases (PKA and p90[rsk], respectively) [149, 150]. In malignant G361 melanoma cells which do not natively express LKB1, reintroduction of a Ser431Ala LKB1 point mutant fails to attenuate cell growth relative to wild-type LKB1 controls [150]. Further, pSer431-LKB1 is enriched in axons of polarised neurons, mirroring the localisation of its downstream effectors, BRSK1/2 [151]. Lastly, co-expression of a Ser431-LKB1 point mutant (S431A) with STRAD in cortical neurons is comparatively poor at promoting formation of supernumerary axons in cortical neurons [151]. These studies strongly implicate LKB1-Ser431 phosphorylation as requisite in BRSK1/2 regulation. Peculiarly, Ser431 phosphorylation is seemingly dispensable for LKB1 activity toward its downstream effectors [152]. Further, forskolin treatment of CCL-13 cells co-expressing LKB1 and BRSK did not enhance BRSK activity in peptide-based kinase assays [45]. Thus, phosphorylation of Ser431 likely serves non-catalytic functions, such as promoting LKB1 association with BRSK1/2. Irrespectively, LKB1 appears to be the primary kinase by which BRSK1/2 activity is regulated. Interestingly, CaMKK has also been reported to phosphorylate the activation loop of BRSK1/2 [42]. BRSK1 was identified as an interacting partner of CaMKK1 in rat brain extract using the CaMKK1-kinase domain (KD) as bait. CaMKK1 robustly phosphorylated the activation loop Thr189 residue of BRSK1, increasing its catalytic activity to comparable levels as LKB1 [42]. In contrast, CaMKK2 was less efficient in phosphorylating and activating BRSK1 [42]. Contradicting these reports, Bright, Carling [45] failed to demonstrate CaMKK2-mediated activation of BRSK1/2 transiently expressed in CCL-13 cells. Whilst co-expression of CaMKK2 and AMPK robustly enhanced AMPK activity, BRSK1/2 were comparatively kinase dead [45]. In summary, these data paint a perplexing and unresolved picture of BRSK regulation. LKB1 clearly activates both BRSK1 and BRSK2 [41, 45]. Further, PKA/p90[rsk] phosphorylate Ser431 of LKB1, enhancing

polarisation of cortical neurons (and thus mirroring the action of its downstream effectors, BRSK1/2 )[151]. In contrast, PKA stimulation by forskolin treatment does not enhance BRSK kinase activity when co-expressed with LKB1 in CCL-13 cells [45]. Further muddying these reports, whilst CaMKK1 phosphorylates and activates BRSK in cell-free assays, PKA attenuates CaMKK activity by phosphorylating and promoting recruitment of 14-3-3 adaptor proteins [42, 153]. This dual requirement for discordant upstream activating kinases with conflicting regulatory requirements could conceivably exist in a system where LKB1 and CaMKK are spatiotemporally segregated *in vivo*. For example, PKA's broad substrate specificity is tempered by A-kinase anchoring proteins (AKAPs) that appropriately distribute PKA holoenzymes to specific cellular addresses. Thus, whilst PKA may enhance LKB1 association and activation of BRSK1/2, this does not preclude CaMKK activation of BRSK1/2 *in vivo*. Further, although CaMKK has been shown to phosphorylate and activate BRSK in cell-free assays, co-expression of CaMKK2 in CCL-13 cells did not measurably activate BRSK *in vitro* [42, 45]. How can these incongruencies be reconciled? In experiments where CaMKK1 robustly phosphorylated and activated BRSK1 *in vitro*, only the N-terminus and kinase domain of CaMKK1 was utilised [42]. In contrast, where CaMKK co-expression failed to enhance BRSK1/2 activity *in vitro*, full-length enzyme was employed. Thus, it is possible that additional regulatory inputs in the C-terminus of CaMKK are needed (post-translational modifications or adaptor proteins) to facilitate CaMKK interaction with BRSK1/2.

In addition to conserved activation loop residues that are critical for BRSK1/2 activity *in vitro*, both enzymes harbour ubiquitin (Ub)-associated (UBA) domains immediately C-terminal to the catalytic core (Figure 1.8) [154]. Interestingly, these UBA domains do not bind ubiquitin but rather modulate the catalytic activity of AMPK-related kinases (in which they are exclusively represented) [155]. In contrast to BRSK1, whose catalytic activity is entirely dependent on a functional UBA domain, BRSK2 harbours UBA-independent activity [45]. As

such, UBA-regulation of BRSK1 may more resemble that of the closely related Par-1/MARK kinases, whose UBA domain stabilises the catalytic architecture of the kinase domain [155]. Conversely, the UBA domain of BRSK2 concomitant with an autoinhibitory sequence (AIS) N-terminal to the kinase association (KA1) domain of the C-terminal tail inhibits kinase activity through an intrasteric mechanism (Figure 1.8) [156]. Whilst the UBA domains of BRSK1 and BRSK2 serve distinct regulatory functions, they collectively localise within one of two short conserved regions (SCR), first characterised by Crump, Zhen [144] (Figure 1.8). The SCR2 domain of BRSK1 has been shown to be important for localising BRSK1 to the synaptic region of cultured neurons [39]. Similarly, the SCR2 domain of BRSK2 may also serve a localising function, as fragments corresponding to the AIS/KA1 domain of BRSK2 bind phospholipids *in vitro* [156]. Lastly, in contrast to BRSK2 which demonstrates diffuse staining spanning the neuronal cell body, BRSK1 is highly membrane-associated [40]. Although BRSK1 lacks discernible membrane-targeting motifs in its primary structure, it was subsequently determined that BRSK1 is palmitoylated *in vivo*, which likely facilitates its interaction with lipid rafts at the presynaptic terminal [40]. Given that the SCR2 domain has been shown to be critical for BRSK1 localisation to synaptic vesicles, it is likely that this region harbors putative palmitoylation sites [39]. Corroborating this, CSS-Palm 2.0 analysis indicates that candidate palmitoylation sites cluster in this region [40]. Finally, lipid emulsions increase the catalytic activity of BRSK1 by 3.5-fold *in vitro*, whilst BRSK2 is unresponsive to lipid vesicle supplementation [40].
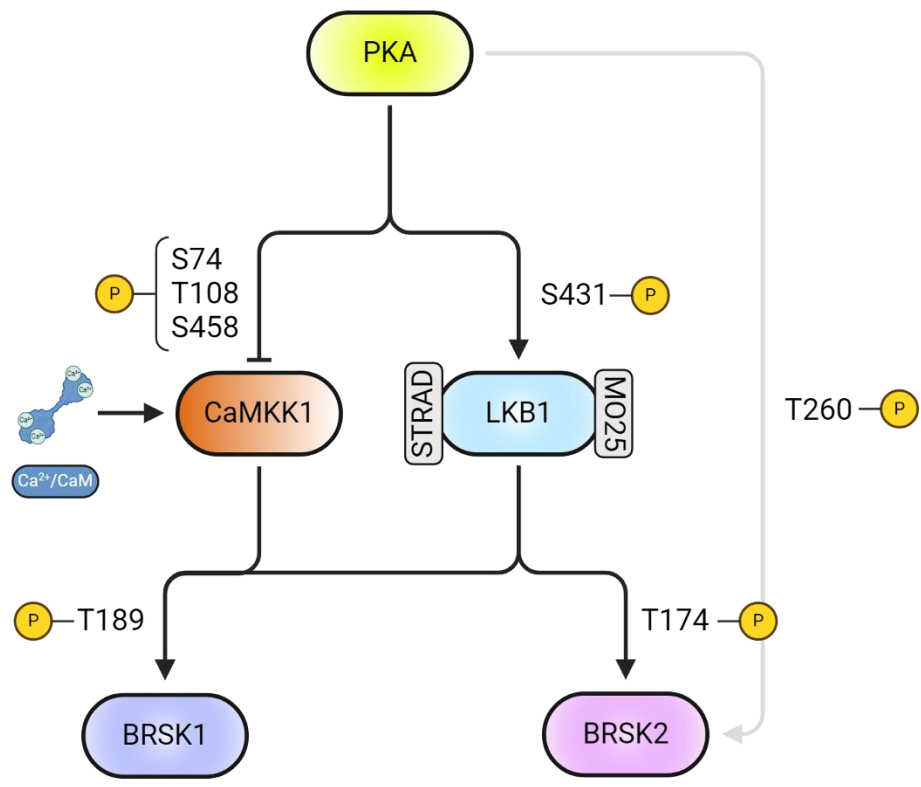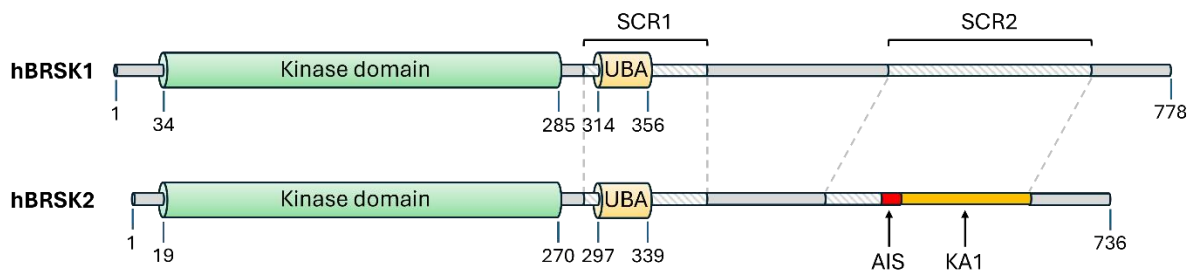
***Figure 1.8. Domain structure and regulation of BRSK1/2****. Domain structure*. The linearised domain structure of BRSK1/2 consists of an N-terminal catalytic domain followed by a lengthy C-terminal extension. The C-terminal tail contains two short conserved regions (SCR). SCR1 harbours a UBA domain, which is integral to the catalytic function of BRSK1, although comparatively dispensable for BRSK2 activity. In BRSK1, the SCR2 domain harbours putative palmitoylation sites and has been shown to be critical for BRSK1 localisation to synaptic vesicles. UNIPROT accession numbers: BRSK1: Q8TDC3; BRSK2: Q8IWQ3. *Regulation of BRSK1/2.* BRSK1/2 are phosphorylated on their activation loops by LKB1 (T189 and T174, respectively). CaMKK1 has also been demonstrated to phosphorylate T189 of BRSK1. PKA exerts differential effects on the upstream activating kinases CaMKK1 and LKB1. PK1 inhibits CaMKK catalytic activity by phosphorylating and promoting recruitment of 14-3-3 adaptor proteins. $Ca^{2+}$/Calmodulin is required for CaMKK1 catalytic activity. In contrast, PKA putatively enhances LKB1 association with BRSK1/2 by phosphorylating a C-terminal serine residue (S431). PKA has also been demonstrated to directly activate BRSK2 by phosphorylating T260. Created with BioRender.com.

*Therapeutic potential*

Mutations to BRSK2 are increasingly correlated with developmental delays and intellectual disabilities in young children (Table 1.2). BRSK2 expression is largely restricted to non-peripheral tissue. Further, BRSK2 is indispensable to the formation and polarisation of mature neurons. Recently, two independent studies reported the identification of various *de novo* mutations in BRSK2 in children presenting with significant neurological impairments, including speech and motor delays, moderate-severe autism spectrum disorder (ASD) and limb tremors [115, 116]. These mutations cluster within the kinase domain and regulatory regions of BRSK2 (Table 1.2). Whilst these mutations have not yet been functionally characterised, several are purported to alter the kinase activity of BRSK2. For example, in the autoinhibited SAD-A (murine BRSK2) crystal structure, the N-lobe R66 (hR65) residue participates in multiple electrostatic interactions with the UBA domain, including Q330 and E331 [156]. Q330 uniquely tethers both lobes of the kinase domain to the UBA [156]. Thus, impaired coordination of this residue in BRSK2-R66C mutants may weaken the mechanism by which BRSK2 activity is controlled. The R621C missense mutation is localised at the purported membrane-binding interface of the KA1 domain. R621 is constituent of a basic cluster that binds acidic phospholipids *in vitro*. Thus, R621C may impair BRSK2 targeting to internal membranes and alter its phospho-proteome *in vivo*. Lastly, the truncated Q244* variant (resultant from a premature stop codon inserted at c. 730C>T) is predicted to be loss of function and correlates with severe neurodevelopmental impairments.

Recent evidence also implicates BRSK2 in neoplasms of the breast and pancreas [50]. Unlike BRSK1, BRSK2 is strongly expressed in healthy, pancreatic tissue [145]. Further, BRSK2 is frequently overexpressed in patient-derived solid tumours and immortalised neoplastic cell lines (PANC-1) [50]. In pancreatic ductual adenocarcinoma (PDAC), cancer cells are thought to mediate their survival via hyperactivation of Akt/PKB. Activating

mutations to *KRAS* indirectly activate PKB via PI3K. However, *KRAS* inhibitors have recently been reported to be non-therapeutic for PDAC [157]. It was later demonstrated by Saiyin et al. (2017) that BRSK2 mediates survival of PDAC tumours by directly phosphorylating TSC-2, thereby inhibiting mTORC activation and subsequent inhibition of PKB (Figure 1.9) [50]. Additionally, co-occurring activating mutations to *KRAS* may further aggravate PKB activation in PDAC. Thus, BRSK2 is an increasingly attractive target for treatment of KRAS G12D/V-resistant PDAC tumours. However, no FDA-approved small molecule inhibitors are currently available.
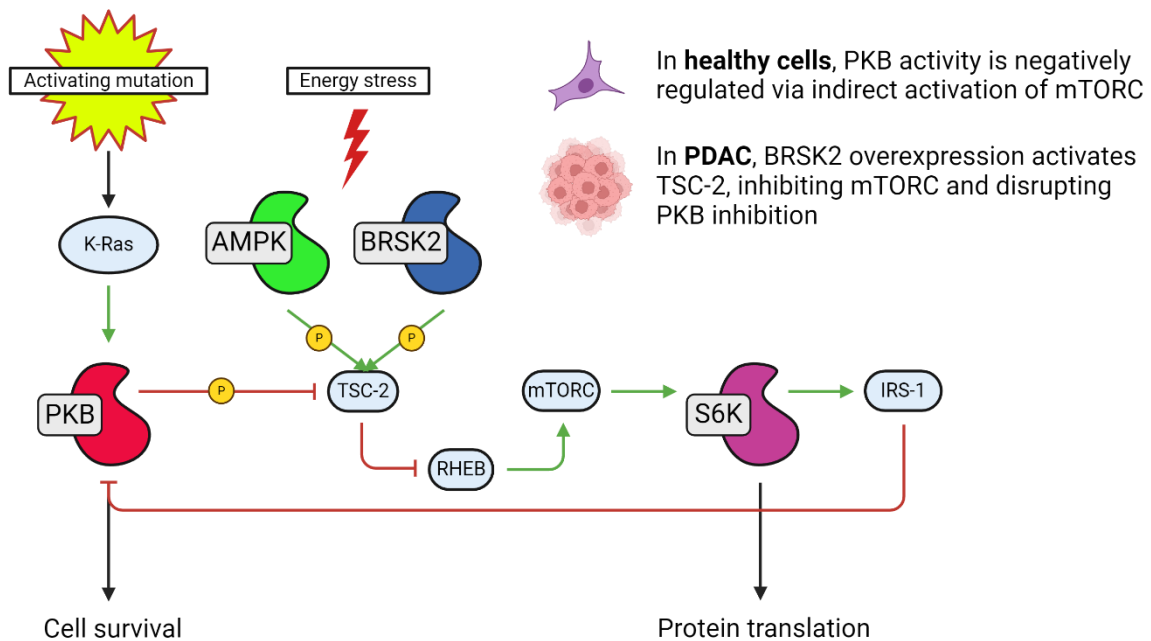


***Figure 1.9. BRSK2 promotes PDAC progression by indirectly inhibiting mTORC activity.*** In non-neoplastic cells, PKB activity is controlled via a negative feedback loop involving TSC-1/2, RHEB, mTORC, S6K and IRS-1. In PDAC, BRSK2 is overexpressed relative to healthy tissue. Further, the hypoxic and nutrient-poor microenvironment of the burgeoning tumour activates BRSK2. This results in hyperactivation of TSC-2 and inhibition of mTORC, altering the regulatory mechanism that keeps PKB activity in check. Concomitant activating mutations to *KRAS* may further enhance PKB activity and cell survival programs. Adapted from Saiyin, Na [50]. Created with BioRender.com.

## 1.7. NUAK family kinase 2

Dissimilar to the closely related AMPK-related kinases previously described, NUAK family kinase 2 (NUAK2) bears no identifiable UBA domain (Figure 1.10) [154]. Indeed, the entire C-terminal tail of NUAK2 bears little homology to all AMPK-related kinase members and remains functionally uncharacterised [51]. Like BRSK1/2, NUAK2's catalytic domain is under direct activation loop control by LKB1, which increases its catalytic activity by more than 50-fold [41]. NUAK2's mRNA and protein expression profiles poorly correlate. For example, whilst *Nuak2* mRNA is strongly expressed in the kidney, small and large intestines, and heart, NUAK2 protein is near undetectable [51, 52]. NUAK2 is readily detectable in the adrenal gland, although peculiarly exhibits its greatest activity in testis [52]. NUAK2's subcellular distribution is highly nuclear and likely mediated via a monopartite nuclear localisation sequence embedded within the N-lobe of the kinase domain (Figure 1.10) [53]. The spatially restricted expression of NUAK2 to the nuclear compartment corroborates its recently reported regulation of the Hippo core kinase cassette comprising the kinases MST1/2 and LATS1/2, the adaptor proteins Salvador family WW domain containing protein 1 (SAV1) and MOB1A/B, and the co-transcriptional activators transcriptional yes-associated protein 1 (YAP) and Tafazzin (TAZ) [54, 118]. Where cell growth is required, YAP/TAZ translocates to the nuclear compartment where it associates with transcriptional enhanced associate domain (TEAD), driving transcription of genes implicated in cell proliferation, survival, and organ formation [158]. When cell density is reached, intracellular cues signalled via the cytoskeletal network direct LATS1/2 to phosphorylate YAP/TAZ, prompting its degradation or retention in the cytoplasm [159-162]. NUAK2 was recently shown to be a direct target of YAP/TAZ signalling in liver cancer [118]. NUAK2 directly phosphorylates LATS1 at Ser613 and Thr246, which inhibits LATS-mediated *trans*-phosphorylation of YAP/TAZ [54]. The consequent nuclear accumulation of YAP/TAZ prompts YAP/TEAD recruitment to enhancer elements of target

genes, including downstream of *Nuak2* [118]. Indeed, YAP overexpression results in increased NUAK2 mRNA and protein expression [118]. Thus, NUAK2 activity toward LATS1/2 feeds forward to promote NUAK2 expression.

The ability of NUAK2 to respond to mechanical cues that prompt LATS1/2 regulation in liver cancer is also reflected in murine skeletal muscle, where contraction *in situ* of tibialis anterior muscle increases NUAK2 catalytic activity [163]. It was later discovered that NUAK2 regulates contraction-mediated glucose transport, a process dependent on LKB1 activation [163]. These dual functions in mediating mechanotransduction inputs corroborate NUAK2's only other established downstream effector, MYPT1. MYPT1 is a regulatory subunit of myosin phosphatase, which promotes muscle contraction by catalysing myosin light chain (MLC) dephosphorylation. NUAK2 directly phosphorylates MYPT1 at residues distinct from the well-characterised Thr696 and Thr853 ROCK kinase phosphorylation sites [55]. Collectively these data strongly implicate NUAK2 in processes involving the cytoskeletal network, including cell morphology and motility programs. Indeed, NUAK2 expression strongly correlates with invasive neoplasms of the bladder. The involvement of NUAK2 in this malignancy, and others, will be discussed below.
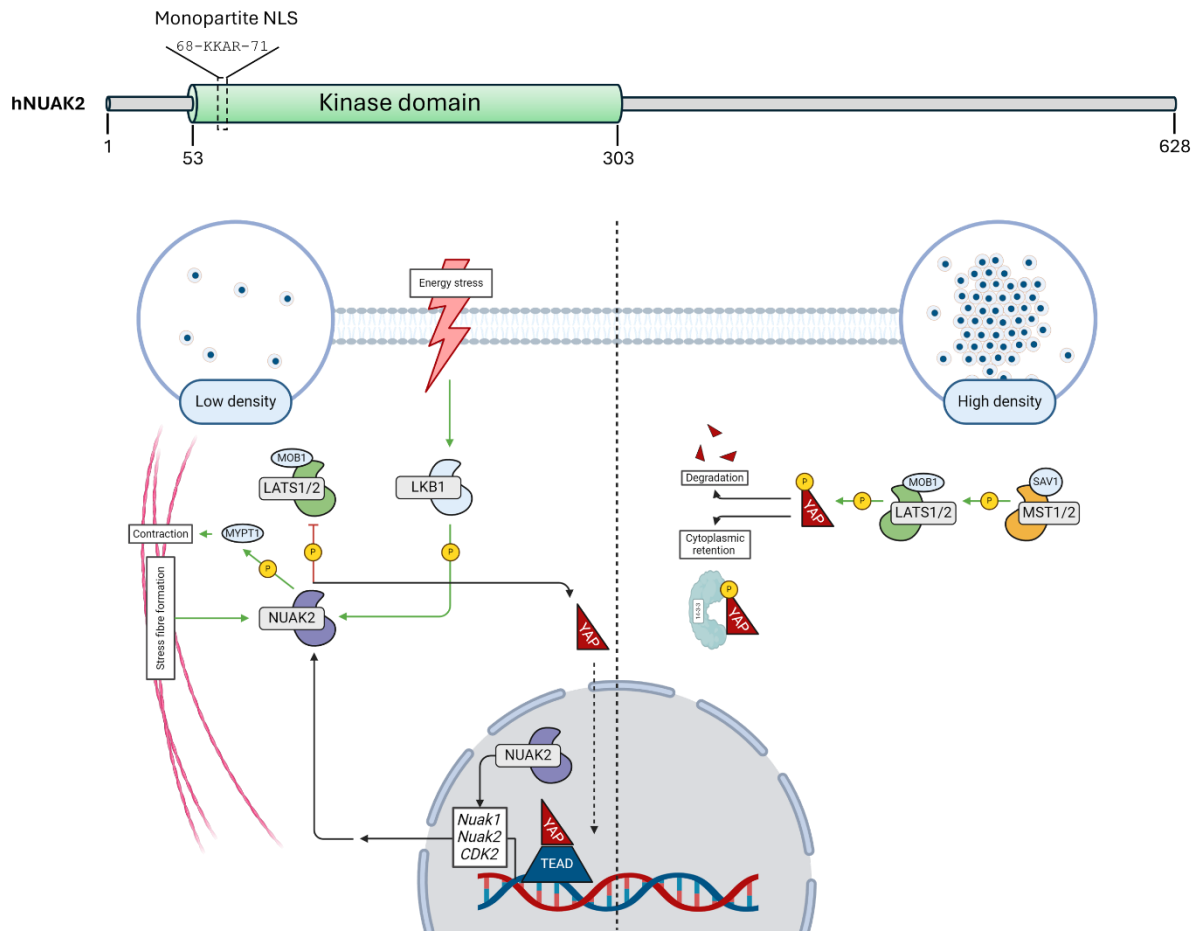
***Figure 1.10. NUAK2 linearised domain structure and regulation.*** NUAK2's domain structure consists of an N-terminal CaMK-kinase domain followed by a C-terminal extension of unknown function [51]. A monopartite NLS embedded within the N-lobe of the kinase domain facilitates NUAK2's subcellular localisation to the nucleus [53]. Under optimal cell growth and nutrient conditions, NUAK2 activity is attenuated. Consequently, LATS1/2:MOB1 can sequester and/or degrade YAP in the cytoplasm by phosphorylating YAP. Low cell densities induce morphological changes including the formation of stress fibres that promote LATS1/2 inactivation, likely via NUAK2 [160]. YAP/TAZ accumulation in the nucleus enhances gene expression concomitantly with the co-transcriptional regulator TEAD. YAP/TEAD directly enhance *Nuak2* expression, thus feeding forward to create a positive feedback loop for YAP/NUAK2 activation [118]. NUAK2 expression has also been shown to directly influence expression of the closely related paralogue *Nuak1* and *CDC2* [117, 119].

*Therapeutic potential*

As previously stated, NUAK2 is a recently characterised regulator of Hippo signalling and promotes hepatomegaly and liver cancer cell proliferation by phosphorylating and inhibiting the action of LATS1/2 [54, 118]. Targeting the Hippo pathway has recently garnered interest as a potential therapeutic for a variety of cancers [164]. However, the Hippo pathway is characterised by a distinct lack of druggable targets. For example, whilst MST1/2 inhibitors are currently available, MST1/2 harbour growth suppressive functions distinct from their capacity to regulate the downstream kinases LATS1/2, making them poor candidates for cancer therapy. NUAK2 inhibition was recently reported to impair neoplastic liver growth *in vivo* and *in vitro* [54, 118]. Further, NUAK2, but not NUAK1, expression positively correlates with penetrant and aggressive subtypes of bladder cancer (HG-MIBC; high-grade muscle-invasive bladder cancer), the fourth leading cause of cancer-related death in men [54]. Samples and cell lines derived from HG-MIBC demonstrate a predominant nuclear accumulation of YAP/TAZ, indicating aberrant Hippo signalling [54]. As such, there is a pressing need to fully evaluate the downstream effectors of NUAK2 signalling (only two such substrates have to date been characterised) and to holistically elucidate the regulatory mechanisms by which NUAK2 signalling integrates into the Hippo core kinase cassette. Further, increased NUAK2 expression frequently co-segregates with melanoma and inversely correlates with prognosis and relapse-free survival [119, 120]. Promisingly, shRNA knockdown of NUAK2 expression impairs melanomagenesis *in vitro* and *in vivo*, including cancer cell growth, migration, and invasion [119, 120].

## 1.8. NIM1 serine/threonine-protein kinase

Studies interrogating NIM1 in mammals are extremely scant. What is currently known largely stems from studies done on orthologues in fission yeast and *Arabidopsis thaliana*. NIM1 (yeast cdr1/nim1) was first characterised in *S. pombe* in the late 1980's and shown to directly promote mitotic entry by phosphorylating and inhibiting the yeast tyrosine kinase Wee1 [165-168]. Autoradiography autophosphorylation experiments indicate yeast nim1 autophosphorylates, primarily on serine residues [165]. Indeed, autophosphorylation appears to be the mechanism by which NIM1 activity is regulated, as GST-NIM1 recombinantly expressed in *E. coli* is constitutively active *in vitro* [56]. Jaleel, McBride [56] posit that the autoactivating site is likely the activation loop residue Thr229, as a Thr229Ala point mutation completely abolishes NIM1 activity *in vitro*. Corroborating this finding, a phosphomimetic point mutation (Thr229Glu) restores NIM1 activity to comparable levels to wild-type [56]. Whilst LKB1 does not demonstrably phosphorylate this site *in vitro*, this does not preclude regulation by alternative, extrinsic kinases *in vivo* [56]. NIM1 is ubiquitously expressed, with greatest activity reported in the brain and testis [56]. NIM1 was recently identified as a novel interacting partner of the retinal rod rhodopsin-sensitive cGMP 3',5'-cyclic phosphodiesterase subunit delta (PDE6D) in HEK293T and mIMCD-3 cell lines [57]. PDE6D drives protein transport toward to the ciliary membrane of primary cilia [169]. PDE6D binds prenylated cysteine moieties typically preceded by a serine residue at position -3. Mutating NIM1-Cys433 to alanine completely abolishes NIM1 localisation to primary cilia in the epithelial cell line mIMCD-3 [57].

*Therapeutic potential*

According to the Clinical Kinase Index (cki.ccs.miami.edu), NIM1 is listed as a relevant drug target for kidney renal clear cell carcinoma (KIRC) [8]. Further, inspection of the Catalogue of Somatic Mutations in Cancer (COSMIC) database (cancer.sanger.ac.uk) reveals that a majority of CNV mutations in NIM1 cluster in lung-associated malignancies [170]. Given NIM1's

recently described cilium-targeting motif, it is entirely reasonable that mutations to NIM1 that

disrupt its homeostatic functioning likely contribute to epithelial malignancies of colon, lung

and kidney origin. However, to date this has not yet been explored.



*Figure 1.11. Linearised domain structure of NIM1.* No papers have to date characterised the domain structure of mammalian NIM1. As such, this infographic is derived from publicly available data on UNIPROT (Accession: Q8IY84). A central catalytic domain is buttressed by N- and C-termini of unknown function. A recently characterised prenylation motif (RHTSKFCSIL) facilitates NIM1 localisation to the ciliary membrane [57]

## 1.8. The testis-specific serine/threonine-protein kinases

The testis-specific serine/threonine protein-kinases (TSSKs) were first described in the early-

1990's with the isolation and characterisation of murine cDNA encoding TSK-1 (henceforth,

TSSK1) [58, 171]. Five more members of the TSSK subfamily were identified during the

subsequent decade: TSSK2 [59], TSSK3 [64], TSSK4 [66] and TSSK6 [70] (for a complete

nomenclature of the TSSK subfamily, see Table 1.1). TSSK5, which is a pseudogene in

primates [172], will not be discussed further. Concurrent analyses of brain and peripheral

tissues revealed highly restricted expression of TSSK mRNA to maturing spermatids in adult

testis [58, 59, 63, 64, 66, 70]. These findings were largely reflected at the translational level

with TSSK1, TSSK2, TSSK4 and TSSK6 detected in and restricted to post-meiotic sperm [59-

62, 64, 70]. Interestingly, several authors note the spatiotemporal segregation of TSSK

expression to defined regions in developing spermatids. TSSK1 and TSSK2 localise to the

cytoplasm and equatorial segment, to residual bodies, and to a ring-shaped structure situated at

the flagellum base [59, 60, 62]. TSSK6 concentrates at the acrosomal/head region [70]. Importantly, TSSK expression is undetectable in immature testis and in the epididymis, where mature sperm are stored, strongly implicating a role for this kinase subfamily to post-meiotic germ cell development and cytodifferentiation [59]. In accordance with these observations, *Tssk1/Tssk2*^{-/-}*, Tssk3*^{-/-} and *Tssk6*^{-/-} male mice are infertile, with *Tssk4*^{-/-} mice presenting with a sub-fertile phenotype [62, 68, 70, 173-175]. Although demonstrably implicated in signalling programs critical for sperm cytodifferentiation, upstream activators and downstream effectors for this kinase subfamily are less clearly defined. All 5 members possess autokinase activity and phosphorylate the generic protein substrate MBP (Table 1) [56, 60, 61, 65, 67, 70]. TSSK1 and TSSK2 phosphorylate the testis-specific kinase substrate (TSKS) which was, concurrently with TSSK1 and TSSK2, characterised by Kueng et al. and parallels the spatiotemporal expression patterns of both upstream enzymes [59, 60]. TSSK6 has also been reported to accept the histone substrates, H1, H2A, H2AX and H3 [70]. Interestingly, the domain structure of several TSSK family members, including TSSK3 and TSSK6, is largely delimited to a kinase domain only (Figure 1.12). How these kinases are regulated despite lacking N and C-termini is not known, but they are believed to form higher-order, heterooligomeric complexes. Indeed, ectopic expression of TSSK6 in HEK293T cells identified 3 interacting partners that co-immunoprecipitated with TSSK6: the heat shock proteins HSP90-1β, HSP70-1 and HSC70 [70]. *Mention activation loop regulation here.*

Bucko-Justyna et al. note a need for an extrinsic kinase to phosphorylate the T168 site in TSSK3's activation loop and demonstrate PDK1 as an *in vitro* candidate, but this has not been confirmed *in vivo*.
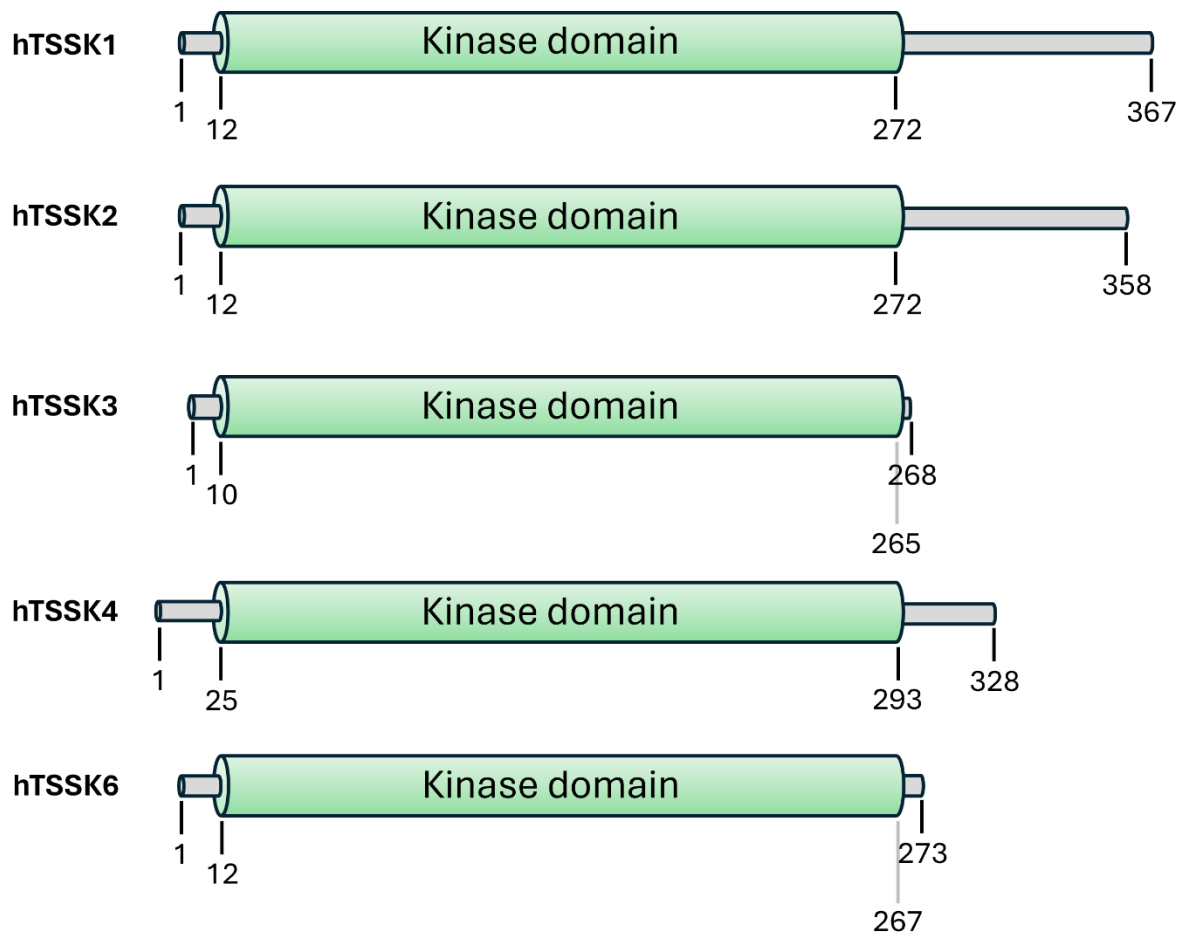
***Figure 1.12. The linearised domain structures of the TSSK subfamily reveals a unique architecture characterised by kinase-domains only.*** The domain architecture of TSSK family members consists of a central catalytic domain buttressed by variable termini of unknown function. Interestingly, TSSK3 and TSSK6 are characterised by a distinct lack of termini and are effectively kinase domains only. Thus, regulation of TSSK3/6 activity would invariably necessitate regulatory action at the catalytic interface.

*Therapeutic potential*

The highly restricted spatiotemporal expression of this kinase subfamily in combination with the observation that *Tssk* KO male mice are sub- or infertile has recently garnered interest in targeting these enzymes as non-hormonal alternatives for reversible male contraception [176]. Further, despite its predominantly restricted expression to testis, TSSK6 was very recently reported as an oncogenic driver of colorectal cancer (CRC) progression [122]. TSSK6 expression was found to negatively correlate with relapse free survival of CRC patients and

cell growth, migration and invasion of CRC cells *in vitro* [122]. In immortalised neoplastic cell lines, TSSK6 colocalises at cell membrane foci with the focal adhesion markers, paxillin and tensin [122]. Further corroborating a role in promoting the migration and invasion of CRC cells, siRNA knockdown of TSSK6 expression significantly impaired CRC invasion in 2D cultures [122]. Importantly, TSSK6-mediated CRC cell growth and migration is dependent on its catalytic activity, as ectopic expression of an activation loop point mutant (T170A) fails to promote neoplastic growth *in vitro* [122]. No upstream activating kinase has, to date, been identified to phosphorylate this site. Further, few substrates have been characterised for TSSK6 and at present, it is not clear through what effectors TSSK6 mediates CRC progression [70]. The dramatic effects TSSK6 expression imparts on neoplastic cell growth is somewhat remarkable for a protein whose structure is largely delimited to a kinase domain only (Figure 1.12). It is likely that TSSK6 activity is regulated by binding to adaptor proteins directly at its catalytic interface. HSP90-1β, HSP70-1 and heat shock cognate protein 70 (HSC70) have been reported to bind TSSK6 when TSSK6 is ectopically expressed in HEK293T cells, but it is not clear if these are native interacting partners [70]. Thus, there is a pressing need to holistically characterise the upstream, downstream, and regulatory effectors of TSSK6 (and indeed, the entire TSSK subfamily) activity.

## 1.9. MAP kinase-interacting serine/threonine-protein kinase 1/2

The 'eIF4E kinases', MAP-kinase-interacting serine/threonine-protein kinase 1 and 2 (MNK1/2, henceforth MKNK1/MKNK2), were concurrently discovered by two, independent groups in screens using ERK as bait [73, 74]. Expectedly, MKNK1/2 harbour MAPK-binding motifs in their C-termini, not dissimilar from the closely related p90[rsk] kinase subfamily (Figure 1.13). In MKNK1, the ERK/p38 docking site is preceded by a leucine-rich nuclear export signal (NES), corroborating its cytoplasmic subcellular distribution in HEK293T cells [72]. Indeed, both MKNK1 and MKNK2 are exclusively expressed in the cytoplasm, despite harbouring polybasic nuclear import signals in their N-termini (Figure 1.13) [72, 75]. Interestingly, a C-terminally truncated splice variant of MKNK2 (MKNK2b) is predominantly expressed in the nucleus, suggesting that this region, as in MKNK1, facilitates MKNK2 exclusion from the nuclear compartment [75]. To date, studies interrogating MKNK subcellular localisation have been delimited to HEK293T cells [72, 75]. In reality, MKNK localisation is likely highly dynamic, mirroring the distribution of its only characterised downstream effector, eIF4E [74]. eIF4E controls the rate-limiting step of protein translation by binding to and recruiting the translational machinery to the nascent mRNA strand [177]. MKNK1/2 phosphorylate eIF4E at Ser209, which modulates eIF4E-mediated translation and nucleo-cytoplasmic export of mRNA [71, 74, 76, 178]. MKNK1/2 *trans*-phosphorylation of eIF4E is dependent on the scaffolding protein eIF4G, which docks via its C-terminus to the N-terminal polybasic cluster of MKNK1/2 (Figure 1.13) [72, 75, 179]. MKNK1 and MKNK2 exhibit stark differences in catalytic activity and affinity for the upstream mitogen and stress-activated MAP-kinases, ERK and p38. Under basal conditions, MKNK2 is significantly more active relative to MKNK1 [76]. Several modifications to MKNK2 putatively explain this increase in catalytic activity. Firstly, a serine residue -6 aa N-terminal to the T-loop phosphorylation sites in MKNK1 is substituted by an aspartic acid in MKNK2 (Figure 1.13). An acidic moiety so close to the regulatory T-loop sites

of MKNK2 may simulate a phosphorylation event that stabilises the local catalytic architecture into a favourable conformation for kinase activity. Artificial substitution of this serine in MKNK1 to aspartic acid increases its catalytic activity [180]. Phospho-peptide mapping indicates that this residue is phosphorylated by an extrinsic kinase, although the identity of this kinase has not yet been validated [180]. Whilst MKNK1-Ser191Glu is more active relative to wild-type controls, kinase activity was still low compared to WT-MKNK2 [180]. It was discovered that the C-terminus of MKNK2a enhances catalytic activity, as a MKNK1-Ser191Glu-C2 (C2: C-terminus of MKNK2a) chimera displays equivalent activity to MKNK2a *in vitro* [180]. The C-terminal MAPK-docking motif of MKNK2 (LAQRR) displays increased preference for ERK and was shown to bind phosphorylated ERK (pERK), which protects ERK from phosphatases and consequent inactivation [74, 76, 180]. Conversely, MKNK1's MAPK-docking motif (LARRR) binds both ERK and p38 but cannot bind pERK [74, 180]. Thus, differences in the kinase domain and C-terminal tail of MKNK2 enhance MKNK2 activity by a) altering the catalytic architecture of MKNK2 and b) preserving ERK activation of MKNK2. Interestingly, despite these differences, MKNK1 and MKNK2 activity (and consequently eIF4E phosphorylation) is seemingly dispensable for normal development [181]. The consequences of eIF4E phosphorylation will be discussed below.

*Therapeutic potential*

As downstream effectors of RAS/RAF/MEK/ERK signalling, MKNK1/2 are increasingly attractive targets for therapeutic intervention of melanoma, of which current clinical efficacy is limited [182]. For example, more than half of cutaneous melanomas harbour activating mutations to BRAF, 90% of which occur at Val600 (V600E) [183]. This residue, which resides in the activation loop of BRAF, is buttressed by two phosphoryl-acceptor sites (Thr598 and Ser601) critical for BRAF activation [184]. The substitution of an acidic moiety at Val600 likely mimics a phosphorylation event, resulting in a constitutively active kinase. Genetic

insults to the upstream activating small GTPase NRAS (for example, Q61L) correlate with a comparatively more aggressive disease phenotype and are present in 28% of cutaneous melanomas [185]. Collectively these mutations compromise homeostatic regulation of downstream RAS/RAF/MEK/ERK effectors, including MKNK1/2. MKNK1/2 are attractive targets for therapeutic intervention as they constitute the only described kinases to phosphorylate the translational activator, eIF4E [71, 76]. Phosphorylated (pSer209) eIF4E is well documented as an oncogenic driver of tumour growth, metastasis, and invasion [186-188]. Due to this restricted substrate profile (to date, eIF4E is the only described *in vivo* target), therapeutically targeting MKNK1/2 will likely prove preferential over BRAF/NRAS inhibition, of which current inhibitors demonstrate severe adverse side effects [189].
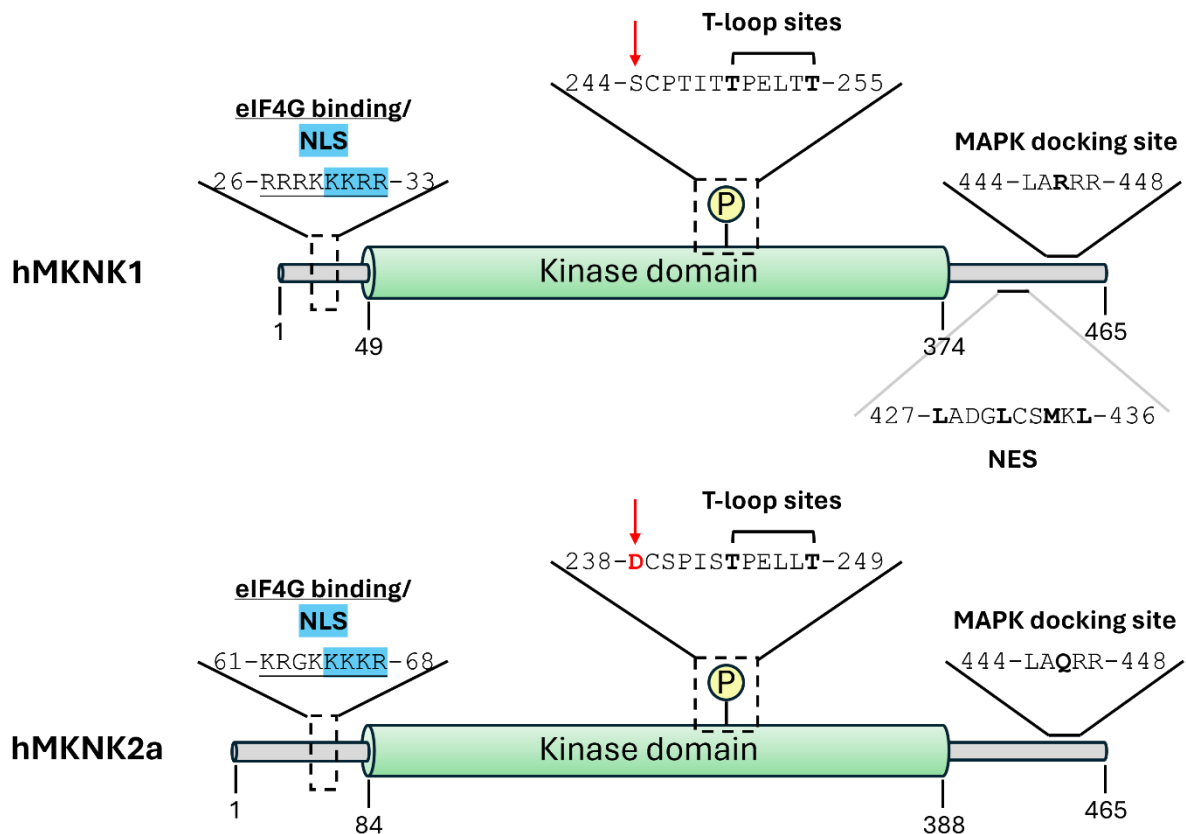
***Figure 1.13. Domain structure of human MKNK1 and MKNK2a.*** MKNK1/2 harbour CaM-kinase domains buttressed by N- and C-termini with high homology. The N-termini contain a polybasic cluster that facilitates eIF4G binding (underlined) and nuclear import (blue). The C-termini of MKNK1/2 contain variable MAPK-docking motifs with differential affinity for the upstream MAP-kinases, ERK and p38. MKNK2 also contains a leucine-rich nuclear export signal (NES) N-terminal the MAPK-docking motif. The regulatory T-loop phosphorylation sites in MKNK2a are preceded -6 aa by an acidic aspartate, which increases the basal activity of MKNK2a. NLS: nuclear localisation signal.

## 1.10. Obscurin-MLCK & obscurin-associated kinases

As its namesake suggests, the giant, sarcomeric protein obscurin remains largely shrouded in mystery. Indeed, its unwieldy size (~720 kDa) has complicated efforts to holistically characterise this protein. Prototypic 'obscurin' (obscurin-A, henceforth 'obscurin') is comprised of 65 tandem immunoglobulin (Ig) domains, 2 fibronectin-III (Fn-III) domains, an isoleucine/glutamine (IQ)/calmodulin-binding domain, a Src-homology 3 (SH3) domain, a Rho-GEF domain, a pleckstrin homology (PH) domain and a C-terminal tail that provides docking sites for ankyrins [190]. Upon obscurin's initial identification by Young et al. (2001), a second variant – Obscurin-B (henceforth 'obscurin-MLCK') – was concurrently discovered [191]. Giant Obscurin-MLCK (870 kDa) shares many of the adhesion and regulatory modules as obscurin but is delineated by tandem serine/threonine kinase domains, 2 Ig domains and an Fn-III domain at its C-terminus (Figure 1.14) [79, 191]. Both proteins result from differential splicing of the same 170 kb DNA fragment on chromosome 1q42.13. Much smaller isoforms (55-145 kDa) have also been reported, including tandem (120-145 kDa) and single (55-70 kDa) MLCK-kinase domain variants [77, 191]. As obscurin bears no CaM-kinase domain, it will not be discussed further. Both large and small isoforms are expressed in sarcomeres of striated skeletal and cardiac tissue but bear differential expression profiles. For example, giant obscurin-MLCK is more strongly expressed in skeletal muscle, whilst the tandem/single MLCK kinase-bearing isoforms are more prevalent in heart [78]. Interestingly, obscurin single-MLCK is more strongly expressed than the tandem-MLCK variant, and 50-fold greater than giant obscurin in murine cardiac tissue [78]. The IQ motif of obscurin-MLCK binds calmodulin in a $Ca^{2+}$-independent manner and is not predicted to be regulatory in nature. Conversely, obscurin tandem-MLCK harbours a predicted overlapping AID/CBD C-terminal to the obscurin kinase 2 domain (OK2), although this has not been functionally characterised (Figure 1.14) [79]. Both kinase domains (OK2 and OK1) were recently demonstrated to possess

autokinase activity [77]. Further, OK2 was able to phosphorylate the generic acceptor substrate, histone [77]. Interestingly, OK2 and OK1 bear little resemblance to one another (~30% sequence homology) and are predicted to serve distinct functional roles [79]. Indeed, yeast two-hybrid screens of adult cardiac cDNA libraries using OK2 and OK1 as bait identified distinct interacting partners for OK2 and OK1 [77]. The short 55-70 kDa isoform (obscurin single-MLCK) which contains the OK1 kinase domain was shown to interact with the extracellular domain of the $Na^+/K^+$ ATPase pump, $NKA\beta_1$ [77]. Further, obscurin single-MLCK is glycosylated at its N-terminus, which is typical of extracellular-associated proteins [77]. OK2, present in the tandem- and giant obscurin-MLCK variants, interacts with the intracellular domain of *N*-Cadherin and phosphorylated *N*-Cadherin *in vitro* [77]. The precise function and phosphorylation sites in OK2-mediated regulation of *N*-Cadherin are not currently understood. Most recently, OK2 was demonstrated to phosphorylate a serine cluster C-terminal to the kinase 2 domain in the inter-kinase region (Figure 1.14) [80]. Phosphorylation of this cluster altered localisation of an OK2-containing fragment transiently expressed in differentiated C2C12 cells to myonuclei of myotubes *in vitro* [80]. Additionally, the C-terminal end of the inter-kinase region harbours further phosphorylation sites homologous to residues in the closely related striated preferentially expressed gene kinase (SPEG) [80]. In SPEG, PKB and CaMK2 phosphorylate this region, altering its catalytic activity [192]. However, these sites have not been characterised in obscurin.
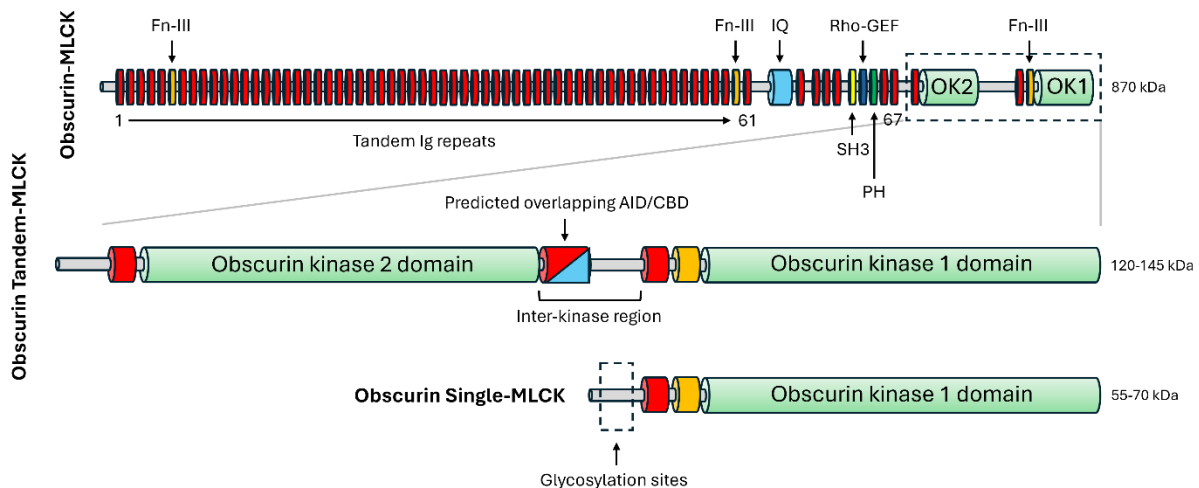
***Figure 1.14. Linearised domain structure of obscurin-MLCK and obscurin-associated kinases.*** Giant obscurin-MLCK comprises 67 Ig domains, 2 Fn-III domains, an IQ motif and a signalling module consisting of tandem SH3/Rho-GEF/PH domains. Alternative splicing of the *OBSCN* gene results in fusion of tandem MLCK kinase domains and additional Ig/Fn-III domains to the C-terminus. Two, truncated kinase-bearing isoforms have also been identified: the 120-145 kDa obscurin tandem-MLCK and the 55-70 kDa obscurin single-MLCK [79, 191]. Obscurin tandem-MLCK harbours a putative AID/CBD C-terminal to the kinase domain in the inter-kinase region. OK2 has also been shown to regulate the inter-kinase region by autophosphorylating a serine cluster [80]. Obscurin single-MLCK harbours glycosylation sites N-terminal the OK1 domain [80]. Fn-III: fibronectin-III; IQ: isoleucine/glutamine motif; SH3: Src-homology 3; PH: pleckstrin homology; OK2: obscurin kinase 2 domain; OK1: obscurin kinase 1 domain; AID/CBD: autoinhibitory/calmodulin-binding domain. Domain structures adapted from Randazzo, Pierantozzi [193] and Grogan, Tsakiroglou [194].

*Therapeutic potential*

Genetic insults to obscurin correlate with a variety of myopathies afflicting the heart and skeletal muscle [193]. The mutations thus characterised generally occur at Ig domains, which impair obscurin's ability to dock at sarcomeric structures. For example, an Arg4344Gln point mutation impairs binding of obscurin to the Z9-Z10 domains of titin/connectin and correlates with hypertrophic cardiomyopathy [125]. Unfortunately, no studies have evaluated the functional impact of obscurin-kinase activity impairment in a disease context. Knock-out of obscurin-MLCK homologues in mice (SPEG) results in cardiac abnormalities and increased neonatal mortality [195]. However, it is not clear if these phenotypic effects are due to impaired MLCK kinase activity or loss of structural motifs (like Ig and Fn-III domains) present on the

SPEG protein. Future studies should holistically evaluate the function and effector proteins of

obscurin-MLCK *in vitro* and *in vivo*.

## 1.11. Concluding commentary

Kinases are analogous to biological 'conductors' that direct the flow of cellular processes by instructing proteins when to execute their physiological function amongst the cacophony of protein signalling ever present inside our cells. Unsurprisingly, their dysregulation frequently leads to catastrophic flow-on effects, destabilising the homeostatic functioning of cells. Fortunately, kinases are inherently druggable and are major targets for therapeutic intervention. According to a recent report by Essegian, Khurana [8], only 8% of the human kinome is currently targeted by FDA-approved anti-cancer therapeutics. No small molecule inhibitors are, at present, approved for CaMK family members [8]. Aggravating efforts, almost two-thirds of the CaMK kinome is comparatively poorly characterised (Figure 1.2). **These understudied, or 'dark' kinases, represent a potentially untapped reservoir for therapeutic intervention of a wide variety of disorders and disease phenotypes, including cancers, neurodevelopmental conditions, metabolic disorders and for non-hormonal contraception.** Recognising this, the Clinical Kinase Index (http://cki.ccs.miami.edu/) was recently established which categorically prioritises understudied kinases for therapeutic intervention [8]. Interestingly, many of the dark CaM-kinases previously described are listed as high-priority anti-cancer targets, including DCLK3 BRSK1, and BRSK2 [8]. As previously discussed, no substrates have currently been defined for DCLK3, and the regulation of BRSK kinases remains inconclusive. As such, there is a pressing need to holistically characterise these dark, CaM-kinases. This literature review demonstrates large gaps in our understanding of the CaMK family and the growing interest in targeting these enzymes for therapeutic intervention of a variety of disorder phenotypes.

## 1.12. Aims and outlines of this thesis

Amongst the dark CaM-kinases previously described, PSKH1 is arguably the least characterised (Table 1.1). Indeed, no upstream activators or downstream effectors have, to date, been defined. Further, the precise function of PSKH1 is currently not known. We decided to interrogate PSKH1 as, initially, it appeared to be a highly probable substrate for CaMKK2, of which remains the focus of our laboratories' research efforts (detailed in Chapter 3.1). Our attempt to biochemically characterise PSKH1 is encapsulated in the following chapters:

Chapter 3 describes efforts to evaluate how PSKH1 activity is regulated *in vitro*. Whilst this study did not reveal an extrinsic, upstream kinase regulating PSKH1 activity, it was discovered that PSKH1 autoactivates itself by phosphorylating its activation loop Thr256 residue in a *cis-*apparent mechanism. Additionally, as a *bona fide* CaM-kinase, PSKH1 is regulated by calmodulin albeit mechanistically distinct from its closely related cousins, CaMK1 and CaMK4. Lastly, a novel family of low-affinity $Ca^{2+}$-binding proteins negatively regulate PSKH1 catalytic activity.

Chapter 4 interrogated PSKH1's role in prostate cancer progression. Our studies demonstrated, for the first time, a direct function for PSKH1 i.e. PSKH1 is a metabolic sensor that promotes prostate cancer cell growth by instructing cells to fuel-switch to fatty acids under glucose deprived conditions.

Chapter 5 provides a summation of the findings previously described and contextualises PSKH1 in a broader context.

# 2. MATERIALS AND METHODS

## 2.1. Reagents and resources

### 2.1.1. Chemicals and consumables

**Table 2.1.1. Chemicals and consumables**

| Supplier | Name | Abbreviation | Catalogue No. |
|---|---|---|---|
| Agilent Technologies | Agilent Seahorse XF XF Calibrant | | 100840-000 |
| Bio-Rad | 4-15% Mini-PROTEAN TGX Stain-Free Gels, 12 well, 20μl | | 4561085 |
| | 4-15% Mini-PROTEAN TGX Stain-Free Gels, 10 well, 50μl | | 4561084 |
| | 4-15% Criterion TGX Stain-Free Protein Gels, 26 well, 15μl | | 5678085 |
| | 4X Laemmli Sample Buffer | | 1610747 |
| BOVOGEN Biologicals | Bovine Serum Albumin | BSA | BSAS-NZ |
| GenScript | DYKDDDDK Peptide | FLAG peptide | RP10586 |
| Ibidi | μ-Slide 18 Well Glass Bottom | | 81817 |
| Merck Life Science | cOmplete™, Mini EDTA-free Protease Inhibitor Cocktail | cOmplete™ | 4693159001 |
| | Immobilon®-FL PVDF Membrane | PVDF | IPFL00010 |
| | Re-Blot Plus Strong Solution | | 2504 |

| | EZview Red Anti-HA Affinity Gel | HA-resin | E6779 |
|---|---|---|---|
| Promega | FuGENE HD Transfection Reagent | FuGENE | E2312 |
| Pure Science Australia | Carbenicillin (Disodium), USP Grade | | C-103-25 |
| Revvity | EasyTides® Adenosine 5'-triphosphate, [gamma-32P] | EASYTIDES ATP,[g-32P] | BLU502A001MC |
| Sigma-Aldrich | 2-Deoxy-D-Glucose | | D6134 |
| | Adenosine 5'-diphosphate sodium salt | | A2754 |
| | Adenosine 5'-monophosphate monohydrate | | A2252 |
| | Anti-FLAG M2 Affinity Gel | | A2220-5ML |
| | Forskolin | | F3917-10MG |
| STEMCELL™ Technologies | Ionomycin | | 73722 |
| Thermo Fisher Scientific | 2.5% Trypsin (10X) | | 15090046 |
| | Human PDGF-BB Recombinant Protein | | PHG0044 |
| | Penicillin-Streptomycin (10,000 U/mL) | Pen Strep | 15140122 |
| | Poly-D-Lysine | PLD | A3890401 |
| | DPBS | PBS | 14190-144 |
| | DPBS (calcium, magnesium) | | 14040133 |

| | | Earle's Balanced Salt Solution | EBSS | 24010043 |
|---|---|---|---|---|
| Qiagen | | HiSpeed Plasmid Midi Kit | | 12643 |

**Table 2.1.2. Buffers**

| | Acronym | Formulation | | |
|---|---|---|---|---|
| **Buffers** | | | | |
| Mammalian lysis buffer | MLB | 50mM Tris pH 7.5, 150mM NaCl, 50mM NaF, 5mM NaPPi, 1mM EGTA, 1mM EDTA | | |
| RIPA buffer | RIPA | As above + 0.5% (v/v) sodium deoxycholate, 0.1% (v/v) SDS and 1% (v/v) Nonidet P 40 Substitute | | |
| High-salt wash buffer | HS | MLB supplemented with 1% (v/v) Triton X-100 and 1M NaCl | | |
| Low-salt wash buffer | LS | MLB supplemented with 1% (v/v) Triton X-100 and 150mM NaCl | | |
| No-salt wash buffer | NS | 50 mM HEPES-NaOH pH 7.4 and 0.1% (v/v) Tween-20 | | |
| Assay buffer | | 50 mM HEPES-NaOH pH 7.4, 0.1% (v/v) Tween-20 and 5mM DTT | | |
| ATP mix | ATP mix | 10$\mu$l 2.5M MgCl$_2$, 10$\mu$l 100mM 'cold' ATP, 50$\mu$l [$\gamma$-32P]-ATP in 930$\mu$l 50mM HEPES pH 7.4 | | |

| | | | | |
|---|---|---|---|---|
| Fractionation Buffer A | | 50mM HEPES pH 7.4, 150mM NaCl, 1M hexylene glycol, 25μg/mL digitonin | | |
| Fractionation Buffer B | | 50mM HEPES pH 7.4, 150mM NaCl, 1M hexylene glycol, 1% (v/v) NP-40 | | |
| Fractionation Buffer C | | 50mM HEPES pH 7.4, 150mM NaCl, 1M hexylene glycol, 0.1% (w/v) SDS, 0.5% (w/v) sodium deoxycholate | | |
| 1 X SDS-Running buffer | | 14.4g/L glycine, 3.03g/L Tris-base, 1g/L SDS, pH 8.3 | | |
| 1 x SDS-Transfer buffer | | | | |

**Table 2.1.3. Media**

| | Acronym | Catalogue No. | Supplier |
|---|---|---|---|
| **Media** | | | |
| DMEM, high glucose | HG DMEM | 11995-065 | Thermo Fisher |
| DMEM, no glucose | - gluc | 11966-025 | |
| DMEM, high glucose, no glutamine | - glut | 11960-044 | |
| RPMI 1640 | | 11875-093 | |
| RPMI 1640, no glucose | | 11879-020 | |
| SOC Outgrowth Medium | SOC | B9020S | NEB |

| | | | 102353-100 | Agilent Technologies |
|---|---|---|---|---|
| XF Base Medium Minimal DMEM | | | | |

### 2.1.2. *Escherichia coli* strains

NEB® 5-alpha Competent *E.coli* (High Efficiency) (#C2987I) cells were purchased from NEB, Australia.

### 2.1.3. Mammalian cell lines

HEK293T, LNCaP-WT and LNCaP PSKH1-KO cells were generously donated by Dr. Naomi Ling (SVI, Fitzroy, Australia).

### 2.1.4. Plasmids

All plasmids were purchased from Gene Universal. These constructs were manufactured (i.e. cloned) and QC'd externally by this supplier. Validation of construct expression is detailed in section 2.3.1.

**Table 2.1.4. Plasmid inventory**

| Vector | Plasmid No. | Plasmid | Selection Marker | Supplier |
|---|---|---|---|---|
| pcDNA3.1(-) | P1057 | FLAG-CaMKK2.1 | Ampicillin/ Carbenicillin$^R$ | Gene Universal |
| | P1693 | PSKH1-HA | | |
| | P1273 | PSKH1-FLAG | | |
| | P1274 | PSKH1-FLAG Thr256Ala | | |
| | - | PSKH1-FLAG D218N | | |
| | P1641 | PSKH1-FLAG G2A | | |
| | P1642 | PSKH1-FLAG C3S | | |

| | | | | |
|---|---|---|---|---|
| | P1643 | PSKH1-FLAG G2A/C3S | | |
| | P1695 | PSKH1-FLAG 1-391 | | |
| | P1696 | PSKH1-FLAG 1-375 | | |
| | P1697 | PSKH1-FLAG 1-359 | | |
| | P1698 | PSKH1-FLAG 86-424 | | |
| | P1705 | PSKH1-FLAG 98-424 | | |
| | P1721 | PSKH1-FLAG Y86A | | |
| | P1722 | PSKH1-FLAG R87A | | |
| | P1723 | PSKH1-FLAG K89A | | |
| | P1724 | PSKH1-FLAG F90A | | |
| | P1725 | PSKH1-FLAG D91A | | |
| | P1726 | PSKH1-FLAG P92A | | |
| | P1727 | PSKH1-FLAG R93A | | |
| | P1728 | PSKH1-FLAG T95A | | |
| | P1729 | PSKH1-FLAG K97A | | |
| | P1730 | PSKH1-FLAG Y98A | | |
| | P1694 | PSKH2-HA | | |
| pEGFP-C1 | P1228 | GFP-hCaMK4-FLAG | Kanamycin[R] | |
| | P1259 | GFP-hCaMKK2.7-FLAG | | |
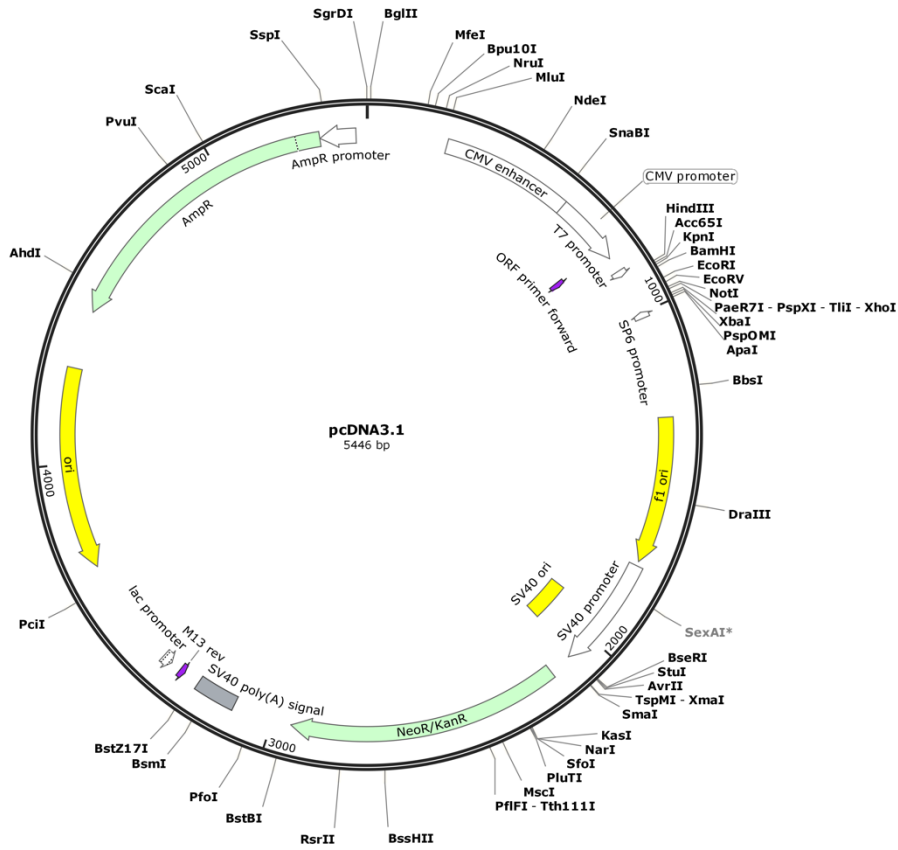
***Figure 2.1. pcDNA3.1(-) vector map.*** Vector map of the pcDNA3.1(-) mammalian expression vector. Prepared using SnapGene.

## 2.1.5. Antibodies

**Table 2.1.5. Primary and secondary antibodies**

| Antibodies | Source | Catalogue No. | Dilution | Supplier |
|---|---|---|---|---|
| **Primary antibodies** | | | | |
| α-14-3-3 (pan) | Rabbit | 8312S | 1:1000 | CST |
| α-DYKDDDDK | Rabbit | 14793S | 1:1000 | CST |
| α-DYKDDDDK | Mouse | 8146T | 1:1000 | CST |
| α-GAPDH | Mouse | 97166S | 1:1000 | CST |
| α-HA | Rabbit | 3724S | 1:1000 | CST |
| α-HA | Mouse | 2367S | 1:1000 | CST |
| α-PSKH1 (E-9) | Mouse | sc-514401 | 1:200 | Santa Cruz |
| α-PSKH1 | Rabbit | HPA053927 | 1:1000 | Atlas |
| α-Puromycin | Mouse | ZMS1016 | 1:10000 | Sigma |
| α-RCN3 | Rabbit | ab204178 | | abcam |
| α-RSK1 (D6D5) | Rabbit | 8408S | 1:1000 | CST |
| **Secondary antibodies** | | | | |
| IRDye® 680RD | Rabbit | LCR-926-68071 | 1:10000 | Millenium Science |
| IRDye® 800CW | Mouse | LCR-926-32210 | 1:10000 | Millenium Science |
| **Phospho-Antibodies** | **Source** | **Catalogue No.** | **Dilution** | **Supplier** |
| α-p-CaMKK2 (Ser511) | Rabbit | 12818S | 1:1000 | CST |
| α-p-eEF2K (Ser366) | Rabbit | 3691T | 1:1000 | CST |

| α-p-p38 | | | 1:1000 | CST |
|---|---|---|---|---|
| α-p-p42/44 | | | 1:1000 | CST |
| α-p-p90RSK (Ser380) | Rabbit | 9341S | 1:1000 | CST |
| α-p-Serine | | | 1:1000 | |
| α-p-Threonine | Mouse | 9386S | 1:1000 | CST |

### 2.1.6. Cell culture growth media

#### 2.1.6.1. E. coli growth media

Luria-Bertani (LB) broth was formulated by dissolving 1% (w/v) NaCl, 1% (w/v) tryptone and 0.5% yeast into deionised water. LB preparations were subsequently autoclaved using standard lab protocols. To prepare bacterial growth plates, 1.5% (w/v) agar was supplemented into LB preparations prior to sterilisation. 1:1000 dilutions of carbenicillin (Pure Science Australia) or kanamycin were inoculated into cooled LB/LB-agar preparations on an as-needed basis.

#### 2.1.6.2. Mammalian cell growth media

Please refer to table 2.1.2 for cell media formulations

## 2.2. Cell culture

### 2.2.1. *E. coli* cell culture and transformation

25μl aliquots of thawed, competent *E. coli* were inoculated with 50ng plasmid DNA and allowed to incubate on ice for 30 minutes. Aliquots were subsequently transferred to a pre-heated water bath (42°C) and briefly heat shocked for 30 seconds. Following a 5-minute incubation on ice, transformed *E. coli* were recovered in 150μl SOC Outgrowth Medium at 37°C for 1 hour with agitation. 30-50μl transformed bacteria were streaked onto LB agar plates containing an appropriate selective antibiotic and allowed to incubate overnight at 37°C. On

day 2, colonies were picked and transferred to 500ml conical flasks containing 50ml LB similarly supplemented with antibiotic and allowed to outgrow overnight at 37°C with agitation.

### 2.2.2. Preparation of glycerol stocks

500μl of transformed bacterial suspension was mixed with 500μl 50% (v/v) autoclaved glycerol by vortexing and stored at -80°C.

### 2.2.3. DNA isolation

45-50ml input of bacterial suspension was used per DNA isolation using a HiSpeed Plasmid Midi Kit (Qiagen) according to manufacturer's protocols.

### 2.2.4 – Mammalian cell culture

HEK293T cells were maintained in HG DMEM supplemented with 10% (v/v) FBS in a humidified incubator at 37°C with 5% $CO_2$ injection. LNCaP cells were maintained in RPMI 1640 medium supplemented with 10% (v/v) FBS in a humidified incubator at 37°C with 5% $CO_2$ injection. To prevent senescence and keep cultures in log phase growth, cell cultures were passaged at ~90% confluency by briefly rinsing in pre-warmed PBS and incubating in 0.25% (v/v) trypsin for 3-5 minutes at 37°C. Trypsin was deactivated by re-suspending cell cultures in equal volumes of supplemented HG DMEM or RPMI 1640, respectively. Suspensions were subsequently centrifuged at 350g for 3 minutes to pellet cells and remove residual trypsin from cell cultures. For maintenance culturing, pellets were resuspended in 5-10ml supplemented media and split according to confluency and the dimensions of the receiving flask.

## 2.3. Mammalian recombinant protein expression

### 2.3.1. Transient transfection of protein expression constructs

3μg pcDNA3.1 or pEGFP C1 vector encoding constructs of desired proteins (Gene Universal, Table 5) were transfected into HEK293T cells seeded onto 100mm culture dishes at a ratio of 6:1 FuGENE® HD Transfection Reagent (Promega):DNA and allowed to incubate for 48 hours. Following transfection and to concentrate yield of recombinant protein, cells were sequentially lysed *in situ* in 150μl/plate MLB (Table 3) supplemented with 1% (v/v) Triton X-100 and cOmplete Protein Inhibitor Cocktail tablet (Roche) by cell scraping and transferred to pre-chilled Eppendorf® tubes for incubation on ice for 30 minutes. All lysates were snap frozen in liquid nitrogen and stored at -80°C. To validate expression of the mutant PSKH1 constructs, cell lysates containing transiently transfected PSKH1 plasmids were probed by western blot using α-FLAG/GFP antibodies. To confirm mutations (i.e. truncations) to PSKH1, all constructs were benchmarked against full-length WT PSKH1 by comparing bandshifts in blots.

### 2.3.2. Immunoprecipitation of protein from cell lysates

FLAG-tagged protein was immunoprecipitated from whole cell lysate (WCL) using pre-equilibrated anti-FLAG M2® Affinity Gel (50% (v/v)) for 1 hour at 4°C on a carousel rotator. Immunoprecipitated protein was pelleted by centrifugation on a bench-top centrifuge at 8200g for 3 minutes. For conducting immobilised [$\gamma^{32}$P]-ATP peptide assays [Section 2.5.1], FLAG-conjugated protein was first rinsed in ice-cold high-salt (HS) and low-salt (LS) wash buffers followed by successive washes in no-salt (NS) wash buffer to remove chelating EGTA (Table 3).

#### 2.3.2.1. FLAG elution

Complexed recombinant FLAG-tagged protein:FLAG agarose was resuspended in synthetic FLAG peptide (1 mg/ml in HEPES buffer, pH 7.4) and allowed to elute overnight at 4°C with agitation.

## 2.4. Protein manipulation

### 2.4.1. SDS-PAGE

Protein samples destined for downstream analysis by western blot were first resolved by 55SDS-PAGE, a technique used to resolve proteins of interest (POI) from a crude mixture by size. All protein samples were denatured at 95°C for 5 minutes in 4X Laemmli's sample buffer (Bio-Rad) supplemented with 50mM DTT. Samples were subsequently resolved by SDS-PAGE using 4-15% pre-cast gradient gels (Table 2) for approximately 1.5 hours at a constant 100V in SDS running buffer (25mM Tris-HCl, pH 8.3, 190mM glycine and 1% (w/v) SDS).

### 2.4.2. Western blotting

Electrophoresed proteins were transferred onto Immobilon-FL (Merck Millipore) PVDF using the Mini Trans-Blot system (Bio-Rad). Transfers were performed on ice for 70 minutes at 80V in SDS-transfer buffer (Table 3). To evaluate transfer efficiency, membranes were stained in Ponceau S (Thermo Fisher Scientific), briefly rinsed in dH20 to remove excess staining solution, and imaged on a ChemiDoc Imaging System (Bio-Rad) using the colorimetric function. Before blocking, membranes were de-stained in repeated washes of TBS-T for 15 minutes. Membranes were blocked in TBS-T supplemented with 5% (v/v) BSA (BOVOGEN Biologicals) for 30 minutes at room temperature.

## 2.5. ADR1G233 peptide activity assay of PSKH1

The *in vitro* kinase activity of PSKH1 was measured by its propensity to incorporate phosphorous-32 ($^{32}$P) into the ADR1G233 peptide. The ADR1G233 peptide (LKKLTRRASFSGQ) is derived from the yeast transcriptional activator ADR1 and is an ideal peptide substrate for the closely related CaM-kinases, CaMK1 and CaMK4 [196].

### 2.5.1. Immobilised PSKH1-FLAG peptide assay

For radiometric assaying involving immobilised PSKH1-FLAG, 10μl ANTI-FLAG M2®/PSKH1-FLAG mixture was assayed in the presence of 5mM $MgCl_2$, 200μM [$\gamma$-32P]-ATP (PerkinElmer), 200μM ADR1G233 peptide substrate, with or without 100μM $CaCl_2$ and 1μM CaM to a total reaction volume of 25μl. The reaction was allowed to proceed for 10 minutes at 30°C for 10 minutes with agitation. To terminate the reaction, 15μl was spotted onto pre-cut squares of phosphocellulose paper (SVI) and submersed in 1% phosphoric acid. Following subsequent washes in 1% phosphoric acid to remove excess unbound [$\gamma$-32P]-ATP, phosphocellulose papers were air dried overnight and transferred to scintillation vials containing 4ml Ultima Gold LSC cocktail (PerkinElmer) and analysed on a liquid scintillator. Radioactivity (32P phosphate incorporation) was quantified by liquid scintillation counting. For studies interrogating functional differences between PSKH1-FLAG mutants, counts were corrected for differences in construct expression by SDS-PAGE/western blot.

### 2.5.2. GFP-PSKH1 peptide assay

PSKH1 peptide assays using purified, recombinant GFP-PSKH1 were carried out as previously described (2.5.1). 10μl immobilised PSKH1-FLAG was substituted with 10-100ng GFP-PSKH1.

# 3. INTERROGATING POTENTIAL MODULATORS OF PSKH1 ACTIVITY

## 3.1. Activation loop regulation of PSKH1

Kinases, from Ancient Greek κινεῖν ('to set in motion'), are aptly named – indeed, their role in coupling extracellular signals to tightly regulated signalling cascades appropriately positions this family of enzymes as master 'metabolic switches' amongst the compendium of proteins in the human body. Unsurprisingly, aberrant kinase activity is correlated with a growing number of human pathologies including cancer, neuropsychiatric conditions such as bipolar disorder [138] and endocrine disorders including Cushing's disease [197]. Fortunately, kinases have evolved a beautiful but complex interplay of regulatory mechanisms that serve to quench catalytic activity in the absence of an upstream activating signal. These include intrasteric autoinhibition of the substrate binding cleft and active site [11, 86, 87, 89, 198-202], allosteric regulation by small molecules including cyclic-AMP [203], long-chain fatty acid (LFCA)-CoA esters [204] and calmodulin (CaM) [14], regulatory modules that attenuate catalytic activity and, most notably, phosphorylation of conserved residues in a segment termed the 'activation loop'. The drastic conformational changes induced by activation loop phosphorylation are best demonstrated in the well-characterised cyclic-AMP-dependent protein kinase A (PKA) (Figure 3.1). Upon disengagement of the regulatory subunits in response to transient increases in intracellular cAMP levels, PKA is phosphorylated at Thr197 [205]. The addition of a single phosphate moiety on the activation segment dramatically alters the conformation of the catalytic architecture of PKA (Figure 3.1) [206]. For example, pT197 coordinates basic N- and C-lobe residues (His87, Arg165 and Lys189) through hydrogen bonding, stabilising the labile activation loop (Figure 3.1: *insert*) [206]. This enables the formation of a 'regulatory (R) spine' via packing of Phe185 into a hydrophobic pocket created by Leu95, Leu106 and Tyr164 (Figure 3.1: *yellow insert*) [207]. Collectively, these conformational changes stabilise the overall architecture of the kinase domain and potentiate the catalytic activity of PKA by correctly positioning key catalytic residues integral for phosphoryl transfer to occur (Figure

3.1: *table*). Alternatively, in the absence of an upstream activating signal, the dephosphorylated activation loops of the receptor tyrosine kinases InRK and FGFR sterically block the substrate binding cleft and active site [208, 209]. Irrespective of the specific mechanistic details, importantly, activation loop phosphorylation increases the catalytic activity of many protein kinases: 3-fold for PKA, 60-fold for BRSK1 and ~150-fold for CaMK1 [24, 42, 210].

Activation loop phosphorylation can be achieved autocatalytically, either *in cis* or *in trans*, or extrinsically by an upstream activating protein kinase [211]. Phosphorylation by heterologous protein kinases typically requires consensus electrostatic and hydrophobic interactions at the αD-helix of the upstream enzyme with residues that surround the recipient phosphorylation site of the substrate polypeptide (Figure 3.2). For example, PKA binds its endogenous peptide inhibitor, PKI, via salt-bridges between acidic residues that occupy (Glu127) and surround (Glu170 and Glu230) the αD-helix and basic residues on PKI (Arg18 and Arg19) (Figure 3.2: *Top panel, insert*) [93]. Specificity for PK1 is further enhanced by packing of Ile22 into a hydrophobic pocket on the C-lobe of PKA created by Leu205 and … (Figure 3.2: *Top panel, insert*) [93]. Collectively, these residues on PKI (Arg18, Arg19, Ile22) mimic the consensus phosphorylation motif for PKA (RRXS/TY, where X is any amino acid and Y is hydrophobic) [212]. Similarly, CaMK1's autoinhibitory domain (AID), it too a pseudosubstrate, straddles both lobes of the catalytic core with bonding chiefly concentrated at the αD-helix (Figure 3.2: *Bottom panel, insert*) [89]. As such, illuminating these kinase-kinase signalling relationships remains an area of intense research interest.

| Residue | Function |
|---------|----------|
| H87 | Basic, tethers C-helix to pT197 |
| L95 | Hydrophobic, constituent of R-spine |
| L106 | Hydrophobic, constituent of R-spine |
| Y164 | Hydrophobic, constituent of R-spine |
| R165 | Basic, xRD motif, H-H bonding with pT197 |
| D166 | Acidic, xRD motif, base catalysed attack of protein substrate –OH group |
| D184 | Acidic, DFG motif, coordinates $Mg^{2+}$ |
| F185 | Hydrophobic, DFG motif, constituent of R-spine |
| K189 | Basic, H-H bonding with pT197 |
| T195 | H-H bonding with pT197 |
| pT197 | Phosphorylation site |

***Figure 3.1. Activation loop phosphorylation stabilises the catalytic architecture of PKA.*** *Top panel.* Surface representations of PKA catalytic subunit in complex with the endogenous peptide inhibitor (PKI) [206]. Lobes and selected subdomains are shown as ribbon structures and coloured as follows: blue: PKI; white: N-lobe; black: subdomain V (linker region); dark grey: C-lobe; lime green: activation loop. *Insert.* Activation loop phosphorylation of T197 coordinates the catalytic machinery of PKA and enables the formation of a regulatory (R) spine (*yellow insert*); hydrogen bonding: dashed lines. *Table.* Conserved residues of PKA kinase domain. Cyan: basic; yellow: hydrophobic; orange red: acidic; green: activation loop; cornflower blue: phosphorylation site. Structures were manipulated on ChimeraX using publicly available crystal structures from the Protein Data Bank (PDB ID: 2cpk).
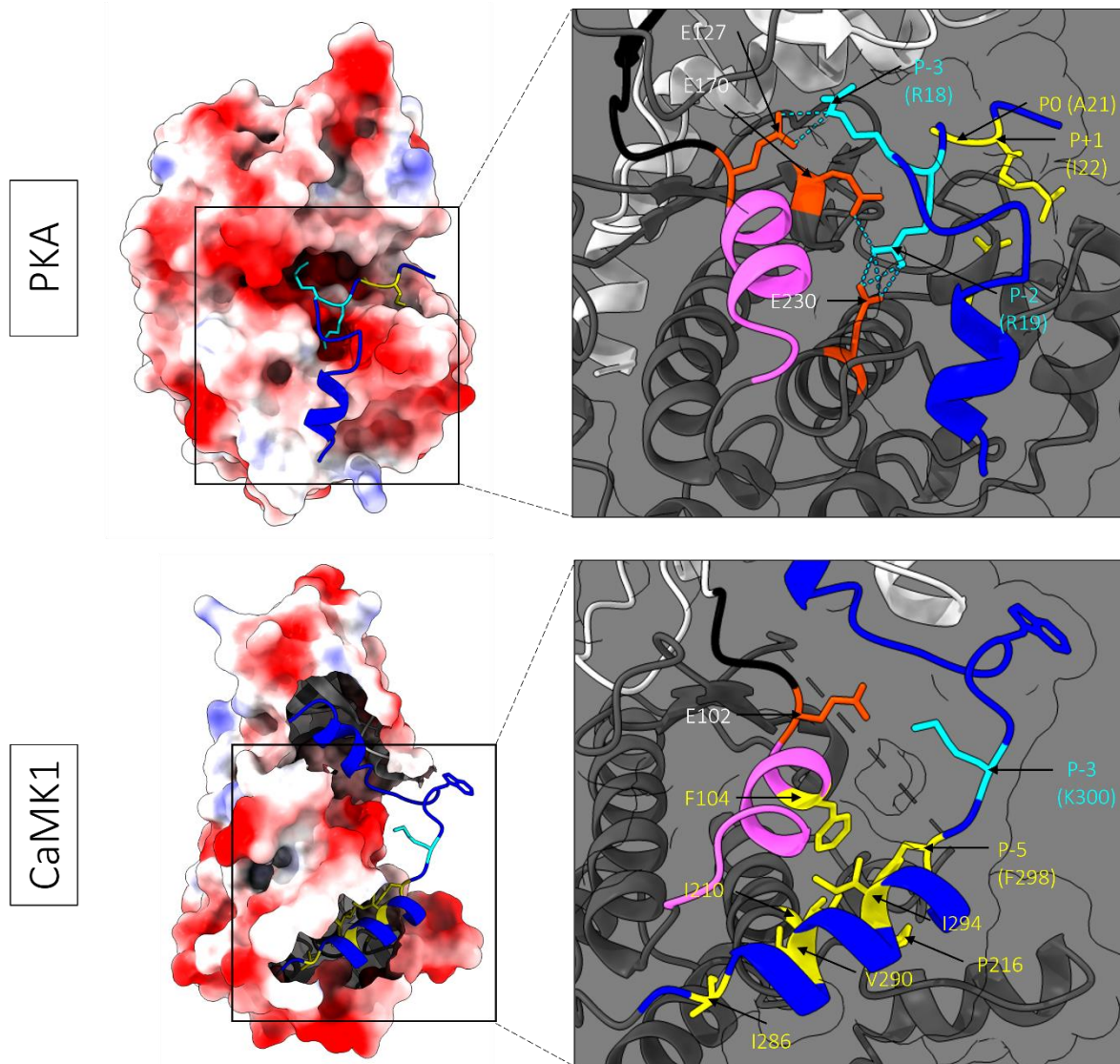
***Figure 3.2. Protein kinase substrate determination is largely determined by consensus electrostatic and hydrophobic interactions between the αD-helix and substrate polypeptide.*** *Top*. PKA is a basophilic kinase. Electrostatic potential map of PKA catalytic core in complex with inhibitor peptide (PKI) [93]. *Top: insert*. PKA binds PKI (dark blue) via electrostatic and hydrophobic interactions at the αD-helix (magenta), visualised as ribbon structures. Highlighted residues and subdomains are coloured as follows: white: N-lobe; black: linker region; orange red: acidic residue; cyan: basic residue; yellow: hydrophobic residue; dashed lines: salt bridge. *Bottom*. CaMK1 is a basophilic kinase. Electrostatic potential map of autoinhibited CaMK1 [89]. *Bottom: insert*. The overlapping AID/CBD (dark blue) of CaMK1, C-terminal to and contiguous with the catalytic core, straddles both lobes of the kinase domain in the absence of $Ca^{2+}$/CaM. Bonding is facilitated by electrostatic and hydrophobic interactions between the AID/pseudosubstrate and the αD-helix. Colouring is as above. Structures were modified on ChimeraX using publicly available data from the Protein Data Bank (PDB ID: PKA: 2cpk; CaMK1: 1a06).

The serine/threonine-protein kinase H1 (PSKH1) has recently emerged as a top-6 candidate driver of prostate cancer progression [6]. However, the precise signalling mechanisms that regulate this kinase have not been investigated. Sequence analysis of PSKH1's activation segment reveals striking similarity to CaMK1, CaMK4 and the AMP-activated protein kinase (AMPK) (Figure 3.3: *Middle panel*), known substrates of CaMKK2 [11]. This observation is corroborated by the kinase prediction tool on PhosphoSitePlus, which ranks the CaMKKs as the top two candidate upstream activating kinases for PSKH1's activation segment (Figure 3.3: *Bottom panel*) [213]. Unlike other CaMK family members, CaMKK2 is unique in that it lacks an αD-helix (Figure 3.3: *Top panel*) [214]. In its place, CaMKK2 possesses a highly hydrophobic β5-αE loop (Figure 3.3: *Insert*). The conserved P-3 interacting acidic residue on PKA, Glu127, is replaced by Pro274 in CaMKK2. Further, Glu170 and Glu230, which collectively bond with the P-2 basic residue present on PKA substrates, are substituted by the polar uncharged and neutral amino acids Ser316 and Cys382, respectively (Figure 3.3: *Top panel*). Consequently, CaMKK2 has a strong tropism for activation loops with hydrophobic binding interfaces [214]. Interestingly, AlphaFold2 simulations of CaMKK2:AMPK-α1, a known activation loop substrate of CaMKK2, and CaMKK2:PSKH1 bear striking similarity (Figure 3.4). Collectively these observations implicate a probable role for CaMKK2-mediated activation loop regulation of PSKH1.
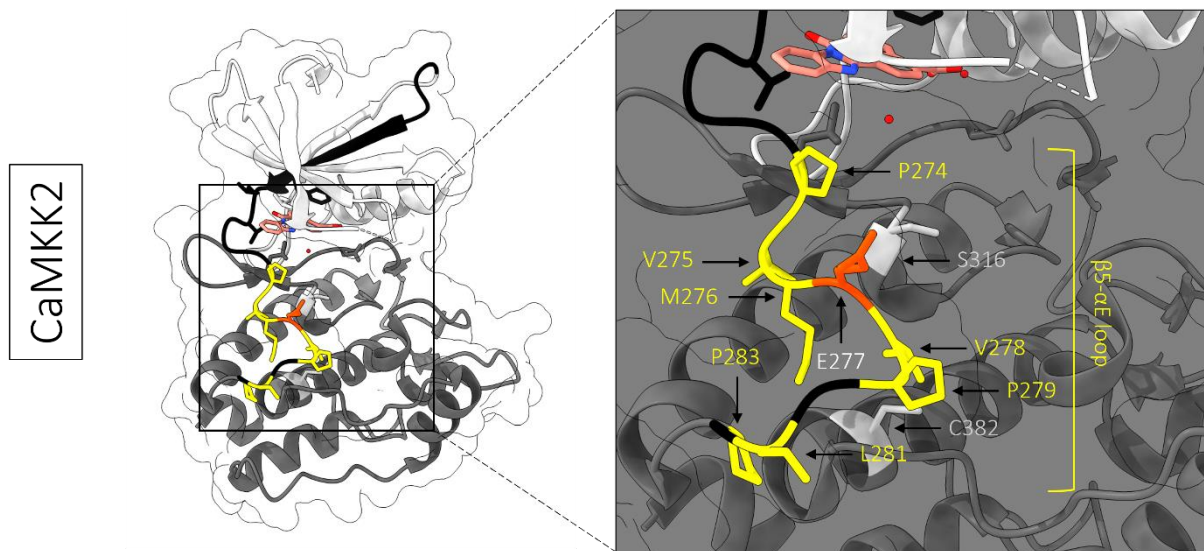
| CaMKKTide: | LSNLYHQGKFLQ**t**FCGAPLYRRR | |
|---|---|---|
| | *P–* *P+* | |
| | 4321 1234 | |
| CaMK1 | DFGLSKMED--PGSVLS**t**ACGTPGYVAPE | 188 |
| CaMK4 | DFGLSKIVE--HQV<u>LMK</u>**t**VCGTPGYCAPE | 211 |
| AMPK, α1 | DFGLSNMMS--DGEFLR**t**SCGSPNYAAPE | 194 |
| PSKH1 | DFGLASARKKGDDC<u>LMK</u>**t**TCGTPEYIAPE | 267 |

**Site sequence**

position: -5 -4 -3 -2 -1 0 1 2 3 4 5 6
sequence: D C L M K S/T T C G T P E

Show 50 ⌄ entries                                          Search: _____

| | kinase | kinase group | log₂(score) | site percentile | percentile rank |
|---|---|---|---|---|---|
| ⊕ | CAMKK1 | Other | 2.468 | 99.886 % | 1 |
| ⊕ | CAMKK2 | Other | 2.360 | 99.854 % | 2 |

***Figure 3.3. PSKH1 is a putative substrate of CaMKK2.*** *Top.* Ribbon diagram of hCaMKK2 kinase domain in complex with the small molecule inhibitor STO-609 [214]. *Insert.* Residues of the overlapping linker region (black)/β5-αE loop are coloured as follows: yellow: hydrophobic; orange red: acidic; medium grey: Ser316 and Cys382 (PDB ID: 2ZV2). *Middle.* UNIPROT sequence alignment of CaMKK2 synthetic peptide (CaMKKTide) and known (hCaMK1, hCaMK4, hAMPK) and unknown (hPSKH1) substrates of CaMKK2. Conservation of hydrophobic residues in the P-2 and P-3 positions in PSKH1 indicative of a CaMKK2 phosphorylation site. *Bottom.* The PSKH1 activation loop site sequence (DCLMKT*TCGTPE) was submitted to the kinase prediction tool on PhosphoSitePlus.
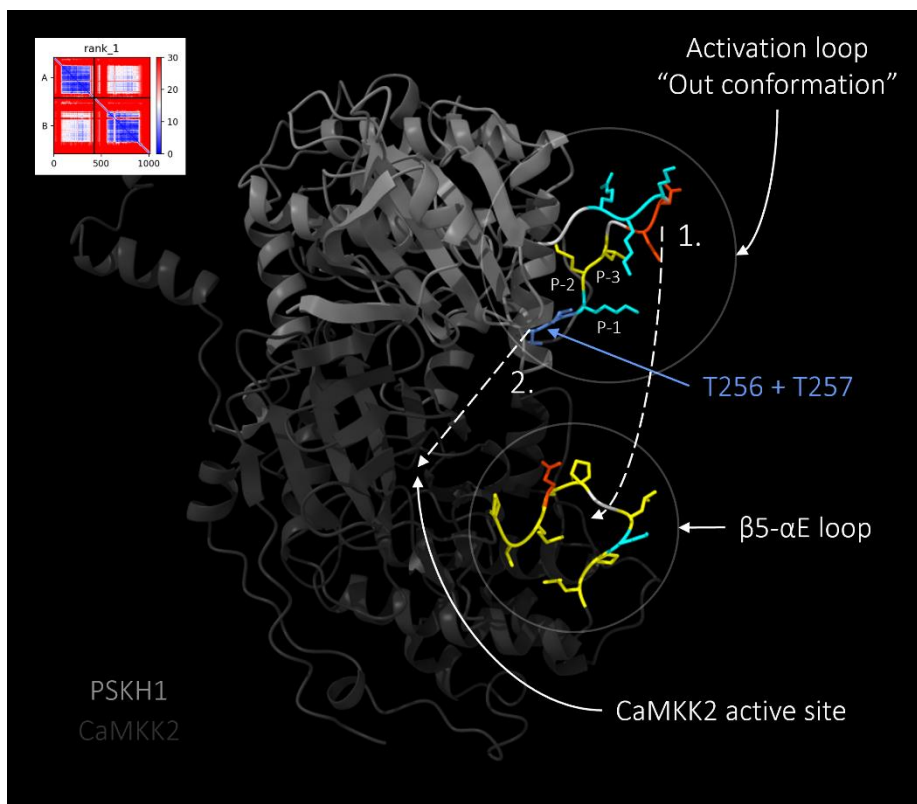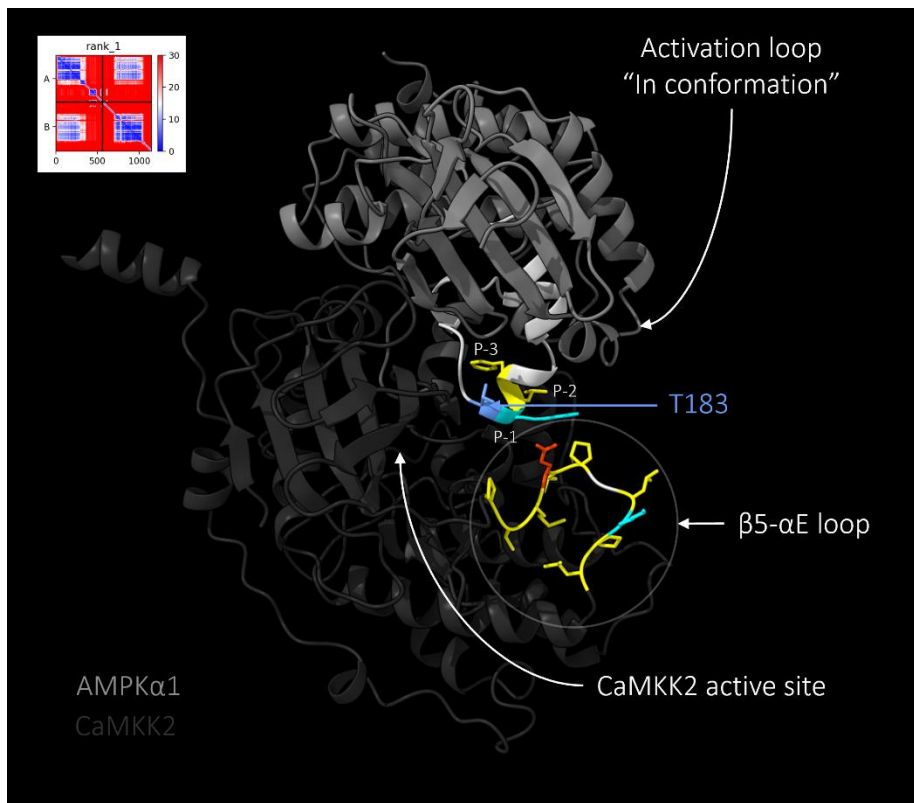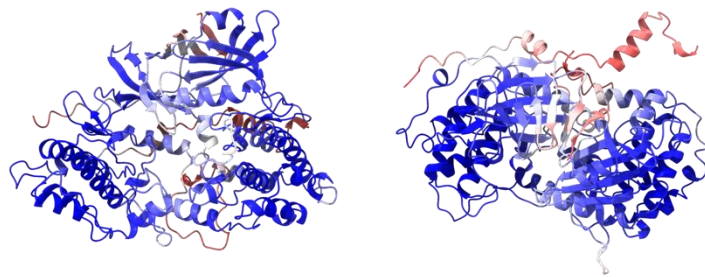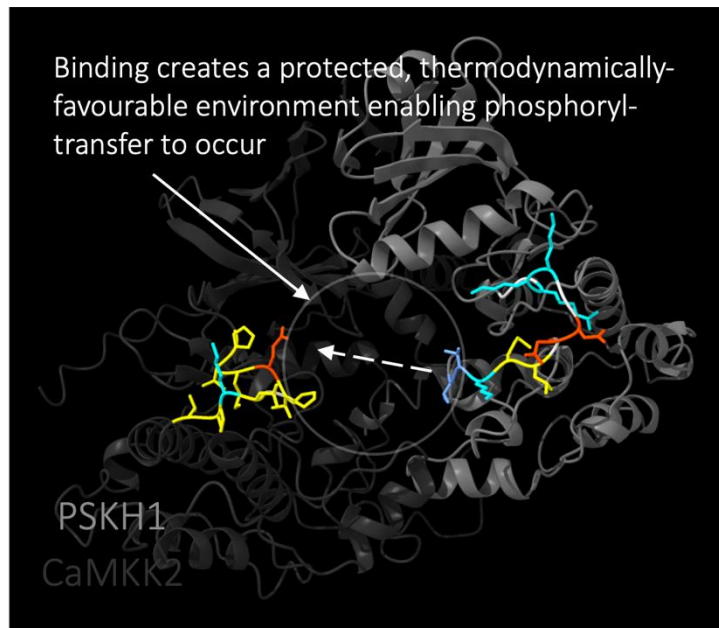
*Figure 3.4. An AlphaFold2 CaMKK2:PSKH1 docking simulation bears striking similarity to CaMKK2:AMPK, a known activation loop substrate of CaMKK2.* Full-length protein sequences of human CaMKK2, AMPK-α1 and PSKH1 (derived from UNIPROT) were submitted to the ColabFold v.1.5.2 Google Colaboratory notebook. Docking simulations between CaMKK2:AMPKα1 (*Top panel*) and CaMKK2:PSKH1 (*Bottom panel*) were run with 3 recycles using the MMseqs2 multiple sequence alignment (MSA) method. 5 protein complexes were generated per docking simulation. The highest-scoring structures are shown. Non-catalytic quaternary structure (N- and C-termini) has been omitted for clarity. Kinase domains are shown (top-down perspective). *Inserts, top left.* Predicted aligned error (PAE) plots for each respective protein:protein simulation. *CaMKK2:AMPKα1.* The CaMKK2 β5-αE loop makes putative electrostatic and hydrophobic contacts with the P-1 and P-2 residues of the AMPKα1 activation loop, coordinating the recipient phosphorylation site (T183) to the active site of CaMKK2. *CaMKK2:PSKH1.* Like CaMKK2:AMPKα1, CaMKK2 docks PSKH1 primarily through catalytic domain contacts (*Insert, top left, PAE plot*). Residues are coloured as follows: yellow: hydrophobic; cyan: basic; orange red: acidic; cornflower blue: recipient phosphorylation site/s. AlphaFold2 ColabFold v.1.5.2 simulated structures of CaMKK2:PSKH1 (*below panels*) are coloured by pLDDT score.

### 3.1.1. Aims

The precise signalling mechanisms that regulate PSKH1 have not been investigated. Given the presence of a putative CaMKK2 phosphorylation consensus sequence in PSKH1's activation segment, the aim of this subchapter was to interrogate activation loop regulation of PSKH1. CaMKK2 and candidate upstream activating kinases, identified by sequence analysis and mass spectrometry proteomics, were probed for their ability to phosphorylate PSKH1 *in vitro* by radiometric assay or by western blot analysis.

### 3.1.2. Materials & Methods

#### 3.1.2.1. Reagents and resources

Recombinant GFP-PSKH1, PAK1, RCN1, RNC3, Calumenin and untagged CHK2 were generously provided by Dr. Chris Horne (WEHI). CaM stocks were similarly provided by Dr. Chris Horne (WEHI).

#### 3.1.2.2. *In vitro* phosphorylation assay

10μl purified PSKH1-FLAG transiently expressed in HEK293T cells was phosphorylated in the presence or absence of 500ng upstream enzyme, 200μM ATP, 5mM $MgCl_2$, 100μM $CaCl_2$ and 1μM CaM (unless stipulated otherwise) at 30°C for 0-60 minutes. Kinase activity was arrested by the addition of 4X Laemmli sample buffer containing 50mM DTT and subsequent denaturation at 95°C for 5 minutes. Phosphorylation of PSKH1 was inferred by western blot using α-mouse phospho-threonine (pThr, CST) and α-mouse IRDye® 800CW infrared secondary (LI-COR) antibodies. Phosphorylated protein was normalised to total protein using α-rabbit DYKDDDDK Tag or α-rabbit GFP (CST) and α-rabbit IRDye® 680RD infrared secondary (LI-COR) antibodies.

#### 3.1.2.3. Immobilised *in vitro* phosphorylation assay

20μl PSKH1-FLAG:ANTI-FLAG M2® bead mixture immunoprecipitated from >1ml WCL was phosphorylated in the presence or absence of 500ng enzyme (PAK1), 200μM ATP, 5mM

MgCl$_2$, 100μM CaCl$_2$ and 1μM CaM at 30°C for 0-45 minutes with agitation (900 RPM) on a benchtop shaker. To terminate the reaction, the mixture was pelleted by centrifugation at 8200g for 3 minutes to pellet the bead-immobilised PSKH1 fraction and to allow subsequent washing (1M 'high-salt', 150mM 'low-salt' and HEPES pH 7.4) to remove contaminating PAK1 from further downstream analysis. Clarified PSKH1 was eluted overnight in 30μl 1mg/ml FLAG peptide (Genscript) at 4°C with rotation. Phosphorylation was detected as previously described. Impact of activation loop phosphorylation on PSKH1 activity was assessed by radiometric kinase assay (Chapter 2.5).

### 3.1.2.4. Concentration dependence studies

To interrogate the mechanism by which PSKH1 autophosphorylates, increasing concentrations of GFP-tagged PSKH1 (50-400ng) were permitted to autophosphorylate in the presence of absence (HEPES buffer) of Mg$^{2+}$ATP for 0-60 minutes. Kinase activity was quenched via addition of 4X Laemmli sample buffer supplemented with 50mM DTT. Phosphate incorporation was inferred via western blot, as previously described. In experiments where kinase activity of autophosphorylated GFP-PSKH1 was measured by radiometric peptide assay (Chapter 2.5), sample buffer was excluded.

### 3.1.2.5. LC-MS/MS analysis of autophosphorylated PSKH1

Liquid chromatography/mass spectrometric analysis of *in vitro* autophosphorylated GFP-PSKH1 was undertaken with the assistance of Dr. Toby Dite from the Walter and Eliza Hall Institute of Medical Research (WEHI).

### 3.1.3. Results

#### 3.1.3.1. CaMKK does not phosphorylate PSKH1-FLAG on threonine residues *in vitro*

To determine if CaMKK2 phosphorylates the activation segment (T256) of PSKH1, initial *in vitro* phosphorylation experiments were undertaken. As no phospho-specific antibodies targeting the T256 activation loop site in PSKH1 are commercially available, a generic phospho-threonine antibody (CST) was utilised. Constructs encoding wild-type PSKH1 (PSKH1-FLAG), an activation loop PSKH1 point mutant (PSKH1 T256A-FLAG) and GFP-CaMK4-FLAG (CaMKK substrate positive control) were transiently expressed in HEK293T cells and immunoprecipitated from whole cell lysate, as previously described. Unlike GFP-CaMK4-FLAG, which demonstrated a CaMKK2 and $Ca^{2+}$/CaM-dependent increase in pThr immunoreactivity over time (indicative of Thr200 *trans* phosphorylation by CaMKK2 – Figure 3.5, A), PSKH1-FLAG was completely non-reactive (Figure 3.5, B). As expected, an activation loop point mutant of PSKH1 whose recipient phosphorylation site (T256) was mutated to alanine (A) was not phosphorylated in the presence of CaMKK2 (Figure 3.5, C). CaMKK1 is closely related to CaMKK2 and phosphorylates the CaMKK2 substrates, CaMK1 and CaMK4 [17, 18]. Thus, CaMKK1-FLAG, expressed and purified from HEK293T cells, was also assayed for its ability to phosphorylate PSKH1's activation segment. Similarly, PSKH1-FLAG was also non-reactive to pThr antibody in the presence of CaMKK1-FLAG (Figure 3.5, E). Corroborating these reports, later *in vitro* phosphorylation experiments utilising GFP-PSKH1 failed to demonstrate pThr immunoreactivity on incubation with CaMKK2 (Supp. Fig. 3.5.1). These data collectively indicate that PSKH1 is likely not an endogenous substrate of the CaMKK family of protein kinases, as had originally been presumed. However, it is important to consider that the generic pThr antibody may not recognise a phosphorylated PSKH1 at the T256 site. This is a considerable limitation of this study, exacerbated by the unavailability of a pThr256-specific antibody at the time of experimentation. Future studies should incorporate

mass spectrometric analysis to holistically characterise phosphorylation of this residue by CaMKK2 and other putative upstream kinases.
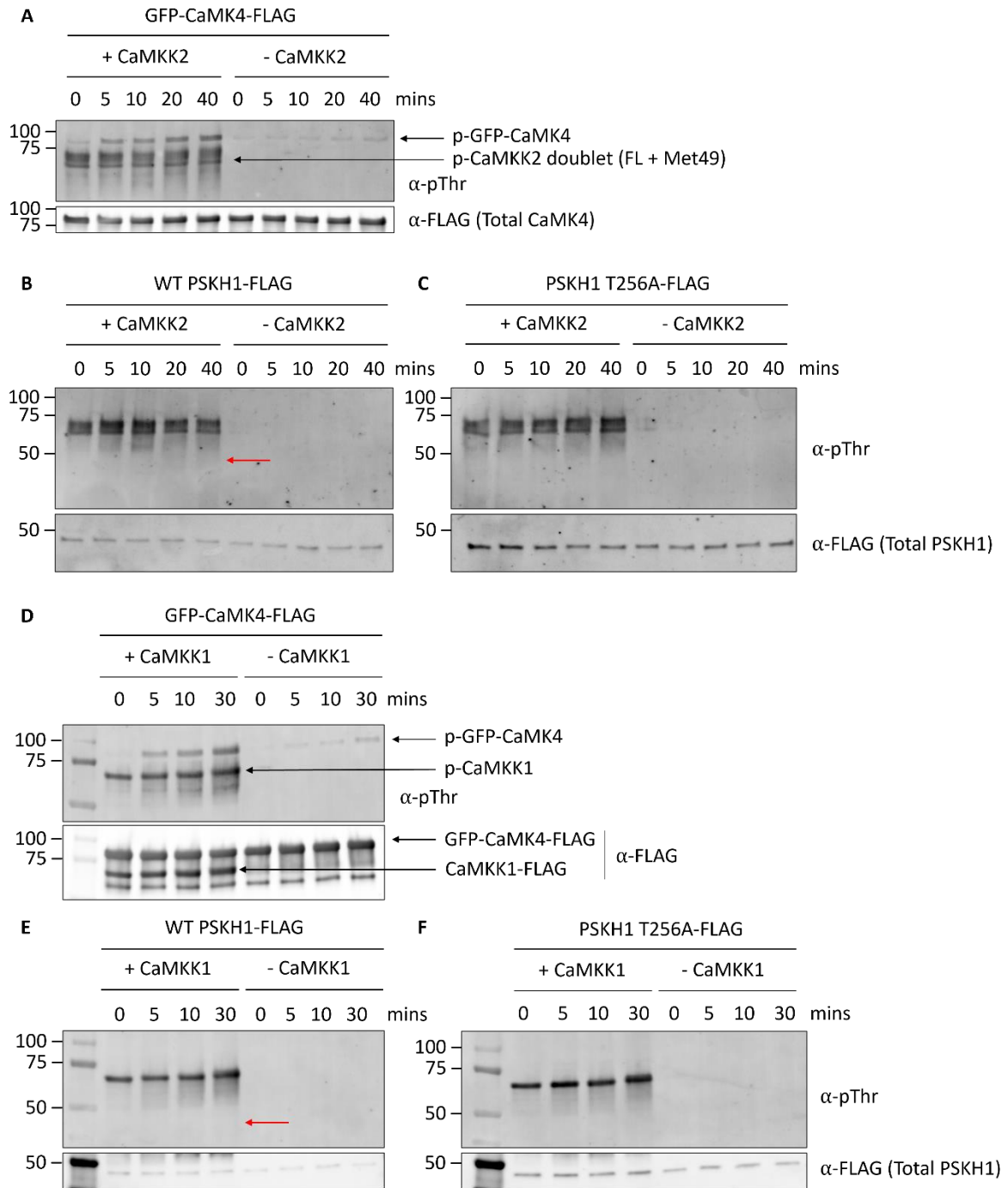
*Figure 3.5. CaMKK2/CaMKK1-FLAG do not phosphorylate PSKH1-FLAG on threonine residues in vitro.* Recombinant WT GFP-CaMK4-FLAG (positive control), WT PSKH1-FLAG or a T256A-FLAG point mutant were immunoprecipitated from transiently transfected HEK293T WCL using an Anti-FLAG® M2 Affinity Gel. Eluted material was phosphorylated in the presence or absence of 500ng recombinant CaMKK1-FLAG (D-F) or CaMKK2-FLAG (A-C) over a maximal period of 40 minutes. Activation loop phosphorylation was inferred by subsequent SDS-PAGE and western blot using α-mouse phospho-threonine (42H4) and α-rabbit FLAG (D6W5B) primary antibodies and α-rabbit IRDye® 680RD and α-mouse IRDye® 800CW near-infrared secondary antibodies. Expected phosphorylated PSKH1 bands are indicated by red arrows. Three independent experiments were performed (n=3). Representative blots are shown. CaMKK1-FLAG and CaMKK2-FLAG preparations were purified from transiently transfected HEK293T whole cell lysate using anti-FLAG® M2 Affinity Gel and eluted overnight using FLAG peptide.

### 3.1.3.2. PAK1 does not phosphorylate the activation loop of PSKH1-FLAG *in vitro*

Concurrent proximity labelling experiments utilising PSKH1-TurboID fusion constructs identified various interacting partners of PSKH1, including p-21 activated protein kinase (PAK) (Dr. Chris Horne, Dr. Toby Dite, unpublished). Like PSKH1, PAK is frequently dysregulated in prostate cancer [215]. To interrogate whether PAK1 activates PSKH1 by phosphorylating its activation loop, PSKH1-FLAG or an activation loop point mutant (T256A) were transiently expressed in HEK293T cells and immunoprecipitated from WCL, as previously described. Immobilised PSKH1-FLAG:α-FLAG M2® bead mixture was phosphorylated in the presence or absence of PAK1, supplemented with 200μM ATP, 5mM MgCl$_2$, 100μM CaCl$_2$ and 1μM CaM. PAK1 presumably phosphorylates the PSKH1 peptide ADR1G233, based on sequence homology of the kinase catalytic core. Unfortunately, due to time constraints, phosphorylation of the ADR1G233 peptide by PAK1 was not investigated. Irrespectively, to remove contaminating PAK1 from downstream analysis and to terminate the reaction, immobilised PSKH1-FLAG was briefly centrifuged and successively rinsed in wash buffers followed by overnight elution in 1mg/ml FLAG peptide. Phosphorylation of PSKH1 was inferred by SDS-PAGE and western blot. As demonstrated, incubation with recombinant PAK1 did not induce pThr immunoreactivity in PSKH1-FLAG or, as expected, a T256A point mutant (Figure 3.6). These data strongly suggest that the conditions tested do not support

PSKH1 activation and further, that PAK1 is unlikely to be an upstream activating kinase for

PSKH1-FLAG.
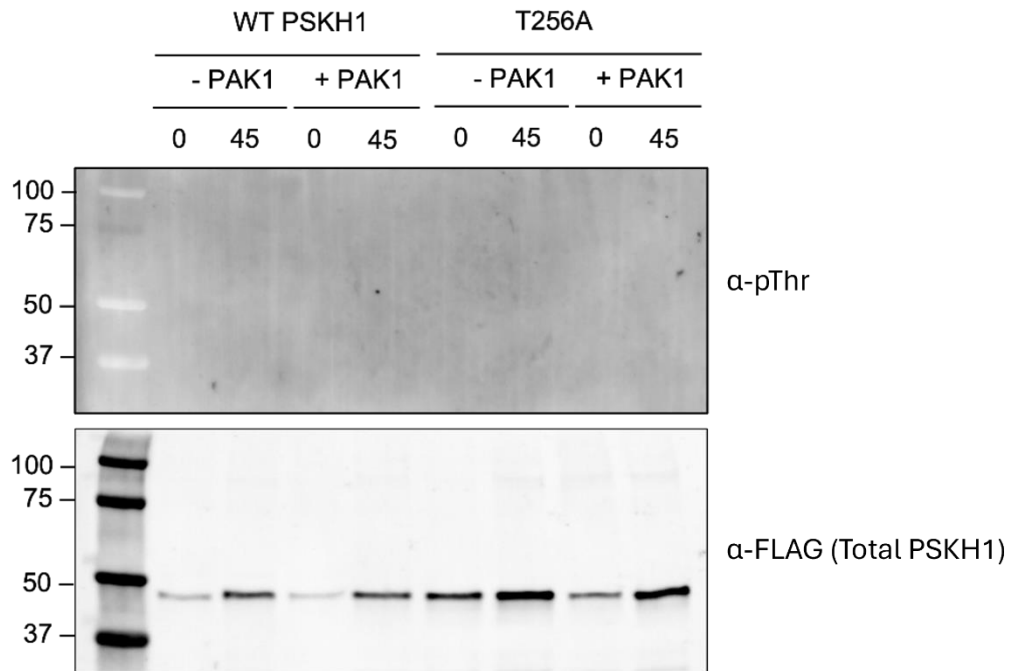


***Figure 3.6. PAK1 does not phosphorylate PSKH1-FLAG on threonine residues in vitro.*** 20μl
PSKH1-FLAG:α-FLAG M2® bead mixture immunoprecipitated from >1ml WCL was
phosphorylated in the presence or absence of 500ng recombinant PAK1, 200μM ATP, 5mM
$MgCl_2$, 100μM $CaCl_2$ and 1μM CaM at 30°C for 0-45 minutes with gentle agitation (900 RPM)
on a benchtop shaker. To terminate the reaction, the mixture was pelleted by centrifugation at
8300g for 3 minutes and subsequently washed in high-salt and low-salt wash buffers (Table
2.1.2. Buffers) to remove contaminating PAK1 from further downstream analysis. Clarified
PSKH1 was eluted overnight in 30μl 1mg/ml FLAG peptide at 4°C with rotation. Activation
loop phosphorylation of PSKH1 was inferred by SDS-PAGE/western blot using an α-mouse
p-Thr antibody and an activation loop point mutant (PSKH1-T256A) as a negative control.
Total PSKH1-FLAG was determined using an α-rabbit FLAG antibody. Three independent
experiments were performed (n=3). A representative blot is shown.

### 3.1.3.3. Evaluating CHK2 as a candidate upstream activating kinase of PSKH1

To identify the as-yet elusive upstream activating kinase of PSKH1, the checkpoint kinase 2 (CHK2) was selected for further interrogation. CHK2 is a critical effector of the DNA damage response (DDR) pathway which, frequently, is dysregulated in cancer. Like PSKH1, mutations in CHK2 correlate with prostate cancer progression [216]. CHK2 is phosphorylated at Thr68 by the phosphatidylinositol kinase-like kinase ataxia telangiectasia mutated (ATM), which promotes its association into a transient homodimer [217, 218]. Oligomerised CHK2 autophosphorylates at Thr383 and Thr387, which maximally activates this protein kinase [219, 220]. Structural studies revealed that CHK2 autophosphorylates *in trans* by T-loop exchange [221]. T-loop exchange is facilitated by CHK2's uniquely rigid activation segment which extends outward from the body of the kinase domain (Figure 3.7). The stable and extended conformation of CHK2's activation loop allows transiently oligomerised CHK2 homodimers to 'handshake' each other and phosphorylate the opposing CHK2 monomer activation segment *in trans* (Figure 3.8, *Kinase schematic*). Interestingly, sequence alignment of CHK2's activation segment bears striking similarity to CaMK4 and PSKH1 (Figure 3.8). It was therefore reasoned that, if CHK2 can phosphorylate its own activation loop *in trans*, can it therefore phosphorylate the activation loop(s) of CaMK4 and principally, PSKH1. Further, CHK2's activation segment harbours a hydrophobic cluster of amino acids C-terminal to the recipient T183 and T187 phosphorylation sites (Figure 3.7). This putative 'hydrophobic substrate binding motif' (HSBM) bears striking similarity to substrate interfacing residues residing in CaMKK2's β5-αE loop (Figure 3.7). Collectively, these observations strongly indicated that CHK2 may be an upstream activating kinase of PSKH1. CHK2 was interrogated for its ability to phosphorylate the activation loop of PSKH1 by *in vitro* phosphorylation assay. Full-length CHK2 (Chk2-FL) or a kinase domain truncation mutant (Chk2-KD, negative control) did not phosphorylate PSKH1 *in vitro* (Figure 3.8). Strikingly, GFP-PSKH1

autophosphorylated, as determined by the time-dependent increase in pThr immunoreactivity in the presence of $Mg^{2+}ATP$ (Figure 3.8). This phenomena was not observed in experiments utilising full-length CHK2 due to occlusion of the autophosphorylated PSKH1 band (GFP-PSKH1 and full-length CHK2 are of comparable size). We decided to incorporate alternatively-tagged PSKH1 (GFP-PSKH1) over PSKH1-FLAG due to the comparatively poor activity of PSKH1-FLAG observed in *in vitro* radiometric kinase assays (for example, Figures 3.17 and 3.19, high nmol versus low pmol, respectively). Autophosphorylation at threonine residues has not previously been reported for PSKH1. Indeed, differentially tagged PSKH1 (PSKH1-FLAG) showed no time-dependent increase in pThr immunoreactivity in the presence of $Mg^{2+}ATP$ in previous experimentation (Figures 3.5/3.6). These data collectively indicate that the location and biochemical characteristics of the respective epitope tag may impact the catalytic activity and/or substrate binding interface of PSKH1. Alternatively, the different expression systems used (suspension culturing of GFP-PSKH1 expressing SF9 cells versus adherent culturing of mammalian HEK293T cells) may differentially affect the catalytic activity of PSKH1. To account for these observations, CaMKK2 as an upstream activating kinase of PSKH1 was revisited. To prevent autophosphorylation of PSKH1 in the presence of $Mg^{2+}ATP$, a kinase dead point mutant (GFP-D218N) was employed. As expected, a dually tagged splice variant of CaMKK2 (GFP-CaMKK2.7-FLAG) immunoprecipitated from transiently transfected HEK293T WCL phosphorylated GFP-CaMK4-FLAG, a known substrate of CaMKK2, in a time and $Ca^{2+}$/CaM-dependent manner (Supplementary Figure 3.5.1). Conversely, although GFP-PSKH1-D218N was basally phosphorylated, GFP-CaMKK2.7-FLAG did not phosphorylate GFP-D218N, as indicated by the absence of additive pThr immunoreactivity on addition of GFP-CaMKK2.7-FLAG. These data collectively validate that PSKH1 is likely not an endogenous substrate of CaMKK2 or CHK2. Importantly, PSKH1 autophosphorylates on threonine residues (Figure 3.8).

CHK2 kinase domain crystal structure (PDB ID: 2w0j)

CHK2 N & C-lobes of kinase domain

ATP cleft

T383

T387

CHK2 activation loop

Core binding motif?

Chk2 'HSBM'    YLAPTVLVSVGTA

CaMKK2 β5-αE loop    GPVMRVPTLKPLS

AlphaFold2 PSKH1

Top-down

Substrate cleft?

Top-down

Side    Substrate cleft?
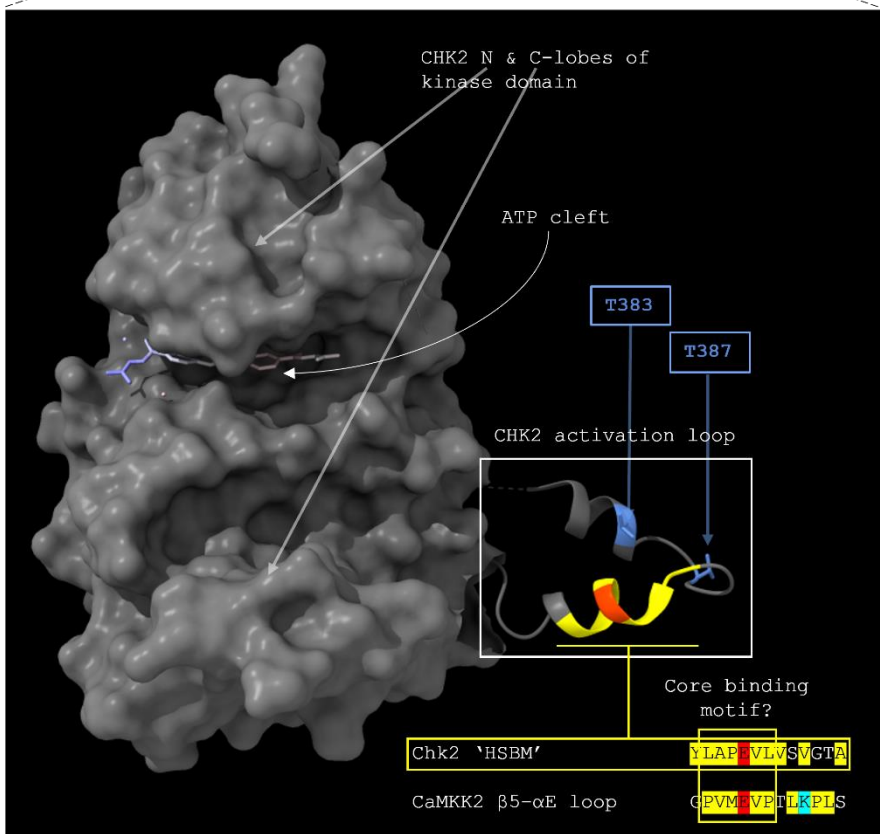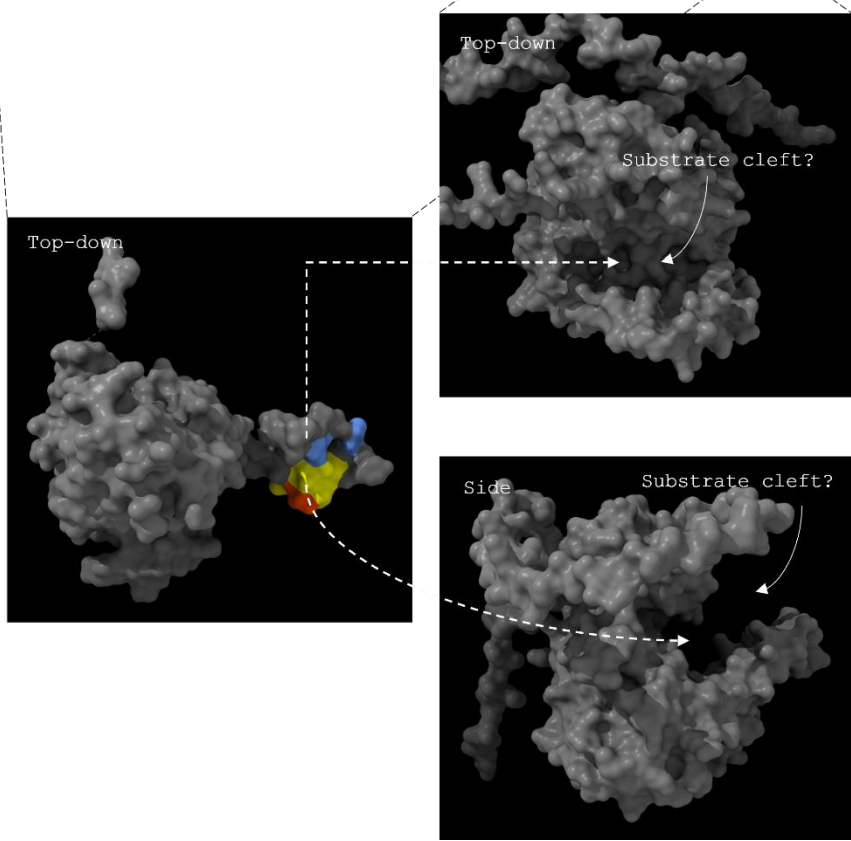
*Figure 3.7. A hypothetical mechanism for CHK2-mediated activation loop phosphorylation of PSKH1.* CHK2 phosphorylates its activation loop *in trans* by T-loop exchange. *Large panel.* CHK2 kinase domain crystal structure in complex with a peptide inhibitor [222]. CHK2's rigid activation loop (boxed white) juts outward from the body of the kinase domain and facilitates *trans* autophosphorylation by T-loop exchange. CHK2's activation loop harbours a structural motif (boxed yellow) with primary and secondary sequence homology to CaMKK2's β5-αE loop. Residues are coloured as follows: yellow: hydrophobic; orange red: acidic; cornflower blue: activation loop phosphorylation site. *Small panels.* Top-down and side perspectives of CHK2 catalytic domain (*left*) and an AlphaFold2 simulation of full-length PSKH1.
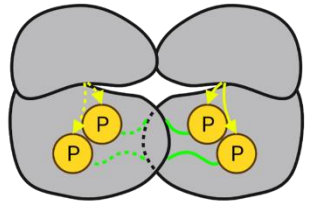
CHK2 *trans* autophos
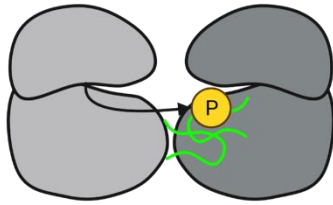
CHK2:PSKH1 *trans* phos?
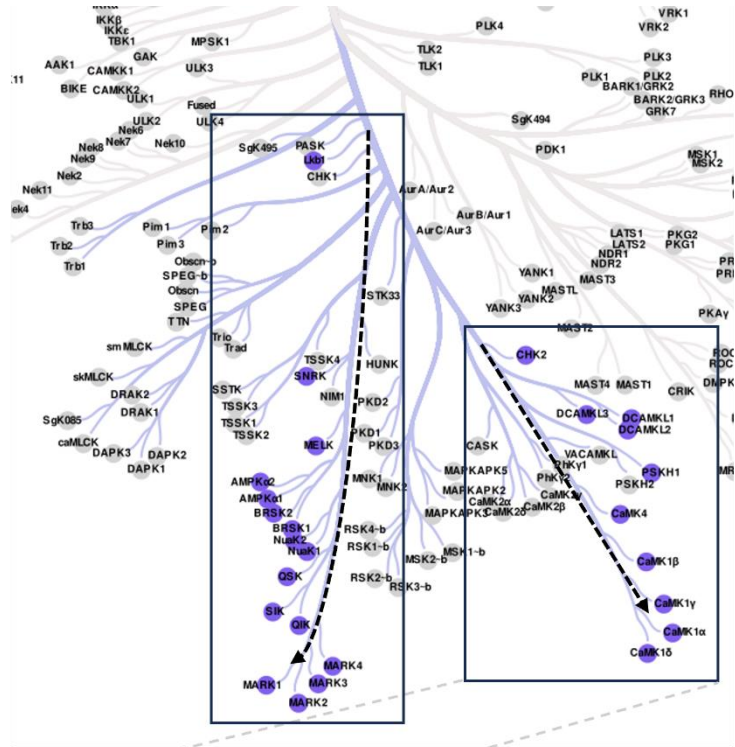
Activation loop

```
sp|O96017|CHK2_HUMAN   EDCLIKIT DFGHSKILGET--SLMRTLCGTPTYLAPE VLVSVGTAGYNRAVDCWSLGVIL   417
sp|O15075|DCLK1_HUMAN  GSKSLKLG DFGLATIVD----GPLYTVCGTPTYVAPE IIA---ETGYGLKVDIWAAGVIT   577
sp|Q8N568|DCLK2_HUMAN  GTKSLKLG DFGLATVVE----GPLYTVCGTPTYVAPE IIA---ETGYGLKVDIWAAGVIT   581
sp|Q9C098|DCLK3_HUMAN  KSTTLKLA DFGLAKHVV----RPIFTVCGTPTYVAPE ILS---EKGYGLEVDMWAAGVIL   543
sp|P11801|KPSH1_HUMAN  TDSKIIIT DFGLASARKKGDDCLMKTTCGTPEYIAPE VLV---RKPYTNSVDMWALGVIA   287
sp|Q16566|KCC4_HUMAN   PDAPLKIA DFGLSKIVEHQ--VLMKTVCGTPGYCAPE ILR---GCAYGPEVDMWSVGIIT   231
sp|Q14012|KCC1A_HUMAN  EDSKIMIS DFGLSKMEDPG--SVLSTACGTPGYVAPE VLA---QKPYSKAVDCWSIGVIA   208
```

P-3
P-2
P-1
P-0

Chk2-FL    -  -  -  -  -  -  -  -      +  +  +  +  +  +  +  +
Ca²⁺/CaM   -  -  -  -  +  +  +  +      -  -  -  -  +  +  +  +

0  1  5  15  0  1  5  15    0  1  5  15  0  1  5  15   mins

100 —
75 —
50 —

α-pThr
pCHK2 FL

100 —
75 —
50 —

α-GFP (Total PSKH1)

Chk2-KD    -  -  -  -  -  -  -  -      +  +  +  +  +  +  +  +
Ca²⁺/CaM   -  -  -  -  +  +  +  +      -  -  -  -  +  +  +  +

100 —
75 —
50 —

α-pThr

100 —
75 —
50 —

α-GFP (Total PSKH1)

97
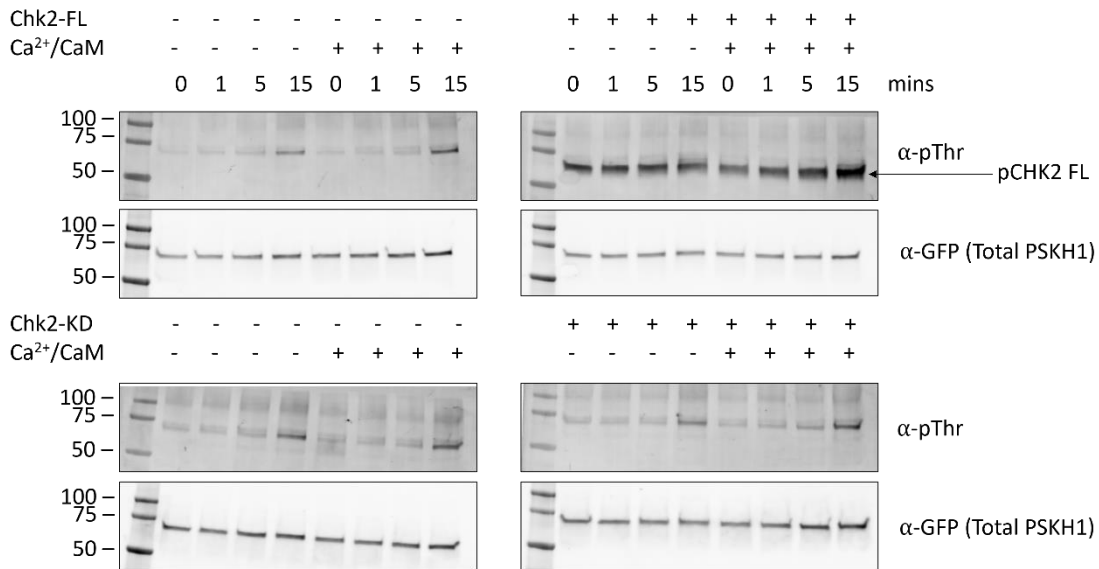
***Figure 3.8. Evaluating CHK2 as a candidate upstream activating kinase of PSKH1.*** *Kinase schematic.* CHK2 (light grey) autophosphorylates its activation loop *in trans* by T-loop exchange [221]. *Kinome tree.* The ancient CaM-kinase LKB1 phosphorylates the activation loops of 13 members downstream on the Manning kinome tree (*left insert*) [41]. Cyan: CaMK family. The phylogenetic tree graphic was prepared using Coral [10]. *Sequence alignment.* The activation segments of DCLK1, DCLK2, DCLK3, PSKH1, CaMK4 (KCC4) and CaMK1 (KCC1A) bear striking similarity to CHK2. UNIPROT sequence alignment of the activation loops of CaMK family members downstream and inclusive of CHK2. The recipient phosphorylation site (T) and surrounding consensus residues are coloured as follows: yellow: hydrophobic; blue: basic; P-0: phosphorylation site. *Western blot*s. Full-length CHK2 (Chk2-FL) or a kinase domain truncation mutant (Chk2-KD) do not phosphorylate GFP-PSKH1 *in vitro*. 500ng GFP-PSKH1 was phosphorylated in the presence of 25ng Chk2-FL, 25ng Chk2-KD, with or without 100µM $Ca^{2+}$/1µM CaM. Phosphorylation of GFP-PSKH1 was subsequently determined by SDS-PAGE and immunoblot analysis using α-mouse phospho-threonine (42H4) and α-rabbit GFP (D5.1) primary antibodies and α-rabbit IRDye® 680RD and α-mouse IRDye® 800CW near-infrared secondary antibodies. Three independent experiments were performed (n=3). Representative blots are shown. Interestingly, GFP-PSKH1 autophosphorylates in a time-dependent manner in the presence of $Mg^{2+}$ATP, irrespective of Chk2.

### 3.1.3.4. GFP-PSKH1 autophosphorylates in the presence of Mg2+ATP, increasing its catalytic activity

To interrogate the previously unreported autophosphorylation of PSKH1 at threonine residues in greater detail, radiometric assaying was employed to evaluate the impact of autophosphorylation on the kinase activity of PSKH1. As previously described, activation loop phosphorylation potentiates the catalytic activity of a multitude of kinases [206, 208, 209]. GFP-PSKH1 maximally pre-treated with $Mg^{2+}$ATP for 30 minutes showed an approximate 4-fold increase (P= in kinase activity as compared to a HEPES control (Figure 3.9). Recombinantly expressed GFP-PSKH1 elutes off in the void fraction (Dr. Chris Horne, unpublished), strongly suggesting that GFP-PSKH1 oligomerises. To account for as-yet uncharacterised extraneous binding partners that could theoretically phosphorylate the ADR1G233 peptide, a kinase dead point mutant of PSKH1 (GFP-PSKH1-D218N) was subsequently assayed in parallel. The ADR1G233 peptide (LKKLTRRASFSGQ) is derived from the yeast transcriptional activator ADR1 and is an ideal peptide substrate for the closely related CaM-kinases, CaMK1 and CaMK4 (and thus likely, PSKH1) [196]. GFP-PSKH1-D218N should theoretically recruit the same substrate complement as catalytically active WT

GFP-PSKH1. GFP-PSKH1-D218N did not detectably phosphorylate a peptide substrate above background levels (Figure 3.9). These data strongly suggest that a) phosphorylation of the ADR1G233 peptide is facilitated by PSKH1 and b) autophosphorylation potentiates the catalytic activity of PSKH1.
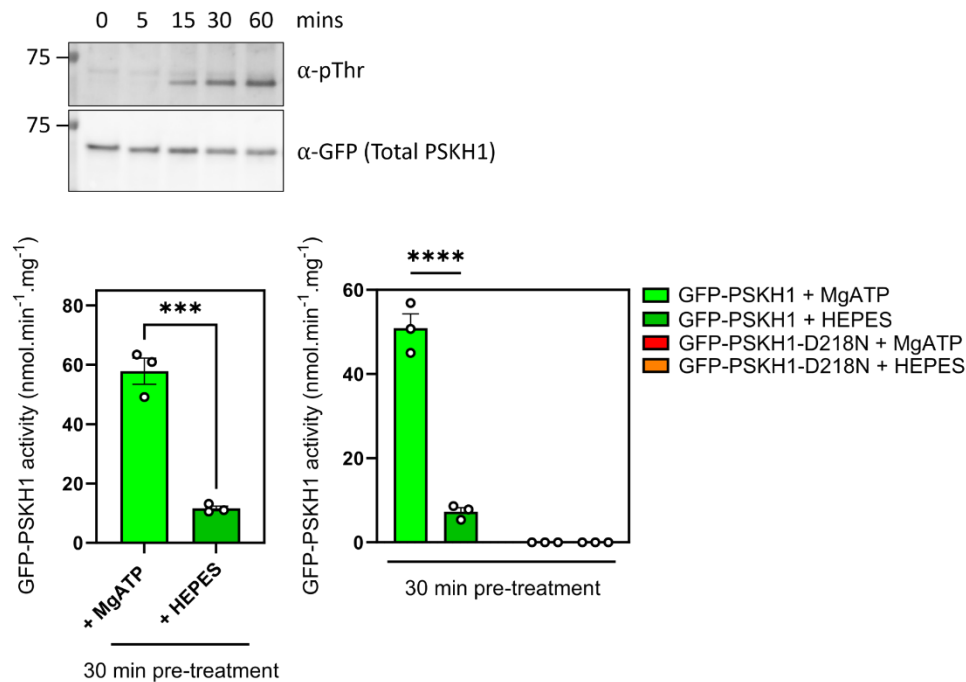


*Figure 3.9. Autophosphorylation of GFP-PSKH1 increases its activity for a peptide substrate. Autophosphorylation is dependent on catalytically active PSKH1.* Western blot. GFP-PSKH1 autophosphorylates in the presence of $Mg^{2+}$ATP in a time-dependent manner. 125ng GFP-PSKH1 was allowed to autophosphorylate in the presence of $Mg^{2+}$ATP over 0-60 minutes at 30°C. Autophosphorylation of GFP-PSKH1 was subsequently determined by SDS-PAGE and immunoblot analysis using α-mouse phospho-threonine (42H4) and α-rabbit GFP (D5.1) primary antibodies and α-rabbit IRDye® 680RD and α-mouse IRDye® 800CW near-infrared secondary antibodies. Three independent experiments were performed (n=3). A representative blot is shown. *Radiometric kinase assay*. Pre-treatment of GFP-PSKH1 with $Mg^{2+}$ATP increases PSKH1's activity toward a peptide substrate. *Left*. Kinase assay data was statistically appraised by unpaired t-test (**: P=0.0005). *Right*. Phosphorylation of the ADR1G233 peptide is facilitated by GFP-PSKH1 and not a contaminating co-purified kinase. A kinase dead variant of PSKH1 (GFP-PSKH1-D218N) pre-treated with or without (HEPES buffer) $Mg^{2+}$ATP did not phosphorylate the ADR1G233 peptide above background levels. Data was statistically appraised by two-way ANOVA and Tukey's multiple comparisons t-test (****: <0.0001). Data is representative of three independent experiments (three technical replicates/experiment).

### 3.1.3.5. Autophosphorylation of GFP-PSKH1 is independent of Ca2+/CaM

It has previously been reported that $Ca^{2+}$/CaM attenuates autophosphorylation of a serine cluster C-terminal to the catalytic domain of PSKH1 [38]. As autophosphorylation on threonine residues, putatively on the activation loop, has not previously been reported for PSKH1, we subsequently decided to interrogate the effect of $Ca^{2+}$/CaM on pThr-autophosphorylation. Autophosphorylation of GFP-PSKH1 was independent of $Ca^{2+}$/CaM, as determined by equivalent time-dependent increases in pThr immunoreactivity, with or without $Ca^{2+}$/CaM (Figure 3.10). To interrogate the inverse operation – i.e. if pThr-autophosphorylation sensitises PSKH1 to $Ca^{2+}$/CaM enhancement, 25ng GFP-PSKH1 pre-treated with or without (HEPES) MgATP was radiometrically assayed in the presence or absence of $Ca^{2+}$, $Ca^{2+}$/CaM, or CaM alone. Concurrent with previous experimentation, pre-treatment with MgATP potentiated the catalytic activity of PSKH1 (P=<0.0001, Figures 3.9/3.10). Conversely, $Ca^{2+}$/CaM did not significantly enhance the activity of autophosphorylated PSKH1 (Figure 3.10). Interestingly, $Ca^{2+}$/CaM potentiated the intrinsic activity of unstimulated PSKH1 (P=0.0096, Figure 3.10), suggesting that $Ca^{2+}$/CaM (discussed later) and activation loop autophosphorylation of PSKH1 independently regulate PSKH1 activity.
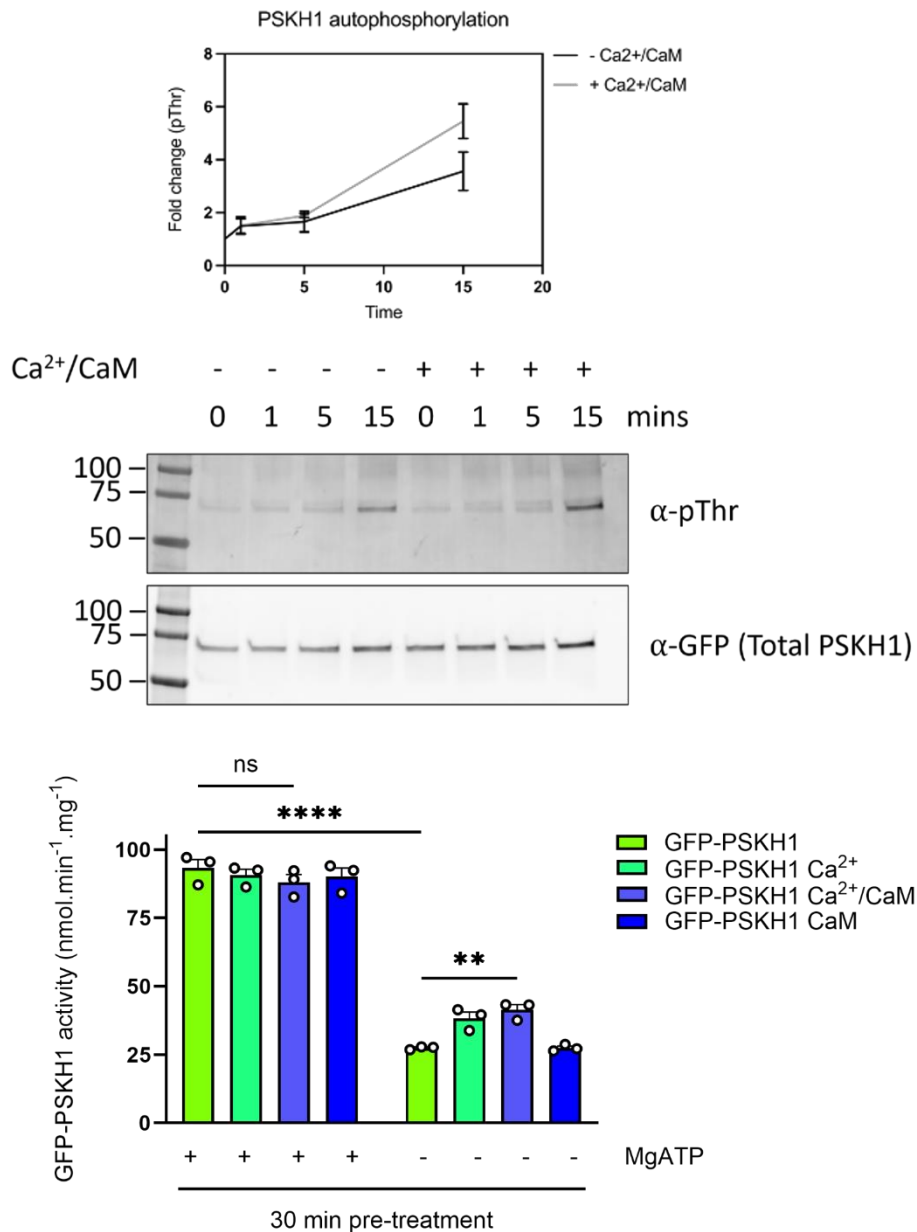
***Figure 3.10. Autophosphorylation of GFP-PSKH1 is independent of Ca2+/CaM.*** Saturating amounts of GFP-PSKH1 (500ng) was allowed to autophosphorylate in the presence of $Mg^{2+}$ATP, with or without 100μM $Ca^{2+}$/1μM CaM, for 15 minutes at 30°C. Autophosphorylation of GFP-PSKH1 was subsequently determined by SDS-PAGE and immunoblot analysis using α-mouse phospho-threonine (42H4) and α-rabbit GFP (D5.1) primary antibodies and α-rabbit IRDye® 680RD and α-mouse IRDye® 800CW near-infrared secondary antibodies. Three independent experiments were performed (n=3). A representative blot is shown. Fold change in autophosphorylation over time (*Top*) was determined by normalising pThr densitometries to total protein (α-GFP). *Radiometric kinase assay.* 25ng of GFP-PSKH1 pre-treated with or without (HEPES) $Mg^{2+}$ATP was radiometrically assayed in the presence of 200μM ATP, [γ-32P] and a peptide substrate (200μM ADR1G233) with or without 100μM $Ca^{2+}$; 100μM $Ca^{2+}$/1μM CaM or 1μM CaM. Data were statistically appraised by two-way ANOVA and Tukey's multiple comparisons t-test (**: P=0.0096; ****: P=

<0.0001). Data is representative of three independent experiments (three technical replicates/experiment).

### 3.1.3.6. Autophosphorylation of GFP-PSKH1 is concentration independent, suggesting *cis* autophosphorylation

GFP-PSKH1, an approximate 75 kDa fusion protein, elutes off a Superdex™ 200 10/300 increase column (Cytiva) into the void fraction (Dr. Chris Horne, unpublished). This observation suggested to us that PSKH1 participates in higher-order complexes. Indeed, homodimerisation of PSKH1 has been previously reported in the literature [38]. As pThr-autophosphorylation has currently only been demonstrated by N-terminally tagged GFP-PSKH1, it was subsequently reasoned that oligomerised PSKH1 *trans*-autophosphorylates in a *cis*-apparent mechanism. To interrogate this further, concentration dependence studies were employed to evaluate the effect of increasing kinase concentration on PSKH1 autophosphorylation. For *cis* autophosphorylating kinases, phosphate incorporation is limited by the intrinsic catalytic rate ($k_{cat}$) of the kinase. Thus, increasing the concentration of kinase has no effect on phosphate incorporation. For *trans* autophosphorylating kinases, the concentration of enzyme, rate of diffusion, and the $k_{cat}$ of the kinase collectively determine the rate of autophosphorylation. Thus, there is a linear relationship between concentration and kinase activity. Increasing concentrations of GFP-PSKH1 (125-500ng) were allowed to autophosphorylate in the presence of $Mg^{2+}$ATP, quenched by SDS sample buffer and analysed by western blot to determine phosphate incorporation on threonine residues. Time dependent fold-change in pThr immunoreactivity was normalised to total protein ($\alpha$-GFP) and statistically appraised by two-way ANOVA (Figure 3.11). Increasing the concentration of GFP-PSKH1 in the autophosphorylation reaction did not significantly alter the kinetics of phosphoryl transfer (Figure 3.11). To further validate these results, increasing concentrations of autophosphorylated GFP-PSKH1 were radiometrically assayed by $^{32}$P kinase assay.

Increasing the concentration of GFP-PSKH1 in the autophosphorylation reaction did not translate to increased kinase activity, as inferred by $^{32}$P-ATP incorporation into the ADR1G233 peptide substrate (Figure 3.11). The relationship between concentration and PSKH1 autoactivation, a relatively flat, linear line, was diagnostic of a *cis* mechanism.
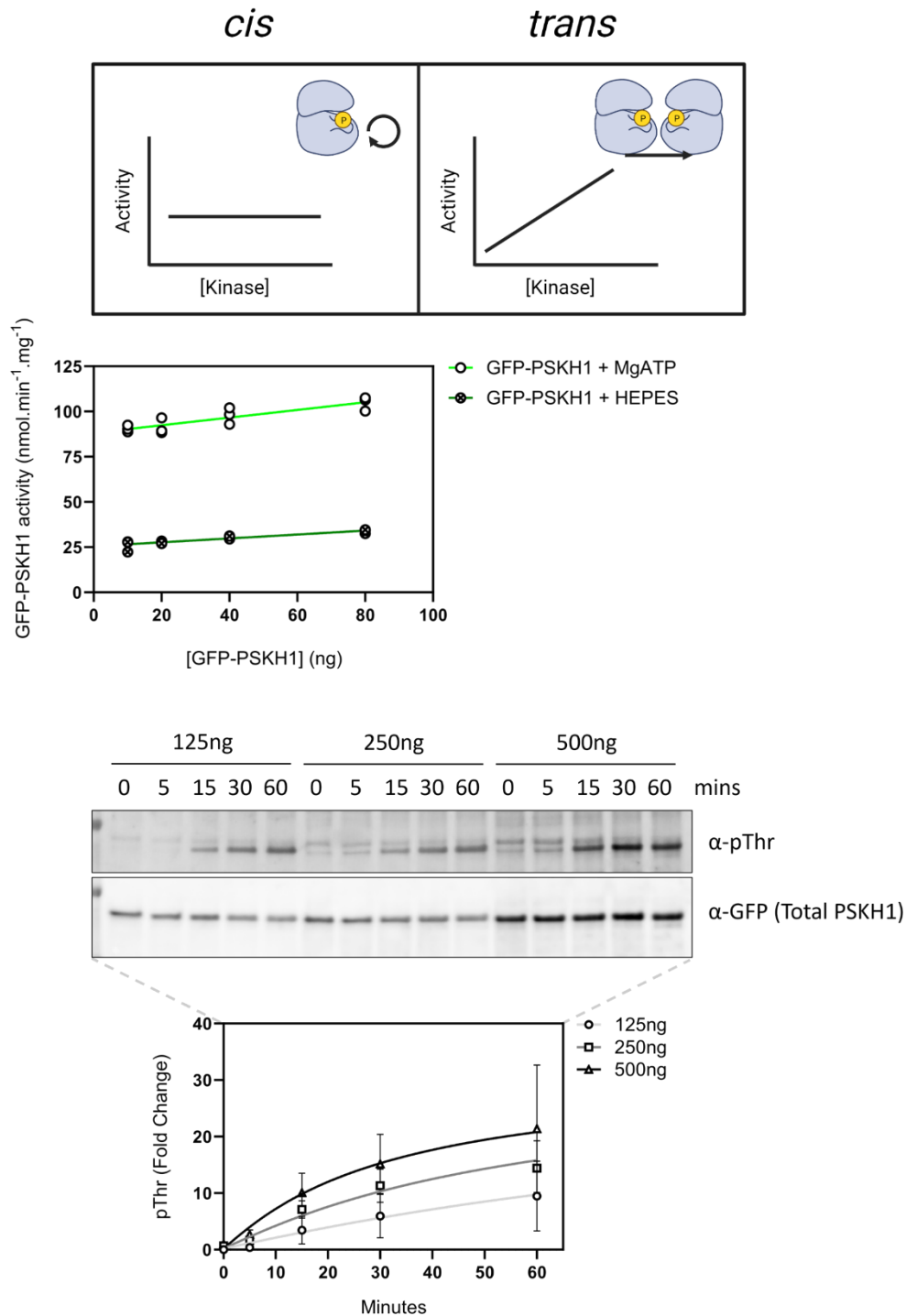
***Figure 3.11. Autophosphorylation of GFP-PSKH1 is concentration independent, suggesting a cis mechanism.*** *Diagram.* For *cis*-autoactivating kinases, autophosphorylation is limited only by the intrinsic catalytic rate ($k_{(cat)}$) of the kinase. For *trans*-autoactivating kinases, concentration, rate of diffusion, and the $k_{(cat)}$ of the kinase collectively determine the rate of autophosphorylation. There is a linear relationship between concentration and kinase activity. Adapted from Reinhardt and Leonard (2023) [211]. *Radiometric kinase assay.* GFP-PSKH1 autoactivation is concentration insensitive, suggesting a *cis* mechanism. Increasing

concentrations of GFP-PSKH1 (50-400ng) were allowed to autophosphorylate in the presence or absence of $Mg^{2+}$ATP for 30 minutes. Autophosphorylated enzyme was radiometrically assayed to determine the impact of changing concentration on the autoactivation and, subsequent activity of, GFP-PSKH1. Activity data were corrected for ng of protein used/per reaction. Data was fit to the equation Y=Bottom + (Top-Bottom)/(1+(EC/X)^Hillslope). n=3. *Western blot*. pThr was normalised to total GFP. Increasing the [PSKH1] did not significantly alter fold-change in pThr immunoreactivity. Three independent experiments were performed (n=3). A representative blot is shown.

### 3.1.3.7. Phosphopeptide analysis by LC-MS/MS of autophosphorylated GFP-PSKH1 reveals enrichment of phosphorylated residues within and C-terminal to the activation segment of PSKH1

To determine what residues were autophosphorylated by PSKH1, phosphopeptide analysis by trypsin digest and liquid chromatography/mass spectrometry (LC-MS/MS) was employed. Briefly, 10μg GFP-PSKH1 was allowed to autophosphorylate in the presence or absence (50mM HEPES buffer, pH 7.4) of $Mg^{2+}$ATP for 0-60 minutes. Autophosphorylated GFP-PSKH1 was subsequently snap frozen in liquid nitrogen and further processed at the Walter and Eliza Hall Institute of Medical Research for phosphopeptide analysis, with the assistance of Dr. Toby Dite. Trypsin digest/LC-MS/MS revealed significant phosphate incorporation at a serine cluster C-terminal to the catalytic domain (Ser363, Ser372) (Figure 3.12). This region has been reported previously as a major autophosphorylation site [38]. Moreover, residues within the activation segment (Thr260) were also autophosphorylated, albeit to a reduced degree (Figure 3.12). Phosphate incorporation at Thr256 – the presumed activation loop site – was not detected in the conditions tested, but likely reflects an inability of peptides containing this site to fly through the mass spectrometry instrument. Indeed, this residue is immediately flanked by a lysine side chain (Lys255), which would result in cleavage and production of a phosphopeptide too large for LC-MS/MS analysis. Perplexingly, no ion intensities were recorded at the 30 minute +$Mg^{2+}$ATP time point (column 7, Figure 3.12), which may reflect poor sample quality or mishandling during the preparation steps.

| Gene name | Amino acid | Position within protein | 0 min + Mg²⁺ATP | 5 min + Mg²⁺ATP | 15 min + Mg²⁺ATP | 30 min + Mg²⁺ATP | 60 min + Mg²⁺ATP |
|---|---|---|---|---|---|---|---|
| PSKH1 | S | 28 | 0 | 0 | 0 | 0 | 24553 |
| PSKH1 | T | 30 | 17424 | 0 | 67292 | 0 | 456910 |
| PSKH1 | S | 32 | 0 | 44075 | 0 | 0 | 24553 |
| PSKH1 | T | 40 | 0 | 0 | 0 | 0 | 119350 |
| PSKH1 | S | 44 | 0 | 0 | 4900.1 | 0 | 81941 |
| PSKH1 | S | 233 | 0 | 0 | 0 | 0 | 9823.4 |
| PSKH1 | T | 260 | 47064 | 50997 | 0 | 0 | 0 |
| PSKH1 | S | 361 | 0 | 0 | 0 | 0 | 0 |
| PSKH1 | S | 362 | 0 | 0 | 0 | 0 | 0 |
| PSKH1 | S | 363 | 239290 | 244870 | 332370 | 0 | 1040900 |
| PSKH1 | S | 372 | 1193800 | 1232100 | 1184700 | 0 | 1225000 |

| Gene name | Amino acid | Position within protein | 0 min + HEPES | 5 min + HEPES | 15 min + HEPES | 30 min + HEPES | 60 min + HEPES |
|---|---|---|---|---|---|---|---|
| PSKH1 | S | 28 | 0 | 0 | 0 | 0 | 0 |
| PSKH1 | T | 30 | 0 | 0 | 0 | 0 | 0 |
| PSKH1 | S | 32 | 0 | 0 | 0 | 0 | 0 |
| PSKH1 | T | 40 | 0 | 0 | 0 | 0 | 0 |
| PSKH1 | S | 44 | 0 | 0 | 0 | 0 | 0 |
| PSKH1 | S | 233 | 0 | 0 | 0 | 0 | 0 |
| PSKH1 | T | 260 | 0 | 0 | 0 | 0 | 0 |
| PSKH1 | S | 361 | 0 | 0 | 0 | 0 | 0 |
| PSKH1 | S | 362 | 0 | 0 | 0 | 0 | 0 |
| PSKH1 | S | 363 | 49046 | 0 | 0 | 0 | 0 |
| PSKH1 | S | 372 | 28862 | 0 | 0 | 0 | 0 |

*Figure 3.12. Phosphopeptide analysis by LC-MS/MS of autophosphorylated GFP-PSKH1 reveals enrichment of phosphorylated residues within and adjacent to the activation segment of PSKH1.* 10 μg GFP-PSKH1 was autophosphorylated in the presence or absence (50mM HEPES buffer) of Mg²⁺ATP for 0-60 minutes. Autophosphorylated sites were subsequently interrogated by phosphopeptide analysis by trypsin digest/LC-MS/MS with the assistance of Dr. Toby Dite, WEHI. Columns 4 through 8 indicate ion intensities at the respective phosphosite positions (position within protein) and time points (0-60 min).

## 3.2. Ca$^{2+}$/CaM-dependence of PSKH1

Upon the advent of multicellularity 600 million years ago, a pressing need for mechanisms by which cells communicate to one another invariably emerged. The third most abundant metal on planet Earth, calcium's unique chemical properties prompted its adoption as this integral signalling molecule by cells [223]. Although Ca$^{2+}$ can, in some cases, signal directly to substrates, it typically is first "decoded" by the complement of Ca$^{2+}$-sensing proteins present in the human body. Upon binding free Ca$^{2+}$, these sensors "translate" the Ca$^{2+}$ signal by adopting a modified conformation that imparts substrate affinity to the desired downstream effector. To enable these Ca$^{2+}$ sensors to detect and translate pulsatile increases in free Ca$^{2+}$, intracellular concentration must necessarily be kept low. Indeed, by myriad pumps, ion channels and Ca$^{2+}$-sequestering proteins like parvalbumin and calbindin, intracellular [Ca$^{2+}$] is kept comparatively low ($10^{-7}$ M), 4-fold lower than the extracellular milieu [223, 224]. Amongst the Ca$^{2+}$-decoding protein complement, calmodulin remains the best characterised. Calmodulin (CaM) is a small (~17 kDa) dumbbell shaped protein with ubiquitous tissue and subcellular expression [224]. Its globular termini each harbour an EF-hand pair (EF + CD) tethered by a flexible linker region (Figure 3.13) [225]. The E-F and C-D helices, reminiscent of an extended forefinger, middle finger, and thumb, are enriched with non-polar, hydrophobic side chains forming a hydrophobic substrate interface (Figure 3.13). In the apo (Ca$^{2+}$-free) state, these hydrophobic 'palmar' pockets are collapsed and largely unavailable for substrate interaction. Upon liganding Ca$^{2+}$, CaM adopts an extended and more open conformation. This exposes the hydrophobic pockets, unleashing considerable free energy and endowing CaM with its Ca$^{2+}$-sensing and substrate binding properties.

***Figure 3.13. Calmodulin, the prototypic Ca2+-sensor in eukaryotic cells, binds Ca2+ by virtue of the EF-hand.*** Sequence alignment of CaM EF/CD-hands, using Parvalbumin as the consensus EF-hand motif. Conserved residues 2, 5, 6, 9, 22, 25, 26 and 29 harbour non-polar/hydrophobic side chains and form the hydrophobic palmar surface of both termini. Conserved residues 10, 12, 14, 18 and 21 harbour oxygen-containing side chains necessary for $Ca^{2+}$ coordination. Residue 15 (glycine) is generally conserved due to geometric constrictions on the carboxylate ligand loop. Manual adjustments to the alignment were made. *Structures and insert*. Crystal structure of $Ca^{2+}$-bound CaM (PDB ID: 1exr), visualised as a ribbon diagram (above) and hydrophobicity surface structure (below). Highlighted motifs and residues are coloured as follows: cyan: EF-hand I; sea green: CD-hand I; deep blue: EF-hand II; purple: CD-hand II; yellow: non-polar/hydrophobic side chain; red: oxygen-containing side chain; green: conserved glycine; white: $Ca^{2+}$ cation. Kretsinger consensus sequence (EF-hand consensus sequence) adapted from Kretsinger (1980) [225].

Calmodulin regulates myriad protein substrates, including phosphodiesterases (PDE), phosphatases, A-kinase anchoring proteins (AKAPs) [226] and, notably, members of the serine/threonine calmodulin-dependent protein kinase (CaMK) subfamily. Mechanistically, this regulation is best illustrated by the substrate specific CaM-kinases skeletal (sk) and smooth muscle (sm) myosin light chain kinase (MLCK) and the multi-functional CaM-kinases CaMK1, CaMK2 and CaMK4. Although not technically a CaM-kinase according to the Manning designation [1], CaMKK has been included for completion, as it forms the basis for the CaMKK signalling cascade (of which CaMK1 and CaMK4 are constituent components) and is itself calmodulin-dependent. All 6 enzymes harbour a calmodulin-binding domain (CBD), a requirement for CaM recognition, C-terminal to the catalytic core (Figure 3.14) [13, 17, 19, 198, 202, 227, 228]. CBDs are characterised by their overall amphipathicity, segregation of hydrophilic and hydrophobic faces, bulky aromatic and aliphatic side chains that serve to anchor the activated CaM molecule, and an α-helical secondary structure. In skMLCK, Trp580 and Phe593, interspersed by 12 spacer amino acids, anchor the COOH- and NH2-lobes of calmodulin, respectively (Figures 3.14/15) [86]. The CaM:skMLCK-CBD complex is further stabilised by electrostatic interactions between the basic residues that cluster around Trp580/Phe593 and the acidic side chains of Glu11, 14, 83, 84 and 87 (Figure 3.14/15) [86]. This 1-(8)-14 motif is also shared with smMLCK, although the position 14 aromatic is substituted by the aliphatic side chain of Leu813 (Figures 3.14) [87]. In CaMK2, the anchoring aromatics of skMLCK are replaced by Leu299 and Leu308, resulting in a significantly shorter spacer region of just 8 amino acids (Figure 3.14) [88]. Additionally, basic residues (Arg296, Arg297, Lys298) that participate in hydrogen bonding and salt-link interactions with calmodulin cluster entirely at the N-terminal end of the CaMK2-CBD peptide. Like skMLCK, CaMKK1's CBD also contains two anchoring aromatics, Trp444 and Phe459, albeit spaced 16 amino acids apart, the largest spacer region yet characterised (Figure 3.14) [14].

Interestingly, in contrast to previously reported calmodulin-binding domains, CaMKK1's CBD is characterised by an N-terminal α-helical segment followed by a hairpin-like loop structure that folds back onto the α-helix (Figure 3.14) [14]. This unique CBD conformation is stabilised by intramolecular interactions between helix (Ile448, Leu449, Met453) and loop (Phe459, Phe463) residues present on the CaMKK1-CBD peptide (Figure 3.15) [14]. Additionally, the electrostatic properties of the CaMKK1-CBD result in a reversed binding orientation, whereby the highly basic C-terminus of the CBD peptide associates with the acidic channel outlet created by the C-lobe of calmodulin (Figure 3.15). This N-N/C-C orientation is unique to CaMKK1 and, likely, CaMKK2, a closely related CaMKK isoform predominantly expressed in brain but whose CBD structure remains unresolved [19]. The CaMKK substrates CaMK1 and CaMK4 are themselves CaM-regulated and collectively these kinases constitute the CaMKK signalling cascade. However, no structures are currently available for the CBD's of CaMK1 or CaMK4 complexed with calmodulin. Fortunately, early biochemical characterisation studies undertaken in the 1990's have shed some light on CaM-regulation of these critical CaMKK-effectors. Truncational analyses by Haribabu et al. (1995) and Yokokura et al. (1995) delineated the minimal CaMK1 CBD to residues 302-321 of the protein polypeptide (Figure 3.14) [198]. Subsequent sequence alignment with defined CaMK-CBD's revealed some similarities with sk- and smMLCK, including a conserved tryptophan (Trp303) at the N-terminal end of the CBD peptide and an intervening spacer region of 12 amino acids. In the autoinhibited CaMK1 crystal structure, Met316 – the proposed C-terminal anchor residue – is buried at the interface with the N-lobe of the kinase domain (Figure 3.16). In contrast, Trp303 is highly solvent-exposed and may be the initial anchor site by which calmodulin binds with CaMK1 (Figure 3.16) [89].
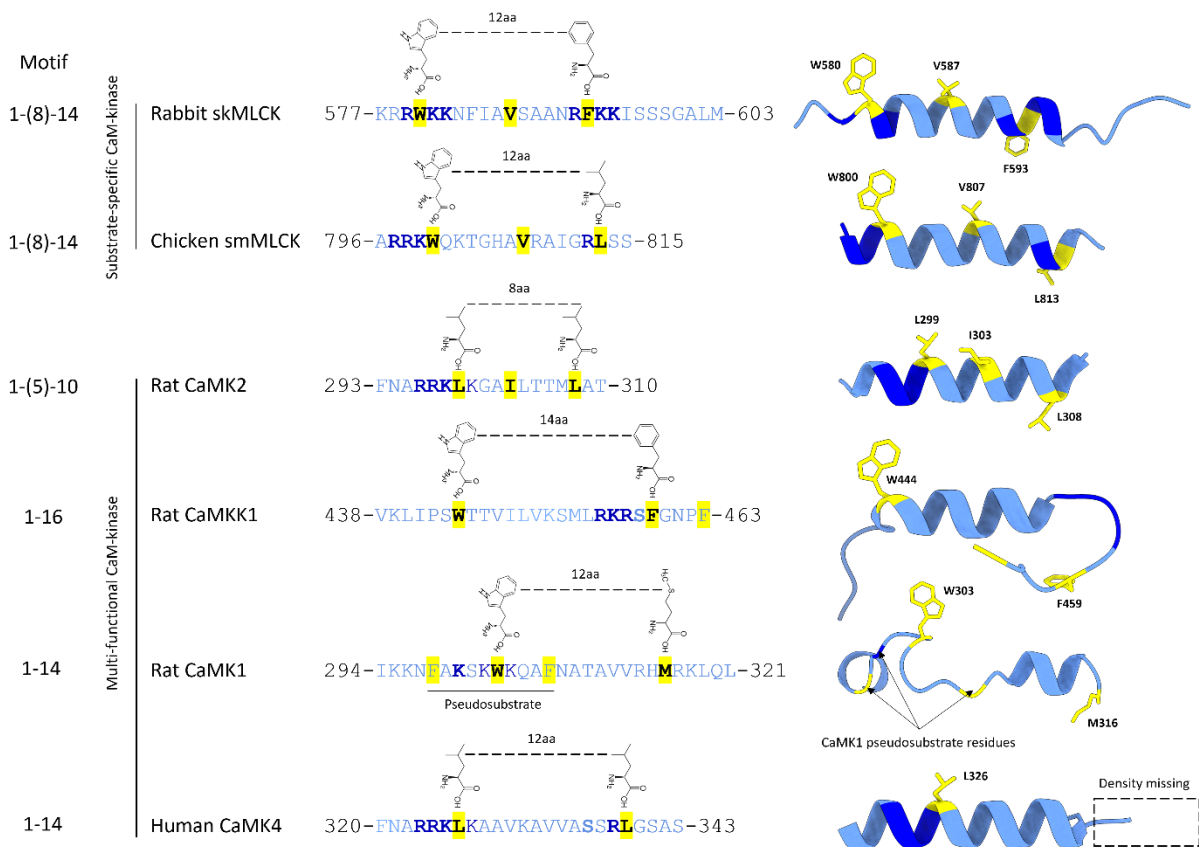
***Figure 3.14. Representative calmodulin-binding domains of the CaMK subfamily.*** Primary and secondary structure of the calmodulin-binding domains of rabbit smMLCK (PDB: 2bbm), chicken smMLCK (PDB: 1cdl), rat CaMK2 (PDB: 1cdm), rat CaMKK1 (PDB: 1ckk), rat CaMK1 (PDB: 1a06) and human CaMK4 (PDB: 2w4o). Key anchoring hydrophobic residues are bolded and highlighted yellow. Key basic residues are bolded blue. Bolded cornflower blue residues indicate phosphorylation sites. aa: amino acid.
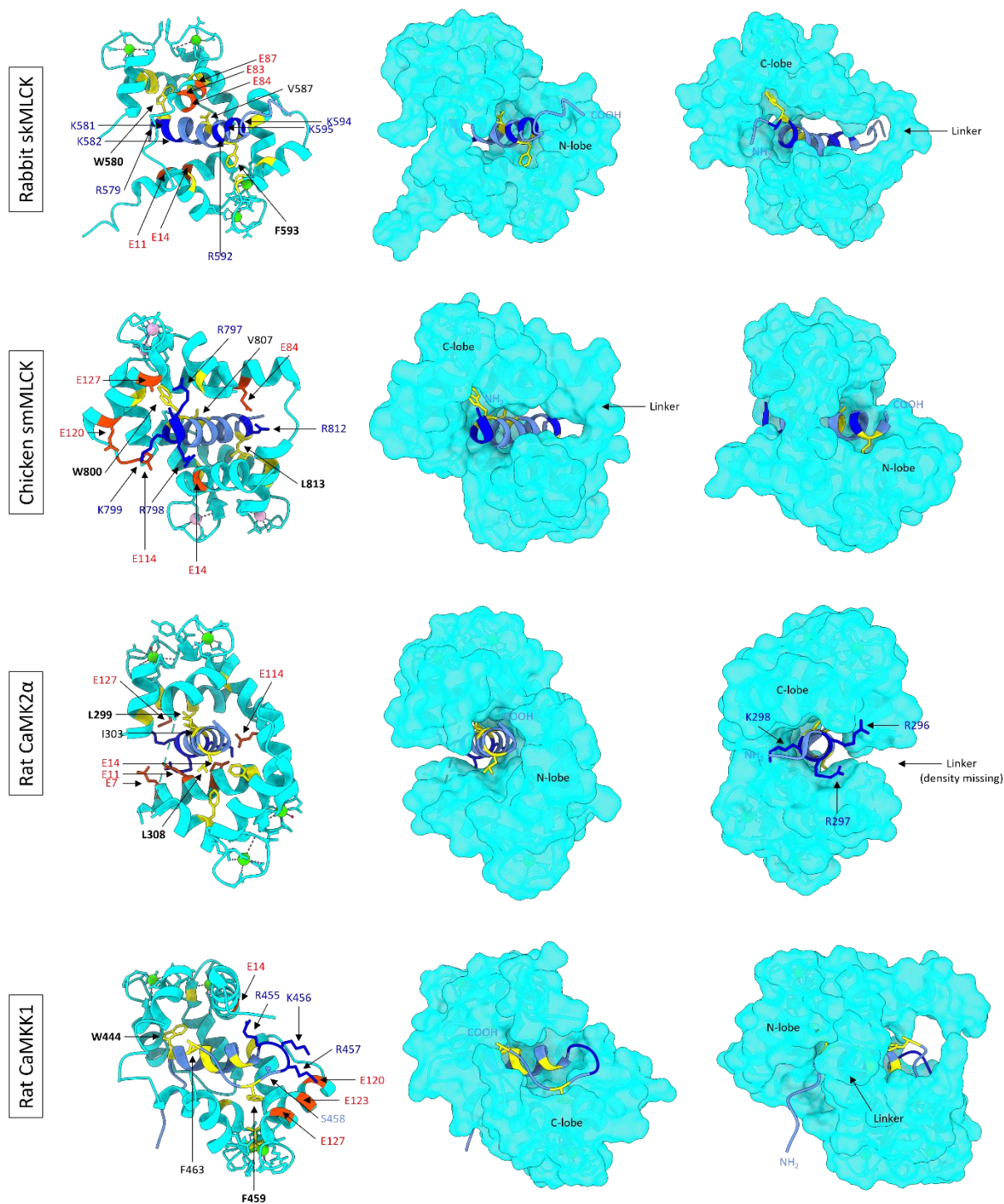
*Figure 3.15. Differential binding orientations of calmodulin with peptides corresponding to the calmodulin-binding domains of its in vivo substrates, skMLCK, smMLCK, CaMK2α and CaMKK1.* Calmodulin (cyan) adopts a globlular conformation upon binding the calmodulin-binding domains of skMLCK (PDB ID: 2bbm), smMLCK (PDB ID: 1cdl), CaMK2α (PDB ID: 1cdm) and CaMKK1 (PDB ID: 1ckk). In skMLCK, smMLCK and CaMK2α, the N- and C-lobes of calmodulin tether to the C- and N- termini of the CBD peptides, respectively. In CaM:CaMKK1, this orientation is reversed. Residues are coloured as follows: dark blue: basic; orange red: acidic; yellow: hydrophobic; cornflower blue: calmodulin-binding domain. Some side chains have been omitted for clarity.

In almost all instances, binding of calmodulin alleviates intrasteric inhibition of the active site. For example, in the autoinhibited CaMK1 crystal structure (PDB ID: 1a06), the overlapping AID/CBD straddles both lobes of the kinase domain, distorting the ATP-binding lobe and sterically obstructing the C-lobe substrate binding cleft (Figure 3.16). $Ca^{2+}$/CaM-binding to a solvent exposed aromatic side chain on the CaMK1-CBD (W303) presumably alleviates this autoinhibition by pulling the AID/CBD away from the kinase domain and altering the conformation of CaMK1's catalytic architecture.

Autoinhibited CaMK1-kinase domain (1a06)
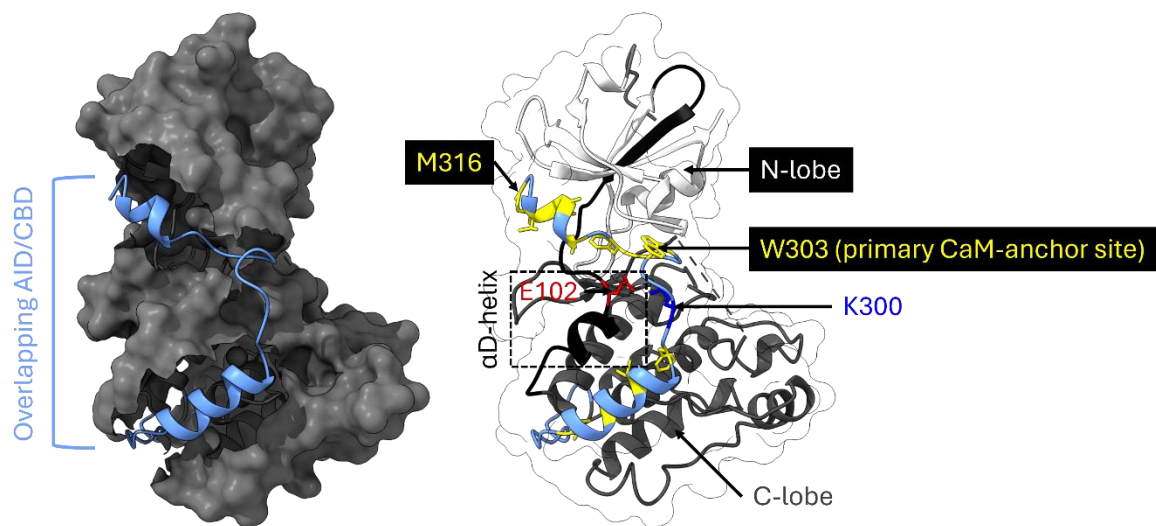


***Figure 3.16. Intrasteric autoinhibition of the kinase domain is relieved by $Ca^{2+}$/CaM-binding.*** In the autoinhibited CaMK1 crystal structure (PDB ID: 1a06), an overlapping autoinhibitory/calmodulin binding domain (AID/CBD) straddles both lobes of the kinase domain, inhibiting activity. The autoinhibitory domain (C-lobe interacting) sterically obstructs the substrate binding cleft through hydrophobic (yellow residues) and electrostatic (red: acidic; dark blue: basic) interactions. For example, a conserved Glu102 (E102) acidic residue on the CaMK1 αD-helix participates in salt-bridge interactions with Lys300 (K300) of the autoinhibitory domain. The calmodulin binding domain (CBD) distorts the ATP-binding architecture of the N-lobe, primarily via hydrophobic interactions. A solvent exposed Trp300 (W300) aromatic side chain provides the initial anchor site for $Ca^{2+}$/CaM. Binding of $Ca^{2+}$/CaM alleviates the intrasteric autoinhibition of the active site, permitting CaMKK activation of CaMK1.

The heterogeneity in calmodulin binding domains make them inherently difficult to identify by sequence information alone. Indeed, unlike skMLCK, smMLCK, CaMK2, CaMKK, CaMK1 or CaMK4, PSKH1 has no discernible calmodulin binding domain in its primary structure. Additionally, in contrast to previous reports [38] $Ca^{2+}$/CaM did not abrogate autoactivation of PSKH1 (Figure 3.10). Consequently, $Ca^{2+}$/CaM regulation of PSKH1 remains inconclusive.

### 3.2.1. Aims

The aim of this subchapter was to elucidate the dependence, if any, of PSKH1 activity on $Ca^{2+}$-signalling.

### 3.2.2. Materials and Methods

### 3.2.2.1. Nutrient stimulation of PSKH1-FLAG

To stimulate the activation of the PSKH1-FLAG transiently expressed in HEK293T cells, following a 48-hour transfection period, cells were briefly washed in pre-warmed DPBS (Gibco) and pre-treated in glucose deplete DMEM medium (Gibco) for 30 minutes to two hours before rapid lysis *in situ*. Lysates were snap frozen in liquid nitrogen before subsequent analysis by radiometric kinase assay, previously described (Materials and Methods, Section 2.5.1).

### 3.2.3. Results

### 3.2.3.1. PSKH1 is a $Ca^{2+}$/CaM regulated protein kinase

In contrast to previous reports, $Ca^{2+}$/CaM did not detectably impact autophosphorylation of GFP-PSKH1 (Figure 3.10). Additionally, given the absence of an identifiable calmodulin binding domain in PSKH1's primary structure, CaM's impact (if any) on the catalytic activity of PSKH1 currently remains undefined. Radiometric assaying was employed to interrogate $Ca^{2+}$/CaM regulation of GFP-PSKH1 activity. CaM potentiated PSKH1's activity toward a peptide substrate in a concentration-dependent matter, with an apparent EC50 of 27.4 nM, congruent with other CaMKs (Figure 3.17).
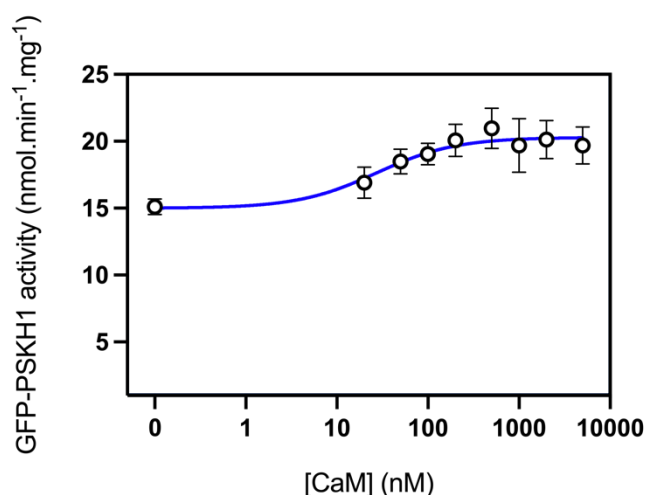


***Figure 3.17. PSKH1 is a Ca2+/CaM regulated protein kinase.*** GFP-PSKH1 activity was measured over a [CaM] gradient (0-5μM) in the presence of 5mM $MgCl_2$, 200μM [$\gamma$-32P]-ATP (PerkinElmer), 200μM ADR1G233 peptide substrate and 100μM $CaCl_2$. Data was fit to the equation: Y=Bottom + X*(Top-Bottom)/(EC50 + X). 2 technical replicates per biological replicate (n=3). EC50 = 27.40 nM CaM.

### 3.2.3.2. Identification of a putative functional calmodulin-binding domain N-terminal to the catalytic domain of PSKH1

Sequence alignment of PSKH1 orthologues across eukaryotes identified a region of high sequence conservation immediately N-terminal to the kinase domain with some features diagnostic of a CBD (Gerard Manning, unpublished). An AlphaFold2 simulation of this 19aa stretch revealed an α-helical architecture (Figure 3.18). Helical wheel plot analysis indicated overall amphipathicity, however no segregation of hydrophilic or hydrophobic faces (Figure 3.18). Candidate anchoring aromatic residues include Tyr85 and Phe90, although it appears unlikely that this putative PSKH1-CBD would interface with calmodulin via the 1-(5)-10,1-(8)-14 or 1-16 motifs previously described (Figure 3.14).
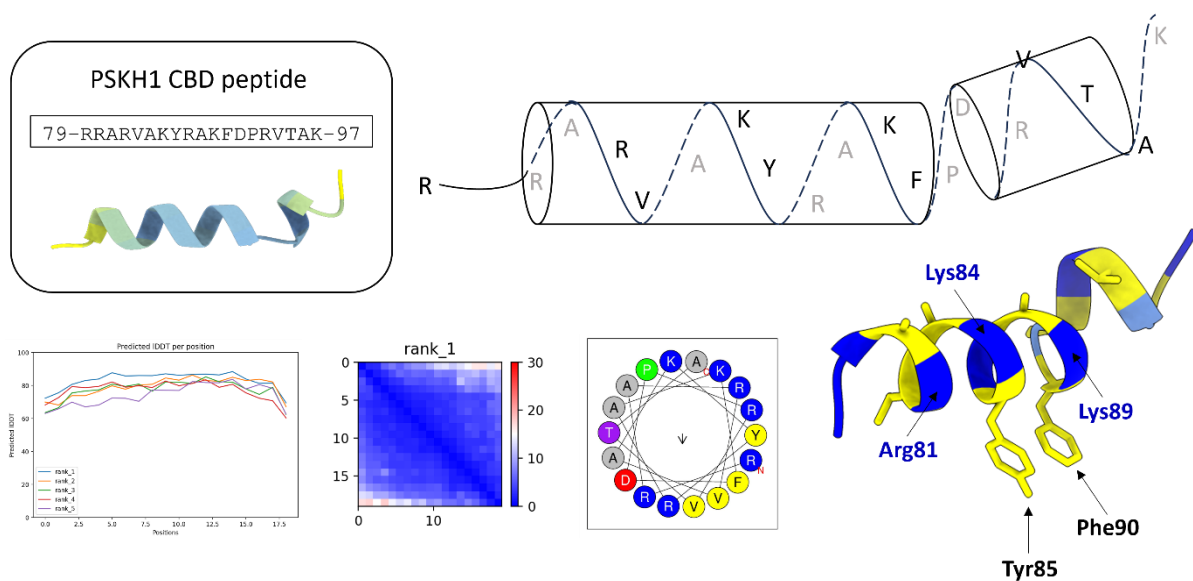


***Figure 3.18. A highly-conserved 19aa region N-terminal to the catalytic domain of PSKH1 shares some features characteristic of a calmodulin-binding domain.*** *Boxed.* A 19aa peptide sequence corresponding to the putative N-terminal CBD of human PSKH1 was simulated on AlphaFold2 using the ColabFold v1.5.5 Google co-laboratory notebook [94]. The simulation was run using the MMseqs2 multiple sequence alignment (MSA) method with 12 recycles. The PSKH1-CBD is coloured by pLDDT score. Corresponding pLDDT and PAE plots are indicated below. *Helical wheel plot.* Helical wheel plot analysis indicates no segregation of hydrophilic and hydrophobic faces. Analysis was performed using HELIQUEST [229]. *Calmodulin-binding domain.* Hydrophobic residues are coloured yellow. Basic residues are coloured blue. Some side chains have been omitted for clarity.

### 3.2.3.3. Truncation analysis of the putative N-terminal PSKH1-CBD

To interrogate the CaM-binding properties of this potential regulatory region, a series of N-terminally truncated PSKH1-FLAG mutants were generated by recombinantly expressing pcDNA3.1-PSKH1-FLAG expression constructs in HEK293T cells. Following a 48-hour transfection period, these constructs were immunoprecipitated from HEK293T whole-cell lysate using an anti-FLAG® M2 affinity resin and radiometrically assayed for their ability to incorporate radiolabelled 32-P into a peptide substrate (ADR1G233). Initial experimentation failed to reliably illustrate PSKH1 activity, which we originally had assumed was related to an epitope-tagging issue. Furthermore, these PSKH1 constructs showed little, if any, pThr immunoreactivity, corroborating previous experimentation. Excitingly, it was later revealed in a concurrent study interrogating the function of PSKH1 in prostate cancer cells that PSKH1-WT but not PSKH1-KO LNCaP cells proliferate under no glucose conditions (Figure 4.3). Although the implications of these findings will not be discussed in this subchapter, it was reasoned that nutrient stress likely activates PSKH1-driven cellular programs and, by extension, PSKH1 itself. Therefore, we revisited these PSKH1-FLAG expression constructs, albeit with the following changes: HEK293T cells transiently transfected with pcDNA3.1-PSKH1-FLAG were briefly washed in pre-warmed DPBS and glucose starved for 30 minutes to 2 hours before rapid lysis *in situ*. Pre-treatment with glucose-deplete DMEM medium (Gibco) caused a moderate, time-dependent increase in PSKH1-FLAG intrinsic (basal) activity (Figure 3.19). Remarkably, glucose stress resulted in an approximate 3-fold increase in PSKH1 activity (when compared with non-treated (NT) controls) when assayed in the presence of 100µM $Ca^{2+}$ and 1µM CaM (Figure 3.19). Relative to glucose-replete (HG) controls which demonstrated a time-dependent increase in catalytic activity, PSKH1-FLAG derived from glucose-starved HEK293T cells showed an immediate (30 minutes) increase in kinase activity (Figure 3.19). This data suggests that PSKH1 activity is stimulated more by conditions where

energy is depleted. Interestingly, there was no corresponding increase in p-threonine immunoreactivity (indicative of PSKH1 autoactivation) following treatment (Figure 3.19). However, as previously stated, it is possible that the generic pThr antibody may not recognise the activation loop (T256) epitope of PSKH1.
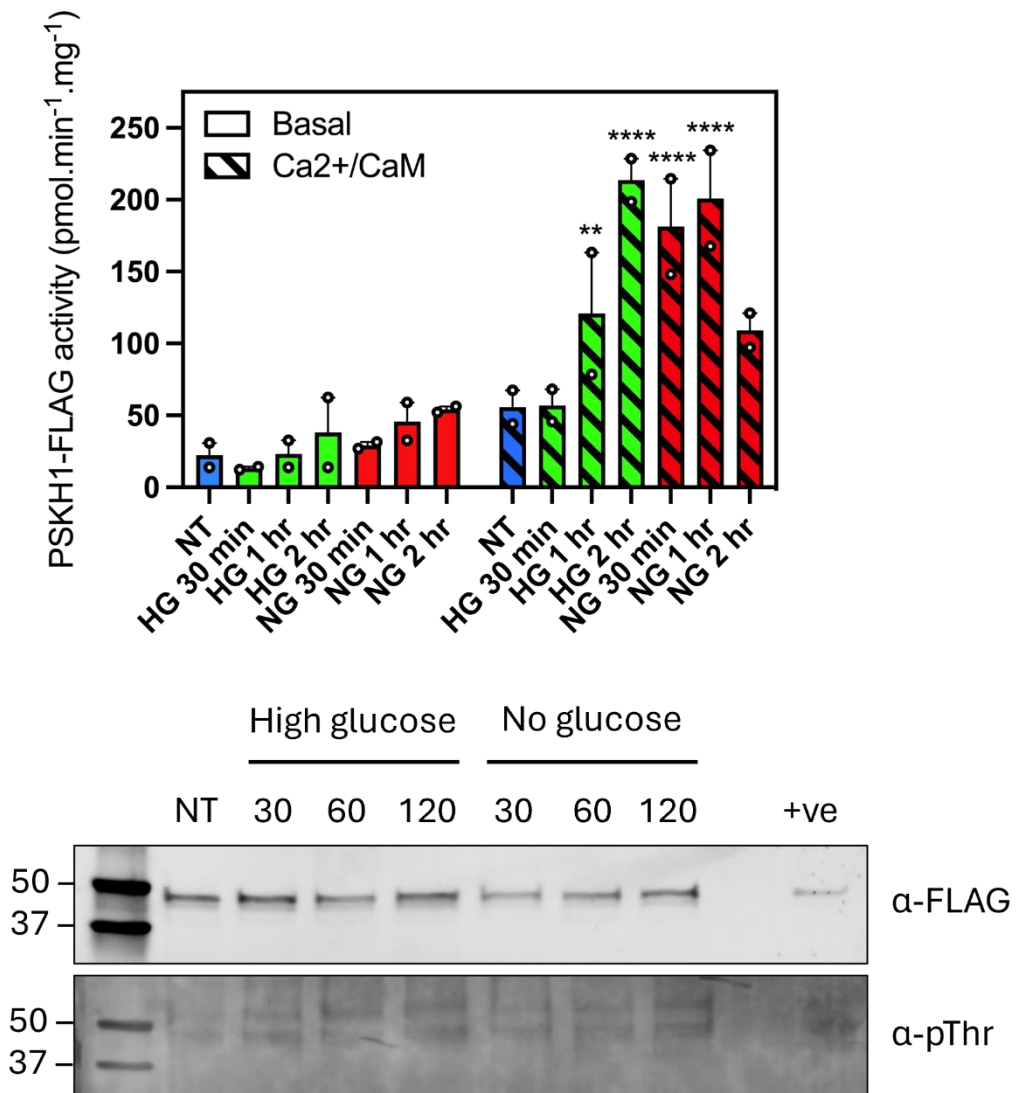


**Figure 3.19. Glucose stress primes PSKH1-FLAG for CaM-activation.** Full-length PSKH1-FLAG was immunoprecipitated from equal volumes whole-cell lysate derived from HEK293T cells either untreated (NT) or pre-treated with glucose deplete DMEM media (Gibco) for 0.5 – 2 hours and radiometrically assayed in the presence of 200μM ATP [γ-32P] and 200μM ADR1G233 synthetic peptide, with or without 100μM $Ca^{2+}$ and 1μM CaM. Activities were corrected for variation in PSKH1 expression by western blot using an anti-FLAG antibody. Data was statistically appraised by two-way ANOVA and Tukey's multiple comparisons test (****: P=<0.0001). Data is representative of two independent experiments (three technical replicates/experiment). Phospho-threonine status was interrogated using an anti-phospho threonine (α-pThr, CST) and anti-mouse IRDye 800CW secondary antibody (LI-COR).

Purified PSKH1-FLAG was utilised as a positive (+ve) control for PSKH1-FLAG expression. A representative blot is shown.

Truncation of the N-terminal region (1-86) severely impaired the intrinsic and $Ca^{2+}$/CaM-mediated ehancement of PSKH1 activity (Figure 3.20). Further removal of an additional 12 aa resulted in complete loss of intrinsic and $Ca^{2+}$/CaM-mediated kinase activity (Figure 3.20). N-terminally truncated PSKH1-FLAG was significantly enriched in WCL and IP supernatants compared to full-length WT, corroborating reports that this region, in addition to putatively facilitating $Ca^{2+}$/CaM-binding, harbours an assortment of membrane-targeting motifs [38].
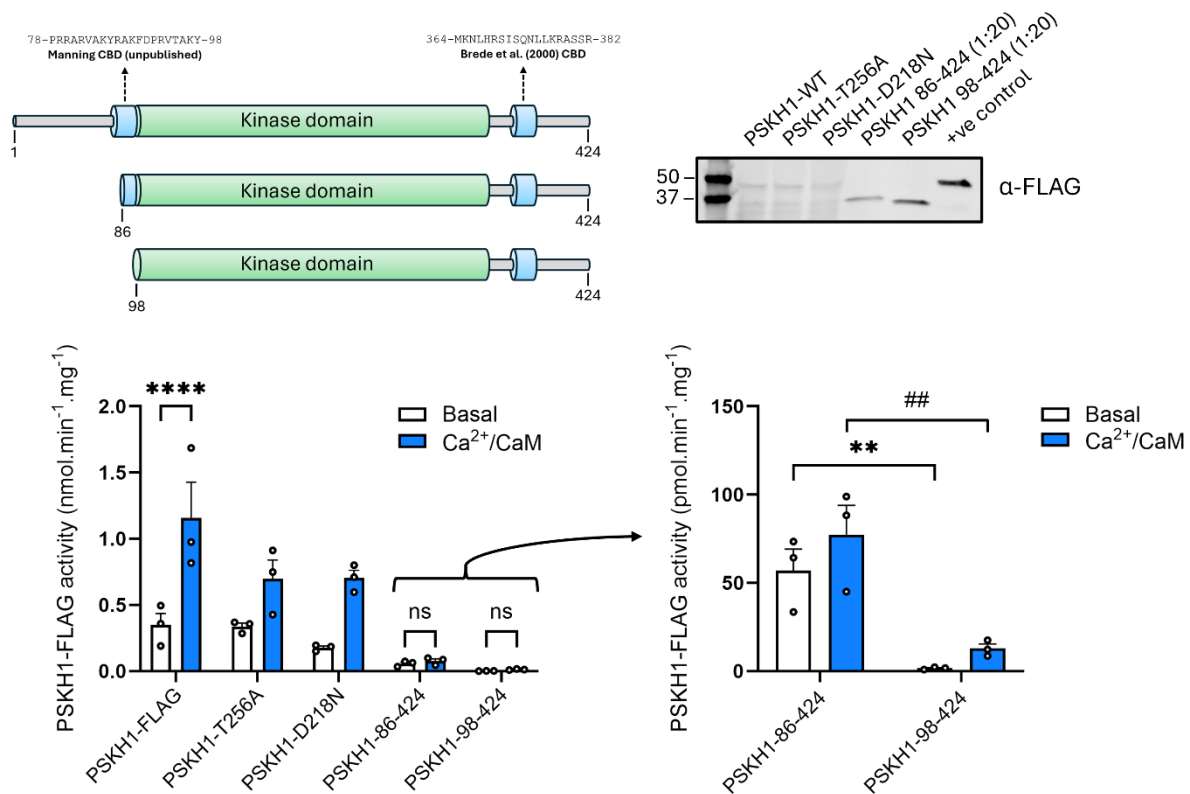


**Figure 3.20. N-terminal truncation of PSKH1-FLAG abrogates its intrinsic and CaM-modulated kinase activity.** Full-length PSKH1-FLAG, an activation loop point mutant (PSKH1-T256A), a kinase dead (PSKH1-D218N) or N-terminally truncated mutants (86-424; 98-424) transiently expressed in HEK293T cells glucose starved for 30 minutes were immunoprecipitated from WCL using anti-FLAG M2® agarose (50% (v/v)) for 1 hour at 4°C. 10µl of 50% (v/v) PSKH1-FLAG:FLAG agarose was aliquoted into a 30µl reaction containing assay buffer (see Table 1), 200µM ATP mix, 200µM PSKH1 peptide substrate (ADR1G233), with or without 100µM CaCl2 and 1µM CaM, and radiometrically assayed for kinase activity. Activities were corrected for variation in PSKH1 expression by western blot using an anti-FLAG antibody. A representative blot is shown. Data was statistically appraised by two-way

ANOVA and Tukey's multiple comparisons test (\*\*:P=0.0052; ##:P=0.0022;\*\*\*\*: P=<0.0001 ). Data is representative of 3 independent experiments (three technical replicates/experiment).

### 3.2.3.4. Alanine scanning of the PSKH1 N-terminal calmodulin-binding domain

Truncation of 86-98aa N-terminal to the kinase domain of PSKH1 severely impairs CaM-enhancement of kinase activity (Figure 3.20). To elucidate which residues are critical for CaM recognition, an alanine scan of the 12aa region was performed. CaM-binding typically requires several bulky, aromatic side chains present on the cognate CBD to anchor the CaM molecule in place (Figures 3.14/15). Consequently, substitution of these residues to alanine, of which bears the shortest R-group amongst the hydrophobic amino acids, should theoretically impair CaM-binding. R87A, K89A and F90A impaired CaM-enhancement relative to a wild-type control (PSKH1-FLAG) by 25-50%, although these results were not statistically significant (Figure 3.21).
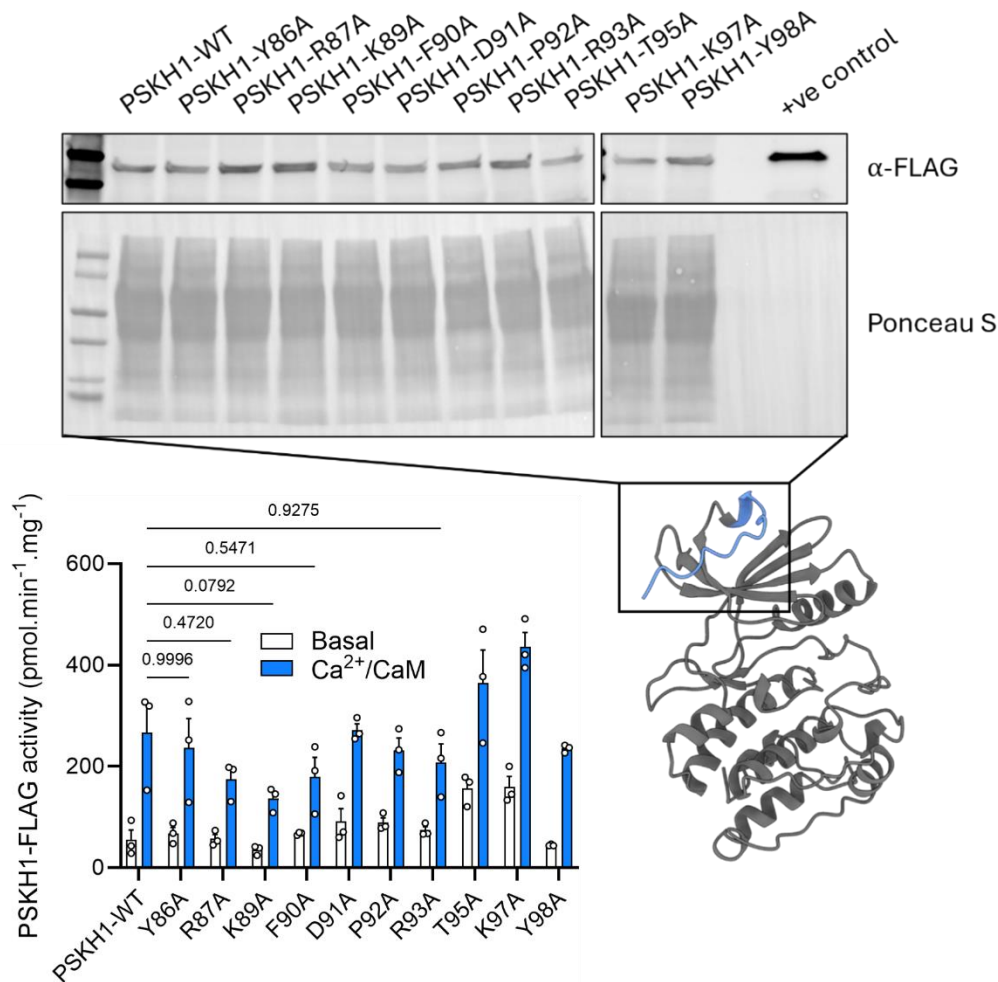
***Figure 3.21. Alanine scan of the putative N-terminal PSKH1 CBD.*** Wild-type (PSKH1-WT) or alanine point mutants were transiently expressed in HEK293T cells. To maximally stimulate CaM-enhancement of kinase activity, cells were briefly (30 minutes) glucose starved before rapid lysis *in situ*. PSKH1-FLAG was immunoprecipitated from WCL using an anti-FLAG M2 Affinity resin and radiometrically assayed on-beads in the presence of of 200μM ATP mix, 200μM PSKH1 peptide substrate (ADR1G233), 100μM CaCl2 and 1μM CaM. Activity measurements were corrected for differences in construct expression by western blot. Data was statistically appraised by two-way ANOVA and Tukey's multiple comparisons test (data is representative of three independent experiments (n=3; three technical replicates/experiment). A ribbon representation of the PSKH1 kinase domain (grey) and putative N-terminal CBD (cornflower blue) is shown (AlphaFold2).

### 3.2.3.5. PSKH1 harbours a putative CBD in an analogous position to the CTM (CBD) of the atypical protein kinase, eEF2K
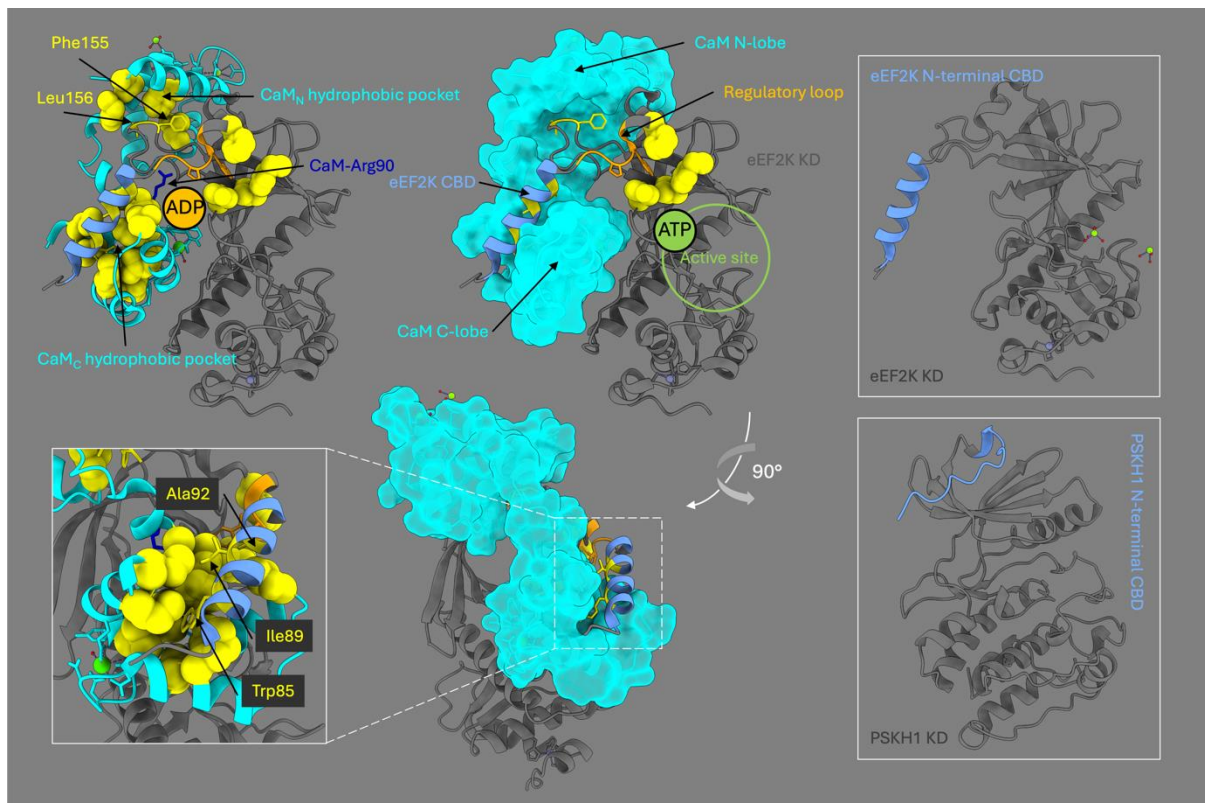


*Figure 3.22. PSKH1's N-terminal CBD lies in an analogous position to eEF2K's calmodulin-binding motif, which docks CaM in an extended conformation.* CaM (light blue) docks the α-kinase eEF2K in an extended conformation. For clarity, only the kinase domain (KD; dark grey) of eEF2K is shown. Binding is facilitated chiefly via contacts at the C-lobe (CaM$_C$) of CaM. The hydrophobic interface (yellow surface representation) of CaM$_C$ anchors the aliphatic side chains (Trp85, Ile89, Ala92) of the eEF2K CBD (cornflower blue). ADP has been demonstrated to bind to a basic pocket on the N-lobe of the kinase domain, enhancing CaM-activation of eEF2K [230]. Correct positioning of the CBD by CaM$_C$ generates an activation spine comprising the CBD, regulatory loop (orange) and conserved hydrophobic residues within the N-lobe of the eEF2K-KD, coupling CaM-signalling to the phosphoryl transfer capabilities of eEF2K [231]. CaM$_N$'s function is supportive, anchoring the kinase complex more stably. *Inserts (right).* eEF2K's CBD lies N-terminal to the kinase domain. PSKH1's putative CBD lies in an analogous position to eEF2Ks (AF2). The described graphic was prepared using publicly available data from the Protein Data Bank (PDB ID: 7SHQ) and ChimeraX. The PSKH1 structure was synthesised using the ColabFold v1.5.5 Colaboratory Notebook [94].

### 3.2.3.6. Sequence alignment of the eEF2K and putative PSKH1 CBD reveals an inverted 1-5-8 motif in PSKH1

As in the CBD's of skMLCK, smMLCK, CaMK2α and CaMKK1 previously described, the eEF2K-CBD is characterised by a unique binding motif essential for its interaction with CaM. The aliphatic side chains W85, I89 and A92 form a "1-5-8" motif that anchors within the hydrophobic channel of the $CaM_C$ lobe (Figure 3.22) [231]. Interestingly, alignment of the primary structure of eEF2K and PSKH1 reveals striking homology at the eEF2K/PSKH1 CBD region (bolded and highlighted residues) (Figure 3.23). Further, on closer inspection, PSKH1 harbours an inverted 1-5-8 motif in its N-terminal CBD (F90, Y86, V83) (Figure 23). Try85 and Phe90 in eEF2K and PSKH1, respectively, appear to be the primary, anchoring aromatics. In AlphaFold2 docking simulations between CaM and the PSKH1-1-5-8 peptide, CaM binds the PSKH1-CBD in a reverse orientation (Figure 3.23). Predicted aligned error (PAE) plots indicate that the position and spatial arrangement of the PSKH1-CBD peptide is moderately confident (black arrows).
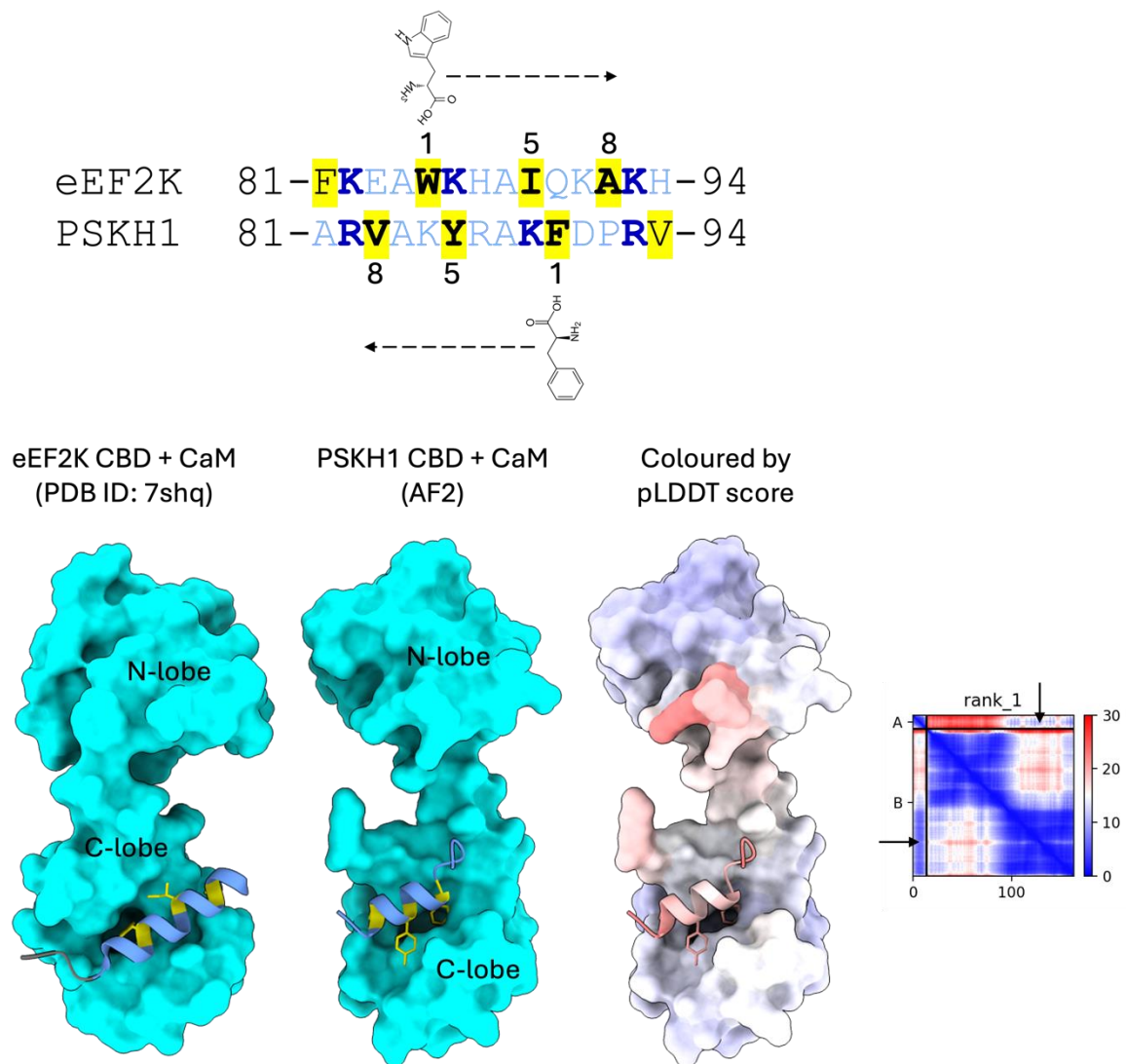
***Figure 3.23. Sequence alignment of the eEF2K and putative PSKH1 CBD reveals an inverted 1-5-8 motif in PSKH1.*** UNIPROT sequence alignment of the eEF2K and PSKH1 primary structures. The 1-5-8 motif (bolded yellow) characteristic to the eEF2K-CBD is represented in the PSKH1 N-terminal CBD as a palindromic motif. Conserved basic and hydrophobic residues are coloured blue (bolded) and yellow, respectively. Modelling on AlphaFold2 between CaM and the PSKH1-1-5-8 peptide indicates a reversed binding orientation. The corresponding predicted aligned error (PAE) plot and pLDDT colouring is shown.

**3.2.3.7. ADP/AMP do not potentiate Ca2+/CaM enhancement of PSKH1-FLAG activity**

The discovery that PSKH1 is activated in response to glucose deprivation in combination with the observation that PSKH1 harbours a putative CBD in an analogous position to eEF2K led to interrogation of the nucleotide sensing properties of PSKH1. ADP allosterically enhances CaM-activation of eEF2K by binding to a basic pocket on the N-lobe of the kinase domain [230]. Unstimulated PSKH1-FLAG transiently expressed in HEK293T cells was immunoprecipitated from WCL and radiometrically assayed on-beads in the presence or absence of ADP or AMP. As previously observed, CaM caused a marked increase (3-fold) in PSKH1 activity (Figure 3.24). Conversely, 100μM ADP or AMP attenuated intrinsic and CaM-mediated catalytic activity. This decrease in kinase activity likely reflects displacement of ATP at the active site by ADP and AMP. Although lower concentrations of ADP and AMP were not explored, it is unlikely that these nucleotides allosterically enhance CaM-activation of PSKH1 *in vitro*.
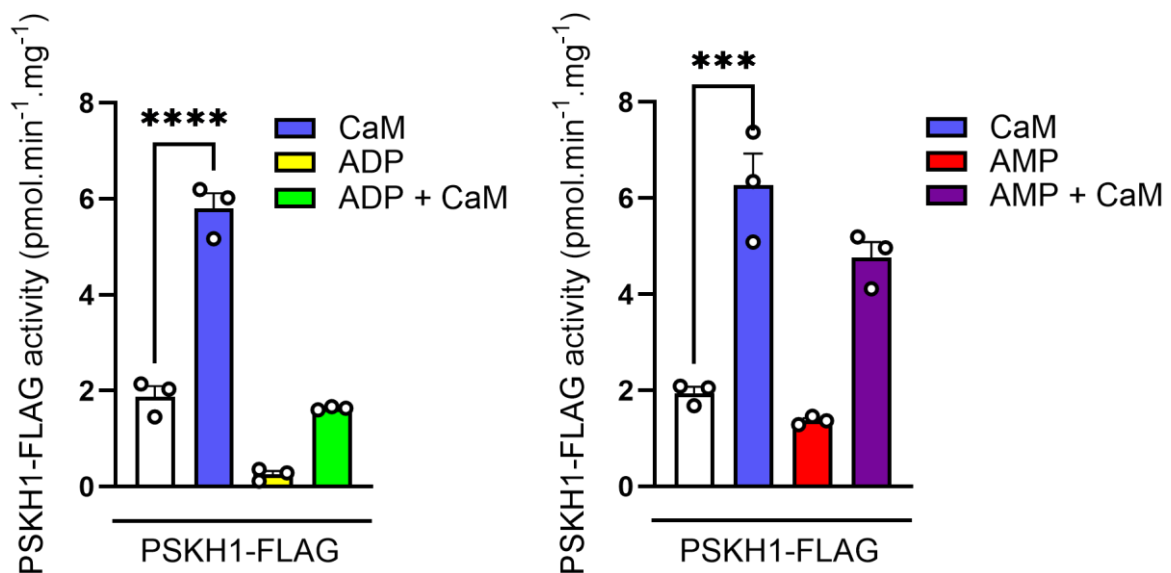


***Figure 3.24. ADP/AMP do not potentiate CaM-enhancement of PSKH1-FLAG activity.*** Unstimulated PSKH1-FLAG immunoprecipitated from HEK293T cells was radiometrically assayed on-beads in the presence of 200μM ATP mix and 200μM PSKH1 peptide substrate (ADR1G233), with or without (basal – boxed white) 1μM CaM, 100μM CaCl2, 100μM ADP

or 100μM AMP. Data was statistically appraised by one-way ANOVA and Tukey's multiple comparisons test. ****: <0.0001; ***: 0.0002. Three technical replicates.

## 3.3. Other modulators of PSKH1 activity

The implications of the findings previously described are several-fold: firstly, PSKH1 can autoactivate in a *cis*-apparent mechanism, independently of $Ca^{2+}$/Calmodulin (Figures 3.9/10/11). Secondly, $Ca^{2+}$/Calmodulin potentiates the catalytic activity of PSKH1 two- (GFP-PSKH1) to eight-fold (PSKH1-FLAG) (Figures 3.17/19). Finally, PSKH1 likely participates in CaM-interaction N-terminal to its kinase domain (Figures 3.18/20/21/22/23). Although the kinetics of PSKH1 autophosphorylation were comparatively slow for a viable *in vivo* system, likely reflecting an absence of additional regulatory inputs *in vitro*, what would prevent unfettered autoactivation of PSKH1 in cells? Like CaMKK2, PSKH1 harbours several putative PKA phosphorylation sites that may be involved in recruitment of 14-3-3 protein to regulate PSKH1 cellular localisation. As such, PKA-mediated 14-3-3 recruitment of PSKH1 was subsequently explored.

### 3.3.1. Results

### 3.3.1.1. PSKH1-FLAG does not co-immunoprecipitate with 14-3-3 following forskolin treatment in HEK293T cells

To explore PKA-mediated 14-3-3 recruitment of PSKH1, HEK293T cells transiently expressing PSKH1-FLAG were treated with or without (DMSO; V) 50μm forskolin and rapidly lysed *in situ*. FLAG-conjugated PSKH1 was immunoprecipitated from WCL using an anti-FLAG M2 Affinity resin and eluted in 1mg/ml FLAG peptide. 14-3-3 recruitment was interrogated by SDS-PAGE and western blot analysis of input (WCL) and IP preparations. 14-3-3 was abundantly present in HEK293T WCL (Figure 3.25). Full-length PSKH1-FLAG is empirically difficult to detect in WCL, likely due to the prevalence of membrane-targeting motifs at its N-terminus and the lysis conditions used (Figure 1.7). Although forskolin stimulation caused a marked increase in Ser511 phosphorylation, an established PKA

phosphorylation and 14-3-3 recruitment site on CaMKK2, 14-3-3 was not detected in forskolin treated PSKH1-FLAG IP preparations. Although this data does not preclude 14-3-3 regulation of PSKH1, 14-3-3 does not coimmunoprecipitate with PSKH1-FLAG under the conditions tested.
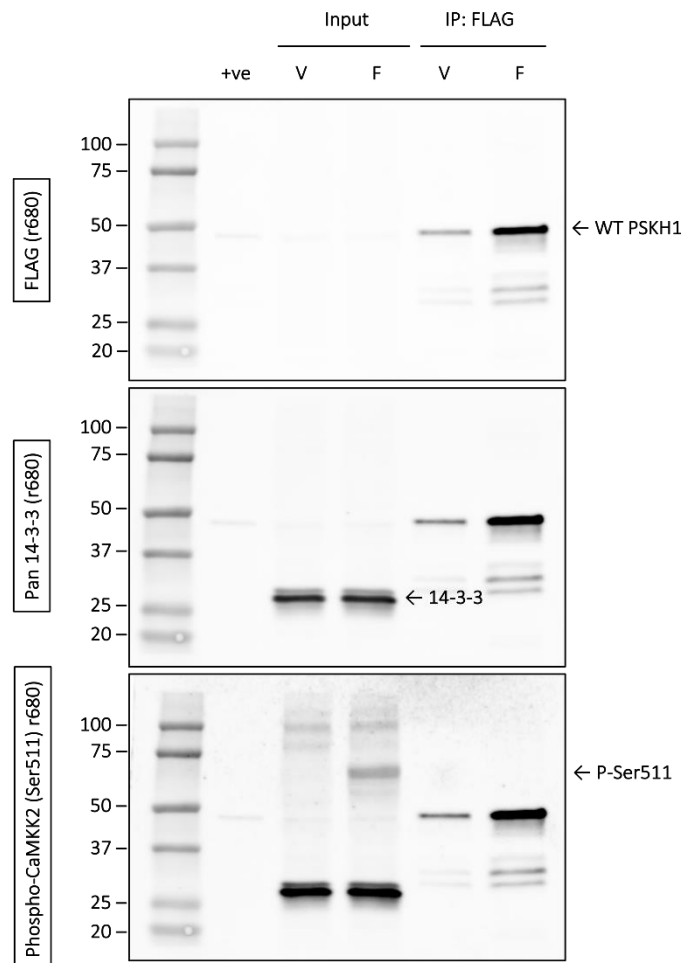


***Figure 3.25. PSKH1-FLAG does not co-immunoprecipitate with 14-3-3 following Forskolin treatment.*** HEK293T cells transiently expressing PSKH1-FLAG were treated with or without (DMSO) 50µM forskolin for 20 minutes and rapidly lysed *in situ*. PSKH1-FLAG was immunoprecipitated from WCL as previously described and eluted overnight in 1mg/ml FLAG peptide. The presence of 14-3-3 in 30µg WCL and 10µL eluted PSKH1-FLAG was interrogated by SDS-PAGE and western blot using a pan-14-3-3 antibody (CST). Phospho-Ser511 was utilised as a positive control for forskolin treatment. PSKH1-FLAG was detected using an anti-FLAG antibody (CST). All primary antibodies were detected using an anti-rabbit fluorescently conjugated (680) secondary antibody. V: vehicle; F: forskolin.

**3.3.1.2. The CREC family of low-affinity Ca$^{2+}$-binding proteins are novel PSKH1 interactors that attenuate autoactivation of GFP-PSKH1 *in vitro***

CaM potentiates the intrinsic activity of PSKH1 but does not attenuate autophosphorylation, in contrast to a previous report (Figure 3.10) [38]. In a concurrent study seeking to elucidate novel interactors of PSKH1, it was revealed that most members of a novel family of low-affinity Ca$^{2+}$-binding proteins (CREC) were enriched and represented (Figure 3.26, Dr. Chris Horne, Dr. Toby Dite). This included the reticulocalbins (RCN) RCN1 and RCN3, and calumenin (CALU). Reticulocalbin-1 (RCN1), notably the most enriched, was selected first for further interrogation. RCN1 retains many features characteristic to CaM: firstly, AlphaFold2 simulations predict a bi-lobate, dumbbell-shaped protein, like CaM (data not shown). Secondly, in contrast to CaM which harbours two pairs of terminal EF-hands, RCN1 has three [232]. These EF-hands bear point substitutions at the position 15 glycine residue (Figure 3.13), which typically is required due to structural constraints on the Ca$^{2+}$-coordinating carboxylate ligand loop [232]. Indeed, EF-hands 2 and 6 appear to have lost their Ca$^{2+}$-binding ability [232]. This reduced Ca$^{2+}$ affinity, in combination with a C-terminal ER-retention signal (HDEL), may explain RCN1's luminal subcellular localisation, where concentrations of Ca$^{2+}$ are high ($10^{-3}$ M) (Table 3.1). In any event, RCN1 was interrogated for its ability to modulate the activity of PSKH1. Purified recombinant GFP-PSKH1 was allowed to autophosphorylate in the presence of MgATP, with or without Ca$^{2+}$ or Ca$^{2+}$/RCN1 (Figure 3.26). As previously observed, there was a time-dependent increase in PSKH1 autophosphorylation on incubation with MgATP, as determined by deepening pThr immunoreactivity (Figure 3.26). In contrast to controls (+MgATP alone, +MgATP/Ca$^{2+}$), RCN1 severely abrogated autophosphorylation of GFP-PSKH1 (Figure 3.26). The closely related Ca$^{2+}$-binding protein RCN3, which was also highly enriched in our PSKH1-TurboID

proteomic screen, also attenuated autophosphorylation of GFP-PSKH1, although to a lesser

degree (Figure 3.26).
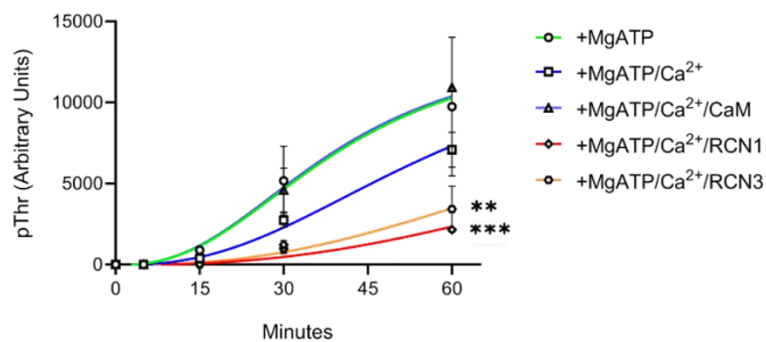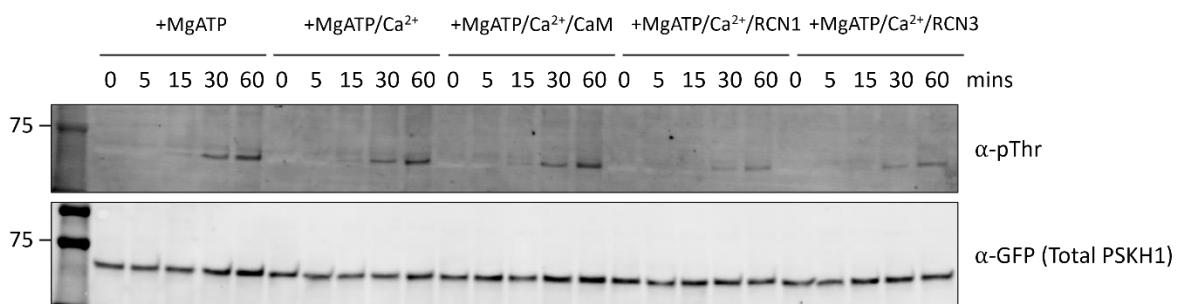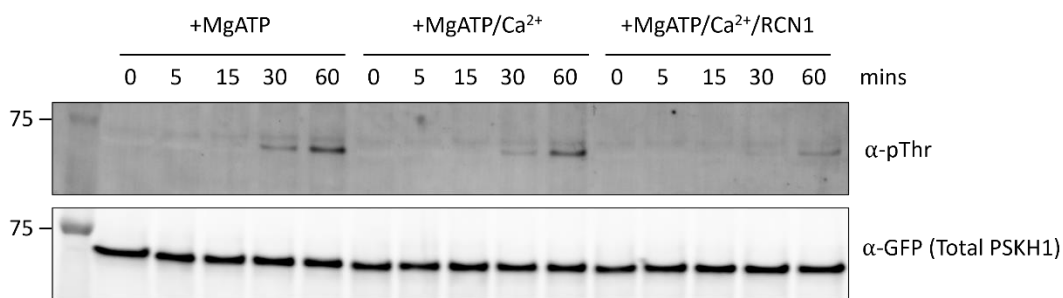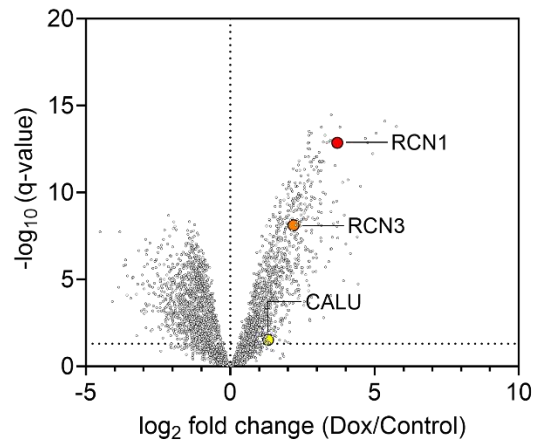
*Figure 3.26. The CREC-family members RCN1 and RCN3 are novel interacting partners of PSKH1 that attenuate autophosphorylation in vitro. Volcano plot.* The CREC proteins RCN1, RCN3 and calumenin were identified as novel interacting partners of PSKH1 in proximity labelling experiments using a doxycycline-inducible TurboID fusion construct of PSKH1 (Dr. Chris Horne, Dr. Toby Dite, unpublished). *In vitro phosphorylation experiment.* 500ng GFP-PSKH1 was allowed to autophosphorylate in the presence of $Mg^{2+}$ATP, with or without 100$\mu$M $Ca^{2+}$, 100$\mu$M $Ca^{2+}$/1$\mu$M CaM, 100$\mu$M $Ca^{2+}$/1$\mu$M RCN1, or 100$\mu$M $Ca^{2+}$/1$\mu$M RCN3 for 0-60 minutes. Autophosphorylation was inferred by SDS-PAGE and western blot using phosphorylated threonine (pThr) as a readout for PSKH1 activation loop autophosphorylation. pThr and total PSKH1 was visualised using $\alpha$-mouse phospho-threonine (42H4) and $\alpha$-rabbit GFP (D5.1) primary antibodies and $\alpha$-rabbit IRDye® 680RD and $\alpha$-mouse IRDye® 800CW near-infrared secondary antibodies. Representative blots are shown (three independent experiments were performed). pThr densitometries were normalised to total protein (GFP-PSKH1) and statistically appraised by two-way ANOVA and Tukey's multiple comparisons test. **: p=0.0025; ***: p=0.0003. Comparisons were made against +MgATP/$Ca^{2+}$ controls.

### 3.3.1.3. The CREC-family members RCN1 and RCN3 attenuate the catalytic activity of GFP-PSKH1

To interrogate the inhibitory effects of RCN on PSKH1 activity further, radiometric assaying was employed. Given the observed differential effects of CaM and RCN on PSKH1, in addition to their contrasting $Ca^{2+}$ affinities (Table 3.1), it was hypothesised that CaM and RCN would co-ordinately modulate PSKH1 activity in response to changing intracellular $Ca^{2+}$ concentration (Figure 3.27). For example, at low $Ca^{2+}$ concentrations, the high-affinity $Ca^{2+}$-decoding protein CaM is activated and increases the intrinsic activity of GFP-PSKH1. Conversely, at high $Ca^{2+}$ concentrations, the low-affinity $Ca^{2+}$-sensing proteins RCN1 and RCN3 are activated and attenuate the autoactivity of PSKH1. GFP-PSKH1 activity toward a peptide substrate (ADR1G233) was measured over a $Ca^{2+}$ gradient (0-1mM) in the presence or absence of CaM, RCN1 or RCN3 (Figure 3.27). Prior to experimentation, potential contaminating $Ca^{2+}$ in CaM/RCN1/RCN3 preparations was investigated by radiometric kinase assay by assaying GFP-PSKH1 in the presence of CaM/RCN1/RCN3 over an EGTA concentration gradient (Supplementary Figure 3.5.3). CaM marginally increased PSKH1 activity over basal, which was somewhat consistent with previous experimentation, although this was not significant (Figure 3.27). An important consideration is that insect cell (SF9)

expressed GFP-PSKH1 exhibits much higher intrinsic activity than PSKH1-FLAG expressed in HEK293T cells (nmol vs pmol, respectively). It is possible that the comparatively stressful environment of suspension culturing (our GFP-PSKH1 preparations are derived from SF9 cells cultured in suspension) activates GFP-PSKH1 and attenuates the stimulatory effect of $Ca^{2+}$/CaM which we typically observe in HEK293T-derived PSKH1-FLAG. Indeed, as previously shown, cell stressors such as glucose deprivation stimulate PSKH1 activity (Figure 3.19). Alternating the $Ca^{2+}$ concentration had no demonstrable effect on CaM-mediated activation of PSKH1 except at high doses (>100μM) (Figure 3.27). RCN1 and RCN3 attenuated the intrinsic activity of PSKH1 by approximately 50% at all $Ca^{2+}$ concentrations tested (Figure 3.27).
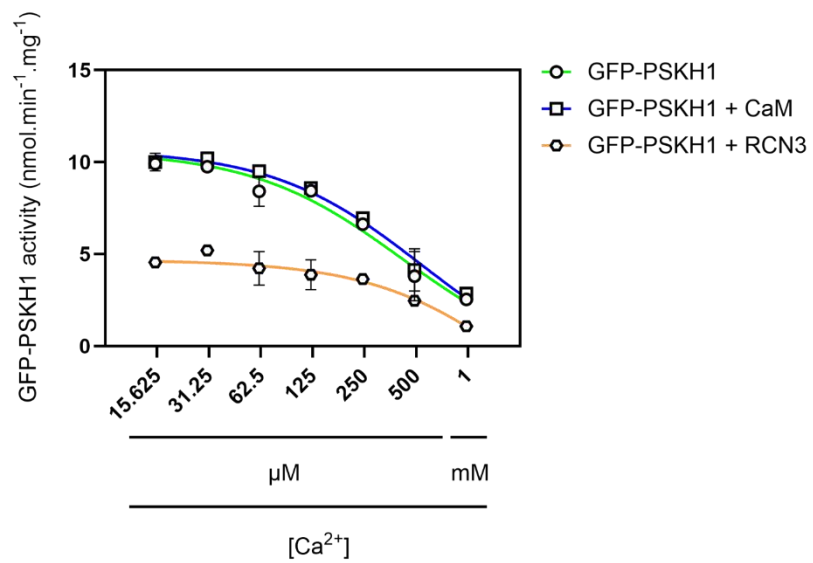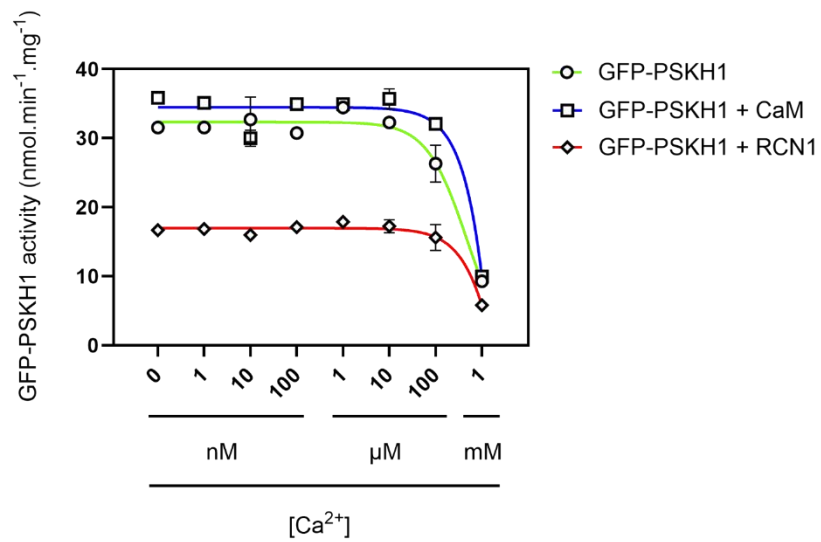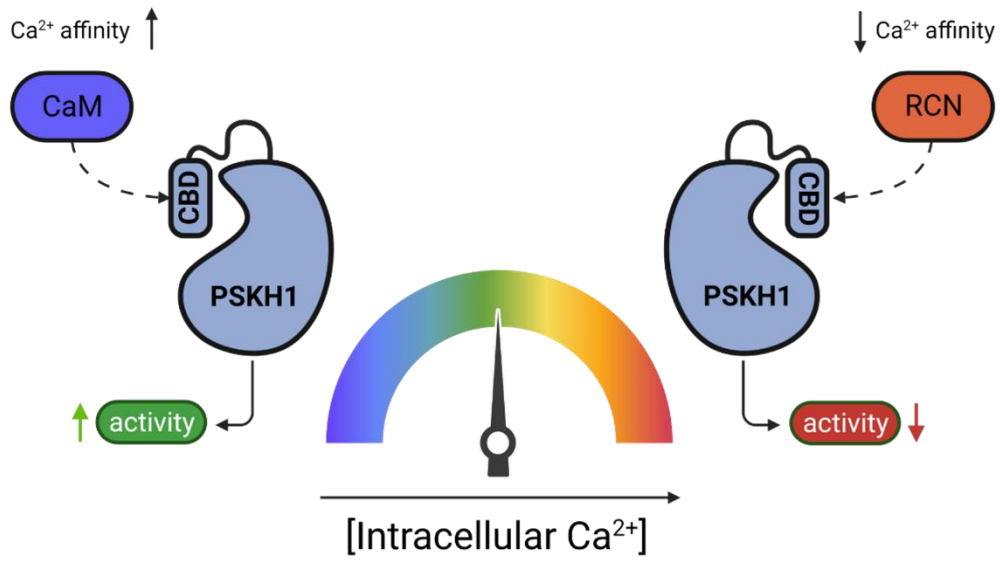
*Figure 3.27. The CREC-family members RCN1 and RCN3 abrogate the catalytic activity of GFP-PSKH1 independently of Ca2+.* 50ng GFP-PSKH1 was radiometrically assayed over a $Ca^{2+}$ gradient (0-1mM) in the presence or absence of 1μM CaM, 1μM RCN1 or 1μM RCN3. Data were fit to the equation: Y=Bottom + (Top-Bottom)/(1+(X/IC50)). Data is representative of three independent experiments (three technical replicates/experiment).

## 3.3.1.4. The CREC-family member, Calumenin, attenuates the autophosphorylation but not the catalytic activity of GFP-PSKH1

Given the dual inhibitory effects of the reticulocalbins on PSKH1 autophosphorylation and intrinsic activity, we decided to also interrogate the effect of the other CREC protein represented in our PSKH1 proteomic screen, calumenin (Figure 3.26). In *in vitro* autophosphorylation experiments, calumenin attenuated autoactivation of GFP-PSKH1 (as determined by decreased pThr immunoreactivity) relative to MgATP/$Ca^{2+}$ controls (Figure 3.27). In radiometric assays, calumenin had no effect on the intrinsic activity of PSKH1 (data not shown).
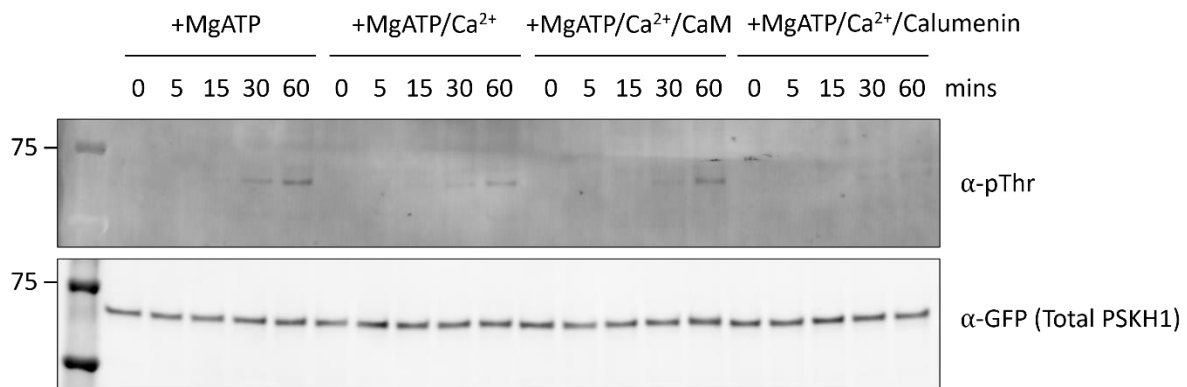


*Figure 3.28. The CREC-family member calumenin attenuates autophosphorylation of GFP-PSKH1. Western blot.* 500ng GFP-PSKH1 was allowed to autophosphorylate in the presence of MgATP, with or without $Ca^{2+}$, $Ca^{2+}$/CaM, or $Ca^{2+}$/Calumenin over a period of 0-60 minutes. Autophosphorylation of GFP-PSKH1 was subsequently determined by SDS-PAGE and immunoblot analysis using α-mouse phospho-threonine (42H4) and α-rabbit GFP (D5.1) primary antibodies and α-rabbit IRDye® 680RD and α-mouse IRDye® 800CW near-infrared secondary antibodies. A representative blot is shown (n=3).

**Table 3.1. Calcium affinities for members of the EF-hand-containing calcium-binding protein superfamily.**

| Cytosolic [Ca$^{2+}$] | nM-μM (10$^{-7}$) | | | | | |
|---|---|---|---|---|---|---|
| ER lumen [Ca$^{2+}$] | mM (10$^{-3}$) | | | | | |
| **Protein** | **Acronym** | **EF-hands** | **Ca$^{2+}$ Kd** | **Ca$^{2+}$ affinity** | **Subcellular localisation** | **Ref** |
| Calmodulin | CaM | 4 | 10$^{-7/6}$ | High | Cytosol, nucleus | [224] |
| Reticulocalbin-1 | RCN; RCN1 | 6 | 10$^{-4/3}$ M | Low | ER | [232] |
| Reticulocalbin-2 | RCN2; ERC-55 | 6 | 10$^{-4/3}$ M | Low | ER, Golgi | [233] |
| Reticulocalbin-3 | RCN3 | 6 | 10$^{-4/3}$ M | Low | ER, Golgi | [234] |
| Calumenin | CALU | 7 | 10$^{-4/3}$ M | Low | ER, Golgi | [235] |
| Cab45 | - | 6 | 10$^{-4/3}$ M | Low | Golgi | [236] |

## 3.4. Discussion

Since its discovery by Hanks [139] in the late 1980's, a growing body of literature has implicated PSKH1 in an array of cellular programs, including pre-mRNA splicing [140], anterograde vesicle trafficking [141] and cell migration [113]. However, a precise function for this elusive enzyme has to date not been described. Moreover, the mechanisms by which PSKH1 is regulated remain unknown. Proper maintenance of kinase activity is critical to mitigating the dramatic pleiotropic effects this family of enzymes impart on biological processes. Thus, it is not surprising that dysregulated kinase activity often correlates with aggressive and fatal disease phenotypes, including metastatic prostate cancer, of which PSKH1 is a top 6 driver [6]. As such, there is a pressing need to elucidate the mechanisms by which kinase activity, and indeed PSKH1, is controlled. The aim of this chapter was to address this question: by what mechanisms is the serine/threonine-protein kinase H1 regulated? The aims of this chapter were:

1. To determine if PSKH1 is regulated by activation loop phosphorylation

2. As a *bona fide* member of the CaMK family, is PSKH1 regulated by calmodulin?

### 3.4.1. Activation loop regulation of PSKH1

Many kinases are regulated by phosphorylation of a segment termed the "activation loop" whereby the covalent attachment of an acidic phosphate moiety coordinates the catalytic architecture of the kinase domain. Although it was initially hypothesised that CaMKK2 would phosphorylate the activation segment (Thr256) of PSKH1, *in vitro* phosphorylation experiments failed to detect pThr immunoreactivity on incubation of PSKH1-FLAG or GFP-PSKH1 with CaMKK1 or 2 (Figure 3.5/Supp Fig. 3.5.1). In retrospect, this is somewhat not surprising. Although PSKH1 is, theoretically, an ideal CaMKK substrate due to congruency with the substrate-binding CaMKK2-β5-αE loop, recent evidence indicates that CaMKK may interface with its substrates primarily through the RP insert [91, 92]. Further, peptides

containing the phosphorylation sites of CaMK1 and CaMK4 perform comparatively poorly as a CaMKK substrate (higher $K_m$ values) in contrast to the native enzymes, indicating a strong preference by CaMKK for substrate tertiary structure [237]. As such, PSKH1 may not possess the necessary structural architecture for CaMKK2 recognition. CHK2 was later selected for interrogation as a putative upstream activating kinase of PSKH1. CHK2 is unique in that it phosphorylates its own activation *in trans* by T-loop exchange (Figure 3.8) [221]. Due to homology between the activation loops of CHK2 and PSKH1, we reasoned that if CHK2 can phosphorylate its own activation loop *in trans*, can it also phosphorylate the activation loop of PSKH1 (Figure 3.8). Interestingly, although recombinant GFP-PSKH1 did not exhibit increased pThr immunoreactivity upon incubation with purified CHK2 (full-length or a kinase domain-only truncation mutant), GFP-PSKH1 autophosphorylated in a time-dependent manner (Figure 3.8). PSKH1 has been reported to autophosphorylate on a serine cluster C-terminal to the kinase domain, but peculiarly, not for threonine residues [38]. Threonine phosphorylation strongly correlates with activation of protein kinases, as threonine typically occupies the recipient phosphorylation site in the activation segment. To determine if pThr-autophosphorylation increased PSKH1 activity, GFP-PSKH1 pre-treated with $Mg^{2+}$ATP was radiometrically assayed for its ability to incorporate γ-32P into a peptide substrate. Autophosphorylated GFP-PSKH1 demonstrated a 4-5 fold increase in catalytic activity compared to a non-phosphorylated (50 mM HEPES buffer) control (Figure 3.8). Further, a kinase dead point mutant (GFP-PSKH1-D218N) pre-treated with $Mg^{2+}$ATP failed to exhibit detectable activity above background controls (Figure 3.9). Both WT and kinase dead GFP-PSKH1 should theoretically bind the same protein complement. Thus, it is unlikely that a contaminating kinase co-purifying with PSKH1 could explain the data previously described. Ergo, these data collectively demonstrate that PSKH1 can autoactivate itself by phosphorylating, presumably, its activation loop.

PSKH1 is a *bona-fide* CaM-kinase [1]. Indeed, early biochemical characterisation studies by Brede, Solheim [38] revealed that $Ca^{2+}$/CaM attenuates autophosphorylation of a serine cluster in PSKH1. As pThr-autophosphorylation had not been reported previously, we decided to investigate the functional relevance of $Ca^{2+}$/CaM in the autoactivation of PSKH1. Interestingly, $Ca^{2+}$/CaM did not demonstrably alter incorporation of $Mg^{2+}$ATP in *in vitro* autophosphorylation experiments (Figure 3.10). Inversely, autophosphorylation did not prime PSKH1 for further regulation by $Ca^{2+}$/CaM (Figure 3.10). However, $Ca^{2+}$/CaM did enhance the intrinsic activity of unstimulated GFP-PSKH1 (Figure 3.10). These data suggest little role for $Ca^{2+}$/CaM in the autophosphorylation of PSKH1, in contrast to a previous report [38]. Our data indicate $Ca^{2+}$/CaM enhances, rather than abrogates, the intrinsic activity of PSKH1 (Figure 3.10), which is consistent with $Ca^{2+}$/CaM regulation the closely related CaM-kinases CaMK1 and CaMK4 [20, 89]. By precisely what mechanism does PSKH1 autophosphorylate? Concentration dependence studies indicated that PSKH1 autophosphorylates in a *cis*-apparent mechanism (Figure 3.11). Increasing the concentration of PSKH1 did not demonstrably alter the kinetics of phosphoryl transfer and, further, did not translate to increase kinase activity in radiometric kinase assays (Figure 3.11). PSKH1 has been reported to form, at minimum, homodimers [38]. Thus, at present it is not clear whether monomeric PSKH1 or a stable homodimer autophosphorylating in a *cis*-apparent mechanism is responsible for the demonstrated autophosphorylation previously described. Irrespectively, these data demonstrate that PSKH1 can autoactivate itself by presumably, phosphorylating its activation loop. To ascertain precisely what residues are autophosphorylated in PSKH1, LC-MS/MS was employed. Trypsin digest/LC-MS/MS analysis of autophosphorylated GFP-PSKH1 revealed significant phosphate incorporation at a serine cluster C-terminal to the catalytic domain of PSKH1 (Figure 3.12). This region has been reported previously as a major autophosphorylation site, corroborating previous reports [38]. Interestingly, Ser272 lies in the predicted C-terminal

Ca$^{2+}$/CaM-binding domain of PSKH1 [38]. The ramifications of this observation will be discussed in greater detail in the following subchapter and figure 3.31. Residues within the activation segment also demonstrated phosphate incorporation upon Mg$^{2+}$ATP addition, including Thr260 (Figure 3.12). This phosphoacceptor site is adjacent to the predicted activation loop residue, Thr256. Unfortunately, in the conditions tested, we were not able to detect phosphorylation of Thr256. This is likely because Thr256 is immediately preceded by a lysine side chain (Lys255) which, by traditional trypsin digest methodologies, would result in a peptide too large for LC-MS/MS analysis. Corroborating this, subsequent work by collaborators incorporating chymotrypsin revealed significant phosphate incorporation at the Thr256 site.

### 3.4.2. Ca$^{2+}$/CaM-regulation of PSKH1

Although PSKH1 is by definition a CaM-kinase, the CaMK designation purely reflects homology of the kinase catalytic core [1]. In other words, CaM-kinases are not inherently CaM-regulated. Indeed, many representative kinases in the CaMK subfamily are not calmodulin regulated at all, including all members of the AMPK-related sub-branch and DCLK1, which is activated by HPCAL1 [238]. Early efforts to biochemically characterise PSKH1 by Brede, Solheim [38] revealed a putative C-terminal CBD with moderate homology to the CaMK1 calmodulin-binding domain. Interestingly, in this study CaM attenuated autophosphorylation of PSKH1 [38]. However, in our hands, autophosphorylation of PSKH1 (as determined by pThr immunoreactivity upon incubation with Mg$^{2+}$ATP) is entirely Ca$^{2+}$/CaM-independent (Figure 3.10). Further, CaM potentiates the intrinsic activity of GFP and FLAG-tagged PSKH1 (Figures 3.17/19). This incongruency in findings may reflect differences in the design of expression constructs and epitope tags used. Irrespectively, we decided to investigate the functional relevance of the Brede C-terminal CBD by truncational analysis. Successive truncations into the C-terminal CBD failed to impair CaM-binding (Supp. Figure 3.5.2).

Consequently, alternative regions of the PSKH1 primary structure were explored. It was later discovered through cross-species sequence comparison that a region immediately N-terminal to the kinase domain of PSKH1 bore extremely strong sequence conservation across eukaryotes (Dr. Gerard Manning, unpublished). From fish to mammals, the retention of near-identical genetic information strongly suggested a critical function for this ~20aa region. Helical wheel plot analysis of a corresponding peptide revealed overall amphipathicity and an α-helix architecture, two features characteristic of calmodulin-binding domains (Figure 3.18). As such, the functional relevance of this region, as it pertains to CaM-binding, was explored. Truncation severely impaired the intrinsic and CaM-modulated activity of PSKH1-FLAG (Figure 3.20). It is worth noting that these activities reflect counts normalised to the expression of the respective PSKH1 construct. Unlike full-length PSKH1-FLAG which is barely detectable in HEK293T WCL, PSKH1-86-424 and PSKH1-98-424 are robustly expressed. This dramatic increase in PSKH1 expression likely reflects liberation from internal membranes (the fraction of WCL which would typically be lost due to the relatively gentle cell lysis conditions used to preserve kinase function) due to the deletion of various membrane-targeting motifs (Figure 1.7). Importantly, PSKH1-86-424 does retain some activity toward a peptide substrate, although CaM-enhancement is significantly attenuated (<2-fold) (Figure 3.20). Conversely, PSKH1-98-424 is completely kinase dead (Figure 3.20). These data collectively demonstrate a critical importance of this region for kinase activity and $Ca^{2+}$/CaM recognition of PSKH1. It was concurrently discovered in an adjacent study investigating the functional relevance of PSKH1 in prostate cancer that PSKH1 promotes cell proliferation under nutrient (glucose) deprivation (Figure 4.2). This would invariably imply that energy stress activates PSKH1. The atypical CaM-binding protein kinase eEF2K is similarly activated under nutrient limiting conditions, which culminate in eEF2K-T348 autophosphorylation and disabling of the downstream effector eEF2, preventing unfettered cell proliferation during energy deplete conditions. CaM-

binding increases the $K_{cat}$ of eEF2K toward a peptide substrate by approximately 2400-fold [239]. Activation is facilitated by binding of the C-lobe of CaM (CaM$_C$) to the eEF2K CBD and subsequent formation of an activation spine, which directly couples CaM-signalling to the phosphoryl-transfer capabilities of eEF2K (Figure 3.22) [231]. The eEF2K CBD is characterised by a 1-5-8 motif of aromatic/aliphatic side chains that serve to anchor the Ca$^{2+}$/CaM molecule in place [231]. It was recently discovered that ADP allosterically enhances CaM-activation of eEF2K by binding to a basic pocket on the N-lobe of the kinase domain, corroborating previous reports that energy stress stimulates eEF2K activity [230]. Interestingly, the putative N-terminal CBD of PSKH1 lies in an analogous position to eEF2K's CBD (Figure 3.22). Strikingly, sequence alignment of the eEF2K and PSKH1 calmodulin-binding domains revealed a palindromic 1-5-8 motif in PSKH1 (Figure 3.23). Given these observations and the dual requirement for energy stress in the activation of eEF2K and PSKH1, ADP regulation of PSKH1 was explored. Interestingly, neither ADP nor AMP enhanced CaM-activation of PSKH1-FLAG (Figure 3.24). Further, an alanine scan of the PSKH1 N-terminal CBD region failed to significantly attenuate CaM-activation of PSKH1-FLAG, although a moderate (25-50%) reduction was observed in the R87, K89 and F90 point mutants (Figure 3.21). F90 is analogous to the W85 anchor residue in eEF2K and is the only aromatic amino acid present in the eEF2K CBD [231]. This residue is critical for CaM-recognition, as the 5 (I89) and 8 (A92) amino acids of the 1-5-8 motif harbour comparatively short hydrophobic side chains [231]. Thus, it was hypothesised that F90A would significantly abrogate CaM-binding of PSKH1. However, as previously stated, CaM-activation was largely retained in the PSKH1 point mutants tested (Figure 3.20). Exactly how CaM-binding is preserved will be explored below.

*Limitations*

A consistent problem plaguing our attempts to functionally characterise PSKH1 was the retention of intrinsic and CaM-modulated activity in catalytically impaired mutants. For

example, an activation loop point mutant (T256A) and kinase dead variant (D218N) of PSKH1, although attenuated compared to a wild-type control, are still responsive to $Ca^{2+}$/CaM and bear some intrinsic activity (Figure 3.20). How is this possible? Yeast two-hybrid and gel filtration studies have demonstrated that PSKH1 forms, at minimum, homodimers [38]. Congruent with this observation, GFP-PSKH1 frequently elutes off in the void fraction, indicating higher order structure (Dr. Chris Horne, unpublished). Modelling by AlphaFold2 predicts the PSKH1 homodimer in a head-to-toe orientation. This would theoretically bring both the N- and C-terminal CBD's in relative proximity to one another (Figure 3.29). The eEF2K-CBD, which is analogous to the PSKH1 N-terminal CBD, interfaces with the C-lobe of calmodulin ($CaM_C$) only (Figures 3.22/23) [231]. AlphaFold2 modelling supports $CaM_C$-binding of the PSKH1 N-terminal CBD peptide (Figure 3.23). Potentially, two molecules of $Ca^{2+}$/CaM stabilise the PSKH1 homodimer by binding the C- and N-terminal CBDs in an extended conformation (Figure 3.29). Indeed, unlike the closely related CaM-kinase CaMK1 and CaMK4, $Ca^{2+}$/CaM is not essential for the intrinsic activity of PSKH1. Rather, $Ca^{2+}$/CaM may enhance the kinetics of phosphoryl transfer or alter the substrate profile of PSKH1. It is entirely possible that the purified PSKH1-FLAG mutants co-immunoprecipitate with endogenous PSKH1, as expression of the PSKH1 constructs is under the control of a CMV promoter (Figure 2.1). As PSKH1 oligomerises primarily via kinase domain contacts [38], it is unlikely that truncation of the N- and C-termini, nor point mutation of catalytic residues, would abrogate the capability of PSKH1 to dimerise [38]. Given this, the PSKH1 mutants could theoretically retain, albeit impaired, intrinsic and $Ca^{2+}$/CaM-modulated activity when oligomerised with active endogenous PSKH1 (Figure 3.30). Thus, co-purification of endogenous PSKH1 with overexpressed PSKH1-FLAG may explain the residual activity frequently observed. Unfortunately, due to the absence of high-quality, commercially available PSKH1 antibodies at the time of this study, it was not possible to determine endogenous PSKH1 expression in

FLAG immunoprecipitates. Future studies should integrate hydrogen deuterium exchange mass spectrometry (HDX-MS) experiments to determine if the N- and C-terminal CBD's of PSKH1 demonstrate increased protection upon $Ca^{2+}$/CaM addition. Further, chemical cross-linking experiments involving PSKH1 and $Ca^{2+}$/CaM should validate the functional importance of F90 and other constituent residues in the PSKH1 N-terminal CBD.

Lastly, whilst the Brede C-terminal CBD was seemingly dispensable for CaM enhancement of PSKH1 activity in the conditions tested (Supp. Fig. 3.5.2), these data do not preclude involvement of this region in CaM-recognition. Interestingly, analysis of the primary structure reveals a 1-5-8 motif (Ile371, Leu367 and Met364, respectively) with some homology to the N-terminal CBD previously identified (Figure 3.31). The acidic aspartic acid that succeeds the putative anchoring aromatic Phe90 in the N-terminal CBD of PSKH1 is replaced by a serine residue in the C-terminal CBD. This residue (Ser372) is a major autophosphorylation site (Figure 3.12). Interestingly, AlphaFold3 docking simulations between CaM and peptides corresponding to the C-terminal CBD indicate that autophosphorylation of Ser372 may impair CaM binding. For example, a phosphomimetic point mutant (Ser372Asp) impairs pLDDT scoring (red) relative to a 'wild-type' control (which docks confidently – blue) (Figure 3.31). This would corroborate data presented in Figure 3.10, which suggests autophosphorylated PSKH1 is unresponsive to $Ca^{2+}$/CaM addition. In contrast, $Ca^{2+}$/CaM significantly increases the catalytic activity of unstimulated PSKH1 (Figure 3.10). The PSKH1 N-terminal CBD, which harbours an acidic moiety at the corresponding Ser372 position, docks confidently with CaM, suggesting other characteristics of the CBD promote CaM recognition (for example, more basic residues and a large aromatic side chain (Phe90) (Figure 3.23). Thus, another possibility is that $Ca^{2+}$/CaM stabilises the PSKH1 homodimer by binding both N- and C-terminal CBDs (binding primarily via the N-terminal peptide), resulting in autophosphorylation of the activation loop and Ser372, promoting CaM dissociation.

Ca$^{2+}$/CaM slightly enhanced the kinetics of autophosphorylation of GFP-PSKH1, although this was not statistically significant (Figure 3.10). However, this was an *in vitro* system utilising a generic pThr antibody as readout for phosphate incorporation. $^{32}$P-based incorporation and quantification experiments may better suited for characterising Ca$^{2+}$/CaM involvement in autoactivation of PSKH1.

N-term CBD

C-term CBD

Kinase domain

Kinase domain

C-term CBD

N-term CBD

C-term CBD

N-term CBD

PSKH1
Monomer 2

PSKH1
Monomer 1

N-term CBD

C-term CBD

Calmodulin
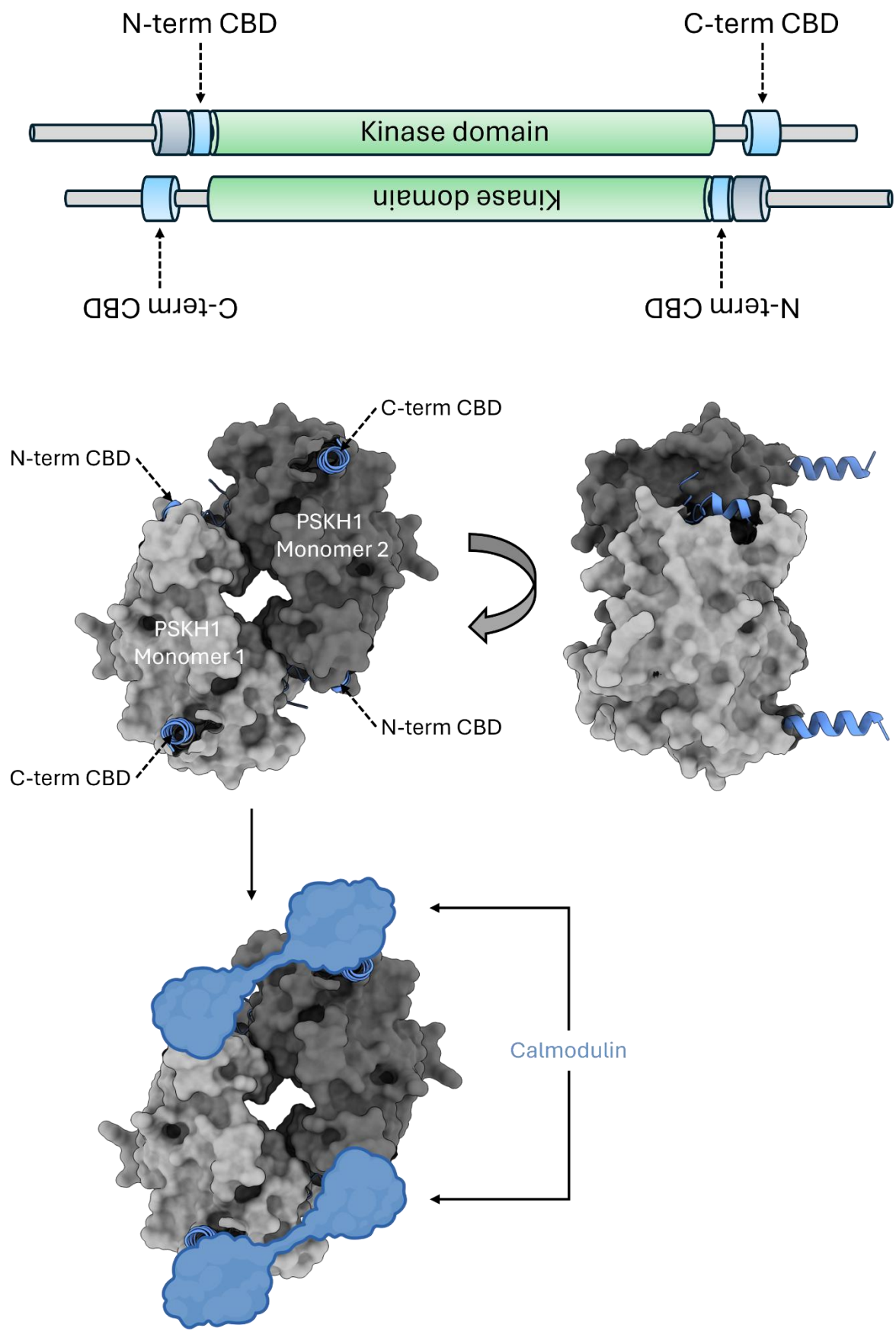
*Figure 3.29. Hypothetical mechanism of CaM activation of PSKH1.* PSKH1 has been reported to form, at minimum, homodimers [38]. Further, GFP-PSKH1 frequently elutes off in the void fraction, indicating higher order structure (Dr. Chris Horne, unpublished). AlphaFold2 modelling of the PSKH1 homodimer consistently predicts the oligomer in a head-to-toe orientation, with binding facilitated primarily via kinase domain contacts. This would theoretically bring the C-terminal Brede CBD of one monomer near the N-terminal CBD of the opposing monomer. Two molecules of $Ca^{2+}$/CaM may stabilise the PSKH1 homodimer by binding the N- and C-terminal CBD's of distinct units of PSKH1 in an extended conformation. Structures were prepared in ChimeraX using simulated data from AlphaFold2 (ColabFold v.1.5.5). Linearised domain structures were created with BioRender.com.
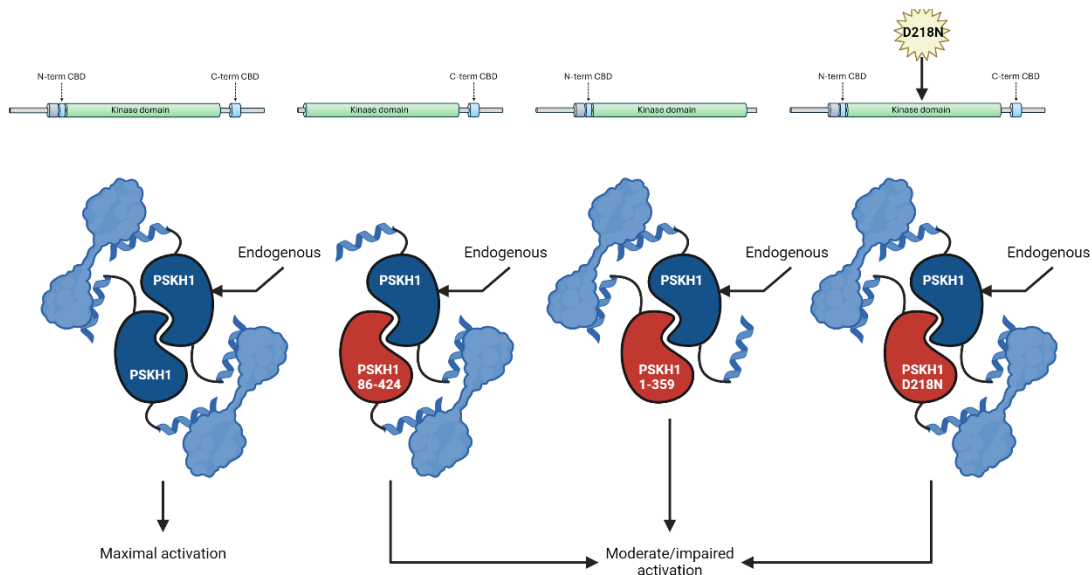


*Figure 3.30. Oligomerisation may protect PSKH1 from truncation and point mutations that typically would attenuate catalytic activity.* Hypothetically, two molecules of $Ca^{2+}$/CaM dock the N- and C-terminal CBD's of distinct PSKH1 monomers and stabilise the PSKH1 homodimer resulting in maximal activation. PSKH1 has been reported to dimerise primarily via kinase domain contacts [38]. As such, point and terminally truncated PSKH1 mutants would theoretically retain oligomerising capability. It was hypothesised that overexpressed PSKH1 could theoretically dimerise with endogenous enzyme present in HEK293T cells. In this scenario, CaM-binding is partially retained in the N- (86-424) and C-terminal (1-359) truncated mutants. Further, in the catalytically dead (D218N) PSKH1 dimer, all tertiary structure and CaM-binding domains are preserved. Consequently, all substrate binding interfaces are theoretically retained. This may allow the active, endogenous PSKH1 subunit to participate in substrate phosphoryl transfer reactions. Created with BioRender.com.

```
                                    -ve acidic moiety
                                          ↓
     PSKH1-N-term CBD:   81-AR V AK Y RAK F D PRV-94
Brede PSKH1-C-term CBD: 364-SS M KN L HRS I S QNL-375
                                          ↑
                            Major autophosphorylation site
```

A          B

Ser372

Asp372

Met364  Leu367  Ile371

Met364  Leu367  Ile371

Reduced pLDDT score

Hydrophobic channel
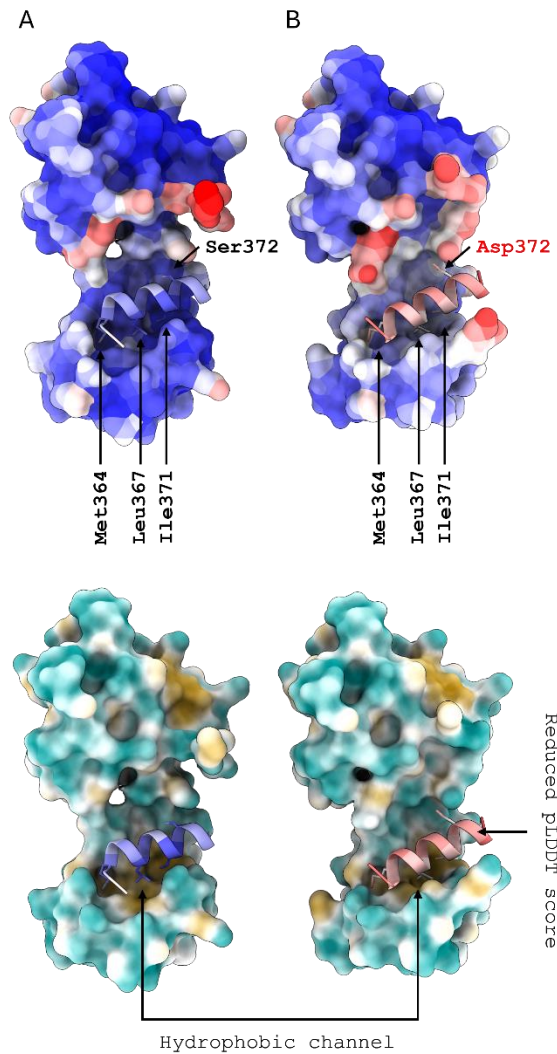
*Figure 3.31. The Brede C-terminal CBD of PSKH1 harbours a major autophosphorylation site which may regulate CaM-binding.* Sequence analysis of the N- and C-terminal putative CBDs reveals shared characteristics, including a 1-5-8 motif. In the N-terminal CBD, the anchoring aromatic Phe90 is followed by an acidic aspartic acid. In the C-terminal CBD, this residue is replaced by serine. Interesting, Ser372 is a major autophosphorylation site (Figure 3.12). AlphaFold3 docking simulations between CaM (surface representation) and C-terminal CBD peptides (ribbon structures) indicate that substitution of this serine residue to an acidic moiety (B – to mimic a phosphorylation event) impairs CaM-binding (reduced pLDDT scoring). Upper structures are coloured by pLDDT score (bfactor palette redblue). Lower structures are coloured by hydrophobicity.

### 3.4.3. CREC-regulation of PSKH1

In concurrent proximity-labelling experiments interrogating the interactome of PSKH1, it was revealed that most members of a novel, low-affinity $Ca^{2+}$-binding protein family (CREC) were enriched and represented (Dr. Chris Horne, Dr. Toby Dite, unpublished). These members included the reticulocalbins RCN1 and RCN3 and calumenin. Interestingly, CREC proteins were also identified in interactome studies of the closely-related pseudokinase, PSKH2 [240]. CREC proteins are largely uncharacterised but are functionally (and presumably structurally) similar to the ubiquitously expressed prototypic $Ca^{2+}$-decoding protein, calmodulin. PSKH1 harbours a putative calmodulin-binding domain in its N-terminus which is indispensable for CaM-mediated enhancement of PSKH1 activity (Figures 3.18/20). As CREC proteins are functionally similar to calmodulin, they presumably interface with calmodulin-like binding domains. Given this, we proceeded to interrogate the effects of the CREC proteins RCN1, RCN3 and calumenin on PSKH1 activity. Calmodulin was previously reported to attenuate the autophosphorylation of PSKH1 *in vitro* [38]. In our hands, calmodulin has no effect on the autoactivation of PSKH1, but does enhance its intrinsic activity (Figures 3.10/17/19). Interestingly, in *in vitro* autophosphorylation experiments, RCN1 abrogated autophosphorylation of GFP-PSKH1 relative to $MgATP/Ca^{2+}$ controls (Figure 3.26, P=0.0003). This effect was similarly demonstrated by the closely related $Ca^{2+}$-binding protein RCN3, albeit to a reduced degree (Figure 3.26, p=0.0025). RCN1 and RCN3 are resident ER proteins with C-terminal HDEL motifs that serve to retain reticulocalbin inside the luminal space [232]. PSKH1 is highly membrane-associated, facilitated by a multitude of membrane targeting motifs in its N-terminus (Figure 1.7) [38, 141]. It was discovered that the acylation status of N-terminal glycine (G2) and cysteine (C3) residues promotes PSKH1 shuttling to internal membranes, including the Golgi apparatus and endosplasmic reticulum (ER) [141]. Dually acylated (myristoylated/palmitoylated) PSKH1 localises at the Golgi and plasma

membrane whilst myristoylated-only (non-palmitoylated) PSKH1 is directed to the ER [141].

Thus, in situations where PSKH1 must necessarily be switched off, it may become myristoylated, which would direct it to the ER and consequently locally enriched pools of reticulocalbin, preventing autoactivation and inhibiting catalytic activity. Consequently, conditions that activate PSKH1 (such as glucose stress) may promote its dual acylation and localisation to the Golgi and plasma membrane, where reticulocalbin is not present but where calmodulin is abundant. Thus, it is entirely possible that the acylation status of PSKH1 governs catalytic activity by shuttling PSKH1 to and from different internal membranes. Congruent with Brede et al. (2003), it is likely that these modifications indirectly affect kinase activity by directing PSKH1 to differential pools of binding partners, including the reticulocalbins and calmodulin, whose allosteric effects on PSKH1 activity are diametrically opposed. Interestingly, the CREC family member calumenin also inhibited the autophosphorylation of PSKH1 but did not affect its intrinsic activity (Figure 3.28). How is this possible? In comparison to the reticulocalbins, calumenin, whilst represented, was not significantly enriched in our PSKH1 proteomic screen relative to RCN1/3 (Figure 3.26). Calmodulin-binding domains frequently exhibit promiscuity toward calmodulin-like proteins. Thus, whilst calumenin may possess some affinity for PSKH1's CBD, given its relatively poor enrichment it is likely not an endogenous regulator of PSKH1.

### 3.4.4. General discussion

The data previously described paint a somewhat complicated picture of PSKH1 regulation. Indeed, PSKH1 seems to exhibit characteristics common to both of its closely related cousins, CaMK1γ and CaMK2 (Figure 3.32). PSKH1 is dually lipidated (myristoylated/palmitoylated) at N-terminal glycine/cysteine residues (G2/C3, respectively), which promotes its translocation to the plasma membrane and Golgi apparatus [141]. Similarly, CaMK1γ is dually lipidated (prenylated/palmitoylated), albeit at its C-terminus (Figure 1.5), which promotes its association

with dendritic lipid microdomains [134]. Interestingly, prenylated/palmitoylated CaMK1γ was reported to self-associate in co-immunoprecipitation experiments, a feature characteristic to dually lipified proteins [134, 241]. Whilst lipidification may indeed target PSKH1 and CaMK1γ to internal membranes, it may also support PSKH1 oligomerisation, like CaMK1γ. PSKH1 has been reported to form homodimers, and GFP-PSKH1 frequently elutes off in the void fraction, indicating higher-order structure [141]. The conditions within which GFP-PSKH1 were expressed (suspension culturing of Sf9 cells) are relatively stressful compared to adherent HEK293T production of PSKH1-FLAG. It is possible that under these conditions (suspension culturing), GFP-PSKH1 is lipified, promoting its self-association (Figure 3.32). On addition of $Mg^{2+}$ATP, oligomerised GFP-PSKH1 autophosphorylates in a *cis*-apparent mechanism, not dissimilar from the closely related CaM-kinase, CaMK2 [242]. Interestingly, under severe stress (EBSS treatment), PSKH1-FLAG is post-translationally modified and becomes phosphorylated on threonine residues (Supp. Fig. 4.4). These considerations support a model where myristoylated-only PSKH1 is the inactive form, associating with reticulocalbin at the endoplasmic reticulum [141, 232]. Like CaMK2, autophosphorylated PSKH1 exhibits $Ca^{2+}$/CaM-independent activity (Figure 3.10). In contrast to CaMK2, which requires $Ca^{2+}$/CaM-binding before autophosphorylation is permitted, $Ca^{2+}$/CaM is seemingly dispensable for PSKH1 autoactivation (Figure 3.10). Additionally, both CaMK1γ and CaMK2 require $Ca^{2+}$/CaM for activity, whilst unstimulated GFP-PSKH1 demonstrates substantial basal activity (low nM) (Figure 3.9). These observations are in stark contrast to HEK293T-derived PSKH1-FLAG, whose activity is considerably enhanced upon $Ca^{2+}$/CaM addition (3-fold for PSKH1-FLAG versus 1.5-fold for GFP-PSKH1) (Figures 3.20/17, respectively). Further, it was discovered that glucose stress primes PSKH1-FLAG for $Ca^{2+}$/CaM enhancement, increasing activity by approximately 8-fold upon $Ca^{2+}$/CaM addition (Figure 3.19). Under these conditions, $Ca^{2+}$/CaM may modulate PSKH1 activity in a distinctly different mechanism to

putative lipidification of GFP-PSKH1. For example, $Ca^{2+}$/CaM-binding may modulate the quaternary structure of monomeric/dimeric PSKH1, altering its substrate profile or enhancing activity by stabilising the catalytic architecture. Thus, it is possible that the differential expression systems used to produce recombinant, purified PSKH1 induce different post-translational modifications with different effects on catalytic activity. Assuming lipidification promotes oligomerisation of PSKH1 and oligomerised PSKH1 autophosphorylates in a *cis*-apparent mechanism, it is not then clear why $Ca^{2+}$/CaM does not induce autophosphorylation of PSKH1-FLAG. It is possible that the different epitope tags used interfere differently with the catalytic architecture of PSKH1, or that lipidification is a necessary step to promote autophosphorylation of PSKH1. Future studies should interrogate the following:

- Determine the acylation status of differentially expressed PSKH1

- Are acylation-defective point mutants (PSKH1-G2A/C3S) unable to autophosphorylate *in vitro*? Is non-lipified PSKH1 monomeric?

The revelation that glucose stress primes PSKH1 for $Ca^{2+}$/CaM activation came relatively late in my candidature. Future experiments should interrogate the effect of glucose starvation (and other cell stressors) on the activity of PSKH1-G2A/C3S point mutants. Further, mass photometry experiments of stimulated WT and G2A/C3S point mutants will reveal if lipidation, like the closely related CaMK1γ kinase, is critical for PSKH1 oligomerisation.

- Where does PSKH1 shuttle to upon glucose starvation?

PSKH1 is highly membrane associated [38, 141]. Dually acylated PSKH1 associates with the plasma membrane and Golgi apparatus, whilst myristoylated-only PSKH1 translocates to the endoplasmic reticulum [141]. Reticulocalbin-1/3, recently characterised inhibitors of PSKH1 autoactivation, are luminal ER proteins [232]. Glucose starvation was previously shown to prime PSKH1 for $Ca^{2+}$/CaM activation and PSKH1 promotes prostate cancer cell growth under glucose stress (Figure 4.2 – discussed later). Thus, does glucose stress promote dual lipidation

of PSKH1 and association at the PM/Golgi apparatus? In contrast, is unstimulated PSKH1 co-localised with reticulocalbin at the ER? *In vitro* subcellular fractionation experiments utilising transiently expressed PSKH1-G2A/C3S point mutants in HEK293T cells under basal and stimulated (glucose stress) conditions should satisfactorily answer these questions.
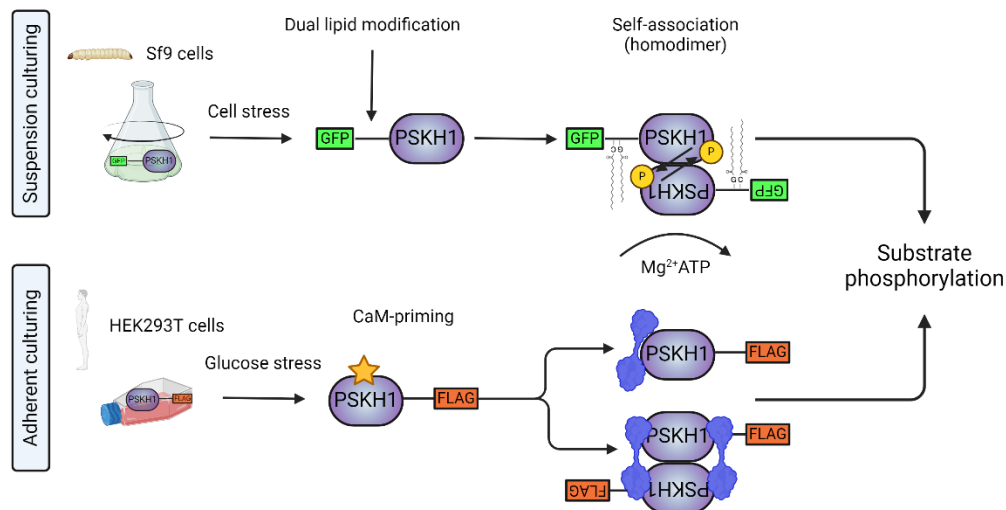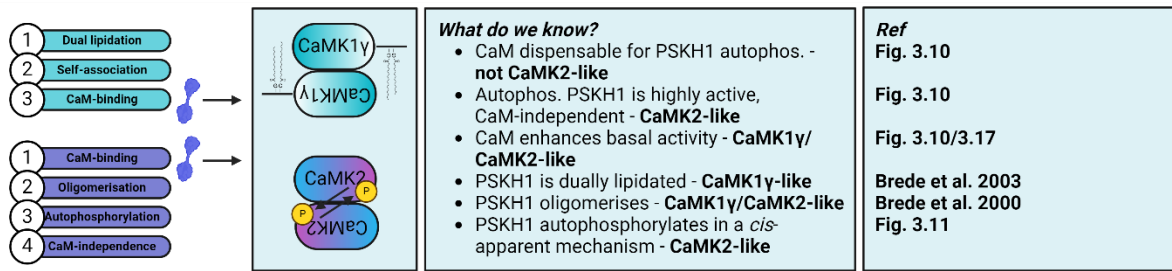
***Figure 3.32. PSKH1 exhibits characteristics common to its closely related cousins, CaMK1γ and CaMK2.*** Differentially expressed PSKH1 (GFP-PSKH1 vs PSKH1-FLAG) exhibit different modes of catalytic activation. For example, GFP-PSKH1 expressed in suspension-cultured Sf9 cells autophosphorylates on incubation with $Mg^{2+}$ATP and frequently elutes off in the void column, indicating higher order structure. $Ca^{2+}$/CaM minimally enhances GFP-PSKH1 activity. In contrast, PSKH1-FLAG expressed in adherent HEK293T cells is significantly activated by $Ca^{2+}$/CaM, an effect enhanced by glucose starvation. It is possible that the different expression systems used induce differential post-translational modifications to PSKH1 with different regulatory effects on the catalytic activity of PSKH1. Created with BioRender.com.

## 3.5. Supplementary Figures

### 3.5.1. GFP-CaMKK2.7-FLAG does not phosphorylate a kinase dead point mutant of GFP-PSKH1 *in vitro*
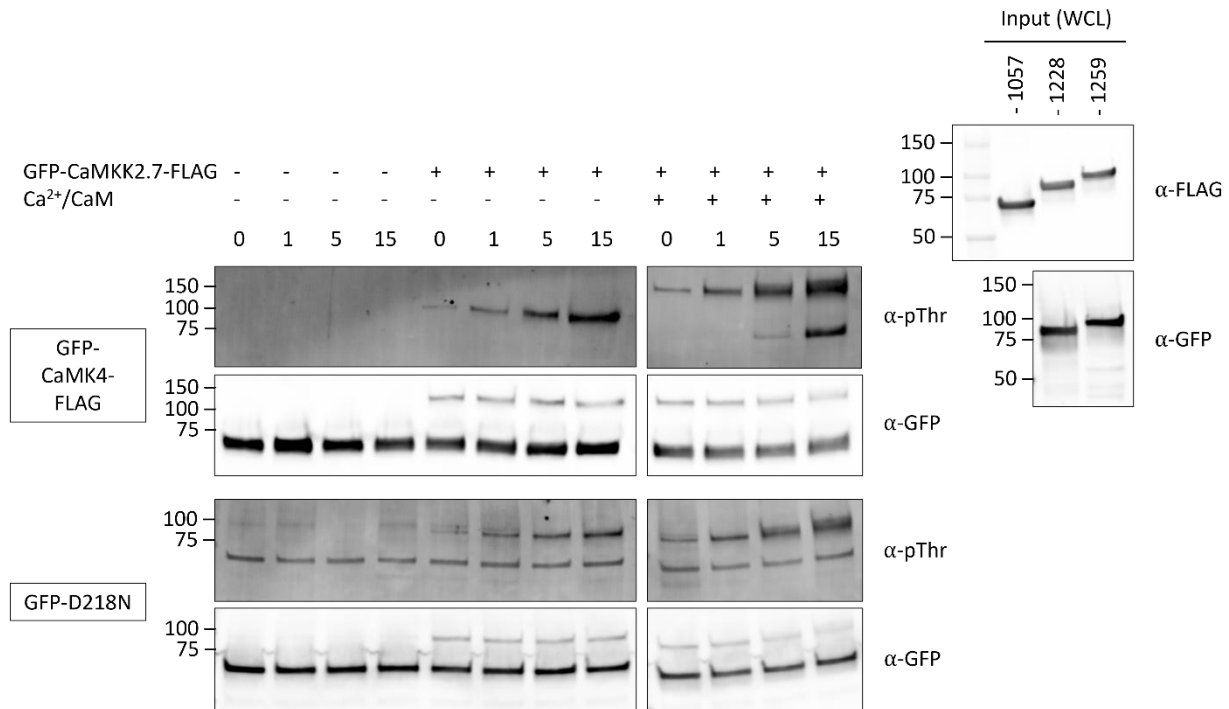


***Supplementary Figure 3.5.1. GFP-CaMKK2.7-FLAG does not phosphorylate a kinase dead point mutant of GFP-PSKH1 in vitro.*** Recombinant GFP-CaMKK2.7-FLAG (1259) and GFP-CaMK4-FLAG (1228, positive control) were immunoprecipitated from transiently transfected HEK293T WCL using an Anti-FLAG® M2 Affinity Gel. 500ng eluted GFP-CaMK4-FLAG or a kinase dead point mutant of PSKH1 (GFP-D218N) were phosphorylated in the presence or absence of 100ng eluted GFP-CaMKK2.7-FLAG, with or without $Ca^{2+}$/CaM, for 0-15 minutes. Activation loop phosphorylation was inferred by subsequent SDS-PAGE and western blot using α-mouse phospho-threonine (42H4) and α-rabbit GFP (D5.1) primary antibodies and α-rabbit IRDye® 680RD and α-mouse IRDye® 800CW near-infrared secondary antibodies. 1057: FLAG-CaMKK2.1; 1228; EGFP-CaMK4-FLAG; 1259: EGFP-CaMKK2.7-FLAG.

### 3.5.2. C-terminal truncation of PSKH1-FLAG does not attenuate $Ca^{2+}$/CaM enhancement of kinase activity
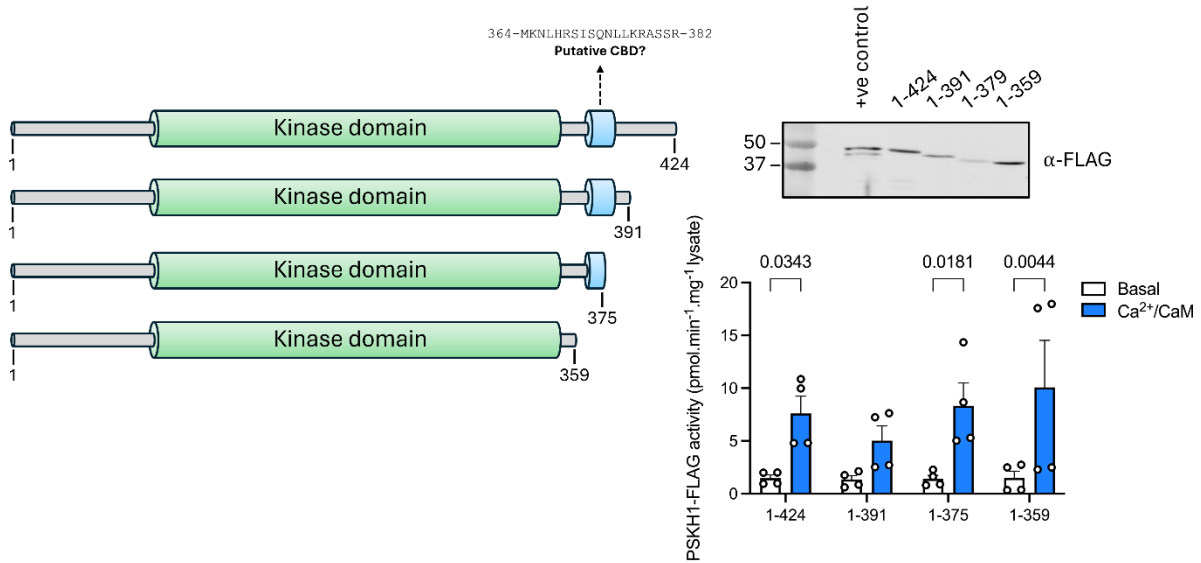


***Supplementary Figure 3.5.2. C-terminal truncation of PSKH1-FLAG does not attenuate Ca2+/CaM enhancement of kinase activity.*** pcDNA3.1(-) expression vectors encoding c-terminal truncation mutants of PSKH1-FLAG (1-391, 1-375, 1-359) were transiently expressed in HEK293T cells for 48 hours. *Western blot.* 30μl WCL was interrogated for PSKH1-FLAG expression using an anti-FLAG antibody. Purified PSKH1-FLAG (100ng) was utilised as a positive control. *Kinase assay.* FLAG-conjugated PSKH1 immunoprecipitated from WCL using an anti-FLAG M2 affinity resin was radiometrically assayed for its propensity to phosphorylate the ADR1G233 peptide *in vitro* in the presence or absence of 100μM $Ca^{2+}$ and 1μM CaM. Two technical replicates per biological replicate. n = 2. Data was statistically appraised by two-way ANOVA and Tukey's multiple comparisons test.

### 3.5.3. Interrogating contaminating Ca²⁺ in CaM/RCN1/RCN3 preparations
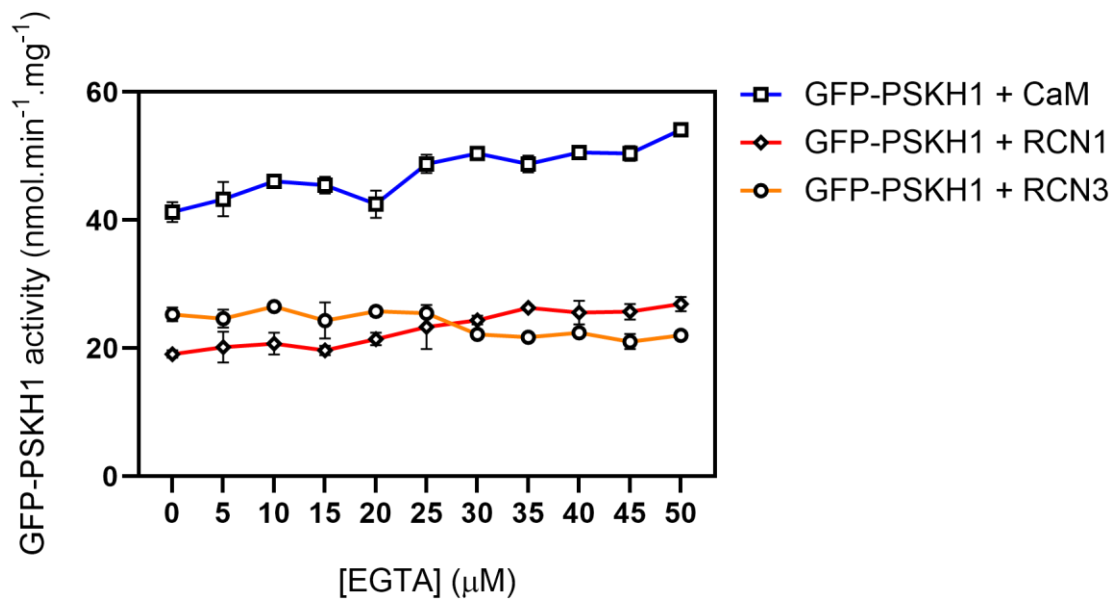


***Supplementary Figure 3.5.3. Interrogating contaminating Ca2+ in CaM/RCN1/RCN3 preparations.*** 50ng GFP-PSKH1 was radiometrically assayed in the presence of 1μM CaM, RCN1 or RCN3 over an EGTA concentration gradient (0-50μM) to chelate contaminating Ca²⁺. Three technical replicates per biological replicate (n=3).

### 3.5.4. PAK1 putatively phosphorylates the activation loop Thr256 residue of PSKH1-FLAG *in vitro*
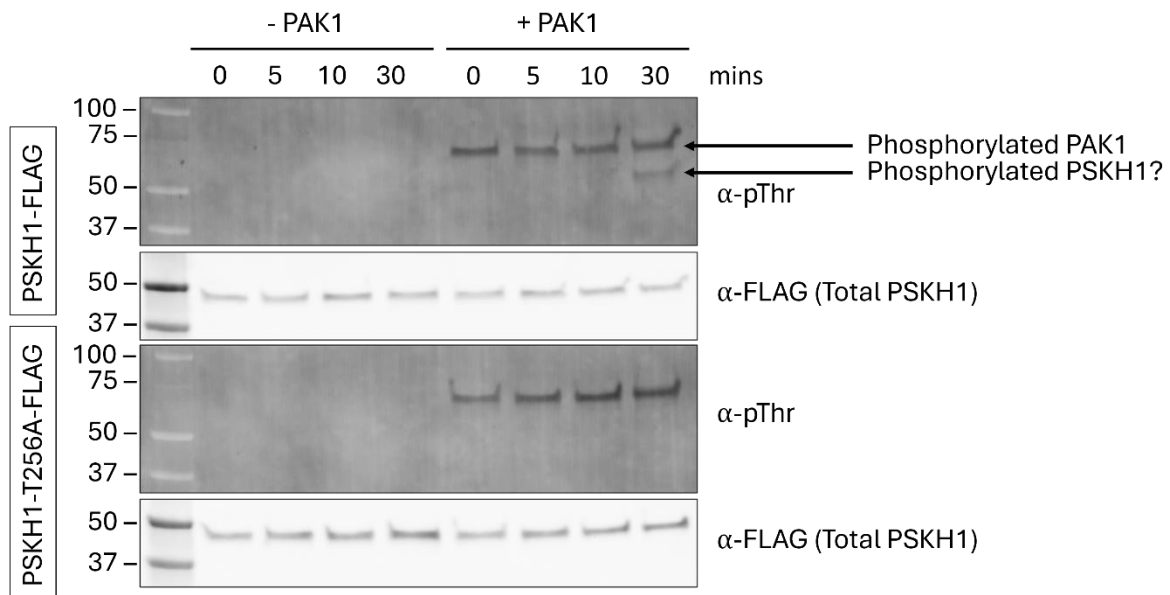


***Supplementary Figure 3.5.4. PAK1 putatively phosphorylates the activation loop Thr256 residue of PSKH1-FLAG in vitro.*** Eluted WT PSKH1-FLAG immunoprecipitated from transiently transfected HEK293T WCL was phosphorylated *in vitro* in the presence or absence of 500ng purified recombinant PAK1 over a period of 30 minutes. Phosphorylation of PSKH1's activation loop was inferred by SDS-PAGE/western blot using an α-phospho threonine (pThr) antibody. In the absence of a commercially available pT256 antibody, phosphorylation of PSKH1's activation loop was indirectly inferred by comparing WT with a non-phosphorylatable activation loop point mutant (PSKH1-T256A-FLAG).

# 4. THE DARK KINASE PSKH1 IS A METABOLIC SENSOR THAT PROMOTES PROSTATE CANCER PROGRESSION BY REGULATING FUEL SWITCHING TO FATTY ACIDS (MANUSCRIPT IN PREPARATION)

**Luke M. McAloon[1,2,3], Chris R. Horne[4], Naomi Ling[2], Jon. S. Oakhill, Jared L. Johnson, James M. Murphy[4], John W. Scott[1]**

**1** Neurometabolism Group, Drug Discovery Biology, Monash Institute of Pharmaceutical Sciences, Parkville, Australia, **2** St Vincent's Institute of Medical Research, Fitzroy, Australia, **3** Australian Catholic University, Fitzroy, Australia, **4** Walter and Eliza Hall Institute of Medical Research, Parkville, Australia

## 4.1. Abstract

Prostate cancer is the second-leading cause of cancer-related death in men. Whilst current therapies are initially effective at stemming disease progression, a subset of patients invariably relapse to a treatment refractory form of disease. Therapies for metastatic castration-resistant prostate cancer (CRPC) are largely palliative in nature, and with incidence of CRPC increasing at 5% annually, new treatments are urgently needed. The dark kinase PSKH1 was recently identified as a top-6 driver of prostate cancer progression. However, the precise signalling mechanisms that regulate this kinase are largely unknown. Further, the function of PSKH1 remains undefined. In this study, we sought to elucidate how PSKH1 promotes prostate cancer progression by using a prostate cancer cell line (LNCaP) with various manipulations. It was discovered that PSKH1 ablation by CRISPR-Cas9 gene editing completely attenuates prostate cancer cell growth under nutrient poor conditions. These data suggested that PSKH1 ameliorates the energetic demands of rapidly dividing cells by prompting fuel switching to alternative energy sources. Corroborating these results, metabolic profiling of PH1-WT and PH1-KO cells revealed that PH1-KO cells are, in general, more glycolytic under energy replete conditions, supporting a role for PSKH1 in alternative energy source utilisation. Lipid profiling by CARS microscopy demonstrated that PSKH1 ameliorates the energetic demands of

nutrient-starved cells by modulating lipid biogenesis. Preliminary data indicate that PSKH1 may mediate these effects through modulating the action of RSK1/eEF2K, established modulators of cell proliferation and, like PSKH1, frequently dysregulated in prostate cancer. In conclusion, these data establish for the first time a direct function for PSKH1 – PSKH1 is a metabolic sensor that promotes prostate cancer progression by controlling fuel switching to fatty acids. Preliminary drug screening results support small molecule inhibition of PSKH1 as a potential novel therapeutic for the treatment of prostate cancer.

## 4.2. Introduction

According to data from the Global Cancer Observatory (GLOBOCAN), prostate cancer (PCa) is the fourth most prevalent malignancy world-wide with approximately 1.47 million incident diagnoses in 2022 (Figure 4.0). Age-standardised prevalence and incidence rates of prostate cancer are disproportionally higher in developed nations (Figure 4.0). These data are reflected domestically where prostate cancer remains the second-most prevalent malignancy across sexes and most common cancer diagnosed amongst men (Figure 4.0). Due to its generally indolent disease course, 5-year survival outcomes for most patients are favourable (~100%) [243]. However, in approximately 20% of cases, progression to an advanced and/or metastatic version of disease inevitably occurs [244]. Since Huggins and Hodges luminary paper in 1972 which detailed the dependence of prostate cancer progression on circulating androgens, androgen deprivation therapy (ADT) has remained the standard of care for metastatic disease [245]. Whilst this treatment is initially effective at inhibiting the action of the androgen receptor (AR) (and thereby limiting prostate cancer progression), the disease inevitably relapses to a hormone refractory form (metastatic castration resistant prostate cancer or, mCRPC) within 2 – 3 years [246]. Clinical outcomes for mCRPC patients are comparatively poor and as incidence of PCa continues to increase and is predicted to overtake tracheal, bronchial and lung malignancies by 2025 (Figure 4.0), new therapies are urgently needed. In an attempt to identify

novel drivers of prostate cancer progression, the human kinome was screened using shRNA targeting 673 kinases in androgen sensitive and insensitive PCa cell lines [6]. Inhibition of just 6 kinases was subsequently shown to attenuate the growth of prostate cancer cells *in vitro*, these included: MAP3K11, DGKD, ICK, CIT, GALK2 and, namely, PSKH1 [6]. Fascinatingly, 5 out of 6 kinases identified enhanced prostate cancer cell growth through AR-independent mechanisms [6]. Promisingly, these kinases demonstrate therapeutic potential, as shRNA inhibition did not attenuate the growth of non-tumorigenic cell lines [6]. PSKH1 is a 48 kDa serine/threonine-protein kinase whose function remains undefined. Further, upstream activators and downstream effectors of PSKH1 signalling are poorly characterised.
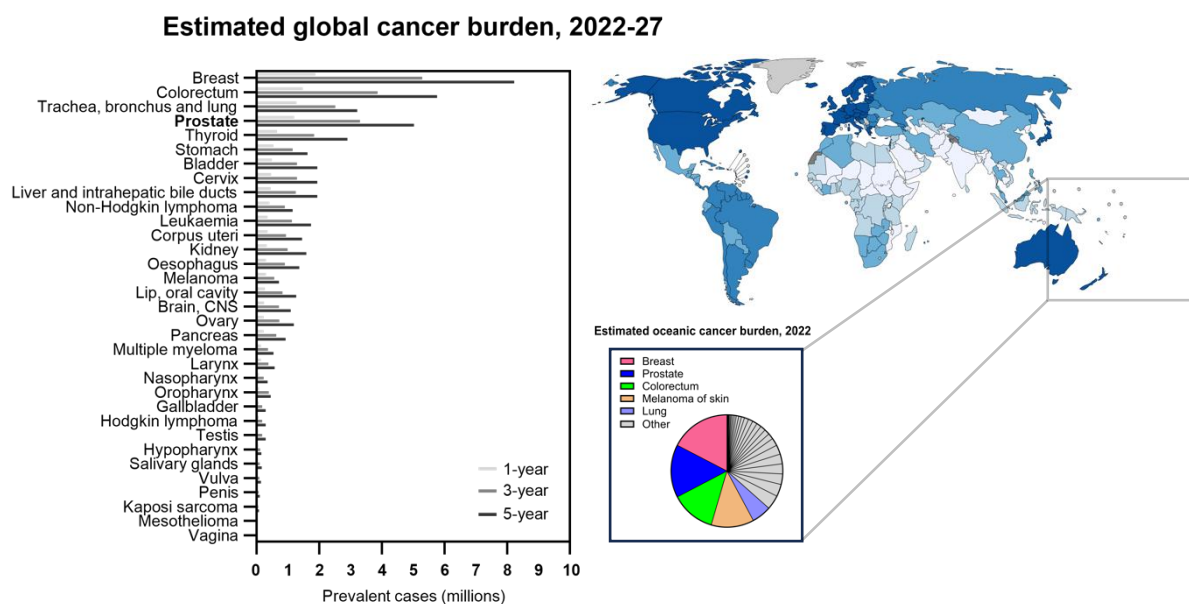


***Figure 4.0. Current and projected geographic burden of prostate cancer.*** Global and domestic (insert) prevalence of cancers using publicly available data from GLOBOCAN (World Health Organisation). Prostate cancer is the fourth most prevalent malignancy globally, second most prevalent malignancy domestically (Oceania) and most commonly diagnosed cancer amongst males.

## 4.3. Aims

The aim of this study was to elucidate the mechanisms by which PSKH1 promotes prostate cancer progression. To do this, PSKH1-KO prostate cancer cell lines (LNCaP) were generated by CRISPR-Cas9 gene editing (Dr. Naomi Ling, SVI). PSKH1-WT (PH1-WT) and PSKH1-KO (PH1-KO) cells were cultured under a battery of conditions and cell growth was monitored.

## 4.4. Materials and Methods

*Cell culture*

LNCaP CRISPRV2 wild-type (PH1-WT) and LNCaP-PSKH1 knock-out (PH1-KO) prostate cancer cells (generously donated by Dr. Naomi Ling, SVI) were cultured in RPMI 1640 medium (Gibco™) supplemented with 10% FBS at 37°C with 5% $CO_2$ injection. HEK293T cells were cultured as previously described.

*HEK293T in vitro cell treatment assays*

HEK293T cells were transiently transfected with PSKH1-FLAG expression constructs, as previously described. To stimulate PSKH1 activity and/or post-translational modification, a battery of treatment conditions was interrogated. This included:

*Nutrient starvation*

To simulate the tumour microenvironment, HEK293T cells transiently expressing PSKH1-FLAG were subjected to nutrient withdrawal, including EBSS treatment, or cultured in DMEM lacking glucose or glutamine (Table 2.1.3. Media), for 2 hours before rapid lysis *in situ*.

*MAPK stimulation of PSKH1*

Many of the kinases identified in our PSKH1-TurboID proteomic screen are members of the MAPK family (Dr. Chris Horn, Dr. Toby Dite, unpublished). To stimulate MAPK signalling and subsequent activation of PSKH1 activity, HEK293T cells transiently expressing PSKH1-FLAG were treated with control (ethanol 1% v/v), EGF (100nM), phorbol ester (10μM), sorbitol (500mM) or exposed under UV light for 30 minutes, before rapid lysis *in situ*.

*Osmotic stress*

The PKC subfamily kinase, PKN1, was identified as a putative interactor of PSKH1. PKN1 is activated by hypotonic swelling [247]. To stimulate PKN1-mediated activation of PSKH1, HEK293T cells transiently expressing PSKH1-FLAG were osmotically stressed by altering the solute concentration of supplemented (10% FBS) HG DMEM. HG DMEM was diluted in sterile milliQ water to yield 50% (1:2) and 25% (1:4) hypotonic cell treatments. Cell media was aspirated and replaced with hypotonic treatments for 5-30 minutes, before rapid lysis *in situ*.

*Prostate cancer cell proliferation assay*

Following initial cell seeding optimisation procedures, $1 \times 10^4$ PH1-WT or PH1-KO cells were seeded into a 96-well PhenoPlate (Revvity) in 100μl supplemented RPMI 1640 medium and allowed to adhere overnight (day 0). For basal cell growth measurements, partial media changes (75%) with fresh, supplemented RPMI 1640 were made 30 minutes prior to data acquisition on an Operetta® CLS High Content Analysis System. Images were captured at 1-hour intervals in a humidified 5% $CO_2$ chamber over a period of 48-60 hours. For cell proliferation experiments involving nutrient stress of PH1-WT and PH1-KO cells, LNCaP cells were seeded onto 96-well PhenoPlates pre-coated with 50μg/mL PDL and allowed to adhere overnight. On day two, wells were carefully rinsed in pre-warmed DPBS (+ calcium/magnesium) followed by media changes to: HG RPMI 1640 supplemented with 2% FBS, serum-free HG RPMI 1640 or glucose-free RPMI 1640 (Table 2.1.3. Media) 30 minutes before insertion into an Operetta® CLS High Content Analysis System. Data was collected as previously described.

*Agilent seahorse XF cell mitochondrial stress test*

$1 \times 10^4$ PH1-WT or PH1-KO cells were seeded onto an Agilent Seahorse XF96-well cell culture microplate, as per the manufacturer's protocol. On day 2, cell culture media was aspirated and replaced with 180μl pre-warmed XF Base Medium Minimal DMEM (Agilent Technologies) containing 2mM glutamine, with or without 10mM glucose and allowed to equilibrate in a $CO_2$-free incubator at 37°C for approximately 1 hour. Concurrently, pre-mixed modulators of cellular respiration (1μM Oligomycin, Carbonyl cyanide-4 (trifluoromethoxy) phenylhydrazone (FCCP), Rotenone and Antimycin) were injected into a pre-calibrated Extracellular Flux Assay cartridge. The combined cell culture plate/cartridge sandwich was analysed on an Agilent Seahorse XF Extracellular Flux Analyser. Oxygen consumption and extracellular acidification rates (OCR and ECAR, respectively) were normalised to total cells/well, as determined by bright field imaging on an Operetta® CLS High Content Imaging System (PerkinElmer).

*Lipid profiling by CARS microscopy*

$10 \times 10^4$ PH1-WT/KO cells were seeded onto glass-bottomed 18-well μSlides pre-coated with 50μg/mL PDL and allowed to adhere overnight. Following overnight incubation, culture media was aspirated and replaced with either HG RPMI 1640 medium or glucose deficient RPMI 1640 medium (Table 2.1.3. Media), both supplemented with 10% FBS, for the indicated time points. CARS microscopy and data collection was facilitated with assistance of the Imaging, FACS and Analysis Core at the Monash Institute of Pharmaceutical Sciences.

*Interrogating PSKH1-mediated phosphorylation of RSK1*

To interrogate PSKH1-mediated *trans*-phosphorylation of putative downstream effectors, PHI-WT and PHI-KO cells were plated onto 6-well tissue culture plates at $0.3 \times 10^6$ cells/well and allowed to adhere overnight. To stimulate PSKH1 activity, cells were briefly rinsed in pre-warmed DPBS and subsequently glucose starved in glucose-free RPMI 1640 medium for 30

minutes before rapid cell lysis *in situ* in 70μl RIPA lysis buffer. To maximally stimulate PSKH1 activity, some wells were also post-treated with 5μM ionomycin (or vehicle control, DMSO) for 10 minutes before rapid lysis *in situ.* Phosphorylation of downstream substrates was inferred by SDS-PAGE and western blot, as previously described.

## 4.5. Results

### 4.5.1. PSKH1 protects LNCaP prostate cancer cell proliferation at high confluency

To first evaluate the effect, if any, of PSKH1 ablation on prostate cancer cell proliferation, PH1-WT and PH1-KO cells were seeded onto 96-well plates in supplemented full growth media (RPMI 1640) and imaged at 1-hour intervals over 60 hours on an Operetta® CLS High Content Imaging System. Interestingly, when cell density reached approximately $10 \times 10^3$ cells/imaged frame (~75% confluency), proliferation of PH1-WT and PH1-KO cells bifurcated, with PH1-KO cells displaying an accelerated growth phenotype (Figure 4.1).
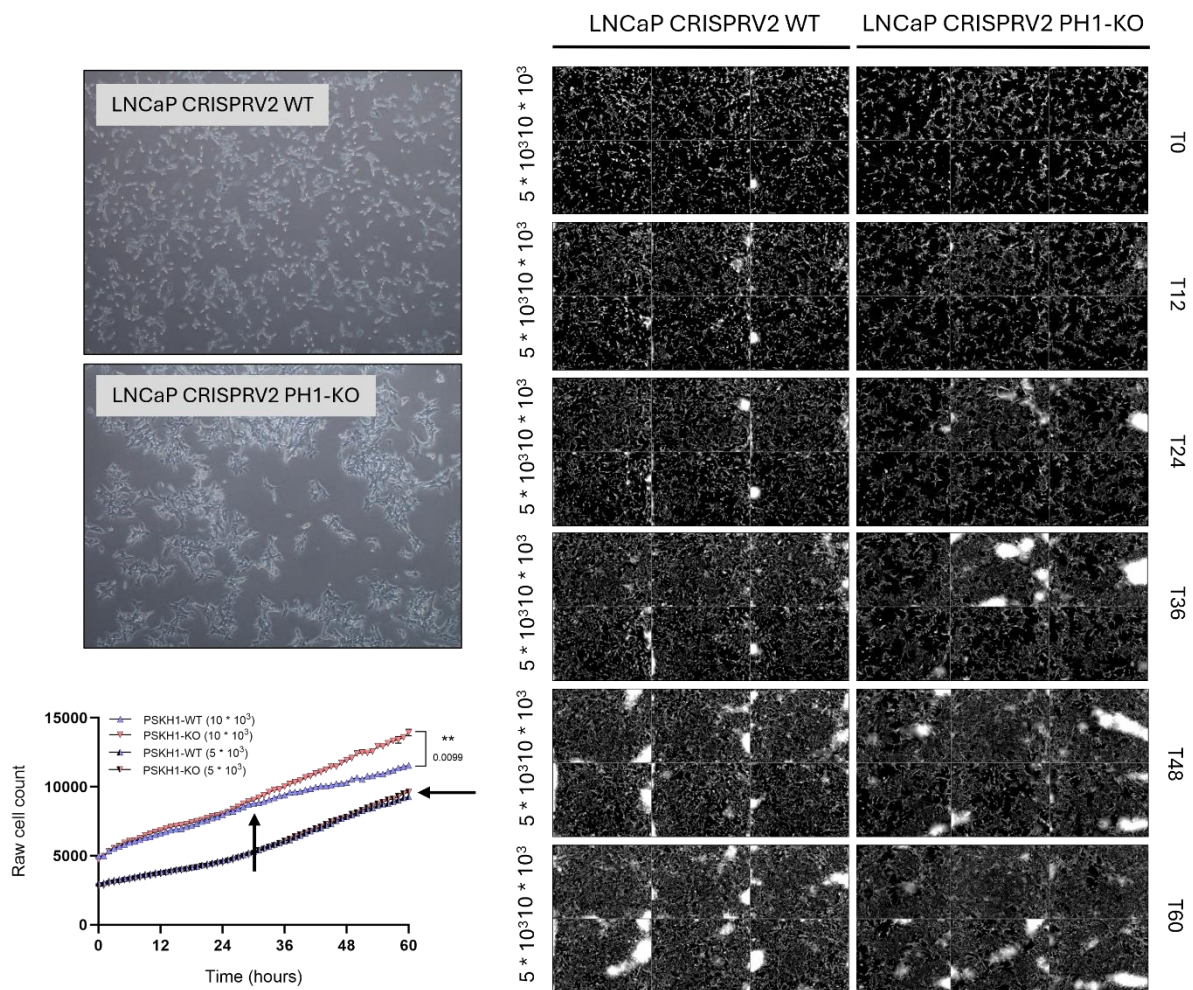
***Figure 4.1. PSKH1 ablation accelerates LNCaP prostate cancer cell growth at high confluency.*** To ascertain the effects of PSKH1 ablation on prostate cancer cell growth, initial basal cell growth measurements were undertaken. 5-10 X $10^3$ LNCaP CRISPRV2 WT (PH1-WT) or PSKH1-KO (PHI-KO) cells were seeded in 96-well PhenoPlates (Revvity) in supplemented RPMI 1640 medium and allowed to adhere overnight. 30 minutes prior to T0 image acquisition, a partial media change was made (75%) with fresh, supplemented RPMI 1640 medium. Images were captured on an Operetta® CLS High Content Imaging System at 1-hour intervals for 60 hours in a humidified chamber with 5% $CO_2$ injection. Data was statistically appraised by two-way ANOVA and Tukey's multiple comparisons t-test (**: 0.0099). 5 technical replicates per genotype. Data is representative of three independent experiments. Black arrows indicate beginning of bifurcation of cell growth rates.

## 4.5.2. PSKH1 exhibits characteristics of a metabolic sensor by mediating prostate cancer growth under nutrient limiting conditions

We initially reasoned that the bifurcation in cell growth rates observed between PH1-WT and PH1-KO cells was due to differential responses to depleted media, as the phenotype was observed late into the experiment (~30 hours) (Figure 4.1). This would invariably imply that PSKH1 is a tumour suppressor that attenuates cell growth under nutrient limiting conditions. However, this hypothesis is incongruent with literature published on PSKH1 and prostate cancer, where ablation of PSKH1 abrogates growth of a panel of prostate cancer cell lines [6]. To interrogate this further, PH1-WT and PH1-KO cells were seeded onto 96-well PhenoPlates pre-coated with 50μg/ml poly-D-lysine (PDL) and cultured under differential growth conditions, including: full growth media (RPMI 1640 supplemented with 10% FBS), serum depleted media (RPMI 1640 supplemented with 2% FBS), serum free media (RPMI 1640) or glucose free media (RPMI 1640, no glucose supplemented with 10% FBS) for a period of approximately 60 hours. No differences in cell growth were observed in 3 out of 4 conditions tested, although a moderate reduction in cell growth rate was observed in the absence of serum (Figure 4.2). Interestingly, proliferation of PH1-KO cells was completely attenuated in the absence of glucose (Figure 4.2).

**12mM glucose, 10% FBS**

**12mM glucose, 2% FBS**

**12mM glucose, serum free**

**No glucose, 10% FBS**

**12mM glucose, 10% FBS**    **No glucose, 10% FBS**

PH1-WT    PH1-KO    PH1-WT    PH1-KO

**12mM glucose**

**No glucose**
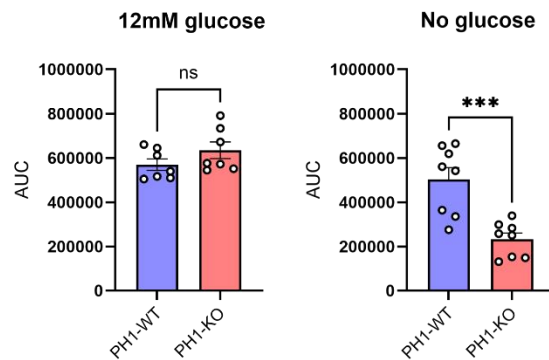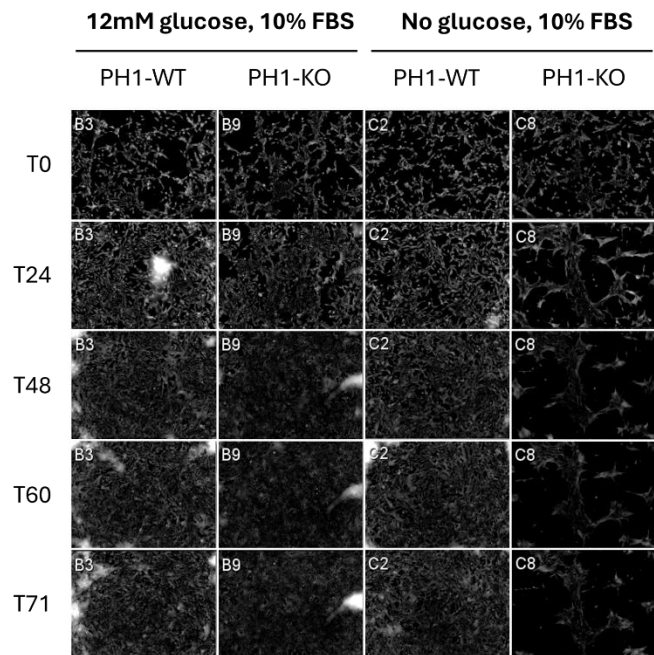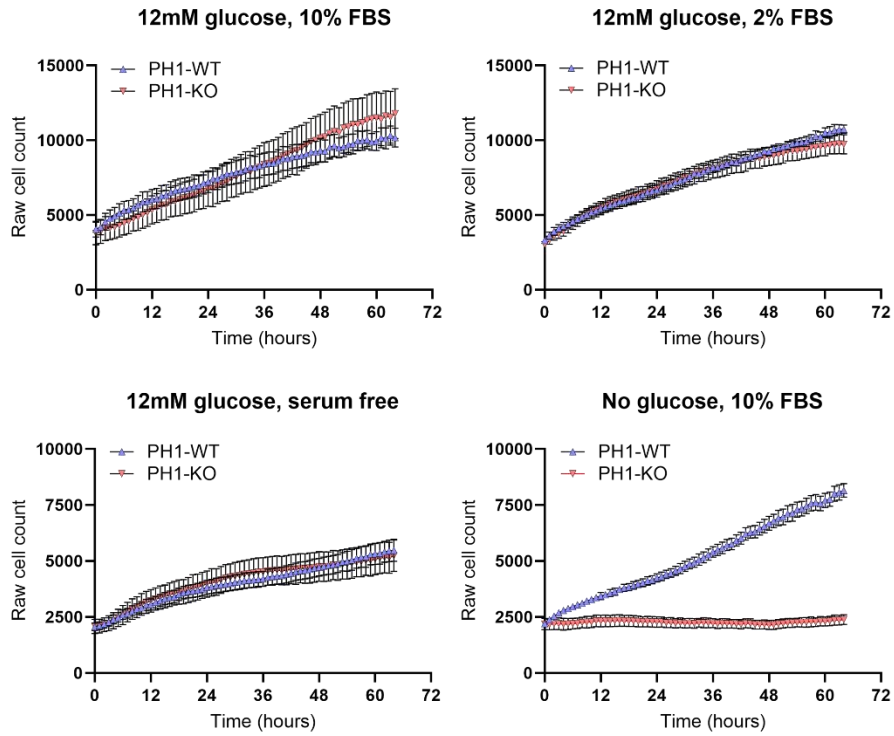
*Figure 4.2. PSKH1 exhibits characteristics of a metabolic sensor by mediating prostate cancer growth under nutrient limiting conditions.* 10 X $10^4$ PH1-WT or PH1-KO LNCaP cells were seeded onto 96-well PhenoPlates pre-coated with 50µg poly-D-lysine and allowed to adhere overnight. 30 minutes prior to T0 acquisition on an Operetta® CLS High Content Imaging System, cells were briefly washed in DPBS (calcium, magnesium) and treated with the indicated growth medium (RPMI 1640 + 10% FBS; RPMI 1640 + 2%; RPMI 1640 serum free or RPMI 1640, no glucose + 10% FBS). Cell growth was monitored at 1 hour intervals over ~64 hours. Representative images at T0-T71 hours are shown. Area under the curve (AUC) was plotted as a column graph and statistically appraised by unpaired t-test (***: P=0.0006). Data is representative of 3 independent experiments.

## 4.5.3. PSKH1-KO LNCaP cells are more glycolytic under glucose-replete conditions and unable to fuel switch during nutrient stress

The inability of PSKH1-KO cells to proliferate in the absence of glucose strongly suggested that PSKH1 regulates cell growth under nutrient stress by promoting fuel switching to alternative energy sources. To interrogate this further, the mitochondrial function of PH1-WT and PH1-KO LNCaP cells was assessed on an XF Extracellular Flux Analyser under glucose replete (10mM glucose) and deplete conditions. The XF Extracellular Flux Analyser is an instrument that concurrently measures the oxygen consumption and extracellular acidification rates (OCR and ECAR, respectively) of live cells in real-time. OCR and ECAR measurements were collected under basal conditions and following injection of 1µM oligomycin, FCCP and rotenone/antimycin A, which alter the bioenergetic profile of cells. Oligomycin is an ATP synthase/complex 5 inhibitor that blocks OXPHOS (oxidative phosphorylation) production of ATP. FCCP is an uncoupling agent that destabilises the proton gradient, promoting unfettered flow of electrons through the electron transport chain (ETC). Thus, the addition of FCCP essentially forces cells to maximally respire by imitating a cellular energy demand. Lastly, rotenone and antimycin A are complex 1/3 inhibitors that completely inhibit the mitochondrial function of cells. Under glucose replete conditions (10mM glucose), no differences in mitochondrial function were observed (Figure 4.3). However, PH1-KO prostate cancer cells were more glycolytic relative to wild-type cells in the presence of glucose, corroborating previously reports that PSKH1-KO cells are heavily dependent on glucose for growth (Figure

4.2). Under glucose deplete conditions, PH1-KO cells appeared to have impaired respiration and ATP production relative to wild-type controls (Figure 4.3). Further, the 3-fold increase in maximal respiration observed in PH1-WT cells following glucose withdrawal was noticeably absent in PH1-KO cells, indicating an impaired ability to exploit increased ETC activity following FCCP injection (P: 0.1902) (Figure 4.3). Taken together, these data strongly suggest that PSKH1 ameliorates the energetic demands of prostate cancer cell growth during nutrient stress by controlling fuel switching, as PSKH1-KO cells are entirely dependent on glucose and are unresponsive to FCCP in glucose-deplete conditions.
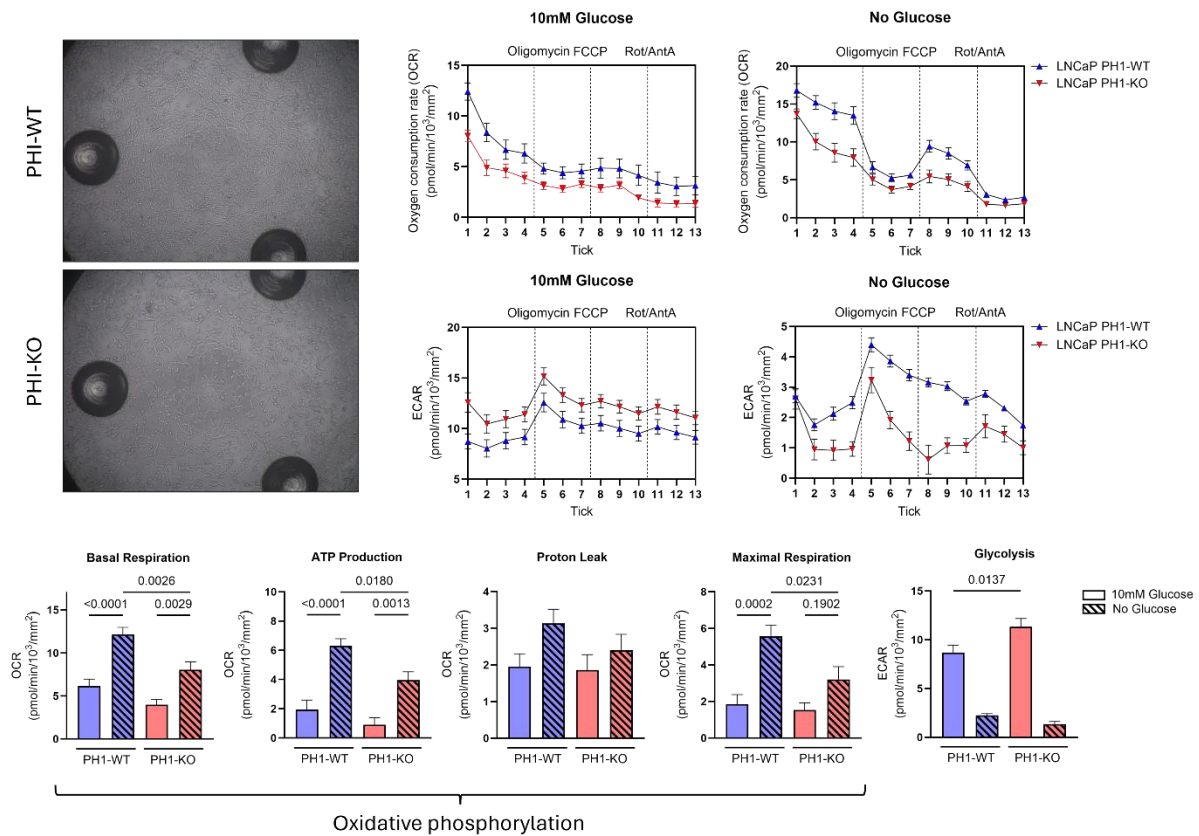


***Figure 4.3. PSKH1-KO LNCaP cells are more glycolytic under glucose-replete conditions and are unable to fuel switch during nutrient stress.*** *Cell images.* Representative images of PH1-WT and PH1-KO cells seeded on an Agilent Seahorse XF96-well microplate. *Mitochondrial stress test.* The Seahorse XF Mitochondrial Stress Test was performed using PH1-WT and PH1-KO cells in minimal DMEM (Agilent) supplemented with 2mM glutamine, with or without 10mM glucose, using an XF Extracellular Flux Analyser. Basal respiration, ATP production, proton leak and maximal respiration were calculated from oxygen consumption rates (OCR) under basal conditions and following injection of 1μM oligomycin,

1μM FCCP or 1μM rotenone/antimycin A. Glycolysis was calculated by averaging the extracellular acidification rates prior to oligomycin injection. Data was normalised to total cells/well on an Operetta® CLS High Content Imaging System. Data was statistically appraised by one-way ANOVA and Tukey's multiple comparisons test. 15 biological replicates per genotype (PH1-WT/KO) were tested under each condition (10mM glucose, no glucose).

### 4.5.4. PSKH1 ablation impairs lipid biogenesis in prostate cancer cells during nutrient stress

PSKH1-KO LNCaP cells are heavily dependent on glucose for growth (Figure 4.2). Further, relative to wild-type controls, PH1-KO cells are more glycolytic under glucose replete conditions and generate less ATP during glucose stress (Figure 4.3). This reduction in ATP production may reflect the increased dependence on glycolysis for growth, which produces just 2 ATP per molecule of glucose [248]. Lastly, PH1-KO cells are unresponsive to FCCP treatment, which uncouples the protein gradient and forces cells to maximally respire (Figure 4.3). Taken together, these data strongly suggest that PSKH1 promotes prostate cancer cell growth by regulating fuel switching to alternative energy sources. Protein catabolism is likely too slow to satisfy the energy demands of rapidly dividing cancer cells. Thus, we reasoned that PSKH1 must regulate the synthesis, processing, or metabolic breakdown of free fatty acids. Interestingly, in contrast to most cancers that generally depend on glucose for growth (see Warburg Effect), prostate cancer is uniquely characterised  by an increased reliance on fatty acids [249-253]. To interrogate this probable role for PSKH1 in fatty acid utilisation, lipid biogenesis in PH1-WT and PH1-KO cells was explored by coherent anti-Stokes Raman scattering (CARS) microscopy. CARS microscopy enables sensitive, real-time acquisition of biomolecular compositional data by exploiting the characteristic vibrational resonance of biomolecules [254]. The combined action of an adjustable Pump beam (720-980 nM) and fixed Stokes beam (1032nM) excite the sample of interest, which result in coherent anti-Stokes Raman scattering (CARS) of transmitted light. The spectra produced directly result from the difference in laser fields (Pump and Stokes beams), which is adjusted to match the vibrational frequency of the biomolecule under study. Consequently, characteristic spectra are

proportional to specific biomolecules, allowing the biomolecular characterisation of cells in real-time. As previously stated, CARS spectroscopy works by promoting the vibrational resonance of atomic bonds. This typically necessitates large quantities of the respective moiety in order to attain a detectable signal. Lipids are ideally suited for CARS microscopy, as their long, aliphatic side chains are abundant in repeated units of -$CH_2$ groups [254]. Lipid biogenesis in PH1-WT and PH1-KO LNCaP cells under glucose stress was subsequently explored. Cells seeded on chambered coverslips (Ibidi) were glucose starved for 1 - 24 hours and analysed on a Leica SP8X CARS microscope with the assistance of Cameron Nowell of the Imaging, FACS and Analysis Core at the Monash Institute of Pharmaceutical Sciences. In general, the number of lipid droplets was not significantly different between cell lines, although the number of lipid droplets did decrease in the PH1-KO cells under glucose duress (Figure 4.4). Analysis of thousands of individual lipid droplets revealed several, interesting phenomena. Firstly, mean signal intensity of lipid droplets increased over time in the PH1-WT cells under glucose stress, whilst the intensity of signal remained unchanged in PH1-KO cells (P=<0.0001 vs P=0.0806, Figure 4.4). Additionally, under severe nutrient stress (24-hour glucose starvation), the size of the lipid droplets was significantly smaller in PH1-KO cells relative to WT controls (P=<0.0001, Figure 4.4). These data are exemplified in the representative images shown, where PH1-WT cells exhibit bright, distinct puncta in comparison to the faintly diffuse lipid droplets observed in PH1-KO cells (Figure 4.4). A comprehensive CARS scan of glucose-starved lipid droplets revealed a distinct difference in the spectroscopic profiles of WT and PH1-KO cells. A peak at 3328 nM is noticeably absent in PH1-KO cells. This peak corresponds hydroperoxides, which are fatty acid derivatives implicated in inflammation and ageing [255].

12mM Glucose, 24hr    No Glucose, 24hr

PH1-WT

PH1-KO

12mM Glucose    No Glucose
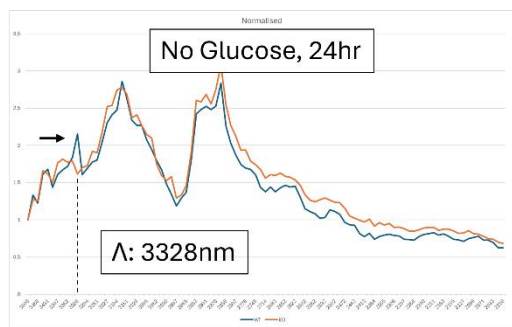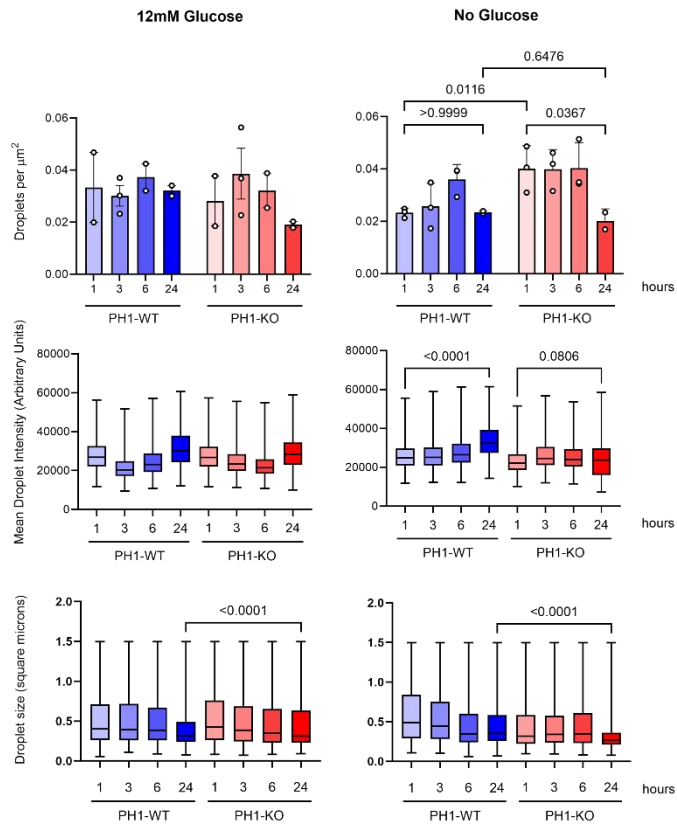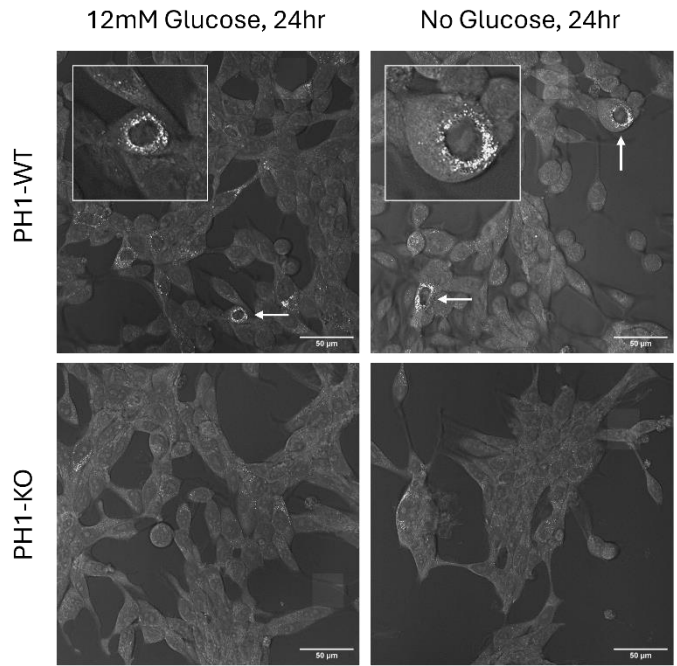
***Figure 4.4. PSKH1 ablation impairs lipid biogenesis in prostate cancer cells under glucose stress.*** $10 * 10^3$ PH1-WT and PH1-KO LNCaP cells were seeded onto glass bottomed 18-well chambered coverslips pre-coated with 50μg/ml PDL and allowed to adhere overnight. On day 2, cell media was aspirated and replaced with either high- or no glucose RPMI 1640 medium supplemented with 10% FBS and culture for the indicated time periods (1-24 hours). Lipid profiling was performed on live cells on a CARS microscope with the assistance of the Imaging, FACS and Analysis Core at the Monash Institute of Pharmaceutical Sciences. Representative CARS scans are shown. White arrows indicate accumulation of lipid puncta. Data was statistically appraised by one-way ANOVA and Tukey's multiple comparisons test.

### 4.5.5. A novel PSKH1 inhibitor attenuates PSKH1-mediated prostate cancer cell proliferation under glucose stress

The data described collectively demonstrated that PSKH1 ameliorates the energetic demands of dividing cells by promoting fuel switching to lipids and fatty acid derivatives. Corroborating these findings, *in vitro* kinase experiments utilising immunoprecipitated PSKH1 from non-malignant cell lines (HEK293T) showed that PSKH1 activity increases upon glucose withdrawal (Figure 3.19). This convergence of phenotype across distinct cell lines strongly positions PSKH1 as a metabolic sensor that preserves cell growth during nutrient stress. Interestingly, the cell culture conditions tested somewhat reflect the tumour microenvironment, where growth of rapidly dividing cancer cells outpaces vascularisation, resulting in a local scarcity of oxygen and, importantly, nutrient availability. Thus, inhibiting PSKH1 may limit the ability of nascent tumours to overcome the localised reduction in energy availability by preventing fuel switching to fatty acids. Supporting this, PSKH1-KO cells are completely quiescent in the absence of glucose (Figure 4.2). To test this, a selection of ATP analogues was screened for their ability to impair PH1-WT LNCaP cell growth under nutrient limiting conditions. These inhibitors were selected from a much wider panel based on initial performance *in vitro* against purified, recombinant GFP-PSKH1. The identities of the compounds utilised in this study have been obfuscated to protect intellectual property. PH1-WT cells were seeded onto 96-well PhenoPlates and cultured in no glucose RPMI 1640 medium, with or without (DMSO) 1μM compound 1 (C1), compound 2 (C2) or compound 3 (C3) for approximately 3 days. Cell growth was monitored on an Operetta® CLS High Content Imaging System at 1-hour intervals. PH1-KO cells cultured in the absence of glucose were utilised as a benchmark for drug efficacy. As expected, PH1-WT cells treated with DMSO control exhibited a time-dependent increase in cell growth comparative to previous experimentation (Figure 4.5). 1μM C1 had no effect on cell growth and C3 was completely cytotoxic (data not shown). As PSKH1 ablation does not kill prostate cancer cells, it is unlikely

that these cytotoxic effects were resultant from PSKH1 inhibition. Interestingly, C2 completely attenuated growth after 12 hours and kept the PH1-WT cells in a quiescent state for the duration of the experiment (Figure 4.5). Although preliminary, these data demonstrate that targeting of PSKH1 by small molecules can limit prostate cancer growth in an *in vitro* context.
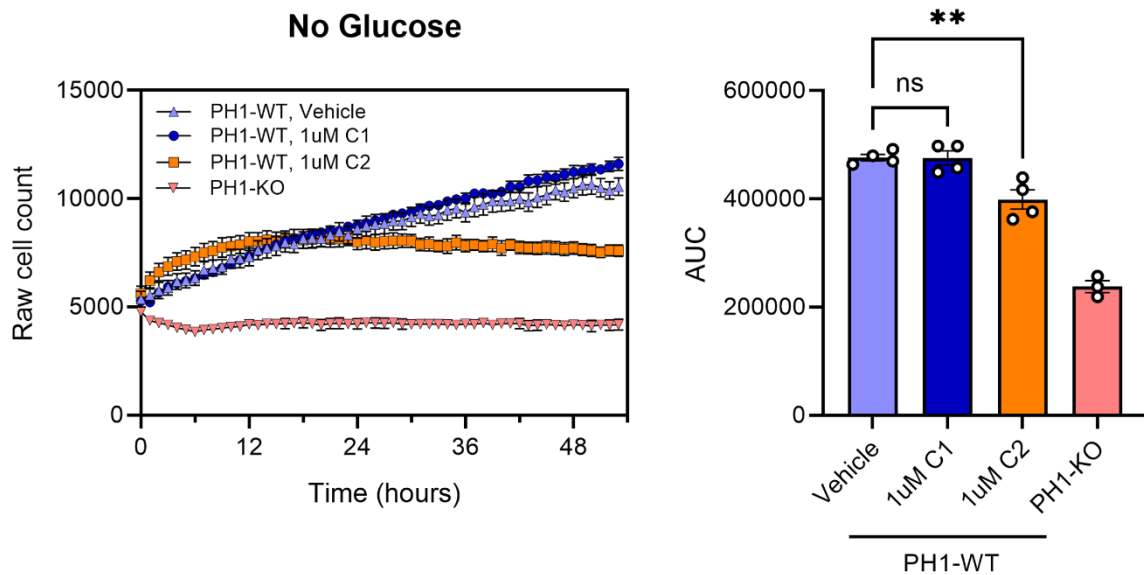


***Figure 4.5. A novel PSKH1 inhibitor attenuates growth of PSKH1-WT cells under glucose stress.*** PH1-WT and PH1-KO cells seeded on a 96-well PhenoPlate were cultured in glucose deplete medium, with or without (DMSO) 1μM compound 1 (C1), 1μM compound 2 (C2), for approximately 48 hours. PH1-KO cells were utilised as a positive control for drug efficacy. Cell growth was monitored on a Operetta CLS High Content Imaging System at 1-hour intervals. Area Under the Curve (AUC) was calculated for individual biological replicates (n=5) and statistically appraised by one-way ANOVA and Tukey's multiple comparisons test (**: P= 0.0055).

### 4.5.6. Elucidating oncogenic effectors of PSKH1: RSK1

Attenuation of prostate cancer cell growth by PSKH1 ablation is not novel, indeed work by Whitworth et al. (2012) and Zhu et al. (2023) have collectively demonstrated that temporal knockdown of PSKH1 expression by RNA interference (RNAi) or short-hairpin RNAs (shRNA) abrogates growth in a panel of prostate and malignant osteosarcoma cell lines [6, 113]. However, the precise mechanisms by which PSKH1 modulates cell growth is not currently understood. Indeed, no downstream effectors of PSKH1 signalling have to date been defined. To identify potential substrates of PSKH1, proximity labelling by TurboID/MS was employed. Briefly, expression of a PSKH1-TurboID fusion construct (pFTRE3G C-FLAG TurboID) was reconstituted in PSKH1 knock-out (PH1-KO) HEL cells using a doxycycline-inducible system. PSKH1 protein-protein interactions (PPIs) were subsequently inferred by streptavidin-affinity purification and mass spectrometric analysis (Dr. Chris R Horne, Dr. Toby Dite, unpublished). These data revealed multiple kinases implicated in Ras/Raf/MEK/ERK signalling, including protein kinase N1 (PKN1), p21 activated kinase 4 (PAK4), eukaryotic elongation factor 2 kinase (eEF2K, henceforth CaMK3) and the 90 kDa ribosomal s6 kinase 1 (RSK1). Simultaneously, concurrent collaborative work with Jared Lee Johnson (Harvard) delineated the preferred PSKH1 substrate motif, revealing a strong preference for serine at the recipient phosphoryl transfer site (P0) and a requirement for leucine, arginine and phenylalanine at P-5, P-3 and P+1, respectively (LxRTx**S\***Fxxx, where x is any amino acid and S* = phosphorylatable residue). Cross-referencing these data identified a single kinase harbouring a perfect PSKH1 phosphorylation site: RSK1.

RSK1 is a constituent member of the p90 ribosomal s6 kinase subfamily of AGC kinases, which in humans includes RSK1-4 [256]. RSK4, whose expression is largely delimited to embryonic development will not be discussed further. Like PSKH1, RSK is strongly implicated in prostate cancer progression [257]. Indeed, amongst the four RSK isoforms, RSK1 is predominately expressed in highly-proliferative tissues [256]. Like the tandem obscurin-MLCK isoforms described earlier, RSK kinases are unusual in that they harbour two catalytic domains tethered by a central linker [258] (Figure 4.6). In canonical RSK signalling, growth factor and mitogen stimulated Ras/Raf/MEK/ERK signalling primes RSK through phosphorylation of the central linker (Ser363) and activation loop (Thr574) of the C-terminal CaM-kinase domain (CTKD) [259, 260] (Figure 4.6). Activated CTKD reportedly autophosphorylates the inter-kinase Ser380 residue through an inter-molecular mechanism [261]. Phosphorylation of this region (the hydrophobic motif) provides a docking site for PDK1, which phosphorylates the N-terminal kinase domain (NTKD) activation loop Ser221, maximally activating RSK [262]. The NTKD mediates phosphorylation of substrates, including the 40S ribosomal S6 subunit, c-Fos, Nur77 and serum response factor (SRF) [259]. Other than the inter-kinase region (Ser380), no substrates have to date been characterised for the CTKD [259]. Several lines of evidence indicate that the CTKD may not be the only mechanism by which Ser380 is phosphorylated *in vivo*. Firstly, a CTKD-truncated RSK1 mutant ectopically expressed in maturing oocytes is 4-fold more active relative to full-length enzyme [263]. In this mutant, the central linker (and hydrophobic motif harbouring the Ser380 PDK1 docking site) is preserved. Corroborating these findings, truncation of the CTKD of RSK2 (1-389) generates an enzyme that is 2.5-fold more active compared to wild-type controls [262]. Astonishingly, RSK2-1-389 is hyperphosphorylated at Ser386 (RSK1-Ser380) despite lacking the CTKD [262]. These data dually suggest that the CTKD sterically obstructs access to the hydrophobic motif and that Ser380 phosphorylation by heterologous protein kinases is

possible *in vivo*. Supporting this, in dendritic cells, p38-activated MK1/2 phosphorylate RSK2-Ser386, completely bypassing a requirement for ERK/CTKD-mediated autophosphorylation of the central linker [264]. Lastly, *in vitro* autophosphorylation experiments demonstrating CTKD-mediated Ser380 phosphorylation have utilised relatively long incubation periods (20 minutes to 1 hour), putting into question the relevance of this phenomenon as a viable explanation for *in vivo* signalling [261]. These revelations, in combination with the observation that RSK1 harbours a perfect PSKH1 consensus motif at the Ser380 regulatory site, led us to interrogate PSKH1-mediated phosphorylation of RSK1. AlphaFold2 docking simulations of the PSKH1 and RSK1 CaM-kinase domains and a peptide corresponding to the Ser380 consensus site suggest that the PSKH1 catalytic surface is a superior binding interface for Ser380 peptide docking (Figure 4.7). For example, the P-3 (Arg377) and P+1 (Phe381) residues previously characterised to be critical for PSKH1 substrate recognition (LxRTxS*Fxxx, where S* = phosphoryl transfer site) interact more stably in the PSKH1:RSK1-Ser380 simulation. Relative to the RSK1-CTKD:RSK1-Ser380 complex, P-3 Arg377 forms multiple salt bridge interactions (dashed lines) with the αD-helix of PSKH1 (Figure 4.7). Further, the P+1 Phe381 aromatic is compactly anchored inside a hydrophobic pocket present in the C-lobe of PSKH1's kinase domain (Figure 4.7). In contrast, this residue appears more labile in the RSK1-CTKD:RSK1-Ser380 simulation (Figure 4.7). pLDDT colouring and PAE plots (black arrows) corroborate a more stable interaction in the PSKH1:RSK1-Ser380 peptide complex. To validate this empirically, PH1-WT and PH1-KO LNCaP cells were seeded onto 6-well plates and allowed to adhere overnight. On day 2, cells were briefly glucose starved to stimulate PSKH1 activity. Interestingly, glucose starvation has also recently been reported to stimulate Ser380 phosphorylation and p90[rsk] activity [265]. Some wells were also post-treated with 1μM ionomycin for 5 minutes to maximally activate PSKH1 by stimulating CaM-enhancement of PSKH1 activity. p-RSK1 (Ser380) was not observably different between cell lines but,

interestingly, total RSK1 expression was increased in the PSKH1-KO cells, particularly under glucose stress (Figure 4.8). Ionomycin treatment increased Ser380 phosphorylation, consistent with previous reports [266]. These data are preliminary – unfortunately, due to time constraints, it was not possible to further validate these observations. The potential ramifications of these data will be explored in the discussion section below.
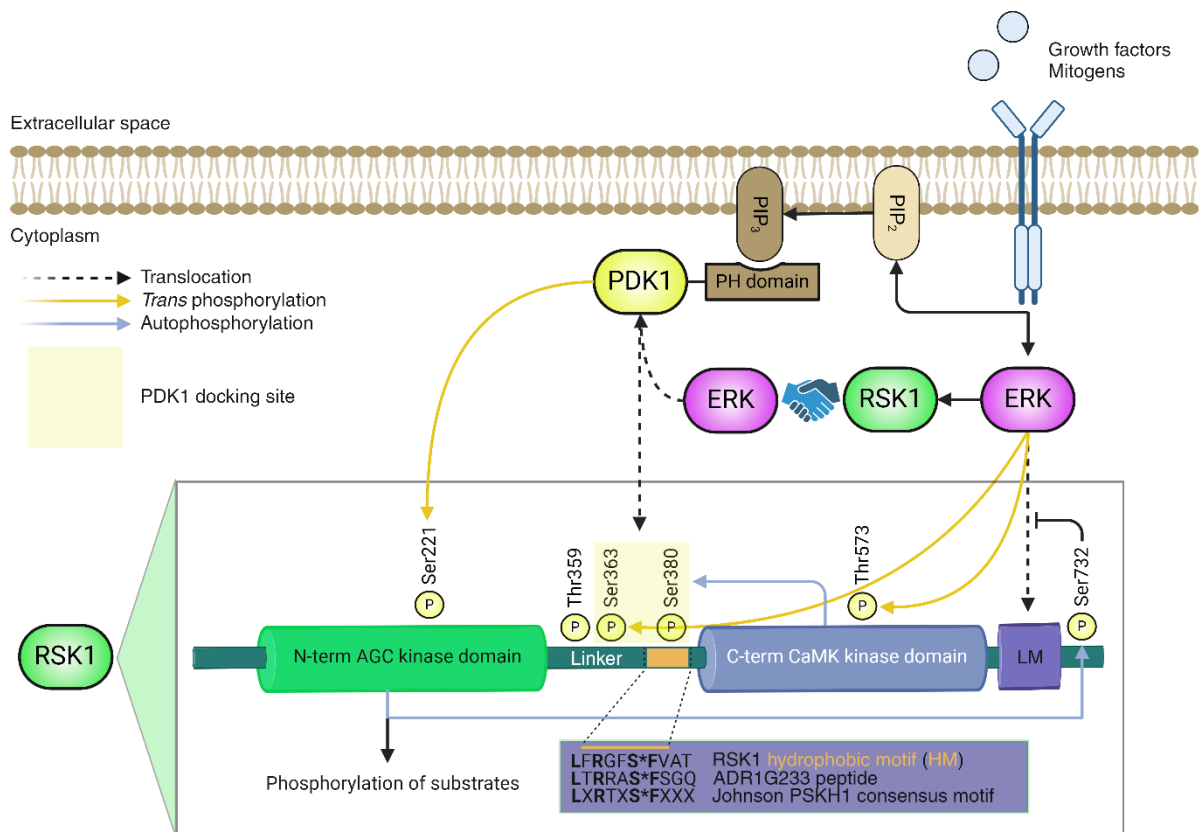
***Figure 4.6. Canonical RSK1 signalling and domain structure.*** Growth factor and mitogen stimulation activates the Ras/Raf/MEK/ERK signal transduction pathway, which promotes ERK-RSK1 association via the c-terminal linear motif (LM) [267]. ERK phosphorylates Ser363 in the central linker region and the activation loop of the C-terminal kinase domain (CTKD) at Thr573, which presumably activates the CTKD [259, 260]. Additionally, non-catalytic functions of ERK have been demonstrated with respect to RSK1 signalling, including rapid and transient translocation of the ERK-RSK1 cognate kinase pair to the plasma membrane [268, 269]. CTKD-mediated autophosphorylation of Ser380 primes a PDK1 docking site on RSK1 and promotes PDK1-mediated transphosphorylation of Ser221 on the activation loop of the N-terminal kinase domain (NTKD). Finally, the activated NTKD phosphorylates downstream exogenous substrates [259]. *Hydrophobic motif insert*. The Ser380 autophosphorylation site, buried within the hydrophobic motif (HM) of RSK1, bears striking similarity to the PSKH1 substrate peptide (ADR1G233) and Johnson PSKH1 consensus motif, which was recently described (unpublished). Phosphosite designation is according to human RSK1 numbering (UNIPROT accession name: KS6A1_HUMAN).
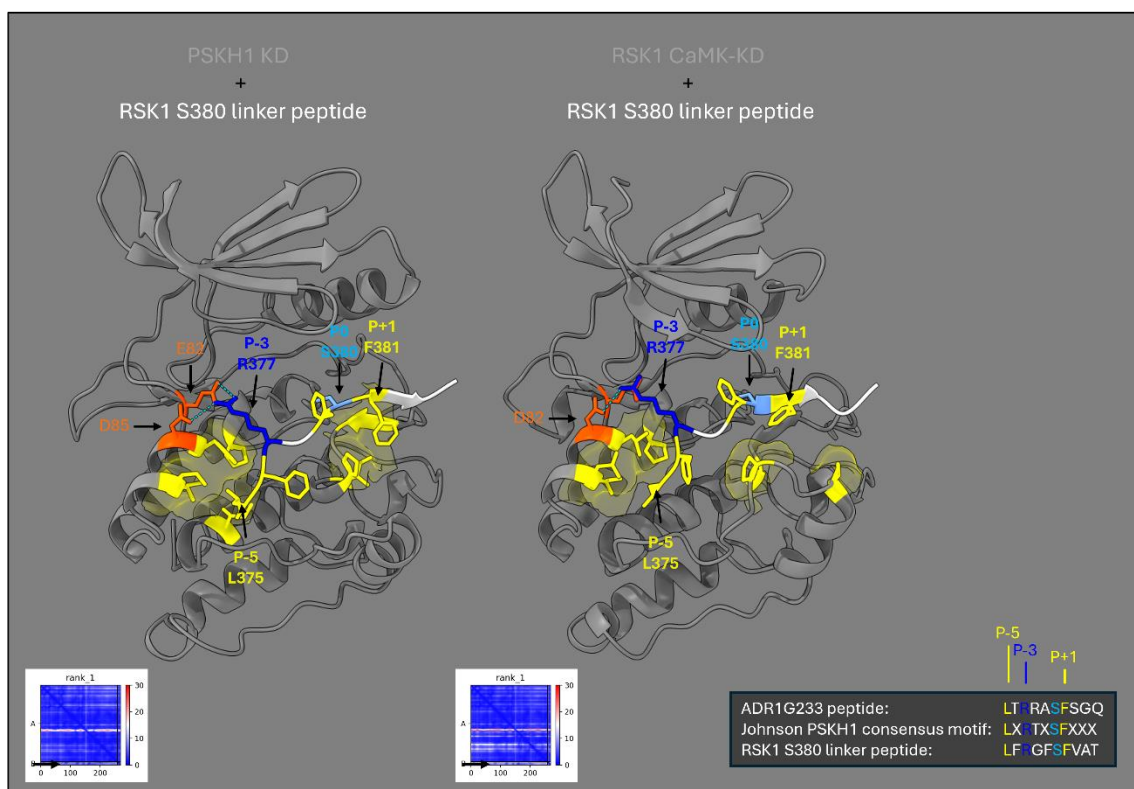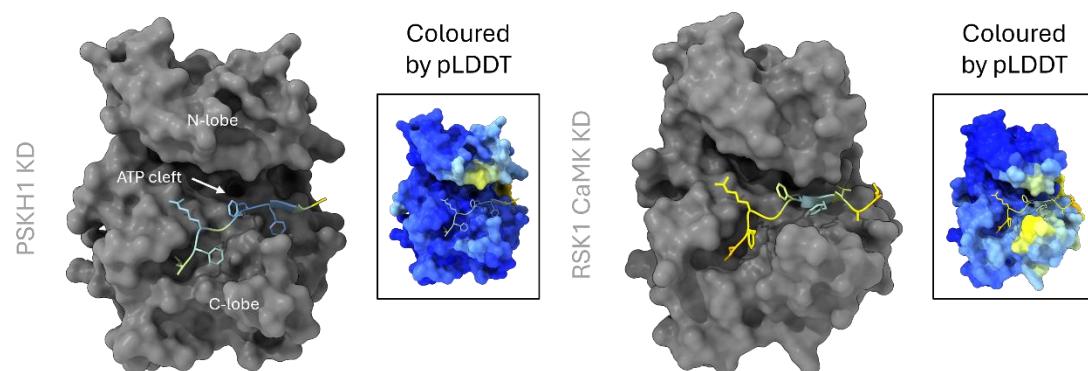
***Figure 4.7. A RSK1 Ser380 peptide docks with greater confidence to the substrate binding cleft of PSKH1.*** AlphaFold2 docking simulations between the kinase domains (KD) of PSKH1 and RSK1 (grey) with a peptide corresponding to the Ser380 'autophosphorylation motif' in RSK1. The Ser380 peptide docks more stably with the catalytic interface of the PSKH1 kinase domain. For example, the critical P-3 Arg377 residue forms multiple salt-bridge interactions with the αD-helix of PSKH1. Further, the P+1 aromatic Phe381 compacts into a hydrophobic pocket present on the C-lobe of the PSKH1 kinase domain simulation. *Surface representations.* The RSK1 Ser380 linker peptide (LFRGFSVAT) docks with improved confidence at the putative substrate binding cleft of PSKH1. Peptides and insert surface representations are coloured by pLDDT score. Predicted aligned error (PAE) plots are indicated below. Yellow: hydrophobic; dark blue: basic; orange red: acidic; cornflower blue: Ser380; white: Ser380 peptide.
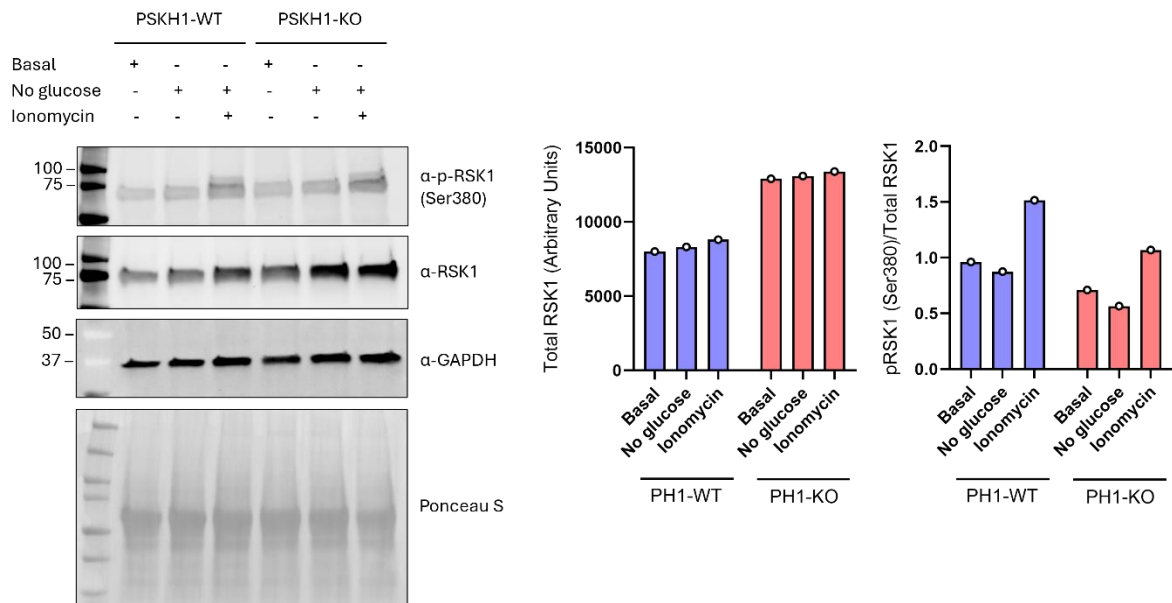
***Figure 4.8. RSK1 expression is increased in PH1-KO cells under glucose stress.*** PH1-WT
and PH1-KO LNCaP cells were seeded onto 6-well plates and cultured in complete media for
24 hours. On day 2, cell media was subsequently replaced with fresh, HG DMEM (basal) or
glucose deficient DMEM (no glucose) for 30 minutes before rapid lysis *in situ*. Some wells
were also post-treated with 1μM ionomycin for 5 minutes before rapid lysis *in situ*. Protein
content was determined by the bicinchoninic acid assay (BCA), according to the
manufacturer's protocol (Thermo Fisher Scientific). Total RSK1 and phospho-RSK1 (Ser380)
were interrogated by western blot using α-RSK1 and α-p-RSK1 (Ser380) antibodies (Table
2.1.5). 50μg total protein was loaded/well. α-GAPDH was used as a positive control for protein
loading. Total RSK1 was normalised to GAPDH. Ponceau S staining was employed to validate
homogenous transfer of protein onto the PVDF membrane.

## 4.6. Discussion

PSKH1 is a top-6 driver of prostate cancer progression, however the mechanisms by which

PSKH1 promotes neoplastic growth are not known [6]. To interrogate this very question,

PSKH1-KO prostate cancer cells (LNCaP) were generated via CRISPR-Cas9 gene editing

(generously provided by Dr. Naomi Ling) It was recently reported that partial PSKH1

knockdown by siRNA interference attenuated growth of a panel of prostate cancer cell lines

[6]. To evaluate the effect of total PSKH1 ablation on cell growth, LNCaP WT and LNCaP-

KO (PH1-WT and PH1-KO, respectively) cells were first cultured under complete growth

conditions. Interestingly, whilst no differences were observed in the initial ~30 hours, PH1-WT and PH1-KO growth curves began to bifurcate >30 hours (Figure 4.1). This effect began to replicate in the lower density seeded cells ($5 * 10^3$) once the same approximate confluency (~$10 * 10^3$) was reached. It was initially reasoned that the difference in cell growth observed was due to differential responses of the PH1-WT/KO cells to nutrient availability. This would imply that PSKH1 is a tumour suppressor that attenuates growth in the absence of nutrients, which is contrary to literature published on PSKH1 and prostate cancer [6]. Irrespectively, we decided to interrogate this further by subjecting PH1-WT/KO cells to various cell culture conditions where energy and growth factor availability were manipulated. Decreasing serum (2%) or removing it entirely (serum free) had no effect on cell growth rates (Figure 4.2). Interestingly, the same bifurcation was observed at approximately the same cell confluency ($10 * 10^3$) under complete growth conditions, indicating that PSKH1 may respond to cell density or mechanical cues and modulate cell growth accordingly (discussed in chapter 5.6). Most importantly, removing glucose completely abolished growth of PH1-KO cells (Figure 4.2). This finding immediately inspired the following hypotheses: 1) PSKH1-KO cells are entirely dependent on glucose for growth and 2) PSKH1 is a metabolic sensor that drives PH1-WT cell growth under low-glucose conditions by regulating utilisation of alternative energy sources. In concurrent *in vitro* experiments in HEK293T cells transiently expressing PSKH1-FLAG, severe nutrient stress was the only condition that promoted post-translational modification of PSKH1 (Supplementary Figure 4.4). EGF stimulation, phorbol ester, sorbitol treatment, and osmotically stressing cells had no observable effect on PSKH1-FLAG (Supplementary Figures 4.1-4.3). Whilst removing glucose did not induce pThr or doublet formation in several experiments, it is entirely possible that the treatment durations were not long enough, although entirely adequate to induce PSKH1 activity (Figures 3.19 and Supp. Fig. 4.4, 30 min and 2-hour glucose starvation, respectively). In contrast, Earle's Balanced Salt Solution (EBSS),

which is deficient in growth factors, nutrients and amino acids and is a comparatively harsh treatment, induced robust post-translational modification of PSKH1 (Supplementary Figure 4.4). By what mechanisms does PSKH1 promote cell growth under low glucose availability? It was reasoned that PSKH1 is likely facilitating fat utilisation, as protein catabolism is too slow to support the growth of neoplastic cells. To test this, PH1-WT and PH1-KO cells were metabolically examined under high- and low-glucose conditions using the Agilent Seahorse XF Analyser. Supporting our hypothesis, under replete (10mM glucose) conditions, PH1-KO cells were more glycolytic, as determined by the increased extracellular acidification rate (ECAR) (P=0.0137, Figure 4.3). ECAR is a measure of lactate production in cells and represents aerobic glycolysis. Thus, PH1-KO cells are more dependent on glucose for growth, indicating impaired alternative energy source utilisation. Further, PH1-KO cells were non-responsive to FCCP treatment under no-glucose conditions (Figure 4.3). FCCP is an uncoupling agent that artificially increases electron flow through the electron transport chain. Thus, FCCP mimics a biological stressor that prompts cells to increase production of ATP by maximally utilising all available energy sources. Maximal respiration was impaired in PH1-KO cells relative to wild-type controls (P=0.0231), suggesting PH1-KO cells are unable to catabolise or synthesise non-glucose derived energy intermediates. Thus, does PSKH1 drive cell growth during low nutrient availability by prompting cells to utilise lipids? To test this, PH1-WT and PH1-KO cells were cultured under high- and no glucose conditions and analysed by coherent anti-Stokes Raman spectroscopy (CARS) microscopy. CARS microscopy is a technique primarily suited to measuring lipid content in samples [254]. By modulating the laser power of concomitant pump and Stokes beams, target biomolecules can be visualised by matching the vibrational resonance characteristic to their atomic bonds [254]. CARS microscopy is limited by its detection sensitivity, which typically requires large quantities of target moiety in order to produce detectable coherent anti-Stokes Raman scattering [254]. Thus,

CARS microscopy is highly suited to lipid profiling, which are abundantly present inside cells. PH1-WT and PH1-KO cells were seeded onto glass-bottomed 18-well µSlides pre-coated with 50µg/mL PDL and glucose starved for 1, 3, 6 and 24 hours. CARS images were collected with the assistance of Cameron Nowell from the Imaging, FACS and Analysis Core at the Monash Institute of Pharmaceutical Sciences. Overall, the number of lipid droplets/$\mu m^2$ were not significantly different under glucose replete conditions but did decrease in the PH1-KO cells during glucose duress (P=0.0367) (Figure 4.4). Interestingly, individual lipid droplet analysis of PH1-WT and PH1-KO cells revealed striking differences in droplet intensity and size (Figure 4.4). For example, mean signal intensity increased in PH1-WT cells during glucose duress but did not change in PH1-KO cells (P=<0.0001 vs P=0.0806, respectively). Furthermore, under severe glucose stress (24 hours), PH1-KO cells exhibited significantly smaller lipid droplets compared to wild-type controls (P=<0.0001). These data are exemplified in the representative images shown, where PH1-WT cells exhibit bright, distinct puncta relative to PH1-KO cells, whose puncta are diffusely faint (Figure 4.4). Interestingly, a comprehensive CARS scan of glucose starved lipid droplets revealed a distinct difference in the spectroscopic profiles of PH1-WT and PH1-KO cells. A peak at 3328 nm was noticeably absent in PH1-KO cells (Figure 4.4). This peak corresponds to lipid hydroperoxides, fatty acid derivatives highly implicated in ageing and inflammation [255]. These data collectively demonstrated that PSKH1 ablation impairs lipid biogenesis *in vitro* and corroborates an expanding body of literature implicating lipids in prostate cancer progression [253, 270]. For example, fatty acid production is frequently upregulated in prostate cancer and fatty acids appear to be the primary metabolic substrate of prostate cancer cells [249, 250]. Further, pharmacological inhibition of fatty acid production impairs prostate cancer growth *in vitro* and *in vivo* [251, 271]. These data provide a direct link between PSKH1-mediated prostate cancer progression and the dependence of prostate cancer on lipid derivatives for growth. Promisingly, our studies also indicate

inhibition of PSKH1 by small molecules as a potential approach to therapeutically block prostate cancer growth (Figure 4.6). Whilst preliminary, the ATP analogue 'compound 2' (C2) halted prostate cancer cell proliferation relative to vehicle-treated controls (P=0.0055, Figure 4.5).

By what mechanisms does PSKH1 modulate fatty acid utilisation to promote prostate cancer cell proliferation? To answer this, we cross referenced the recently characterised PSKH1 substrate motif (LxRTxSFxxx) with >2-fold enriched interacting proteins from our PSKH1-TurboID proteomic screen. This analysis identified a single kinase harbouring a perfect PSKH1 recognition site: RSK1. To satisfactorily explain the dramatic growth phenotype observed upon PSKH1 ablation, downstream effectors of PSKH1 signalling must invariably regulate cell growth pathways. RSK1 is implicated in a wide variety of cellular processes but, notably, promotes cell proliferation and is frequently dysregulated in prostate cancer [257]. The p90[rsk] kinases are unusual in that they harbour tandem kinase domains tethered by an inter-kinase linker. The N-terminal kinase domain (NTKD) bears significant homology to AGC family members (59% similarity), whilst the C-terminal kinase domain (CTKD) more closely resembles a CaM-kinase domain (54% similarity) [258]. In canonical RSK signalling, ERK docks RSK1 at its linear motif (LM) and phosphorylates the inter kinase region (Ser363) and activation loop (Thr573) of the CTKD (Figure 4.7) [259, 260]. CTKD-mediated intermolecular autophosphorylation of Ser380 primes RSK1 for PDK1 docking and subsequent phosphorylation of the NTKD activation loop residue (Ser221), maximally activating RSK1 [261, 262]. Activated RSK1 translocates to the nuclear compartment where it regulates the action of transcription factors CREB and c-Fos, modulating gene expression of a wide variety of downstream effectors implicated in cell growth, differentiation, and cell survival pathways [266]. Interestingly, RSK1 has been reported to associate with the plasma membrane rapidly and transiently before shuttling to the nuclear compartment [269] (Figure 4.6). Richards et al.

(2001) speculate that ERK's primary function is to chaperone RSK to the plasma membrane (PM), rather than phosphorylate the inter-kinase Ser363 site [269]. Forcibly myristoylating a linear motif-deficient RSK1 mutant (thereby promoting its association with the PM but preventing ERK association) results in an enzyme of equivalent activity to wild-type protein [269]. Further, the 'ERK Ser363' site is phosphorylated in myristoylated C-terminal truncated RSK1 mutants, suggesting that ERK action on this residue is largely dispensable [269]. PDK1 possesses a pleckstrin homology domain, enabling stable interaction at the plasma membrane. Thus, transient translocation of RSK1 to the plasma membrane would theoretically bring RSK1 in close proximity to PDK1, its primary upstream activator, but also PSKH1, which similarly associates with internal membranes [141] (Figure 4.6). Earlier we speculated that active PSKH1 may associate with the plasma membrane, whilst inactive PSKH1 may localise to the endoplasmic reticulum, and that this process was mediated by palmitoylation/myristoylation of N-terminal glycine/cysteine residues (Chapter 3.4.3, CREC regulation of PSKH1). Corroborating a role for PSKH1-mediated Ser380 phosphorylation of RSK1, several studies suggest that the CTKD is largely dispensable in RSK1 activation [262-264]. For example, truncating the CTKD yields active enzyme whose Ser380 site is hyperphosphorylated *in vitro* [262, 263]. If the CTKD is indeed the primary mechanism by which Ser380 is phosphorylated *in vivo*, how is this possible? We speculate that the role of the CTKD is predominantly structural in function and may, in addition to providing an essential ERK docking site at its C-terminus (the linear motif), regulate Ser380 phosphorylation by sterically obstructing access to upstream heterologous protein kinases. To test this, PSKH1-WT and PSKH1-KO LNCaP cells were cultured under glucose duress and rapidly lysed *in situ*. Some cells were post-treated with ionomycin to further activate PSKH1 by promoting CaM-enhancement of PSKH1 activity. Interestingly, whilst p-RSK1 (Ser380) was not significantly different between cell lines, total RSK1 expression was significantly higher in PH1-KO cells, particularly under glucose stress

(Figure 4.8). It is tempting to speculate that this increase in RSK1 expression is a compensatory mechanism to account for decreased PSKH1 phosphorylation of Ser380 in the PH1-KO cells. RSK1 can autophosphorylate Ser380, albeit comparatively slowly [259, 261]. Increasing RSK1 expression could theoretically overcome the slow kinetics of Ser380 autophosphorylation and enable PDK1-driven activation of the RSK1-NTKD and subsequent phosphorylation of downstream effectors, including CREB and c-Fos. These data are preliminary and it is not possible to draw definitive conclusions. Nonetheless, it is exciting to envision such a system, which could theoretically explain the dramatic growth defect observed in PH1-KO prostate cancer cells during nutrient withdrawal (Figure 4.2). Like PSKH1, RSK1 is activated during glucose duress and frequently co-segregates with prostate cancer progression [257, 265]. Interestingly, eEF2K was also identified in our PSKH1-TurboID proteomic screen (Dr. Chris Horne, Dr. Toby Dite, unpublished) and was enriched to comparable levels as RSK1. eEF2K inhibits protein synthesis by phosphorylating eEF2 [272]. RSK1 inactivates eEF2K by phosphorylating Ser366 [273]. Like PSKH1 and RSK1, glucose stress modulates eEF2K activity [230]. It is possible that these kinases comprise a signalling network to regulate cell growth pathways during nutrient stress. A hypothetical model of PSKH1:RSK1:eEF2K-driven prostate cancer progression is detailed in figure 4.9. In this model, low glucose in the prostate cancer tumour microenvironment activates PSKH1, possibly by promoting dual acylation of N-terminal palmitoylation/myristoylation sites, or via binding of an undescribed allosteric molecule. Dual acylation promotes PSKH1's translocation to the plasma membrane [141]. The PSKH1 homo-oligomer phosphorylates its activation loops in a *cis*-apparent mechanism (Figure 3.11). Further binding by CaM (Figures 3.17/19) and UNC119B enhance the catalytic activity of PSKH1. UNC119B is a recently identified novel interactor of PSKH1 that binds palmitoylated/myristoylated moieties (unpublished). We have shown that UNC119B increases PSKH1 activity independently of $Ca^{2+}$/Calmodulin (unpublished). Activated PSKH1

phosphorylates PM-localised RSK1 at Ser380, enabling PDK1-mediated *trans*-phosphorylation of the NTKD, maximally activating RSK1 [262]. RSK1 phosphorylates eEF2K at Ser366, disabling eEF2K activity and indirectly promoting protein translation [273]. RSK1 also translocates to the nuclear compartment where it regulates the action of transcription factors CREB and c-Fos, promoting gene expression of proteins implicated in fat mobilisation, ameliorating the energetic demands of rapidly dividing prostate cancer cells [266]. Prostate cancer malignancies are frequently reported to preferentially metastasize to bone [274]. A local abundance of $Ca^{2+}$ may drive constitutive activation of PSKH1 by enhancing $Ca^{2+}$/CaM-enhancement of PSKH1 activity. Alternatively, PSKH1 may indirectly regulate the translation of genes that promote fat utilisation by localising RSK1 to the translation initiation complex. The translation initiation complex (eukaryotic initiation factor 4F, henceforth eIF4F) comprises various subunits implicated in protein translation, including the mRNA helicase eIF4A, the cap-binding eIF4E translation initiation factor and eIF4G, which serves a scaffolding function [275]. Interestingly, several of these subunits were highly represented in our PSKH1 proximity labelling experiments by TurboID/mass spectrometry, including eIF4G1 and eIF4G3 (Figure 4.10). The closely related 'eIF4E kinases' (MKNK1/2, described earlier in Chapter 1) modulate the action of the eIF4F complex by phosphorylating Ser209 on eIF4E [71, 179]. This process is facilitated by an overlapping N-terminal NLS/eIF4G-binding motif that anchors MKNK1/2 to the eIF4F complex [179]. Interestingly, PSKH1 also harbours a putative N-terminal NLS in an analogous position to MKNK1/2, although this has not yet been functionally characterised (Figure 1.7) [38]. As both eIF4G1 and eIF4G3 were demonstrated to be strongly PSKH1-interacting, it is tempting to speculate
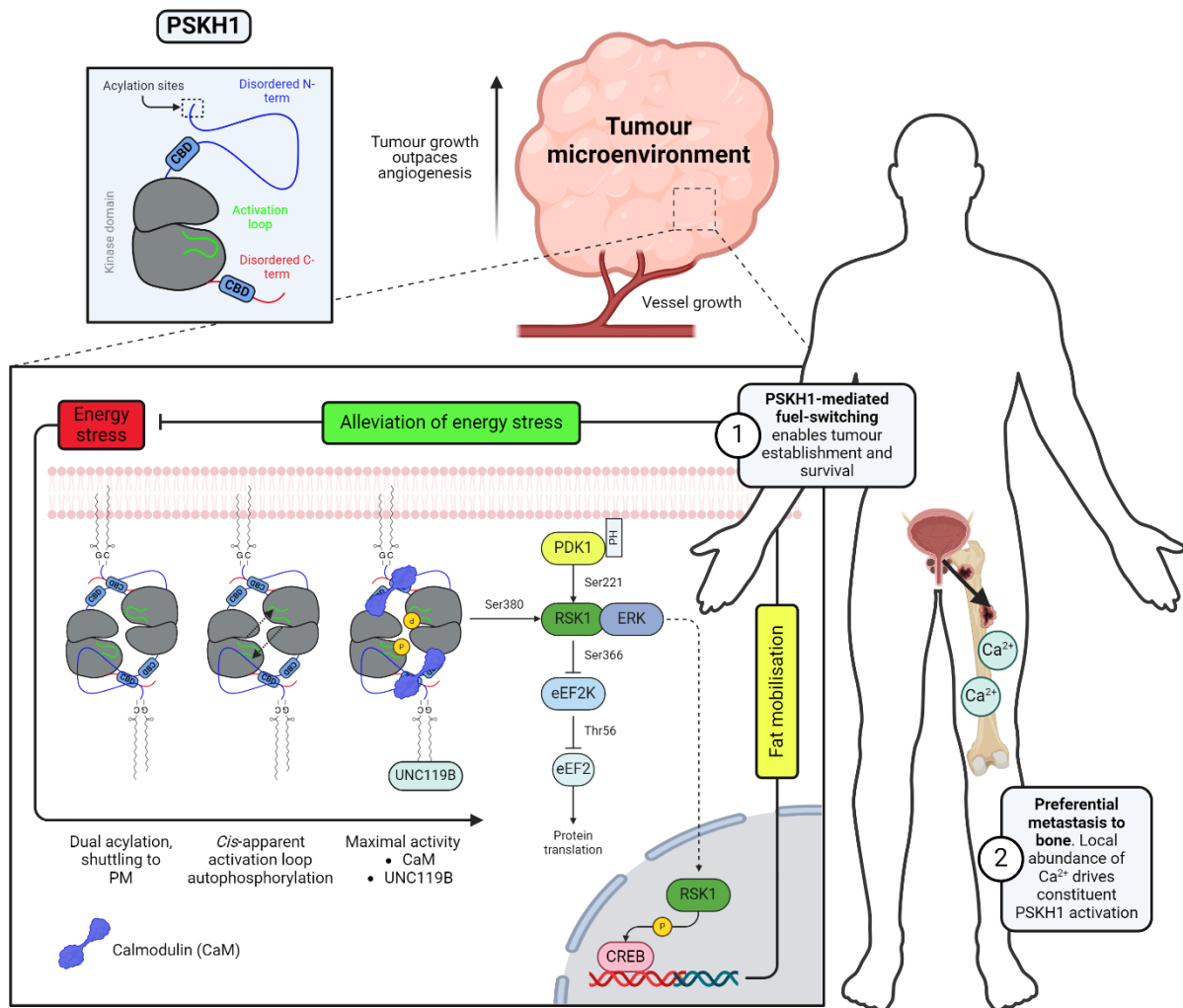
***Figure 4.9. Hypothetical model of PSKH1 activation and mechanism for prostate cancer progression.*** In this hypothetical model of PSKH1-driven prostate cancer progression, energy stress (low glucose) in the tumour microenvironment activates PSKH1 by priming PSKH1 for CaM activation and promoting dual acylation of N-terminal glycine/cysteine residues. Dually acylated PSKH1 co-localises at the plasma membrane [141]. Dimerised PSKH1 autophosphorylates its activation loop in a *cis*-apparent mechanism (Figure 3.10). CaM- and UNC119B-binding maximally activate PSKH1. PSKH1 phosphorylates Ser380 in RSK1's inter-kinase linker, priming it for PDK1 docking and phosphorylation of the NTKD Ser221 residue [262]. Activated RSK1 inhibits eEF2K by phosphorylating Ser366, promoting protein translation [273]. Further, RSK1 translocates to the nuclear compartment, where it regulates the action of transcription factors CREB and c-Fos, promoting gene expression of proteins implicated in fat mobilisation, thereby alleviating the energetic demands for prostate cancer cell growth. Prostate tumours preferentially metastasise to bone [274]. Local abundance of $Ca^{2+}$ drives constituent $Ca^{2+}$/CaM activation of PSKH1. PH: pleckstrin homology domain; CaM: calmodulin. Created with BioRender.com.

that PSKH1 mediates this interaction via its N-terminal NLS. Further, RSK1 has been shown to modulate the helicase activity of eIF4A by phosphorylating eIF4B on Ser422 [276]. It is widely accepted that substrate phosphorylation by RSK1 is chiefly facilitated by the N-terminal AGC-like kinase domain [259]. In contrast, the function of the CaMK-like C-terminal kinase domain remains undefined but may be structural in nature. Due to relative similarity in the CaM-kinase domains of PSKH1 and RSK1-CTKD (Figure 4.10, panel D), it is entirely possible that the non-functional RSK1-CTKD and PSKH1 kinase domains oligomerise. Indeed, PSKH1 has been shown to homodimerise primarily via kinase domain contacts [38]. In this model, eIF4G bound PSKH1 localises RSK1 to the translation initiation complex by oligomerising with the RSK1-CTKD. Active RSK1-NTKD phosphorylates eIF4B on Ser422, which subsequently modulates helicase activity of eIF4A (Figure 4.10, panel C). Truncational studies will determine if the N-terminal NLS of PSKH1 is indeed important for eIF4G recognition. Further, co-immunoprecipitation experiments incorporating RSK1-CTKD and the kinase domain of PSKH1 will elucidate whether PSKH1 and RSK1-CTKD oligomerise *in vitro*.
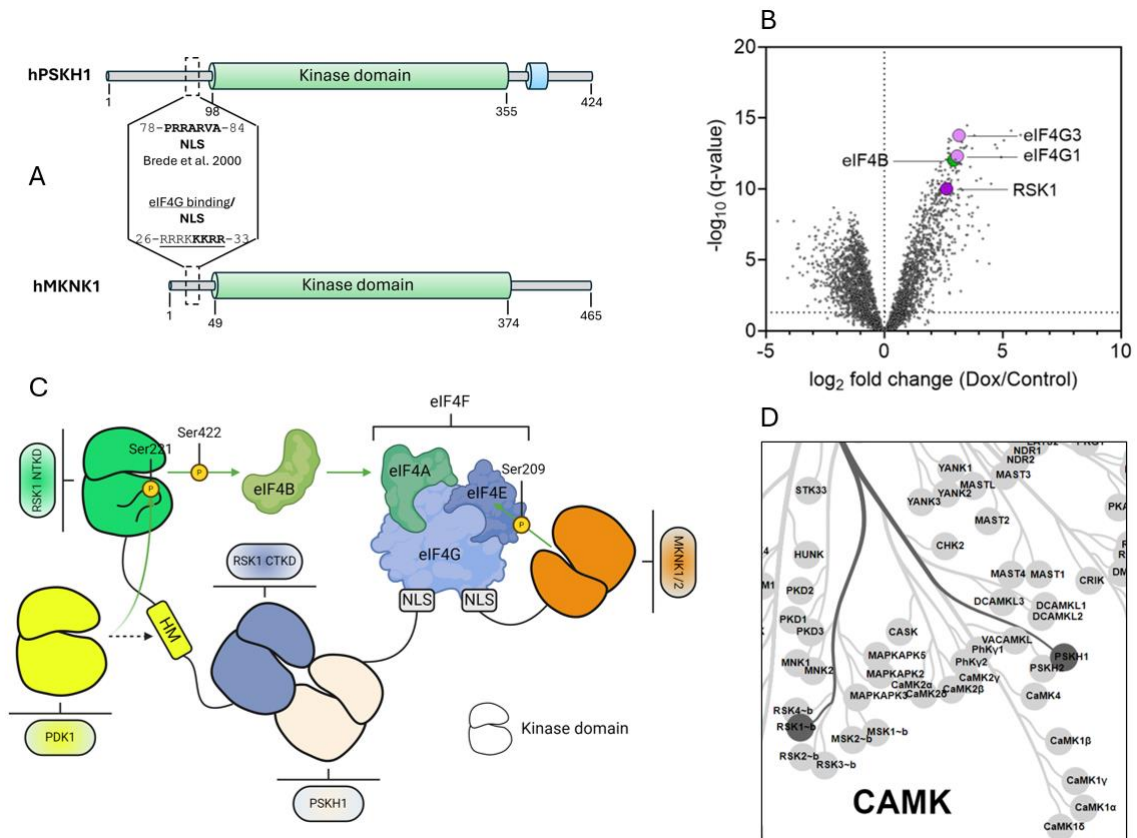
***Figure 4.10. PSKH1 may mediate RSK1 modulation of translation initiation by docking and targeting RSK1 to the eIF4F complex.*** A. PSKH1 and the closely related MKNK1/2 kinases harbour an NLS N-terminal to the catalytic domain [38]. In MKNK1/2, this NLS facilitates interaction with the scaffolding protein eIF4G. B. Components of the eIF4F complex were identified as strongly PSKH1-interacting in proximity labelling experiments by TurboID/MS (Dr. Chris Horne, Dr. Toby Dite, unpublished). C. MKNK1/2 modulate the action of the eIF4F complex by phosphorylation eIF4E on Ser209. An N-terminal NLS binds eIF4G, bringing MKNK1/2 in close proximity to the translational machinery. RSK1 was also identified as PSKH1 interacting and phosphorylates eIF4B at Ser422, indirectly regulating the helicase activity of eIF4A [276]. In this hypothetical model, PSKH1 binds eIF4G by virtue of its N-terminal NLS. The kinase domains of PSKH1 and RSK1 (CTKD) oligomerise, anchoring RSK1 at the eIF4F complex. This allows subsequent phosphorylation of eIF4B at Ser422 by the N-terminal kinase domain of RSK1, modulating the rate-limiting step (helicase activity) of translation initiation. D. The kinase domains of PSKH1 and RSK1-CTKD are closely related. NLS: nuclear localisation signal; HM: hydrophobic motif. Created with BioRender.com and CORAL [10].

As a recently characterised metabolic sensor, PSKH1 modulates cell growth pathways by translating information from the 'energy dial' (Figure 4.11). When energy is plentiful, cell growth is limited by density limits and mechanotransduction signalling between cells. As available energy decreases, PSKH1 ameliorates the energetic demands of cells by prompting fuel-switching to alternative energy sources (i.e. lipids). Under severe energy stress, increased AMP concentration activates AMPK, which halts anabolic processes by inhibiting the action of mTOR.
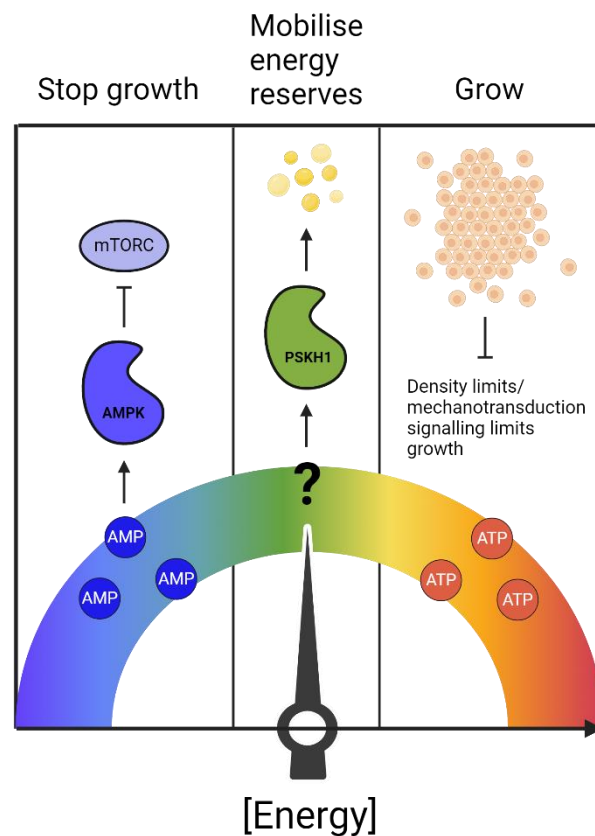


***Figure 4.11. The energy dial regulates cell growth by modulating the action of metabolic sensor kinases.*** Under energy replete conditions, cell growth is limited by cell density limits and mechanotranduction signalling pathways. As energy (glucose) levels decrease, PSKH1 mobilises energy reserves (lipids) to ameliorate the energetic demands of dividing cells. Under severe nutrient stress, increased AMP concentration activates AMPK, which halts anabolic processes by inhibiting the action of mTOR, conserving energy. Created with BioRender.com.

**Supplementary Figures**

**Supplementary Figure 4.1. EGF, TNF and UV do not induce pThr phosphorylation of PSKH1-FLAG in HEK293T cells.**
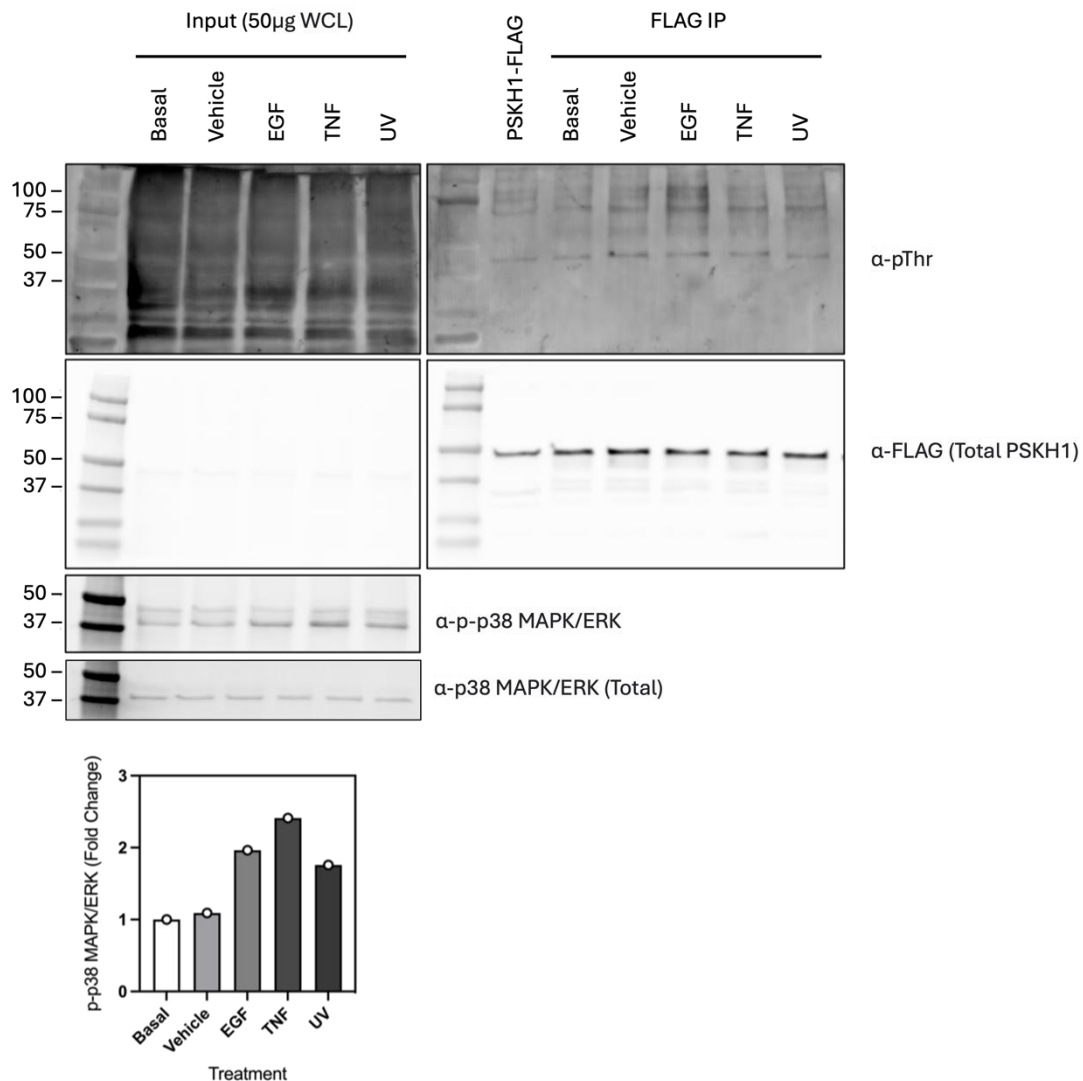


*Supplementary Figure 4.1. EGF, TNF or UV treatment does not induce threonine phosphorylation of PSKH1-FLAG in HEK293T cells.* HEK293T cells transiently expressing PSKH1-FLAG were treated with vehicle (1% ethanol v/v), 100nM EGF, 100nM TNF or exposed to UV light for 30 minutes followed by rapid lysis in MLB (Table 2.1.2. Buffers) *in situ*. PSKH1-FLAG was immunoprecipitated from HEK293T whole cell lysate (WCL) using pre-equilibrated α-FLAG® M2 Affinity resin. Immobilised PSKH1-FLAG was eluted off the FLAG Affinity resin using 50µl FLAG peptide (1mg/mL). 50 µg WCL and 10µL purified PSKH1-FLAG was subjected to SDS-PAGE and western blot. Total PSKH1 expression and phosphor-threonine (pThr) status were interrogated using α-rabbit FLAG (D6W5B) and α-

mouse pThr (42H4) primary antibodies. Secondary antibodies used included α-rabbit IRDye® 680RD and α-mouse IRDye® 800CW near-infrared antibodies. Phospho-p-38 (MAPK/ERK) was used as a positive control for EGF treatment efficacy.

**Supplementary Figure 4.2. EGF, phorbol ester and sorbitol do not induce Thr-phosphorylation of PSKH1-FLAG in HEK293T cells.**
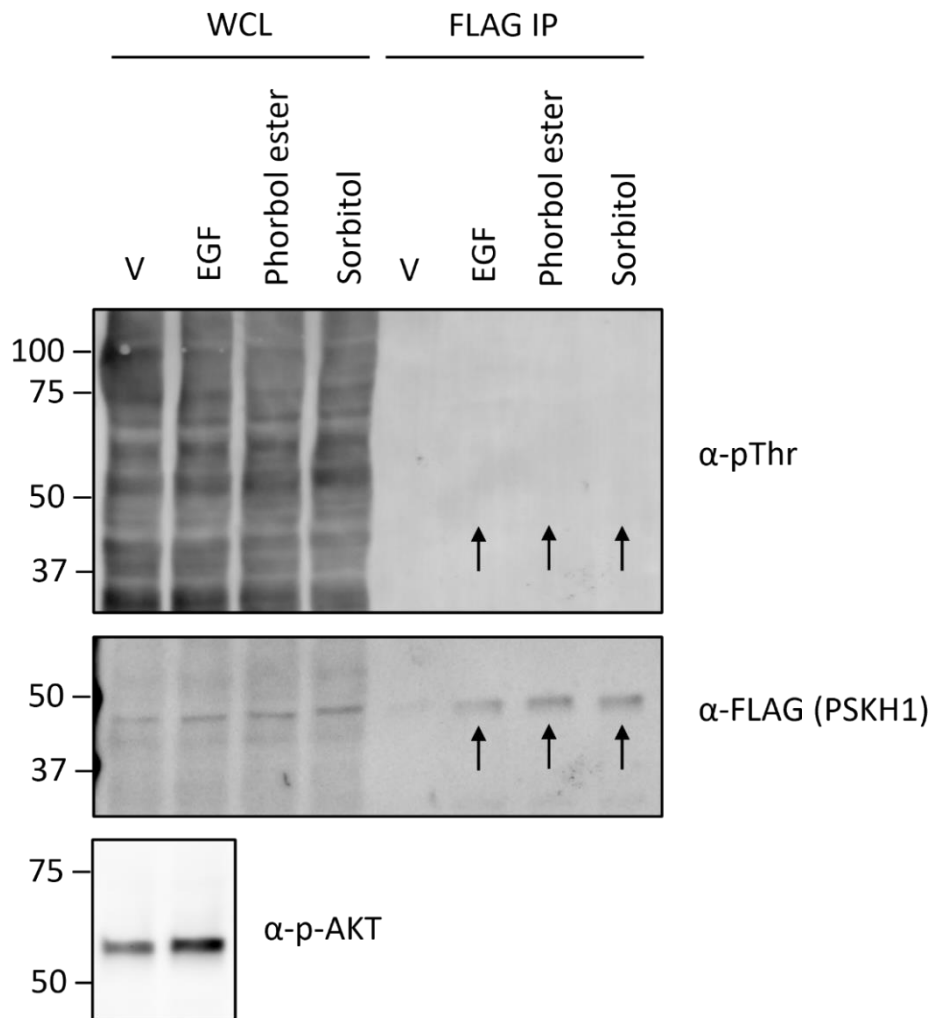


***Supplementary Figure 4.2. EGF, phorbol ester and sorbitol do not induce Thr-phosphorylation of PSKH1-FLAG in HEK293T cells.*** HEK293T cells transiently expressing PSKH1-FLAG were treated with vehicle (1% ethanol v/v), 100nM EGF, 10μM phorbol ester or 500mM sorbitol followed by rapid lysis in MLB (Table 2.1.2. Buffers) *in situ*. PSKH1-FLAG was immunoprecipitated from HEK293T whole cell lysate (WCL) using pre-equilibrated α-FLAG® M2 Affinity resin. Immobilised PSKH1-FLAG was eluted off the FLAG Affinity resin using 50μl FLAG peptide (1mg/mL). 50 μg WCL and 10μL purified PSKH1-FLAG was subjected to SDS-PAGE and western blot. Total PSKH1 expression and phosphor-threonine (pThr) status were interrogated using α-rabbit FLAG (D6W5B) and α-mouse pThr (42H4) primary antibodies. Secondary antibodies used included α-rabbit IRDye® 680RD and α-mouse IRDye® 800CW near-infrared antibodies. Phospho-AKT (α-p-AKT) was utilised as a positive control for EGF treatment.

**Supplementary Figure 4.3. Osmotically stressing HEK293T cells transiently expressing PSKH1-FLAG fails to induce Thr/Ser-phosphorylation.**
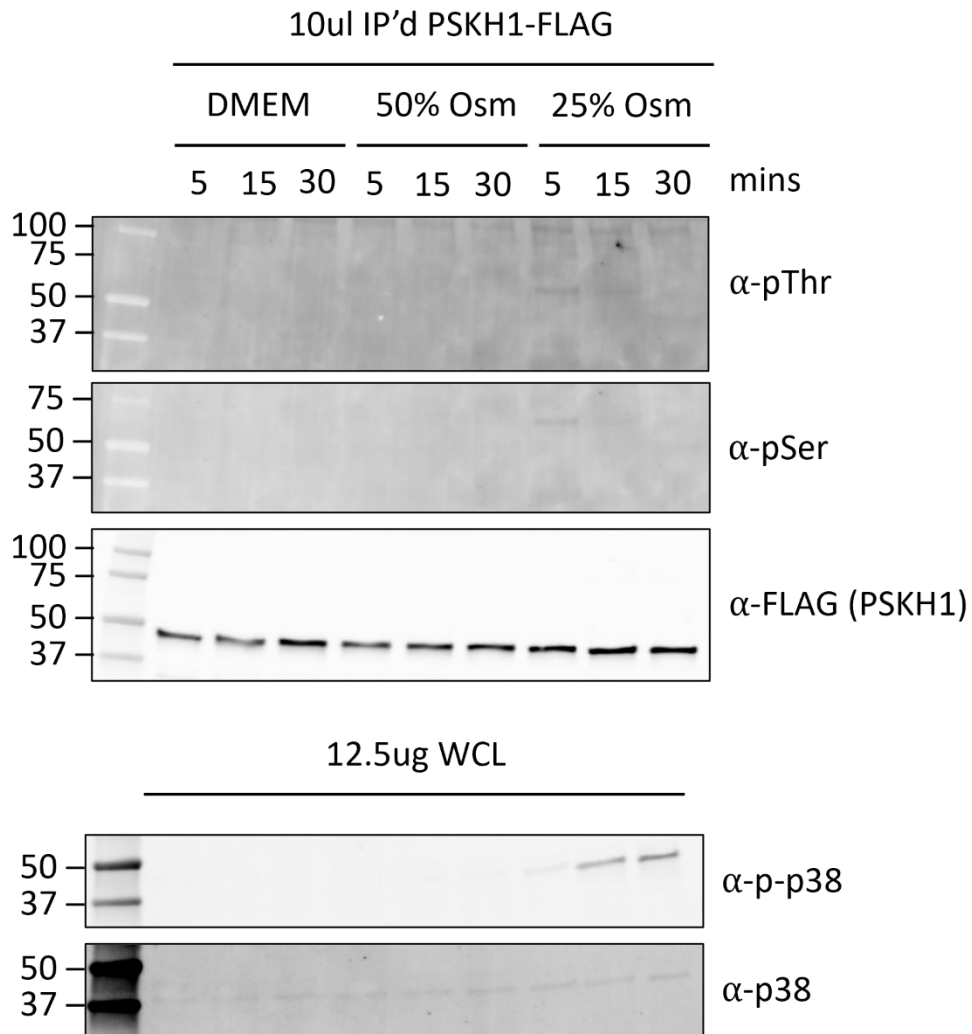


***Supplementary Figure 4.3. Osmotically stressing HEK293T cells transiently expressing PSKH1-FLAG fails to induce PKN1 trans-phosphorylation of PSKH1.*** HEK293T cells transiently expressing PSKH1-FLAG were osmotically stressed for 5-30 minutes by diluting standard, supplemented DMEM cell culture media in milli-Q water. Following treatment, HEK293T cells were rapidly lysed *in situ*. PSKH1-FLAG was immunoprecipitated from WCL as previously described. PSKH1 expression and pThr/Ser status was interrogated by western blot using α-FLAG/p-Thr/p-Ser antibodies (Table 2.1.5). p38 phosphorylation status (p-p38) was used as a positive control to confirm the effectiveness of osmotically stressing HEK293T cells. Hypotonic swelling induces p38/MAPK phosphorylation via PKN1 [247].

**Supplementary Figure 4.4. Severe nutrient stress promotes a novel post-translational modification of PSKH1 and induces Thr-phosphorylation.**
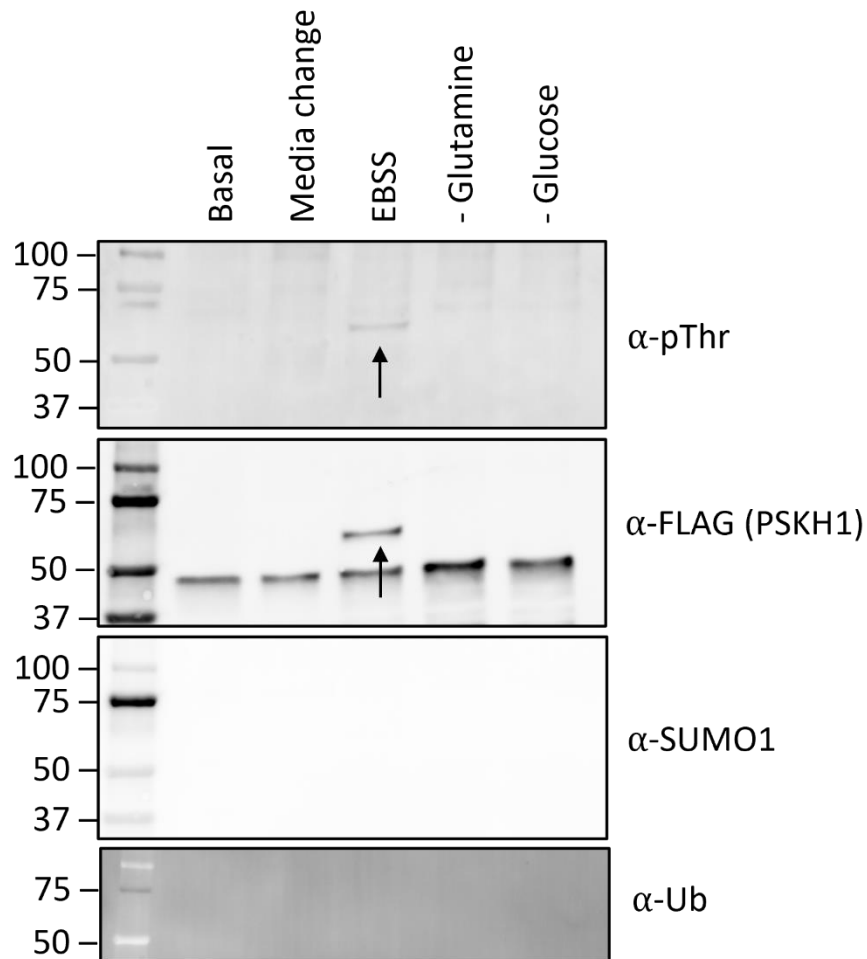


*Supplementary Figure 4.4. Emergence of a putative post-translationally modified form of PSKH1-FLAG under nutrient limiting conditions.* HEK293T cells transiently transfected with pcDNA3.1-PSKH1-FLAG were subjected to nutrient deprived conditions (EBSS, - glutamine, - glucose) for 2 hours and subsequently lysed. Recombinant PSKH1-FLAG was immunoprecipitated from WCL using an α-FLAG® M2 Affinity resin for 1 hour. Bound protein was eluted overnight using 50μl FLAG peptide (1mg/ml). Potential post-translational modifications to PSKH1-FLAG were subsequently interrogated by SDS-PAGE and immunoblot analysis using α-rabbit FLAG (D6W5B), α-mouse phospho-threonine (42H4), α-() SUMO1 () and α-() Ub () primary antibodies and α-rabbit IRDye® 680RD and α-mouse IRDye® 800CW near-infrared secondary antibodies.

# 5. GENERAL DISCUSSION

## 5.1. Preface

Recent literature characterising PSKH1 point mutations in patients with paediatric cholestasis [277] constitutes the 18th paper published on PSKH1 since its discovery in the late 1980's [139]. Thus, relative to closely related and comparatively well-characterised kinases like CaMK2, little is currently understood of PSKH1's biochemistry. Consequently, this thesis was highly results driven and propelled us to be dynamic and prepared to take risks. This involved learning new techniques (for example, CARS microscopy) to further characterise results as they appeared, and to source new collaborators to assist us with our studies. Despite these challenges, new insights were inevitably gleaned on PSKH1, and will be discussed in the following chapter.

## 5.2. Introduction

Despite constituting just ~2% of protein-encoded genes, kinases are arguably among the most important enzymes represented in the human proteome. Indeed, without kinases, crucial biological processes such as carbohydrate metabolism are not possible. Kinases affect this important charge by coordinating complex signalling cascades in response to extracellular stimuli, including energy availability, growth factor stimulation or circulating cytokines. Put plainly, kinases translate extracellular signals into intracellular responses. Activation of protein kinases can be achieved allosterically, for example, by the binding of small second messenger molecules such as cAMP to the regulatory subunits of PKA, or by disrupting intrasteric autoinhibition of the active site (see $Ca^{2+}$/CaM-regulation of CaM-kinases). This characteristic of kinase regulation is multi-faceted – firstly, it is essential to maintaining kinases in an inactive state in the absence of an upstream activating signal. More importantly, it is what makes kinases inherently druggable. Dysregulation of kinase activity frequently correlates with aggressive and often fatal disease phenotypes, such as cancer, metabolic disorders, or catastrophic neurodegenerative conditions (Table 1.2). Despite these dramatic pleiotropic effects, many

kinases remain 'dark' or understudied. This includes members of the Ca$^{2+}$/Calmodulin-regulated kinase family, more than two-thirds of which are comparatively poorly characterised (Figure 1.2). Recently, there has been appreciating interest in therapeutically targeting these dark kinases to treat myriad disorders, including cancer [8]. Strikingly, many of the dark CaM-kinases described earlier in this thesis are top 10 high priority anti-cancer targets, including DCLK3, BRSK2 and BRSK1 [8]. However, without holistic knowledge of the function and biochemical characteristics of these enzymes, therapeutic invention by small molecules remains a challenging and potentially dangerous endeavour. PSKH1 is a 48 kDa serine/threonine-protein kinase whose function and effector substrates remain undefined. Since its discovery in the late 1980's, most findings pertaining to PSKH1 have been incidental, with few studies directly targeting PSKH1 for holistic evaluation. Concerningly, PSKH1 is increasingly correlated with inflammatory disorders of the colon, of colon cancer, and is a recently characterised top 6 driver of prostate cancer progression (Table 1.2) [6, 111, 112]. Thus, there is a pressing need to determine the precise function of PSKH1 and to elucidate the mechanisms by which PSKH1 is regulated. This chapter seeks to synthesise findings from chapters 3 and 4 and is segmented into several subsections.

## 5.3. PSKH1 and inflammation

Arguably the most profound realisation from this thesis was the discovery that PSKH1 is a metabolic sensor that promotes prostate cancer cell growth by regulating fuel switching to fatty acids (Figures 4.2-4.4). It is widely accepted that altered lipid biogenesis promotes inflammatory-associated phenotypes, including various cancers, liver disease and atherosclerosis [278]. Interestingly, recently identified genetic insults to PSKH1 (a newly characterised metabolic sensor that modulates fatty acid utilisation *in vitro*) co-segregate with patients afflicted by Chron's disease and ulcerative colitis, both inflammatory disorders [111]. These mutations, P66L and R79L, cluster in the PxxP/SH3-domain binding motif of PSKH1

[38]. Cross-referencing the >2-fold enriched PSKH1-interacting proteins from our PSKH1-TurboID proteomic screen against the SH3-domain containing proteome (SH3DCP) reveals various proteins implicated in inflammatory pathways (Figure 5.1) [279]. Pathway analysis by Metascape 4.0 (https://metascape.org) of the PSKH1-SH3DCP interactome validated enrichment of inflammatory-associated pathways [280].
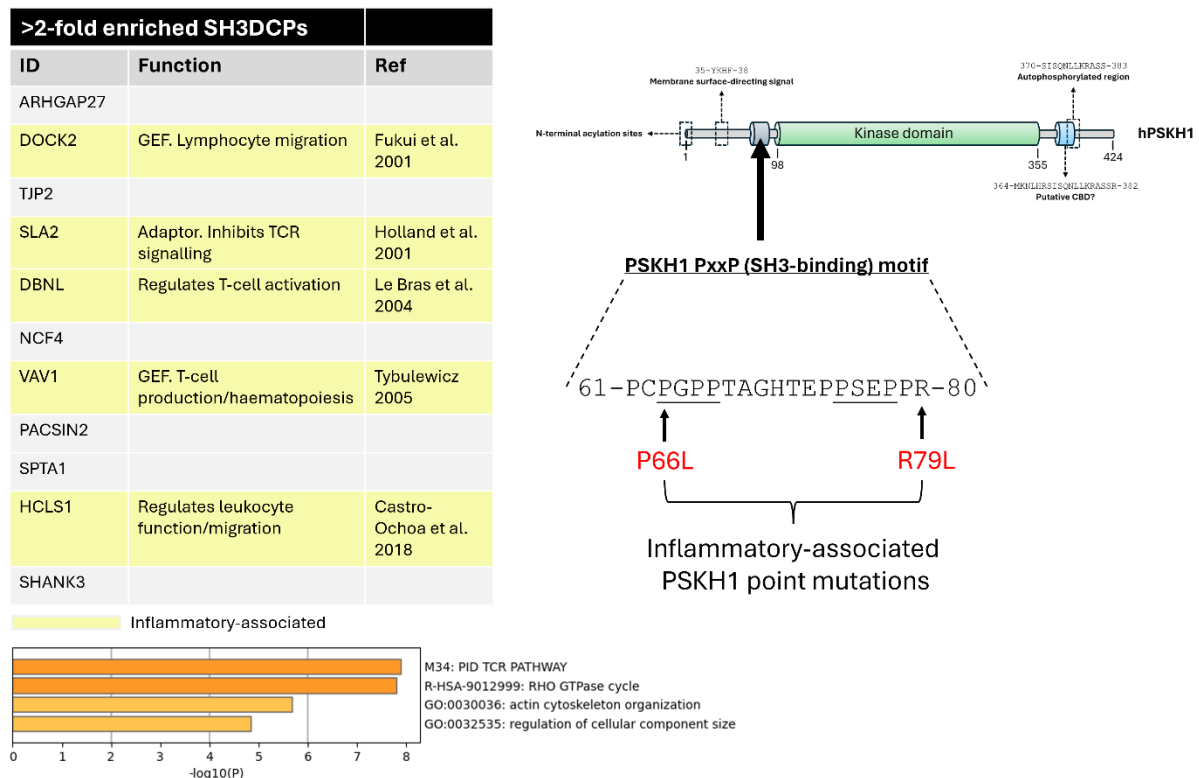


***Figure 5.1. The metabolic sensor kinase PSKH1 is implicated in inflammatory-associated phenotypes.*** Recently identified point mutations in PSKH1 co-segregate with patients afflicted with inflammatory-associated disorders, including ulcerative colitis and Chron's disease [111]. These mutations (P66L and R79L) cluster in the putative PxxP/SH3 domain-binding motif N-terminal to the catalytic domain of PSKH1. Data derived from our PSKH1-TurboID proteomic screen were manually screened for >2-fold enriched SH3 domain containing proteins (SH3DCPs) using publicly available SH3DCP proteomic data from Mehrabipour, Jasemi [279]. Interestingly, many of the SH3DCPs identified are implicated in inflammatory pathways, including DOCK2, SLA2, DBNL, VAV1, and HCLS1 (yellow). Network mapping by Metascape (https://metascape.org) validates enrichment of inflammatory pathways (T-cell receptor pathways) [280].

## 5.4. PSKH1, reticulocalbin, and prostate cancer

PSKH1 proteomic screening coupled with *in vitro* autophosphorylation experiments revealed that a novel family of low-affinity $Ca^{2+}$-binding proteins attenuate the autoactivation and intrinsic activity of GFP-PSKH1 (Figures 3.26-3.28). These CaM-like proteins (RCN1/3) exhibit highly localised expression within the luminal space of the endoplasmic reticulum [232]. PSKH1 is known to translocate to the ER following myristoylation of an N-terminal glycine (G2) residue [141]. Indeed, acylation of this region is likely highly dynamic, as dual lipidation (G2-myristoylation/C3-palmitoylation) promotes PSKH1 localisation to the plasma membrane and Golgi apparatus (GA) [141]. Given the inhibitory effect of reticulocalbin on PSKH1 activity, earlier we speculated that the active form of PSKH1 may localise at the PM/GA, whilst the inactive variant may translocate to the ER (which would theoretically bring it in close proximity to RCN1/3). Like PSKH1, reticulocalbin is also implicated in prostate cancer progression [281, 282]. Interestingly, RCN1 has been reported to express on the cell surface of several prostate cancer cell lines, including LNCaP and C4-2B4 cells [281]. How RCN1 translocates to the cell surface is not currently understood, as RCN1 contains an ER-retention signal (K/HDEL) at its C-terminus [232]. However, hypothetically, cell-surface localisation of RCN1 in PCa could abrogate engagement of ER-localised myristoylated-PSKH1, preventing inhibition of its catalytic activity. PSKH1 drives prostate cancer progression by, partly, ameliorating the energetic demands of dividing cancer cells by promoting fuel-switching to fatty acids (Figures 4.2-4.4). Thus, cell surface expression of RCN1 may further exacerbate prostate cancer progression but maintaining PSKH1 in a constitutively active state. Interestingly, rescue of RCN1 expression in cisplatin-resistant non-small cell lung cancer cell lines restores sensitivity to cisplatin treatment, suggesting that homeostatic RCN1 expression is anti-tumorigenic in nature [283]. These data corroborate our observations on RCN1-mediated inhibition of PSKH1 activity and prostate cancer progression.

Further work is needed holistically evaluate the RCN/PSKH1 interaction *in vivo*. Unfortunately, for the duration of this thesis, high quality commercial antibodies for PSKH1 were not available. This inhibited efforts to evaluate co-localisation of PSKH1 and RCN1 in cells by immunocytochemistry (ICC). Furthermore, we recently discovered that energy (glucose) stress stimulates PSKH1-FLAG activity, corroborating our reports that PSKH1 drives prostate cancer cell growth during nutrient stress (Figures 3.19 and 4.2). We hypothesised that energy stress may modulate the acylation status of the N-terminal membrane targeting motif and thus the subcellular distribution of PSKH1. As previously stated, PSKH1 can localise to various internal compartments, a process dependent on myristoylation/palmitoylation of N-terminal glycine/cysteine residues [141]. It would be interesting to evaluate whether glucose stress prompts PSKH1 translocation to the PM/GA by transient expression of PSKH1-FLAG constructs and subsequent subcellular fractionation experiments. Furthermore, is PSKH1 localised to the endoplasmic reticulum under basal (unstimulated) conditions (which would theoretically bring PSKH1 in proximity to its *in vitro* inhibitor, RCN1/3)? Future studies should evaluate these considerations.

## 5.5. PSKH1 – between a ROCK and a hard place

Preliminary data indicates that the small molecule ATP analogue, compound 2, stems prostate cancer cell growth *in vitro* by, presumably, inhibiting PSKH1 (Figure 4.5). Compound 2 is conventionally marketed as a selective Rho-kinase (ROCK) inhibitor. The ROCK kinases comprise two, very large (160 kDa) isozymes (ROCK1 and ROCK2) with overlapping substrate profiles. They are characterised by an N-terminal AGC kinase domain buttressed by variable N- and C-termini (Figure 5.2). Like PSKH1, ROCK oligomerises, which is essential for its catalytic activity. An interlocked helical bundle (dark blue, Figure 5.3) formed by conjoined, leucine-rich N-terminal extensions of opposing ROCK monomers facilitates dimerisation [284, 285]. A hydrophobic motif (HM), common to most AGC kinases, immediately C-terminal to the catalytic domain makes contacts with the N-terminal bundle, which stabilises the ROCK oligomer [286]. In RSK1, the hydrophobic motif contains an integral phosphorylation site (Ser380) which, on addition of a phosphate moiety, provides a platform for PDK1 docking and subsequent activation of the N-terminal CaM-kinase domain [262]. In contrast, the corresponding residue in ROCK2 (Thr414) is not phosphorylated, and enhances ROCK dimerisation by participating in polar interactions with Asp39 of the N-terminal extension [286]. The catalytic module precedes a lengthy C-terminal extension containing a coiled-coil domain and C-terminal Rho-binding and pleckstrin homology domains (RBD and PH, respectively). Dual PH domains enable stable interaction of the ROCK oligomer at internal membranes, where it binds its primary activator, the small GTPase RhoA [287]. RhoA binding activates ROCK by sterically displacing the C-terminal tail (comprising the RBD and PH) from the active site, which is autoinhibitory in nature [288]. As a *bona fide* Rho-effector, ROCK is highly implicated in cell motility and proliferation programs, including stress fibre and focal adhesion assembly, actin-cytoskeletal remodelling, and cell detachment [288-290]. Fascinatingly, many of ROCK's effectors (or predicted interactors by

computational modelling) were highly enriched in our PSKH1 proteomic screen by proximity labelling and mass spectrometry (Figure 5.2). This includes the lipid kinase PIKFYVE, the phosphatase inhibitor protein PPP1R(16B), RSK1, and BRCA2. RSK1 is a potential downstream effector of PSKH1 signalling (Figures 4.7-4.9). Interestingly, ROCK2 ablation by siRNA knockdown attenuates RSK1-Ser380 phosphorylation in C2C12 cells [291]. These data may be entirely coincidental but given the dual inhibitory effects of compound 2 on ROCK and PSKH1 activity, it is likely that their catalytic architectures, whilst distantly related, share structural characteristics. At minimum, the ATP clefts of ROCK and PSKH1 are clearly similar, as both can accommodate the small molecule ATP analogue compound 2. This similarity may also extend to local tertiary structure, including the closely associated substrate binding groove. Thus, this may putatively explain the overlapping substrate/proteomic profiles of ROCK and PSKH1. Furthermore, both kinases are membrane associated and homodimerise [38, 141, 284, 285, 287]. The oligomeric arrangement of ROCK is such that the kinase domains of both monomers face the same plane [284, 285]. Some authors speculate that this dimeric arrangement may participate in substrate recognition [285]. At present, it is not clear whether monomeric or dimeric PSKH1 (or both) phosphorylates its downstream effectors. Nonetheless, insights into PSKH1 function may be gleaned from examining ROCK1/2's structural characteristics.
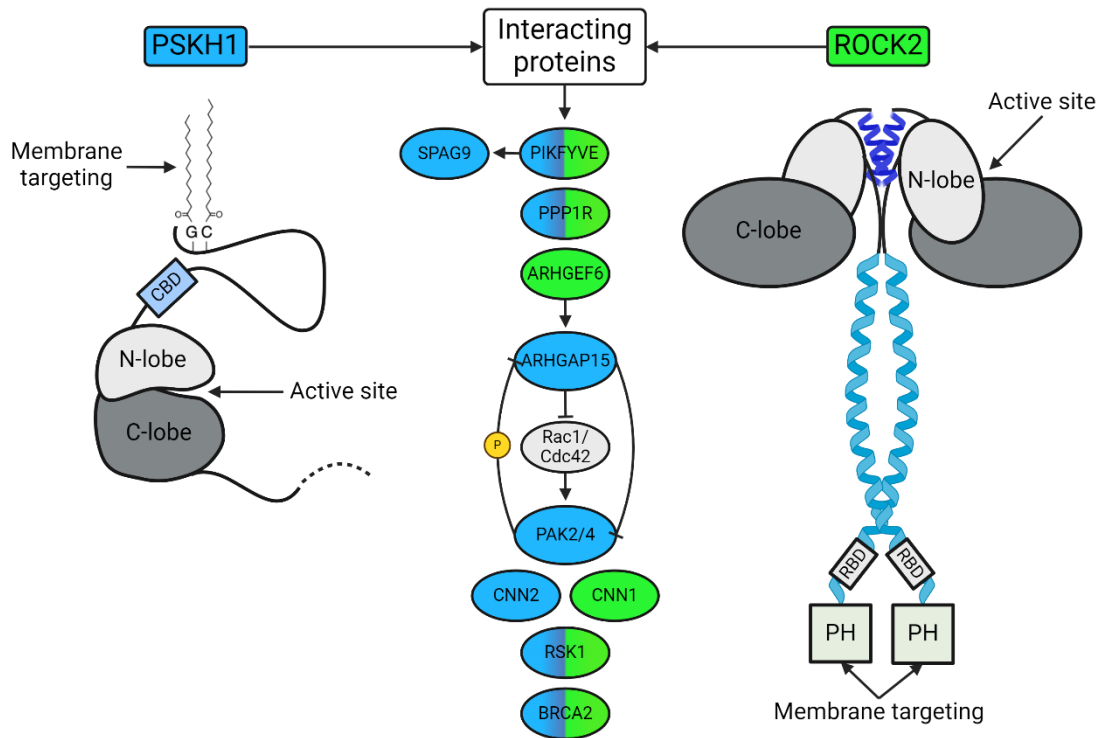
***Figure 5.2. PSKH1 and ROCK2 exhibit overlapping proteomes, dimerise and are membrane-associated.*** Intriguingly, many of ROCK's downstream effectors (or predicted protein interactors by computational modelling – see Giansanti, Stokes [292]) were highly enriched and represented in our PSKH1-TurboID proteomic screen by proximity labelling/MS. This includes, but is not limited to, the lipid kinase PIKFYVE, PPP1R, RSK1 and BRCA2. SPAG9 is a direct effector of PIKFYVE signalling and was also enriched in our PSKH1 proteomic screen. RSK1 is a potential downstream substrate of PSKH1 (Ser380). Interestingly, ROCK2 ablation by siRNA knockdown abrogates RSK1-Ser380 phosphorylation *in vitro*. The calmodulin-binding protein calponin-1 (CNN1) is directly phosphorylated by ROCK at Thr184 [293]. The closely related isozyme CNN2 was highly enriched in our PSKH1 proteomic screen. Furthermore, both kinases are membrane associated and dimerise *in vitro* [38, 141, 284, 285, 287]. ROCK kinase schematic adapted from Yamaguchi, Kasa [284]. Colouring is as follows: blue: PSKH1-interacting; green: ROCK2-interacting; blue/green: dual interacting. Kinase domains are coloured grey (light grey: N-lobe; dark grey: C-lobe). Abbreviations: CBD: calmodulin-binding domain; RBD: Rho-binding domain; PH: pleckstrin homology (domain). Dashed lines indicate the C-terminal tail of PSKH1, which was omitted for clarity. Created with BioRender.com.

## 5.6. PSKH1 and contact inhibition locomotion

A peculiar observation made during our prostate cancer studies was that PSKH1-KO cells exhibit undisturbed cell growth at high confluency (Figure 4.1). In contrast, proliferation of PSKH1-WT cells consistently tapered off. This bifurcation in cell growth, distinct from the phenotype observed under no glucose conditions, was repeatedly observed in separate, independent experiments (Figure 4.2, 12mM glucose + 10% FBS). These data suggest that PSKH1 may participate in programs that prevent unfettered cellular expansion when space is limited. Indeed, PSKH1-KO LNCaP cells exhibit a clustered morphology and continue to proliferate at high confluency (T60) despite evident spatial constraints (Figure 4.1). This behaviour is distinct from healthy cells, which preferentially proliferate as a uniform monolayer by re-orienting their migratory trajectory upon cell-to-cell contact (i.e. contact inhibition locomotion) [294]. Contact inhibition is highly complex, but typically involves mechanotransduction cues signalled by components of the extracellular matrix (ECM), including glycoproteins (e.g. laminin) that ligand transmembrane cellular adhesion molecules (CAMs) or activation of the non-canonical Wnt-Frizzled planar cell polarity (PCP) signalling pathway [295, 296]. CAMs (i.e. integrin) regulate the action of the small GTPases Rac1, Cdc42, and RhoA, previously described [296]. Rac1 and Cdc42 promote F-actin polymerisation at the leading edge (lamellipodium) of migrating cells, forming membranous protrusions (filopodia) that propel the cell forward (Figure 5.3) [297, 298]. The direction of lamellipodium/filopodium formation is driven by hapto- and chemotactic stimuli, including components of the ECM and growth factors (e.g. PDGF), which activate Rac1/Cdc42. Rac1/Cdc42 co-localised at the leading edge of migrating cells activate and/or localise p21-activated kinase (PAK) family members to the plasma membrane, which phosphorylate the LIM domain kinase 1 (LIMK1) [299, 300]. LIMK1 inactivates cofilin, a negative regulator of F-actin polymerisation, thereby supporting cell propulsion [301]. Upon cell-to-cell contact,

Rac1/Cdc42 activity is sequestered in favour of RhoA/ROCK signalling, prompting a collapse of membrane ruffling and re-polarisation of the protruding face to the trailing edge of the migrating cell [302]. Interestingly, a variety of proteins implicated in cell motility were highly enriched in our PSKH1-TurboID proximity label proteomic screen (Figure 5.3). This includes PAK2 (represented) and PAK4 (highly enriched), ARHGAP15, CAP/Ponsin (henceforth, SORBS1) and CD2AP. As previously discussed, PAK family members promote F-actin polymerisation (and thus cell movement in the direction of the leading edge of the migrating cell) by regulating the LIMK1/Cofilin signalling pathway [299-301]. Interestingly, SORBS1 has been reported to inhibit the activity of the PAK pathway in REF52 cells [303]. Transient siRNA knockdown of SORBS1 lead to enhanced migration and activation of PAK signalling [303]. SORBS1 is a large (143 kDa) adaptor protein comprising several SH3 domains [304]. PSKH1 harbours a putative SH3 domain-binding domain (PxxP) in its N-terminus (Figure 1.7) [38]. Interestingly, according to Scansite 4.0, this motif is a *bona fide* SORBS1 binding domain [305]. PAK4 also harbours a putative SH3 domain-binding motif N-terminal to its catalytic domain [306]. This proline-rich region is purported to be autoinhibitory in nature, with Src-SH3 (but not β-PIX-SH3) alleviating autoinhibition of kinase activity [306]. It is possible that PSKH1 may mediate SORBS1 inhibition of PAK4 by co-localising SORBS1/PAK4 via its PxxP/SORBS1-binding domain. It is unlikely that PSKH1 directly regulates PAK4's catalytic architecture, as PAK4 is constitutively phosphorylated on its activation loop at Ser474 [307]. PSKH1 may also regulate the action of ARHGAP15, which has been shown to indirectly inhibit PAK(2) by abrogating Rac1/Cdc42 activity, or by directly binding PAK2 [308]. PAK phosphorylation of PSKH1 is currently unclear. Initial experiments indicated PAK1 might phosphorylate PSKH1's activation loop (Supplementary Figure 3.5.4). For example, a phosphorylated band (pThr) appeared after incubating PSKH1-FLAG with recombinant PAK1 *in vitro*. This band was noticeably absent in an activation loop point mutant of PSKH1

(PSKH1-FLAG-T256A). However, there was no corresponding band shift in the FLAG-reactive band (indicative of PSKH1 phosphorylation), which muddied these results. Furthermore, phosphate incorporation was comparatively slow (30 minutes) (Supplementary Figure 3.5.4). Indeed, PAK1 phosphorylation of PSKH1 was not able to be reproduced (Figure 3.6). However, these data do not preclude PAK2/4 phosphorylation of PSKH1, which were highly enriched in our PSKH1 proteomic screen. Thus, another possibility is such that PAK2/4 may phosphorylate PSKH1, causing reciprocal inhibition of PAK activity (ergo, a negative feedback loop). These considerations support a model where PSKH1 ablation (PSKH1-KO LNCaP cells) promotes cell clustering and overgrowth via increased PAK activity.

## 5.7. Thesis conclusion

This thesis sought to address fundamental gaps in our understanding of PSKH1 regulation and function. Utilising a diverse array of lab-based and bioinformatic techniques, we described, for the first time, a precise function for PSKH1. Further, new insights were gleaned on the regulatory inputs that modulate PSKH1 activity. It is hoped that the findings encapsulated within this thesis will provide a platform for future studies to holistically characterise the complex and, until now, elusive features of PSKH1 function, regulation and activity.
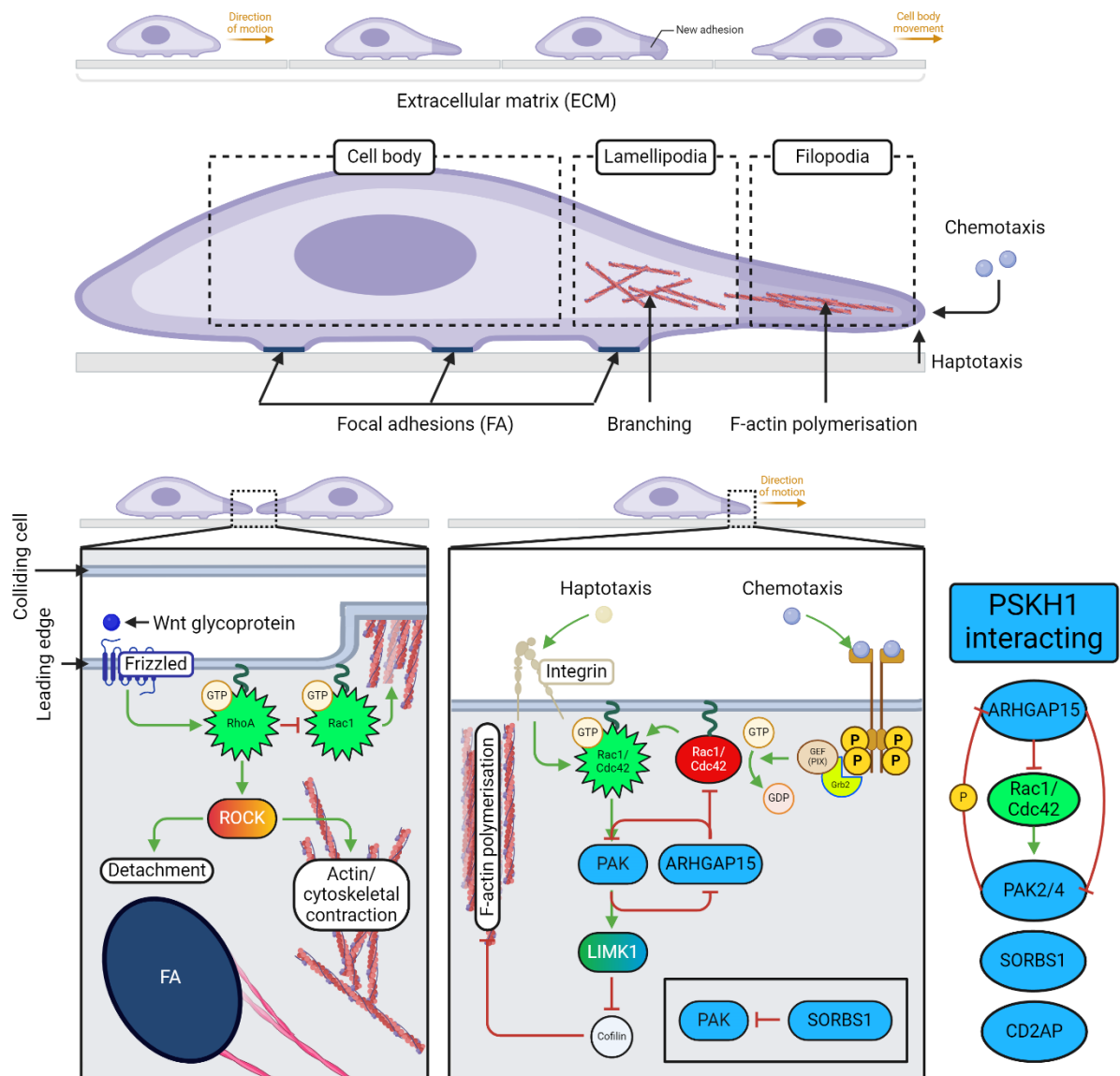
***Figure 5.3. PSKH1 may regulate cell motility programs through modulation of components implicated in Rho/Rac/Cdc42 signalling.*** Cells migrate by dynamically altering the actin/cytoskeletal network. Chemo- and haptotactic stimuli activate the small GTPases RhoA, Rac1 and Cdc42. Rac1/Cdc42, co-localised at the leading edge (lamellipodium) of migrating cells, stimulate F-actin polymerisation by regulating the activity of PAK/LIMK1/cofilin, prompting formation of adhesive protrusions (filopodia) that propel the cell forward. Conversely, RhoA/ROCK signalling impairs F-actin assembly by inhibiting the action of Rac1. ROCK is also implicated in focal adhesion detachment and contraction of the actin/cytoskeletal network, which facilitates cell movement. Interestingly, many components of this highly complex regulatory pathway were identified as PSKH1-interacting in our PSKH1-TurboID proximity label proteomic screen, including PAK2/4, ARHGAP15, SORBS1 and CD2AP. Created with BioRender.com.

References

1. Manning, G., et al., *The protein kinase complement of the human genome.* Science, 2002. **298**(5600): p. 1912-34.
2. Fischer, E.H. and E.G. Krebs, *Conversion of phosphorylase b to phosphorylase a in muscle extracts.* J Biol Chem, 1955. **216**(1): p. 121-32.
3. Krebs, E.G. and E.H. Fischer, *The phosphorylase b to a converting enzyme of rabbit skeletal muscle.* Biochim Biophys Acta, 1956. **20**(1): p. 150-7.
4. Cohen, P., *The subunit structure of rabbit-skeletal-muscle phosphorylase kinase, and the molecular basis of its activation reactions.* Eur J Biochem, 1973. **34**(1): p. 1-14.
5. Han, H.S., et al., *Regulation of glucose metabolism from a liver-centric perspective.* Exp Mol Med, 2016. **48**(3): p. e218.
6. Whitworth, H., et al., *Identification of kinases regulating prostate cancer cell growth using an RNAi phenotypic screen.* PloS one, 2012. **7**(6): p. e38950.
7. Galvan, L., et al., *The striatal kinase DCLK3 produces neuroprotection against mutant huntingtin.* Brain, 2018. **141**(5): p. 1434-1454.
8. Essegian, D., et al., *The Clinical Kinase Index: A Method to Prioritize Understudied Kinases as Drug Targets for the Treatment of Cancer.* Cell Rep Med, 2020. **1**(7): p. 100128.
9. Berginski, M.E., et al., *The Dark Kinase Knowledgebase: an online compendium of knowledge and experimental results of understudied kinases.* Nucleic Acids Res, 2021. **49**(D1): p. D529-D535.
10. Metz, K.S., et al., *Coral: Clear and Customizable Visualization of Human Kinome Data.* Cell Syst, 2018. **7**(3): p. 347-350 e1.
11. Tokumitsu, H., et al., *Activation mechanisms for Ca2+/calmodulin-dependent protein kinase IV. Identification of a brain CaM-kinase IV kinase.* J Biol Chem, 1994. **269**(46): p. 28640-7.
12. Okuno, S., T. Kitani, and H. Fujisawa, *Evidence for the existence of Ca2+/calmodulin-dependent protein kinase IV kinase isoforms in rat brain.* J Biochem, 1996. **119**(6): p. 1176-81.
13. Tokumitsu, H., et al., *Calcium/calmodulin-dependent protein kinase kinase: identification of regulatory domains.* Biochemistry, 1997. **36**(42): p. 12823-7.
14. Osawa, M., et al., *A novel target recognition revealed by calmodulin in complex with Ca2+-calmodulin-dependent kinase kinase.* Nat Struct Biol, 1999. **6**(9): p. 819-24.
15. Okuno, S., T. Kitani, and H. Fujisawa, *Regulation of Ca(2+)/calmodulin-dependent protein kinase kinase alpha by cAMP-dependent protein kinase: I. Biochemical analysis.* J Biochem, 2001. **130**(4): p. 503-13.
16. Lee, J.C. and A.M. Edelman, *A protein activator of Ca(2+)-calmodulin-dependent protein kinase Ia.* J Biol Chem, 1994. **269**(3): p. 2158-64.
17. Haribabu, B., et al., *Human calcium-calmodulin dependent protein kinase I: cDNA cloning, domain structure and activation by phosphorylation at threonine-177 by calcium-calmodulin dependent protein kinase I kinase.* EMBO J, 1995. **14**(15): p. 3679-86.
18. Selbert, M.A., et al., *Phosphorylation and activation of Ca(2+)-calmodulin-dependent protein kinase IV by Ca(2+)-calmodulin-dependent protein kinase Ia kinase.*

*Phosphorylation of threonine 196 is essential for activation.* J Biol Chem, 1995. **270**(29): p. 17616-21.

19.    Kitani, T., S. Okuno, and H. Fujisawa, *Molecular cloning of Ca2+/calmodulin-dependent protein kinase kinase beta.* J Biochem, 1997. **122**(1): p. 243-50.

20.    Anderson, K.A., et al., *Components of a calmodulin-dependent protein kinase cascade. Molecular cloning, functional characterization and cellular localization of Ca2+/calmodulin-dependent protein kinase kinase beta.* J Biol Chem, 1998. **273**(48): p. 31880-9.

21.    Scott, J.W., et al., *Autophosphorylation of CaMKK2 generates autonomous activity that is disrupted by a T85S mutation linked to anxiety and bipolar disorder.* Sci Rep, 2015. **5**: p. 14436.

22.    Green, M.F., et al., *Ca2+/Calmodulin-dependent protein kinase kinase beta is regulated by multisite phosphorylation.* J Biol Chem, 2011. **286**(32): p. 28066-79.

23.    Langendorf, C.G., et al., *CaMKK2 is inactivated by cAMP-PKA signaling and 14-3-3 adaptor proteins.* J Biol Chem, 2020. **295**(48): p. 16239-16250.

24.    Tokumitsu, H., H. Enslen, and T.R. Soderling, *Characterization of a Ca2+/calmodulin-dependent protein kinase cascade. Molecular cloning and expression of calcium/calmodulin-dependent protein kinase kinase.* J Biol Chem, 1995. **270**(33): p. 19320-4.

25.    Okuno, S. and H. Fujisawa, *Requirement of brain extract for the activity of brain calmodulin-dependent protein kinase IV expressed in Escherichia coli.* J Biochem, 1993. **114**(2): p. 167-70.

26.    Okuno, S., T. Kitani, and H. Fujisawa, *Purification and characterization of Ca2+/calmodulin-dependent protein kinase IV kinase from rat brain.* J Biochem, 1994. **116**(4): p. 923-30.

27.    Hurley, R.L., et al., *The Ca2+/calmodulin-dependent protein kinase kinases are AMP-activated protein kinase kinases.* J Biol Chem, 2005. **280**(32): p. 29060-6.

28.    Gocher, A.M., et al., *Akt activation by Ca(2+)/calmodulin-dependent protein kinase kinase 2 (CaMKK2) in ovarian cancer cells.* J Biol Chem, 2017. **292**(34): p. 14188-14204.

29.    Fujimoto, T., et al., *Identification of a novel CaMKK substrate.* Biochem Biophys Res Commun, 2011. **410**(1): p. 45-51.

30.    Wen, L., et al., *Ca2+/calmodulin-dependent protein kinase kinase beta phosphorylation of Sirtuin 1 in endothelium is atheroprotective.* Proc Natl Acad Sci U S A, 2013. **110**(26): p. E2420-7.

31.    Stork, B.A., et al., *Calcium/calmodulin-dependent protein kinase kinase 2 regulates hepatic fuel metabolism.* Mol Metab, 2022. **62**: p. 101513.

32.    Nairn, A.C. and P. Greengard, *Purification and characterization of Ca2+/calmodulin-dependent protein kinase I from bovine brain.* J Biol Chem, 1987. **262**(15): p. 7273-81.

33.    Takemoto-Kimura, S., et al., *Molecular cloning and characterization of CLICK-III/CaMKIgamma, a novel membrane-anchored neuronal Ca2+/calmodulin-dependent protein kinase (CaMK).* J Biol Chem, 2003. **278**(20): p. 18597-605.

34.    Ishikawa, Y., et al., *Identification and characterization of novel components of a Ca2+/calmodulin-dependent protein kinase cascade in HeLa cells.* FEBS Lett, 2003. **550**(1-3): p. 57-63.

35.    Verploegen, S., et al., *Identification and characterization of CKLiK, a novel granulocyte Ca(++)/calmodulin-dependent kinase.* Blood, 2000. **96**(9): p. 3215-23.

36.     Ohmae, S., et al., *Molecular identification and characterization of a family of kinases with homology to Ca2+/calmodulin-dependent protein kinases I/IV.* J Biol Chem, 2006. **281**(29): p. 20427-39.

37.     Varjosalo, M., et al., *The protein interaction landscape of the human CMGC kinase group.* Cell Rep, 2013. **3**(4): p. 1306-20.

38.     Brede, G., et al., *Characterization of PSKH1, a novel human protein serine kinase with centrosomal, golgi, and nuclear localization.* Genomics, 2000. **70**(1): p. 82-92.

39.     Inoue, E., et al., *SAD: a presynaptic kinase associated with synaptic vesicles and the active zone cytomatrix that regulates neurotransmitter release.* Neuron, 2006. **50**(2): p. 261-75.

40.     Rodriguez-Asiain, A., et al., *Brain specific kinase-1 BRSK1/SAD-B associates with lipid rafts: modulation of kinase activity by lipid environment.* Biochim Biophys Acta, 2011. **1811**(12): p. 1124-35.

41.     Lizcano, J.M., et al., *LKB1 is a master kinase that activates 13 kinases of the AMPK subfamily, including MARK/PAR-1.* EMBO J, 2004. **23**(4): p. 833-43.

42.     Fujimoto, T., et al., *Activation of SAD kinase by Ca2+/calmodulin-dependent protein kinase kinase.* Biochemistry, 2008. **47**(13): p. 4151-9.

43.     Mochida, S., et al., *SAD-B Phosphorylation of CAST Controls Active Zone Vesicle Recycling for Synaptic Depression.* Cell Rep, 2016. **16**(11): p. 2901-2913.

44.     Yoshida, H. and M. Goedert, *Phosphorylation of microtubule-associated protein tau by AMPK-related kinases.* J Neurochem, 2012. **120**(1): p. 165-76.

45.     Bright, N.J., D. Carling, and C. Thornton, *Investigating the regulation of brain-specific kinases 1 and 2 by phosphorylation.* J Biol Chem, 2008. **283**(22): p. 14946-54.

46.     Guo, Z., et al., *BRSK2 is activated by cyclic AMP-dependent protein kinase A through phosphorylation at Thr260.* Biochem Biophys Res Commun, 2006. **347**(4): p. 867-71.

47.     Lu, R., H. Niida, and M. Nakanishi, *Human SAD1 kinase is involved in UV-induced DNA damage checkpoint function.* J Biol Chem, 2004. **279**(30): p. 31164-70.

48.     Nie, J., et al., *Synapses of amphids defective (SAD-A) kinase promotes glucose-stimulated insulin secretion through activation of p21-activated kinase (PAK1) in pancreatic beta-Cells.* J Biol Chem, 2012. **287**(31): p. 26435-44.

49.     Kishi, M., et al., *Mammalian SAD kinases are required for neuronal polarization.* Science, 2005. **307**(5711): p. 929-32.

50.     Saiyin, H., et al., *BRSK2 induced by nutrient deprivation promotes Akt activity in pancreatic cancer via downregulation of mTOR activity.* Oncotarget, 2017. **8**(27): p. 44669-44681.

51.     Lefebvre, D.L., et al., *Identification and characterization of a novel sucrose-non-fermenting protein kinase/AMP-activated protein kinase-related protein kinase, SNARK.* Biochem J, 2001. **355**(Pt 2): p. 297-305.

52.     Lefebvre, D.L. and C.F. Rosen, *Regulation of SNARK activity in response to cellular stresses.* Biochim Biophys Acta, 2005. **1724**(1-2): p. 71-85.

53.     Kuga, W., et al., *Nuclear localization of SNARK; its impact on gene expression.* Biochem Biophys Res Commun, 2008. **377**(4): p. 1062-6.

54.     Gill, M.K., et al., *A feed forward loop enforces YAP/TAZ signaling during tumorigenesis.* Nat Commun, 2018. **9**(1): p. 3510.

55.     Yamamoto, H., et al., *Identification of a novel substrate for TNFalpha-induced kinase NUAK2.* Biochem Biophys Res Commun, 2008. **365**(3): p. 541-7.

56.	Jaleel, M., et al., *Identification of the sucrose non-fermenting related kinase SNRK, as a novel LKB1 substrate.* FEBS Lett, 2005. **579**(6): p. 1417-23.

57.	Faber, S., et al., *PDE6D Mediates Trafficking of Prenylated Proteins NIM1K and UBL3 to Primary Cilia.* Cells, 2023. **12**(2).

58.	Bielke, W., et al., *Characterization of a novel murine testis-specific serine/threonine kinase.* Gene, 1994. **139**(2): p. 235-9.

59.	Kueng, P., et al., *A novel family of serine/threonine kinases participating in spermiogenesis.* J Cell Biol, 1997. **139**(7): p. 1851-9.

60.	Hao, Z., et al., *Expression analysis of the human testis-specific serine/threonine kinase (TSSK) homologues. A TSSK member is present in the equatorial segment of human sperm.* Mol Hum Reprod, 2004. **10**(6): p. 433-44.

61.	Li, Y., et al., *Expression and localization of five members of the testis-specific serine kinase (Tssk) family in mouse and human sperm and testis.* Mol Hum Reprod, 2011. **17**(1): p. 42-56.

62.	Shang, P., et al., *Functional transformation of the chromatoid body in mouse spermatids requires testis-specific serine/threonine kinases.* J Cell Sci, 2010. **123**(Pt 3): p. 331-9.

63.	Visconti, P.E., et al., *Cloning and chromosomal localization of a gene encoding a novel serine/threonine kinase belonging to the subfamily of testis-specific kinases.* Genomics, 2001. **77**(3): p. 163-70.

64.	Zuercher, G., et al., *A novel member of the testis specific serine kinase family, tssk-3, expressed in the Leydig cells of sexually mature mice.* Mech Dev, 2000. **93**(1-2): p. 175-7.

65.	Bucko-Justyna, M., et al., *Characterization of testis-specific serine-threonine kinase 3 and its activation by phosphoinositide-dependent kinase-1-dependent signalling.* FEBS J, 2005. **272**(24): p. 6310-23.

66.	Chen, X., et al., *TSSK5, a novel member of the testis-specific serine/threonine kinase family, phosphorylates CREB at Ser-133, and stimulates the CRE/CREB responsive pathway.* Biochem Biophys Res Commun, 2005. **333**(3): p. 742-9.

67.	Wei, Y., et al., *Testis specific serine/threonine kinase 4 (Tssk4) maintains its kinase activity by phosphorylating itself at Thr-197.* Mol Biol Rep, 2013. **40**(1): p. 439-47.

68.	Wang, X., et al., *Tssk4 is essential for maintaining the structural integrity of sperm flagellum.* Mol Hum Reprod, 2015. **21**(2): p. 136-45.

69.	Wang, X., et al., *Testis-specific serine/threonine protein kinase 4 (Tssk4) phosphorylates Odf2 at Ser-76.* Sci Rep, 2016. **6**: p. 22861.

70.	Spiridonov, N.A., et al., *Identification and characterization of SSTK, a serine/threonine protein kinase essential for male fertility.* Mol Cell Biol, 2005. **25**(10): p. 4250-61.

71.	Waskiewicz, A.J., et al., *Phosphorylation of the cap-binding protein eukaryotic translation initiation factor 4E by protein kinase Mnk1 in vivo.* Mol Cell Biol, 1999. **19**(3): p. 1871-80.

72.	Parra-Palau, J.L., et al., *Features in the N and C termini of the MAPK-interacting kinase Mnk1 mediate its nucleocytoplasmic shuttling.* J Biol Chem, 2003. **278**(45): p. 44197-204.

73.	Fukunaga, R. and T. Hunter, *MNK1, a new MAP kinase-activated protein kinase, isolated by a novel expression screening method for identifying protein kinase substrates.* EMBO J, 1997. **16**(8): p. 1921-33.

74. Waskiewicz, A.J., et al., *Mitogen-activated protein kinases activate the serine/threonine kinases Mnk1 and Mnk2.* EMBO J, 1997. **16**(8): p. 1909-20.

75. Scheper, G.C., et al., *The N and C termini of the splice variants of the human mitogen-activated protein kinase-interacting kinase Mnk2 determine activity and localization.* Mol Cell Biol, 2003. **23**(16): p. 5692-705.

76. Scheper, G.C., et al., *The mitogen-activated protein kinase signal-integrating kinase Mnk2 is a eukaryotic initiation factor 4E kinase with high levels of basal activity in mammalian cells.* Mol Cell Biol, 2001. **21**(3): p. 743-54.

77. Hu, L.Y. and A. Kontrogianni-Konstantopoulos, *The kinase domains of obscurin interact with intercellular adhesion proteins.* FASEB J, 2013. **27**(5): p. 2001-12.

78. Borisov, A.B., M.O. Raeker, and M.W. Russell, *Developmental expression and differential cellular localization of obscurin and obscurin-associated kinase in cardiac muscle cells.* J Cell Biochem, 2008. **103**(5): p. 1621-35.

79. Fukuzawa, A., S. Idowu, and M. Gautel, *Complete human gene structure of obscurin: implications for isoform generation by differential splicing.* J Muscle Res Cell Motil, 2005. **26**(6-8): p. 427-34.

80. Fleming, J.R., et al., *Exploring Obscurin and SPEG Kinase Biology.* J Clin Med, 2021. **10**(5).

81. Marcelo, K.L., A.R. Means, and B. York, *The Ca(2+)/Calmodulin/CaMKK2 Axis: Nature's Metabolic CaMshaft.* Trends Endocrinol Metab, 2016. **27**(10): p. 706-718.

82. Tokumitsu, H., et al., *Differential regulatory mechanism of Ca2+/calmodulin-dependent protein kinase kinase isoforms.* Biochemistry, 2001. **40**(46): p. 13925-32.

83. Hsu, L.S., et al., *Human Ca2+/calmodulin-dependent protein kinase kinase beta gene encodes multiple isoforms that display distinct kinase activity.* J Biol Chem, 2001. **276**(33): p. 31113-23.

84. Wayman, G.A., H. Tokumitsu, and T.R. Soderling, *Inhibitory cross-talk by cAMP kinase on the calmodulin-dependent protein kinase cascade.* J Biol Chem, 1997. **272**(26): p. 16073-6.

85. Psenakova, K., et al., *14-3-3 protein directly interacts with the kinase domain of calcium/calmodulin-dependent protein kinase kinase (CaMKK2).* Biochim Biophys Acta Gen Subj, 2018. **1862**(7): p. 1612-1625.

86. Ikura, M., et al., *Solution structure of a calmodulin-target peptide complex by multidimensional NMR.* Science, 1992. **256**(5057): p. 632-8.

87. Meador, W.E., A.R. Means, and F.A. Quiocho, *Target enzyme recognition by calmodulin: 2.4 A structure of a calmodulin-peptide complex.* Science, 1992. **257**(5074): p. 1251-5.

88. Meador, W.E., A.R. Means, and F.A. Quiocho, *Modulation of calmodulin plasticity in molecular recognition on the basis of x-ray structures.* Science, 1993. **262**(5140): p. 1718-21.

89. Goldberg, J., A.C. Nairn, and J. Kuriyan, *Structural basis for the autoinhibition of calcium/calmodulin-dependent protein kinase I.* Cell, 1996. **84**(6): p. 875-87.

90. Kylarova, S., et al., *CaMKK2 kinase domain interacts with the autoinhibitory region through the N-terminal lobe including the RP insert.* Biochim Biophys Acta Gen Subj, 2018. **1862**(10): p. 2304-2313.

91. Tokumitsu, H., et al., *Substrate recognition by Ca2+/Calmodulin-dependent protein kinase kinase. Role of the arg-pro-rich insert domain.* J Biol Chem, 1999. **274**(22): p. 15803-10.

92.     Kaneshige, R., et al., *Substrate recognition by Arg/Pro-rich insert domain in calcium/calmodulin-dependent protein kinase kinase for target protein kinases.* FEBS J, 2022. **289**(19): p. 5971-5984.

93.     Knighton, D.R., et al., *Structure of a peptide inhibitor bound to the catalytic subunit of cyclic adenosine monophosphate-dependent protein kinase.* Science, 1991. **253**(5018): p. 414-20.

94.     Mirdita, M., et al., *ColabFold: making protein folding accessible to all.* Nat Methods, 2022. **19**(6): p. 679-682.

95.     Barden, N., et al., *Analysis of single nucleotide polymorphisms in genes in the chromosome 12Q24.31 region points to P2RX7 as a susceptibility gene to bipolar affective disorder.* Am J Med Genet B Neuropsychiatr Genet, 2006. **141B**(4): p. 374-82.

96.     Xy Ling, N., et al., *Functional analysis of an R311C variant of Ca(2+) -calmodulin-dependent protein kinase kinase-2 (CaMKK2) found as a de novo mutation in a patient with bipolar disorder.* Bipolar Disord, 2020. **22**(8): p. 841-848.

97.     Kataoka, M., et al., *Exome sequencing for bipolar disorder points to roles of de novo loss-of-function and protein-altering mutations.* Mol Psychiatry, 2016. **21**(7): p. 885-93.

98.     Nelson, M.R., et al., *An abundance of rare functional variants in 202 drug target genes sequenced in 14,002 people.* Science, 2012. **337**(6090): p. 100-4.

99.     Lin, F., et al., *The camKK2/camKIV relay is an essential regulator of hepatic cancer.* Hepatology, 2015. **62**(2): p. 505-20.

100.    Clark, V.E., et al., *Genomic analysis of non-NF2 meningiomas reveals mutations in TRAF7, KLF4, AKT1, and SMO.* Science, 2013. **339**(6123): p. 1077-80.

101.    O'Brien, M.T., et al., *Impact of Genetic Variation on Human CaMKK2 Regulation by Ca(2+)-Calmodulin and Multisite Phosphorylation.* Sci Rep, 2017. **7**: p. 43264.

102.    Frigo, D.E., et al., *CaM kinase kinase beta-mediated activation of the growth regulatory kinase AMPK is required for androgen-dependent migration of prostate cancer cells.* Cancer Res, 2011. **71**(2): p. 528-37.

103.    Massie, C.E., et al., *The androgen receptor fuels prostate cancer by regulating central metabolism and biosynthesis.* EMBO J, 2011. **30**(13): p. 2719-33.

104.    Karacosta, L.G., et al., *A regulatory feedback loop between Ca2+/calmodulin-dependent protein kinase kinase 2 (CaMKK2) and the androgen receptor in prostate cancer progression.* J Biol Chem, 2012. **287**(29): p. 24832-43.

105.    Kang, X., et al., *CAMKs support development of acute myeloid leukemia.* J Hematol Oncol, 2018. **11**(1): p. 30.

106.    Bergamaschi, A., et al., *CAMK1D amplification implicated in epithelial-mesenchymal transition in basal-like breast cancer.* Mol Oncol, 2008. **2**(4): p. 327-39.

107.    Jin, Q., et al., *CAMK1D Inhibits Glioma Through the PI3K/AKT/mTOR Signaling Pathway.* Front Oncol, 2022. **12**: p. 845036.

108.    Mullins, N., et al., *Genome-wide association study of more than 40,000 bipolar disorder cases provides new insights into the underlying biology.* Nat Genet, 2021. **53**(6): p. 817-829.

109.    Liu, N.Q., et al., *The non-coding variant rs1800734 enhances DCLK3 expression through long-range interaction and promotes colorectal cancer progression.* Nat Commun, 2017. **8**: p. 14418.

110. Langfelder, P., et al., *Integrated genomics and proteomics define huntingtin CAG length-dependent networks in mice.* Nat Neurosci, 2016. **19**(4): p. 623-33.

111. Wu, F., et al., *Genome-wide gene expression differences in Crohn's disease and ulcerative colitis from endoscopic pinch biopsies: insights into distinctive pathogenesis.* Inflamm Bowel Dis, 2007. **13**(7): p. 807-21.

112. Zhang, Y., et al., *MiR-566 mediates cell migration and invasion in colon cancer cells by direct targeting of PSKH1.* Cancer Cell Int, 2019. **19**: p. 333.

113. Zhu, X., et al., *PSKH1 affects proliferation and invasion of osteosarcoma cells via the p38/MAPK signaling pathway.* Oncol Lett, 2023. **25**(4): p. 144.

114. Wang, H., et al., *Decreased expression and prognostic role of cytoplasmic BRSK1 in human breast carcinoma: correlation with Jab1 stability and PI3K/Akt pathway.* Exp Mol Pathol, 2014. **97**(2): p. 191-201.

115. Hu, Y., et al., *Case report: A novel frameshift mutation in BRSK2 causes autism in a 16-year old Chinese boy.* Front Psychiatry, 2023. **14**: p. 1205204.

116. Hiatt, S.M., et al., *Deleterious Variation in BRSK2 Associates with a Neurodevelopmental Disorder.* Am J Hum Genet, 2019. **104**(4): p. 701-708.

117. Bonnard, C., et al., *A loss-of-function NUAK2 mutation in humans causes anencephaly due to impaired Hippo-YAP signaling.* J Exp Med, 2020. **217**(12).

118. Yuan, W.C., et al., *NUAK2 is a critical YAP target in liver cancer.* Nat Commun, 2018. **9**(1): p. 4834.

119. Namiki, T., et al., *AMP kinase-related kinase NUAK2 affects tumor growth, migration, and clinical outcome of human melanoma.* Proc Natl Acad Sci U S A, 2011. **108**(16): p. 6597-602.

120. Namiki, T., et al., *NUAK2 Amplification Coupled with PTEN Deficiency Promotes Melanoma Development via CDK Activation.* Cancer Res, 2015. **75**(13): p. 2708-15.

121. Fu, W., et al., *NUAK family kinase 2 is a novel therapeutic target for prostate cancer.* Mol Carcinog, 2022. **61**(3): p. 334-345.

122. Delgado, M., et al., *Testis Specific Serine Kinase 6 (TSSK6) is abnormally expressed in colorectal cancer and promotes oncogenic behaviors.* J Biol Chem, 2024: p. 107380.

123. Zhan, Y., et al., *MNK1/2 inhibition limits oncogenicity and metastasis of KIT-mutant melanoma.* J Clin Invest, 2017. **127**(11): p. 4179-4192.

124. Chrestensen, C.A., et al., *MNK1 and MNK2 regulation in HER2-overexpressing breast cancer lines.* J Biol Chem, 2007. **282**(7): p. 4243-4252.

125. Arimura, T., et al., *Structural analysis of obscurin gene in hypertrophic cardiomyopathy.* Biochem Biophys Res Commun, 2007. **362**(2): p. 281-7.

126. Hu, L.R., et al., *Deregulated Ca(2+) cycling underlies the development of arrhythmia and heart disease due to mutant obscurin.* Sci Adv, 2017. **3**(6): p. e1603081.

127. Takemoto-Kimura, S., et al., *Calmodulin kinases: essential regulators in health and disease.* J Neurochem, 2017. **141**(6): p. 808-818.

128. Sugita, R., et al., *Ca2+/calmodulin-dependent protein kinase kinase cascade.* Biochem Biophys Res Commun, 1994. **203**(1): p. 694-701.

129. DeRemer, M.F., R.J. Saeli, and A.M. Edelman, *Ca(2+)-calmodulin-dependent protein kinases Ia and Ib from rat brain I. Identification, purification, and structural comparisons.* J Biol Chem, 1992. **267**(19): p. 13460-5.

130. Kennedy, M.B. and P. Greengard, *Two calcium/calmodulin-dependent protein kinases, which are highly concentrated in brain, phosphorylate protein I at distinct sites.* Proc Natl Acad Sci U S A, 1981. **78**(2): p. 1293-7.

131.    Yokokura, H., et al., *Isolation and comparison of rat cDNAs encoding Ca2+/calmodulin-dependent protein kinase I isoforms.* Biochim Biophys Acta, 1997. **1338**(1): p. 8-12.

132.    Picciotto, M.R., A.J. Czernik, and A.C. Nairn, *Calcium/calmodulin-dependent protein kinase I. cDNA cloning and identification of autophosphorylation site.* J Biol Chem, 1993. **268**(35): p. 26512-21.

133.    Picciotto, M.R., et al., *Immunochemical localization of calcium/calmodulin-dependent protein kinase I.* Synapse, 1995. **20**(1): p. 75-84.

134.    Takemoto-Kimura, S., et al., *Regulation of dendritogenesis via a lipid-raft-associated Ca2+/calmodulin-dependent protein kinase CLICK-III/CaMKIgamma.* Neuron, 2007. **54**(5): p. 755-70.

135.    Volpin, V., et al., *CAMK1D Triggers Immune Resistance of Human Tumor Cells Refractory to Anti-PD-L1 Treatment.* Cancer Immunol Res, 2020. **8**(9): p. 1163-1179.

136.    Burgess, H.A., S. Martinez, and O. Reiner, *KIAA0369, doublecortin-like kinase, is expressed during brain development.* J Neurosci Res, 1999. **58**(4): p. 567-75.

137.    Brochier, C., et al., *Quantitative gene expression profiling of mouse brain regions reveals differential transcripts conserved in human and affected in disease models.* Physiol Genomics, 2008. **33**(2): p. 170-9.

138.    Kaiser, J., et al., *CaMKK2 as an emerging treatment target for bipolar disorder.* Mol Psychiatry, 2023.

139.    Hanks, S.K., *Homology probing: identification of cDNA clones encoding members of the protein-serine kinase family.* Proc Natl Acad Sci U S A, 1987. **84**(2): p. 388-92.

140.    Brede, G., J. Solheim, and H. Prydz, *PSKH1, a novel splice factor compartment-associated serine kinase.* Nucleic Acids Res, 2002. **30**(23): p. 5301-9.

141.    Brede, G., et al., *Mutants of the protein serine kinase PSKH1 disassemble the Golgi apparatus.* Exp Cell Res, 2003. **291**(2): p. 299-312.

142.    Shrestha, S., et al., *Cataloguing the dead: breathing new life into pseudokinase research.* FEBS J, 2020. **287**(19): p. 4150-4169.

143.    Kim, S.T., et al., *Exploratory biomarker analysis for treatment response in KRAS wild type metastatic colorectal cancer patients who received cetuximab plus irinotecan.* BMC Cancer, 2015. **15**: p. 747.

144.    Crump, J.G., et al., *The SAD-1 kinase regulates presynaptic vesicle clustering and axon termination.* Neuron, 2001. **29**(1): p. 115-29.

145.    Hezel, A.F., et al., *Pancreatic LKB1 deletion leads to acinar polarity defects and cystic neoplasms.* Mol Cell Biol, 2008. **28**(7): p. 2414-25.

146.    Baas, A.F., et al., *Activation of the tumour suppressor kinase LKB1 by the STE20-like pseudokinase STRAD.* EMBO J, 2003. **22**(12): p. 3062-72.

147.    Hawley, S.A., et al., *Complexes between the LKB1 tumor suppressor, STRAD alpha/beta and MO25 alpha/beta are upstream kinases in the AMP-activated protein kinase cascade.* J Biol, 2003. **2**(4): p. 28.

148.    Zeqiraj, E., et al., *Structure of the LKB1-STRAD-MO25 complex reveals an allosteric mechanism of kinase activation.* Science, 2009. **326**(5960): p. 1707-11.

149.    Collins, S.P., et al., *LKB1, a novel serine/threonine protein kinase and potential tumour suppressor, is phosphorylated by cAMP-dependent protein kinase (PKA) and prenylated in vivo.* Biochem J, 2000. **345 Pt 3**(Pt 3): p. 673-80.

150.    Sapkota, G.P., et al., *Phosphorylation of the protein kinase mutated in Peutz-Jeghers cancer syndrome, LKB1/STK11, at Ser431 by p90(RSK) and cAMP-dependent protein*

*kinase, but not its farnesylation at Cys(433), is essential for LKB1 to suppress cell vrowth.* J Biol Chem, 2001. **276**(22): p. 19469-82.

151.     Barnes, A.P., et al., *LKB1 and SAD kinases define a pathway required for the polarization of cortical neurons.* Cell, 2007. **129**(3): p. 549-63.

152.     Fogarty, S. and D.G. Hardie, *C-terminal phosphorylation of LKB1 is not required for regulation of AMP-activated protein kinase, BRSK1, BRSK2, or cell cycle arrest.* J Biol Chem, 2009. **284**(1): p. 77-84.

153.     Matsushita, M. and A.C. Nairn, *Inhibition of the Ca2+/calmodulin-dependent protein kinase I cascade by cAMP-dependent protein kinase.* J Biol Chem, 1999. **274**(15): p. 10086-93.

154.     Jaleel, M., et al., *The ubiquitin-associated domain of AMPK-related kinases regulates conformation and LKB1-mediated phosphorylation and activation.* Biochem J, 2006. **394**(Pt 3): p. 545-55.

155.     Murphy, J.M., et al., *Conformational instability of the MARK3 UBA domain compromises ubiquitin recognition and promotes interaction with the adjacent kinase domain.* Proc Natl Acad Sci U S A, 2007. **104**(36): p. 14336-41.

156.     Wu, J.X., et al., *Structural insight into the mechanism of synergistic autoinhibition of SAD kinases.* Nat Commun, 2015. **6**: p. 8953.

157.     Bournet, B., et al., *Targeting KRAS for diagnosis, prognosis, and treatment of pancreatic cancer: Hopes and realities.* Eur J Cancer, 2016. **54**: p. 75-83.

158.     Zhao, B., et al., *TEAD mediates YAP-dependent gene induction and growth control.* Genes Dev, 2008. **22**(14): p. 1962-71.

159.     Dupont, S., et al., *Role of YAP/TAZ in mechanotransduction.* Nature, 2011. **474**(7350): p. 179-83.

160.     Wada, K., et al., *Hippo pathway regulation by cell morphology and stress fibers.* Development, 2011. **138**(18): p. 3907-14.

161.     Zhao, B., et al., *A coordinated phosphorylation by Lats and CK1 regulates YAP stability through SCF(beta-TRCP).* Genes Dev, 2010. **24**(1): p. 72-85.

162.     Liu, C.Y., et al., *The hippo tumor pathway promotes TAZ degradation by phosphorylating a phosphodegron and recruiting the SCFbeta-TrCP E3 ligase.* J Biol Chem, 2010. **285**(48): p. 37159-69.

163.     Koh, H.J., et al., *Sucrose nonfermenting AMPK-related kinase (SNARK) mediates contraction-stimulated glucose transport in mouse skeletal muscle.* Proc Natl Acad Sci U S A, 2010. **107**(35): p. 15541-6.

164.     Cheng, X., et al., *Clinical potential of the Hippo-YAP pathway in bladder cancer.* Front Oncol, 2022. **12**: p. 925278.

165.     Wu, L. and P. Russell, *Nim1 kinase promotes mitosis by inactivating Wee1 tyrosine kinase.* Nature, 1993. **363**(6431): p. 738-41.

166.     Russell, P. and P. Nurse, *The mitotic inducer nim1+ functions in a regulatory network of protein kinase homologs controlling the initiation of mitosis.* Cell, 1987. **49**(4): p. 569-76.

167.     Parker, L.L., et al., *Phosphorylation and inactivation of the mitotic inhibitor Wee1 by the nim1/cdr1 kinase.* Nature, 1993. **363**(6431): p. 736-8.

168.     Tang, Z., T.R. Coleman, and W.G. Dunphy, *Two distinct mechanisms for negative regulation of the Wee1 protein kinase.* EMBO J, 1993. **12**(9): p. 3427-36.

169.     Zhang, H., et al., *Photoreceptor cGMP phosphodiesterase delta subunit (PDEdelta) functions as a prenyl-binding protein.* J Biol Chem, 2004. **279**(1): p. 407-13.

170.  Tate, J.G., et al., *COSMIC: the Catalogue Of Somatic Mutations In Cancer.* Nucleic Acids Res, 2019. **47**(D1): p. D941-D947.

171.  Bielke, W., et al., *Expression of the B cell-associated tyrosine kinase gene Lyn in primary neuroblastoma tumours and its modulation during the differentiation of neuroblastoma cell lines.* Biochem Biophys Res Commun, 1992. **186**(3): p. 1403-9.

172.  Zhang, Z.D., et al., *Identification and analysis of unitary pseudogenes: historic and contemporary gene losses in humans and other primates.* Genome Biol, 2010. **11**(3): p. R26.

173.  Xu, B., et al., *Targeted deletion of Tssk1 and 2 causes male infertility due to haploinsufficiency.* Dev Biol, 2008. **319**(2): p. 211-22.

174.  Nayyab, S., et al., *TSSK3, a novel target for male contraception, is required for spermiogenesis.* Mol Reprod Dev, 2021. **88**(11): p. 718-730.

175.  Sosnik, J., et al., *Tssk6 is required for Izumo relocalization and gamete fusion in the mouse.* J Cell Sci, 2009. **122**(Pt 15): p. 2741-9.

176.  Salicioni, A.M., et al., *Testis-specific serine kinase protein family in male fertility and as targets for non-hormonal male contraceptiondagger.* Biol Reprod, 2020. **103**(2): p. 264-274.

177.  Proud, C.G., *Regulation of mammalian translation factors by nutrients.* Eur J Biochem, 2002. **269**(22): p. 5338-49.

178.  Topisirovic, I., M. Ruiz-Gutierrez, and K.L. Borden, *Phosphorylation of the eukaryotic translation initiation factor eIF4E contributes to its transformation and mRNA transport activities.* Cancer Res, 2004. **64**(23): p. 8639-42.

179.  Pyronnet, S., et al., *Human eukaryotic translation initiation factor 4G (eIF4G) recruits mnk1 to phosphorylate eIF4E.* EMBO J, 1999. **18**(1): p. 270-9.

180.  Parra, J.L., M. Buxade, and C.G. Proud, *Features of the catalytic domains and C termini of the MAPK signal-integrating kinases Mnk1 and Mnk2 determine their differing activities and regulatory properties.* J Biol Chem, 2005. **280**(45): p. 37623-33.

181.  Ueda, T., et al., *Combined deficiency for MAP kinase-interacting kinase 1 and 2 (Mnk1 and Mnk2) delays tumor development.* Proc Natl Acad Sci U S A, 2010. **107**(32): p. 13984-90.

182.  Prabhu, S.A., et al., *The MNK1/2-eIF4E Axis as a Potential Therapeutic Target in Melanoma.* Int J Mol Sci, 2020. **21**(11).

183.  Sun, J., M.J. Carr, and N.I. Khushalani, *Principles of Targeted Therapy for Melanoma.* Surg Clin North Am, 2020. **100**(1): p. 175-188.

184.  Zhang, B.H. and K.L. Guan, *Activation of B-Raf kinase requires phosphorylation of the conserved residues Thr598 and Ser601.* EMBO J, 2000. **19**(20): p. 5429-39.

185.  Nassar, K.W. and A.C. Tan, *The mutational landscape of mucosal melanoma.* Semin Cancer Biol, 2020. **61**: p. 139-148.

186.  Furic, L., et al., *eIF4E phosphorylation promotes tumorigenesis and is associated with prostate cancer progression.* Proc Natl Acad Sci U S A, 2010. **107**(32): p. 14134-9.

187.  Robichaud, N., et al., *Phosphorylation of eIF4E promotes EMT and metastasis via translational control of SNAIL and MMP-3.* Oncogene, 2015. **34**(16): p. 2032-42.

188.  Wendel, H.G., et al., *Dissecting eIF4E action in tumorigenesis.* Genes Dev, 2007. **21**(24): p. 3232-7.

189.  Welsh, S.J. and P.G. Corrie, *Management of BRAF and MEK inhibitor toxicities in patients with metastatic melanoma.* Ther Adv Med Oncol, 2015. **7**(2): p. 122-36.

190. Young, P., E. Ehler, and M. Gautel, *Obscurin, a giant sarcomeric Rho guanine nucleotide exchange factor protein involved in sarcomere assembly.* J Cell Biol, 2001. **154**(1): p. 123-36.

191. Russell, M.W., et al., *Identification, tissue expression and chromosomal localization of human Obscurin-MLCK, a member of the titin and Dbl families of myosin light chain kinases.* Gene, 2002. **282**(1-2): p. 237-46.

192. Quan, C., et al., *A PKB-SPEG signaling nexus links insulin resistance with diabetic cardiomyopathy by regulating calcium homeostasis.* Nat Commun, 2020. **11**(1): p. 2186.

193. Randazzo, D., et al., *The potential of obscurin as a therapeutic target in muscle disorders.* Expert Opin Ther Targets, 2017. **21**(9): p. 897-910.

194. Grogan, A., P. Tsakiroglou, and A. Kontrogianni-Konstantopoulos, *Double the trouble: giant proteins with dual kinase activity in the heart.* Biophys Rev, 2020. **12**(4): p. 1019-1029.

195. Liu, X., et al., *Disruption of striated preferentially expressed gene locus leads to dilated cardiomyopathy in mice.* Circulation, 2009. **119**(2): p. 261-8.

196. Denis, C.L., B.E. Kemp, and M.J. Zoller, *Substrate specificities for yeast and mammalian cAMP-dependent protein kinases are similar but not identical.* J Biol Chem, 1991. **266**(27): p. 17932-5.

197. Omar, M.H., et al., *Classification of Cushing's syndrome PKAc mutants based upon their ability to bind PKI.* Biochem J, 2023. **480**(12): p. 875-890.

198. Yokokura, H., et al., *The regulatory region of calcium/calmodulin-dependent protein kinase I contains closely associated autoinhibitory and calmodulin-binding domains.* J Biol Chem, 1995. **270**(40): p. 23851-9.

199. Ohmstede, C.A., K.F. Jensen, and N.E. Sahyoun, *Ca2+/calmodulin-dependent protein kinase enriched in cerebellar granule cells. Identification of a novel neuronal calmodulin-dependent protein kinase.* J Biol Chem, 1989. **264**(10): p. 5866-75.

200. Kemp, B., et al., *The calmodulin binding domain of chicken smooth muscle myosin light chain kinase contains a pseudosubstrate sequence.* Journal of Biological Chemistry, 1987. **262**(6): p. 2542-2548.

201. Bagchi, I.C., Q.H. Huang, and A.R. Means, *Identification of amino acids essential for calmodulin binding and activation of smooth muscle myosin light chain kinase.* J Biol Chem, 1992. **267**(5): p. 3024-9.

202. Blumenthal, D.K., et al., *Identification of the calmodulin-binding domain of skeletal muscle myosin light chain kinase.* Proc Natl Acad Sci U S A, 1985. **82**(10): p. 3187-91.

203. Hardie, D.G., D. Carling, and M. Carlson, *The AMP-activated/SNF1 protein kinase subfamily: metabolic sensors of the eukaryotic cell?* Annu Rev Biochem, 1998. **67**: p. 821-55.

204. Pinkosky, S.L., et al., *Long-chain fatty acyl-CoA esters regulate metabolism via allosteric control of AMPK beta1 isoforms.* Nat Metab, 2020. **2**(9): p. 873-881.

205. Steinberg, R.A., et al., *Autoactivation of catalytic (C alpha) subunit of cyclic AMP-dependent protein kinase by phosphorylation of threonine 197.* Mol Cell Biol, 1993. **13**(4): p. 2332-41.

206. Knighton, D.R., et al., *Crystal structure of the catalytic subunit of cyclic adenosine monophosphate-dependent protein kinase.* Science, 1991. **253**(5018): p. 407-14.

207. Kornev, A.P., et al., *Surface comparison of active and inactive protein kinases identifies a conserved activation mechanism.* Proc Natl Acad Sci U S A, 2006. **103**(47): p. 17783-8.

208. Hubbard, S.R., *Crystal structure of the activated insulin receptor tyrosine kinase in complex with peptide substrate and ATP analog.* EMBO J, 1997. **16**(18): p. 5572-81.

209. Mohammadi, M., et al., *Structures of the tyrosine kinase domain of fibroblast growth factor receptor in complex with inhibitors.* Science, 1997. **276**(5314): p. 955-60.

210. Adams, J.A., et al., *Phosphorylation modulates catalytic function and regulation in the cAMP-dependent protein kinase.* Biochemistry, 1995. **34**(8): p. 2447-54.

211. Reinhardt, R. and T.A. Leonard, *A critical evaluation of protein kinase regulation by activation loop autophosphorylation.* Elife, 2023. **12**.

212. Kemp, B.E., R.B. Pearson, and C.M. House, *Pseudosubstrate-based peptide inhibitors.* Methods Enzymol, 1991. **201**: p. 287-304.

213. Johnson, J.L., et al., *An atlas of substrate specificities for the human serine/threonine kinome.* Nature, 2023. **613**(7945): p. 759-766.

214. Kukimoto-Niino, M., et al., *Crystal structure of the Ca(2)(+)/calmodulin-dependent protein kinase kinase in complex with the inhibitor STO-609.* J Biol Chem, 2011. **286**(25): p. 22570-9.

215. Radu, M., et al., *PAK signalling during the development and progression of cancer.* Nat Rev Cancer, 2014. **14**(1): p. 13-25.

216. Dong, X., et al., *Mutations in CHEK2 associated with prostate cancer risk.* Am J Hum Genet, 2003. **72**(2): p. 270-80.

217. Matsuoka, S., et al., *Ataxia telangiectasia-mutated phosphorylates Chk2 in vivo and in vitro.* Proc Natl Acad Sci U S A, 2000. **97**(19): p. 10389-94.

218. Melchionna, R., et al., *Threonine 68 is required for radiation-induced phosphorylation and activation of Cds1.* Nat Cell Biol, 2000. **2**(10): p. 762-5.

219. Ahn, J.Y., et al., *Phosphorylation of threonine 68 promotes oligomerization and autophosphorylation of the Chk2 protein kinase via the forkhead-associated domain.* J Biol Chem, 2002. **277**(22): p. 19389-95.

220. Xu, X., L.M. Tsvetkov, and D.F. Stern, *Chk2 activation and phosphorylation-dependent oligomerization.* Mol Cell Biol, 2002. **22**(12): p. 4419-32.

221. Oliver, A.W., et al., *Trans-activation of the DNA-damage signalling protein kinase Chk2 by T-loop exchange.* EMBO J, 2006. **25**(13): p. 3179-90.

222. Lountos, G.T., et al., *Crystal structure of checkpoint kinase 2 in complex with NSC 109555, a potent and selective inhibitor.* Protein Sci, 2009. **18**(1): p. 92-100.

223. Carafoli, E. and J. Krebs, *Why Calcium? How Calcium Became the Best Communicator.* J Biol Chem, 2016. **291**(40): p. 20849-20857.

224. Chin, D. and A.R. Means, *Calmodulin: a prototypical calcium sensor.* Trends Cell Biol, 2000. **10**(8): p. 322-8.

225. Kretsinger, R.H., *Crystallographic studies of calmodulin and homologs.* Ann N Y Acad Sci, 1980. **356**: p. 14-9.

226. Faux, M.C. and J.D. Scott, *Regulation of the AKAP79-protein kinase C interaction by Ca2+/Calmodulin.* J Biol Chem, 1997. **272**(27): p. 17038-44.

227. Lukas, T.J., et al., *Calmodulin binding domains: characterization of a phosphorylation and calmodulin binding site from myosin light chain kinase.* Biochemistry, 1986. **25**(6): p. 1458-64.

228. Kemp, B.E., et al., *The calmodulin binding domain of chicken smooth muscle myosin light chain kinase contains a pseudosubstrate sequence.* J Biol Chem, 1987. **262**(6): p. 2542-8.

229. Gautier, R., et al., *HELIQUEST: a web server to screen sequences with specific alpha-helical properties.* Bioinformatics, 2008. **24**(18): p. 2101-2.

230. Piserchio, A., et al., *ADP enhances the allosteric activation of eukaryotic elongation factor 2 kinase by calmodulin.* Proc Natl Acad Sci U S A, 2023. **120**(17): p. e2300902120.

231. Piserchio, A., et al., *Structural basis for the calmodulin-mediated activation of eukaryotic elongation factor 2 kinase.* Sci Adv, 2022. **8**(27): p. eabo2039.

232. Ozawa, M. and T. Muramatsu, *Reticulocalbin, a novel endoplasmic reticulum resident Ca(2+)-binding protein with multiple EF-hand motifs and a carboxyl-terminal HDEL sequence.* J Biol Chem, 1993. **268**(1): p. 699-705.

233. Ludvigsen, M., et al., *Identification and characterization of novel ERC-55 interacting proteins: evidence for the existence of several ERC-55 splicing variants; including the cytosolic ERC-55-C.* Proteomics, 2009. **9**(23): p. 5267-87.

234. Tsuji, A., et al., *A proteomic approach reveals transient association of reticulocalbin-3, a novel member of the CREC family, with the precursor of subtilisin-like proprotein convertase, PACE4.* Biochem J, 2006. **396**(1): p. 51-9.

235. Vorum, H., et al., *Human calumenin localizes to the secretory pathway and is secreted to the medium.* Exp Cell Res, 1999. **248**(2): p. 473-81.

236. Scherer, P.E., et al., *Cab45, a novel (Ca2+)-binding protein localized to the Golgi lumen.* J Cell Biol, 1996. **133**(2): p. 257-68.

237. Okuno, S., T. Kitani, and H. Fujisawa, *Studies on the substrate specificity of Ca2+/calmodulin-dependent protein kinase kinase alpha.* J Biochem, 1997. **122**(2): p. 337-43.

238. Cheng, L., et al., *DCLK1 autoinhibition and activation in tumorigenesis.* Innovation (Camb), 2022. **3**(1): p. 100191.

239. Tavares, C.D., et al., *The molecular mechanism of eukaryotic elongation factor 2 kinase activation.* J Biol Chem, 2014. **289**(34): p. 23901-16.

240. Byrne, D.P., et al., *Evolutionary and cellular analysis of the 'dark' pseudokinase PSKH2.* Biochem J, 2023. **480**(2): p. 141-160.

241. Zacharias, D.A., et al., *Partitioning of lipid-modified monomeric GFPs into membrane microdomains of live cells.* Science, 2002. **296**(5569): p. 913-6.

242. Miller, S.G. and M.B. Kennedy, *Regulation of brain type II Ca2+/calmodulin-dependent protein kinase by autophosphorylation: a Ca2+-triggered molecular switch.* Cell, 1986. **44**(6): p. 861-70.

243. Litwin, M.S. and H.J. Tan, *The Diagnosis and Treatment of Prostate Cancer: A Review.* JAMA, 2017. **317**(24): p. 2532-2542.

244. Studer, U.E., et al., *Immediate versus deferred hormonal treatment for patients with prostate cancer who are not suitable for curative local treatment: results of the randomized trial SAKK 08/88.* J Clin Oncol, 2004. **22**(20): p. 4109-18.

245. Huggins, C. and C.V. Hodges, *Studies on prostatic cancer. I. The effect of castration, of estrogen and androgen injection on serum phosphatases in metastatic carcinoma of the prostate.* CA Cancer J Clin, 1972. **22**(4): p. 232-40.

246. Chandrasekar, T., et al., *Mechanisms of resistance in castration-resistant prostate cancer (CRPC).* Transl Androl Urol, 2015. **4**(3): p. 365-80.

247.    Kajimoto, K., et al., *Hypotonic swelling-induced activation of PKN1 mediates cell survival in cardiac myocytes.* Am J Physiol Heart Circ Physiol, 2011. **300**(1): p. H191-200.

248.    Melkonian, E.A. and M.P. Schury, *Biochemistry, Anaerobic Glycolysis*, in *StatPearls*. 2024: Treasure Island (FL).

249.    Rossi, S., et al., *Fatty acid synthase expression defines distinct molecular signatures in prostate cancer.* Mol Cancer Res, 2003. **1**(10): p. 707-15.

250.    Liu, Y., L.S. Zuckier, and N.V. Ghesani, *Dominant uptake of fatty acid over glucose by prostate cells: a potential new diagnostic and therapeutic approach.* Anticancer Res, 2010. **30**(2): p. 369-74.

251.    Schlaepfer, I.R., et al., *Lipid catabolism via CPT1 as a therapeutic target for prostate cancer.* Mol Cancer Ther, 2014. **13**(10): p. 2361-71.

252.    Schlaepfer, I.R., et al., *Hypoxia induces triglycerides accumulation in prostate cancer cells and extracellular vesicles supporting growth and invasiveness following reoxygenation.* Oncotarget, 2015. **6**(26): p. 22836-56.

253.    Watt, M.J., et al., *Suppressing fatty acid uptake has therapeutic effects in preclinical models of prostate cancer.* Sci Transl Med, 2019. **11**(478).

254.    Pezacki, J.P., et al., *Chemical contrast for imaging living systems: molecular vibrations drive CARS microscopy.* Nat Chem Biol, 2011. **7**(3): p. 137-45.

255.    Miyazawa, T., *Lipid hydroperoxides in nutrition, health, and diseases.* Proc Jpn Acad Ser B Phys Biol Sci, 2021. **97**(4): p. 161-196.

256.    Anjum, R. and J. Blenis, *The RSK family of kinases: emerging roles in cellular signalling.* Nat Rev Mol Cell Biol, 2008. **9**(10): p. 747-58.

257.    Clark, D.E., et al., *The serine/threonine protein kinase, p90 ribosomal S6 kinase, is an important regulator of prostate cancer cell proliferation.* Cancer Res, 2005. **65**(8): p. 3108-16.

258.    Jones, S.W., et al., *A Xenopus ribosomal protein S6 kinase has two apparent kinase domains that are each similar to distinct protein kinases.* Proc Natl Acad Sci U S A, 1988. **85**(10): p. 3377-81.

259.    Fisher, T.L. and J. Blenis, *Evidence for two catalytically active kinase domains in pp90rsk.* Mol Cell Biol, 1996. **16**(3): p. 1212-9.

260.    Dalby, K.N., et al., *Identification of regulatory phosphorylation sites in mitogen-activated protein kinase (MAPK)-activated protein kinase-1a/p90rsk that are inducible by MAPK.* J Biol Chem, 1998. **273**(3): p. 1496-505.

261.    Vik, T.A. and J.W. Ryder, *Identification of serine 380 as the major site of autophosphorylation of Xenopus pp90rsk.* Biochem Biophys Res Commun, 1997. **235**(2): p. 398-402.

262.    Frodin, M., et al., *A phosphoserine-regulated docking site in the protein kinase RSK2 that recruits and activates PDK1.* EMBO J, 2000. **19**(12): p. 2924-34.

263.    Gross, S.D., et al., *Induction of metaphase arrest in cleaving Xenopus embryos by the protein kinase p90Rsk.* Science, 1999. **286**(5443): p. 1365-7.

264.    Zaru, R., et al., *Structural and functional basis for p38-MK2-activated Rsk signaling in toll-like receptor-stimulated dendritic cells.* Mol Cell Biol, 2015. **35**(1): p. 132-40.

265.    Ma, Y., et al., *P90 ribosomal S6 kinase confers cancer cell survival by mediating checkpoint kinase 1 degradation in response to glucose stress.* Cancer Sci, 2022. **113**(1): p. 132-144.

266.    Boglari, G. and J. Szeberenyi, *Nuclear translocation of p90Rsk and phosphorylation of CREB is induced by ionomycin in a Ras-independent manner in PC12 cells.* Acta Biol Hung, 2002. **53**(3): p. 325-34.

267.    Alexa, A., et al., *Structural assembly of the signaling competent ERK2-RSK1 heterodimeric protein kinase complex.* Proc Natl Acad Sci U S A, 2015. **112**(9): p. 2711-6.

268.    Shimamura, A., et al., *Rsk1 mediates a MEK-MAP kinase cell survival signal.* Curr Biol, 2000. **10**(3): p. 127-35.

269.    Richards, S.A., et al., *Characterization of regulatory events associated with membrane targeting of p90 ribosomal S6 kinase 1.* Mol Cell Biol, 2001. **21**(21): p. 7470-80.

270.    Fidelito, G., M.J. Watt, and R.A. Taylor, *Personalized Medicine for Prostate Cancer: Is Targeting Metabolism a Reality?* Front Oncol, 2021. **11**: p. 778761.

271.    Zadra, G., et al., *A novel direct activator of AMPK inhibits prostate cancer growth by blocking lipogenesis.* EMBO Mol Med, 2014. **6**(4): p. 519-38.

272.    Nairn, A.C., et al., *Elongation factor-2 phosphorylation and the regulation of protein synthesis by calcium.* Prog Mol Subcell Biol, 2001. **27**: p. 91-129.

273.    Wang, X., et al., *Regulation of elongation factor 2 kinase by p90(RSK1) and p70 S6 kinase.* EMBO J, 2001. **20**(16): p. 4370-9.

274.    Wong, S.K., et al., *Prostate Cancer and Bone Metastases: The Underlying Mechanisms.* Int J Mol Sci, 2019. **20**(10).

275.    Merrick, W.C., *eIF4F: a retrospective.* J Biol Chem, 2015. **290**(40): p. 24091-9.

276.    Shahbazian, D., et al., *The mTOR/PI3K and MAPK pathways converge on eIF4B to control its phosphorylation and activity.* EMBO J, 2006. **25**(12): p. 2781-91.

277.    Maddirevula, S., et al., *Large-scale genomic investigation of pediatric cholestasis reveals a novel hepatorenal ciliopathy caused by PSKH1 mutations.* Genet Med, 2024. **26**(11): p. 101231.

278.    Day, C.P., *From fat to inflammation.* Gastroenterology, 2006. **130**(1): p. 207-10.

279.    Mehrabipour, M., et al., *A Systematic Compilation of Human SH3 Domains: A Versatile Superfamily in Cellular Signaling.* Cells, 2023. **12**(16).

280.    Zhou, Y., et al., *Metascape provides a biologist-oriented resource for the analysis of systems-level datasets.* Nat Commun, 2019. **10**(1): p. 1523.

281.    Cooper, C.R., et al., *Novel surface expression of reticulocalbin 1 on bone endothelial cells and human prostate cancer cells is regulated by TNF-alpha.* J Cell Biochem, 2008. **104**(6): p. 2298-309.

282.    Liu, X., et al., *Downregulation of reticulocalbin-1 differentially facilitates apoptosis and necroptosis in human prostate cancer cells.* Cancer Sci, 2018. **109**(4): p. 1147-1157.

283.    Hirano, T., et al., *Identification of postoperative adjuvant chemotherapy responders in non-small cell lung cancer by novel biomarker.* Int J Cancer, 2005. **117**(3): p. 460-8.

284.    Yamaguchi, H., et al., *Molecular mechanism for the regulation of rho-kinase by dimerization and its inhibition by fasudil.* Structure, 2006. **14**(3): p. 589-600.

285.    Jacobs, M., et al., *The structure of dimeric ROCK I reveals the mechanism for ligand selectivity.* J Biol Chem, 2006. **281**(1): p. 260-8.

286.    Couzens, A.L., V. Saridakis, and M.P. Scheid, *The hydrophobic motif of ROCK2 requires association with the N-terminal extension for kinase activity.* Biochem J, 2009. **419**(1): p. 141-8.

287.    Leung, T., et al., *A novel serine/threonine kinase binding the Ras-related RhoA GTPase which translocates the kinase to peripheral membranes.* J Biol Chem, 1995. **270**(49): p. 29051-4.

288.    Leung, T., et al., *The p160 RhoA-binding kinase ROK alpha is a member of a kinase family and is involved in the reorganization of the cytoskeleton.* Mol Cell Biol, 1996. **16**(10): p. 5313-27.

289.    Nakagawa, O., et al., *ROCK-I and ROCK-II, two isoforms of Rho-associated coiled-coil forming protein serine/threonine kinase in mice.* FEBS Lett, 1996. **392**(2): p. 189-93.

290.    Shi, J., et al., *Distinct roles for ROCK1 and ROCK2 in the regulation of cell detachment.* Cell Death Dis, 2013. **4**(2): p. e483.

291.    Pelosi, M., et al., *ROCK2 and its alternatively spliced isoform ROCK2m positively control the maturation of the myogenic program.* Mol Cell Biol, 2007. **27**(17): p. 6163-76.

292.    Giansanti, P., et al., *Interrogating cAMP-dependent kinase signaling in Jurkat T cells via a protein kinase A targeted immune-precipitation phosphoproteomics approach.* Mol Cell Proteomics, 2013. **12**(11): p. 3350-9.

293.    Kaneko, T., et al., *Identification of calponin as a novel substrate of Rho-kinase.* Biochem Biophys Res Commun, 2000. **273**(1): p. 110-6.

294.    Abercrombie, M. and J.E. Heaysman, *Observations on the social behaviour of cells in tissue culture. II. Monolayering of fibroblasts.* Exp Cell Res, 1954. **6**(2): p. 293-306.

295.    Carmona-Fontaine, C., et al., *Contact inhibition of locomotion in vivo controls neural crest directional migration.* Nature, 2008. **456**(7224): p. 957-61.

296.    Zhou, H. and R.H. Kramer, *Integrin engagement differentially modulates epithelial cell motility by RhoA/ROCK and PAK1.* J Biol Chem, 2005. **280**(11): p. 10624-35.

297.    Ridley, A.J., et al., *The small GTP-binding protein rac regulates growth factor-induced membrane ruffling.* Cell, 1992. **70**(3): p. 401-10.

298.    Nobes, C.D. and A. Hall, *Rho, rac, and cdc42 GTPases regulate the assembly of multimolecular focal complexes associated with actin stress fibers, lamellipodia, and filopodia.* Cell, 1995. **81**(1): p. 53-62.

299.    Edwards, D.C., et al., *Activation of LIM-kinase by Pak1 couples Rac/Cdc42 GTPase signalling to actin cytoskeletal dynamics.* Nat Cell Biol, 1999. **1**(5): p. 253-9.

300.    Dan, C., et al., *Cytoskeletal changes regulated by the PAK4 serine/threonine kinase are mediated by LIM kinase 1 and cofilin.* J Biol Chem, 2001. **276**(34): p. 32115-21.

301.    Nishita, M., et al., *Spatial and temporal regulation of cofilin activity by LIM kinase and Slingshot is critical for directional cell migration.* J Cell Biol, 2005. **171**(2): p. 349-59.

302.    Matthews, H.K., et al., *Directional migration of neural crest cells in vivo is regulated by Syndecan-4/Rac1 and non-canonical Wnt signaling/RhoA.* Development, 2008. **135**(10): p. 1771-80.

303.    Zhang, M., et al., *CAP interacts with cytoskeletal proteins and regulates adhesion-mediated ERK activation and motility.* EMBO J, 2006. **25**(22): p. 5284-93.

304.    Kioka, N., K. Ueda, and T. Amachi, *Vinexin, CAP/ponsin, ArgBP2: a novel adaptor protein family regulating cytoskeletal organization and signal transduction.* Cell Struct Funct, 2002. **27**(1): p. 1-7.

305.    Obenauer, J.C., L.C. Cantley, and M.B. Yaffe, *Scansite 2.0: Proteome-wide prediction of cell signaling interactions using short sequence motifs.* Nucleic Acids Res, 2003. **31**(13): p. 3635-41.

306.    Ha, B.H., et al., *Type II p21-activated kinases (PAKs) are regulated by an autoinhibitory pseudosubstrate.* Proc Natl Acad Sci U S A, 2012. **109**(40): p. 16107-12.

307.    Baskaran, Y., et al., *Group I and II mammalian PAKs have different modes of activation by Cdc42.* EMBO Rep, 2012. **13**(7): p. 653-9.

308.    Radu, M., et al., *ArhGAP15, a Rac-specific GTPase-activating protein, plays a dual role in inhibiting small GTPase signaling.* J Biol Chem, 2013. **288**(29): p. 21117-21125.